Investigations of electrophysiological mechanisms related to myocardial ischaemia in hypertrophic cardiomyopathy: implications for arrhythmic risk, ECG diagnosis, and antiarrhythmic therapy

James Alec Coleman
St Catherine's College



Department of Computer Science
University of Oxford

Hilary 2024

This thesis is submitted to the Department of Computer Science, University of Oxford, for the degree of Doctor of Philosophy. This thesis is entirely my own work, and, except where otherwise indicated, describes my own research.

Abstract

Hypertrophic cardiomyopathy (HCM) is a leading cause of sudden cardiac death in the young. Acute myocardial ischaemia (a sudden myocardial blood supply/demand mismatch) and pre-existing chronic ionic remodelling (which causes slowed cellular repolarisation) are acknowledged as two key contributors to lethal arrhythmias, but the assessment of these disease factors is absent from HCM clinical guidelines. Using multiscale modelling of cardiac electrophysiology, this thesis aimed to investigate the electrophysiological effects of myocardial ischaemia and ionic remodelling in HCM, to benefit arrhythmic risk predictions, the ECG diagnosis of ischaemia, and antiarrhythmic therapy.

Computational models of human HCM cardiomyocytes with ionic remodelling were subjected to ischaemia and action potential biomarkers were measured, then validated *in vitro* with human HCM patch-clamp experimental data from collaborators. Biventricular simulations with regional ischaemia, informed by clinical HCM perfusion imaging data, were used to measure independent arrhythmic risk contributions from ionic remodelling using S1-S2 pacing protocols. ECGs were further derived from ischaemic biventricular simulations, and compared to those under benign exercise effects, to investigate HCM-specific stress ECG diagnostic markers of ischaemia. Finally, arrhythmic risk was measured in HCM biventricular simulations under the pharmacologic effects of ranolazine.

HCM cardiomyocytes had enhanced sensitivity to ischaemia, where the presence of ionic remodelling increased arrhythmic risk in ischaemic simulations, particularly for transmural insults. This enhanced ischaemic cellular response manifested as pseudonormalisation of ECG repolarisation abnormalities, but benign exercise effects also contributed, possibly mimicking signs of ischaemia on the ECG and complicating its diagnosis. Finally, the antiarrhythmic efficacy and safety of ranolazine was dependent on the severity of ionic remodelling and may be predicted using the ECG, with optimal effects in cases of moderate ionic remodelling, but potential proarrhythmic effects in severe-extreme cases.

Ionic remodelling in HCM makes independent contributions to ischaemic arrhythmic risk, facilitates HCM-specific manifestations of ischaemia on the ECG, and may be a therapeutic target for the amelioration of arrhythmias with ranolazine.

Publications

- **James A Coleman**, Ruben Doste, Matteo Beltrami, Alessia Argirò, Raffaele Coppini, Iacopo Olivotto, Betty Raman and Alfonso Bueno-Orovio. "Effects of ranolazine on the arrhythmic substrate in hypertrophic cardiomyopathy". In: *Front Pharmacol* 15 (2024). DOI: 10.3389/fphar.2024.1379236.

- **James A Coleman**, Ruben Doste, Zakariye Ashkir, Raffaele Coppini, Rafael Sachetto, Hugh Watkins, Betty Raman and Alfonso Bueno-Orovio. "Mechanisms of ischaemia-induced arrhythmias in hypertrophic cardiomyopathy: a large-scale computational study". In: *Cardiovasc Res* (2024). DOI: 10.1093/cvr/cvae086.

- Julia Camps, Lucas Arantes Berg, Zhinuo Jenny Wang, Rafael Sebastian, Leto Luana Riebel, Ruben Doste, Xin Zhou, Rafael Sachetto, **James A Coleman**, Brodie Lawson, Vicente Grau, Kevin Burrage, Alfonso Bueno-Orovio, Rodrigo Weber dos Santos and Blanca Rodriguez. "Digital twinning of the human ventricular activation sequence to clinical 12-lead ECGs and magnetic resonance imaging using realistic Purkinje networks for in silico clinical trials". In: *Med Image Anal* 94 (2024), p. 103108. DOI: 10.1016/j.media.2024.103108.

- **James A Coleman**, Ruben Doste, Matteo Beltrami, Raffaele Coppini, Iacopo Olivotto, Betty Raman and Alfonso Bueno-Orovio. "Electrophysiological mechanisms underlying T wave pseudonormalisation on stress ECGs in hypertrophic cardiomyopathy". In: *Comput Biol Med* 169 (2024), p. 107829. DOI: 10.1016/j.compbiomed.2023.107829.

- **James A Coleman**, Zakariye Ashkir, Betty Raman and Alfonso Bueno-Orovio. "Mechanisms and prognostic impact of myocardial ischaemia in hypertrophic cardiomyopathy". In: *Int J Cardiovasc Imaging* 39.10 (2023), pp. 1979–1996. DOI: 10.1007/s10554-023-02894-y.

- **James A Coleman**, Ruben Doste and Alfonso Bueno-Orovio. "Differential response of hypertrophic cardiomyopathy to ischemia caused by remodelling of late sodium and rapidly delayed rectifier channels". In: *Comput Cardiol* 498 (2022). DOI: 10.22489/CinC.2022.045.

Conferences

- **Gordon Research Seminar and Conference on Cardiac Arrhythmia Mechanisms**. Poster: "Myocardial ischaemia and abnormal repolarisation as causes of arrhythmias and ECG abnormalities in hypertrophic cardiomyopathy", Galveston, TX, USA (2023). *British Heart Foundation Travel Award*.

- **Oxford Symposium on the Future of Therapy Discovery and Development**. Talk: "Pro-arrhythmic ischaemia in hypertrophic cardiomyopathy: in silico versus clinical investigations", Oxford, UK (2022).

- **British Heart Foundation Centre of Research Excellence Annual Symposium**. Poster: "Contribution of ionic remodelling and fibrosis to arrhythmic risk during ischaemia in hypertrophic cardiomyopathy", Oxford, UK (2022).

- **Computing in Cardiology**. Poster: "Contribution of ionic remodelling and fibrosis to arrhythmic risk during ischaemia in hypertrophic cardiomyopathy", Tampere, Finland (2022).

- **European Society of Cardiology Working Group on Cardiac Cellular Electrophysiology Annual Meeting**. Poster: "Contribution of ionic remodelling and fibrosis to arrhythmic risk during ischaemia in hypertrophic cardiomyopathy", Toledo, Spain (2022).

- **Computing in Cardiology**. Poster: "Increased re-entry inducibility in ischaemic hypertrophic cardiomyopathy tissue caused by remodelling in late sodium and rapidly delayed rectifier channels", Brno, Czech Republic (2021). *The Rosanna Degani Young Investigator Semi-Finalist Award*.

Acknowledgements

Firstly, I'd like to thank Prof. Alfonso Bueno-Orovio for the continuous excellent supervision throughout the last three years. I am especially grateful for the positive mentorship and for keeping motivation high, particularly through the initial lockdown lows, as well as providing the opportunity to attend conferences in exciting new places. I am further thankful to Prof. Betty Raman for the excellent clinical input, access to data, and insight provided as co-supervisor.

I'd like to thank the collaborators, in relation to the unique access to clinical and experimental data and/or clinical feedback, Dr. Raffaele Coppini, Dr. Matteo Beltrami, Dr. Alessia Argirò, Dr. Zakariye Ashkir, Prof. Iacopo Olivotto and Prof. Hugh Watkins. I'd like to thank Prof. Rafael Sachetto in relation to the development of MonoAlg3D, as well as guidance on using the software.

I'd like to thank the entire Computational Cardiovascular Science group for the continuous presentations and discussions, in which I was fortunate to learn about a range of new research. I am particularly grateful to Dr. Hector Martinez-Navarro and Dr. Lucas Berg for their efforts in securing access to computational resources, as well as Dr. Ruben Doste for the continuous input and feedback. I'd also like to thank Prof. Blanca Rodriguez and Dr. Rina Ariga as the examiners of my Transfer and Confirmation vivas, for their questions and feedback. I am further grateful to the nine anonymous peer reviewers for their constructive criticism and insight.

I'd like to thank the Engineering and Physical Sciences Research Council and Department of Computer Science at University of Oxford for providing the DPhil tuition fees and stipend. I acknowledge the further support from the Partnership for Advanced Computing in Europe for access to Piz Daint at the Swiss National Supercomputing Centre, Switzerland [ICEI-PRACE grants icp005, icp013 and icp019], the Edinburgh Parallel Computing Centre for access to Cirrus, and the use of the University of Oxford Advanced Research Computing facility (DOI: 10.5281/zenodo.22558).

Finally, I'd like to thank my friends in Oxford and London for making the last three years so entertaining, as well as my family (Mum, Dad, Sam and Beckie) for their constant support.

Acronyms

AF atrial fibrillation

AP action potential

APD action potential duration

ATP adenosine triphosphate

BOLD blood oxygen level dependent

BZ border zone

CAD coronary artery disease

CFR coronary flow reserve

CFVR coronary flow velocity reserve

CMR cardiac magnetic resonance

CT computed tomography

CV conduction velocity

CZ core zone

DM diabetes mellitus

ECG electrocardiogram

ECGI electrocardiographic imaging

ECV extracellular volume

ERP effective refractory period

GPU graphics processing unit

HCM hypertrophic cardiomyopathy

ICD implantable cardioverter-defibrillator

JSR junctional sarcoplasmic reticulum

LA left arm

LAD left anterior descending

LGE late gadolinium enhancement

LL left leg

LQT long QT

LV left ventricle

LVOT left ventricular outflow tract

MBF myocardial blood flow

MCE myocardial contrast echocardiography

MPR myocardial perfusion reserve

MPRI myocardial perfusion reserve index

NSR network sarcoplasmic reticulum

NZ normal zone

ODE ordinary differential equation

PDE partial differential equation

PET positron emission tomography

PRR post-repolarisation refractoriness

PVC premature ventricular complex

RA right arm

RL right leg

RMP resting membrane potential

RV right ventricle

SCD sudden cardiac death

SEM standard error of the mean

SERCA sarcoendoplasmic reticulum Ca^{2+} ATPase

SPECT single positron emission computed tomography

SS junctional subspace

VF ventricular fibrillation

VT ventricular tachycardia

WMA wall motion abnormality

Contents

1 Introduction **17**
- 1.1 Background . . . 17
- 1.2 Aims . . . 21
- 1.3 Outline . . . 21

2 Cardiac electrophysiology **23**
- 2.1 Gross cardiac anatomy, function and electrophysiology . . . 23
- 2.2 Fine cardiac structure and electrophysiology . . . 26
  - 2.2.1 Cardiomyocytes . . . 26
  - 2.2.2 Ion channels, pumps and exchangers . . . 26
  - 2.2.3 Action potentials . . . 27
  - 2.2.4 Ca^{2+} subsystem . . . 30
  - 2.2.5 Cardiomyocyte-cardiomyocyte coupling . . . 30
  - 2.2.6 Myocardial heterogeneities . . . 31
- 2.3 Electrocardiograms . . . 33
  - 2.3.1 Recording an ECG . . . 33
  - 2.3.2 Biomarkers of the ECG . . . 36
- 2.4 Electrophysiological effects of acute myocardial ischaemia . . . 37
  - 2.4.1 Acute myocardial ischaemia . . . 37
  - 2.4.2 Ischaemic action potentials . . . 38
  - 2.4.3 Regional acute myocardial ischaemia . . . 40
  - 2.4.4 Effects on the ECG . . . 41
- 2.5 Ventricular arrhythmias . . . 42
  - 2.5.1 Cellular arrhythmias . . . 42
  - 2.5.2 Types of ventricular arrhythmias . . . 42
  - 2.5.3 Mechanisms of ventricular arrhythmias . . . 44

3 Literature review of myocardial ischaemia and ionic remodelling in HCM **45**
- 3.1 Hypertrophic cardiomyopathy . . . 45
  - 3.1.1 General background . . . 45
  - 3.1.2 Causes of mortality in HCM . . . 47
  - 3.1.3 Sudden cardiac death . . . 47
  - 3.1.4 Prevention of sudden cardiac death . . . 47
- 3.2 Myocardial ischaemia . . . 50
  - 3.2.1 Imaging of ischaemia in HCM . . . 50
  - 3.2.2 Pathophysiological mechanisms of ischaemia in HCM . . . 53
  - 3.2.3 Relationships between markers of disease severity and ischaemia . . . 55
  - 3.2.4 Clinical manifestations of myocardial ischaemia in HCM . . . 59
  - 3.2.5 Mechanisms of myocardial ischaemia progression in HCM . . . 59
  - 3.2.6 Prognostic value of myocardial ischaemia in HCM . . . 62
- 3.3 Ionic remodelling . . . 67
  - 3.3.1 Experimental evidence . . . 67
  - 3.3.2 ECG evidence . . . 68
  - 3.3.3 Spatial distribution of ionic remodelling . . . 69
  - 3.3.4 Prognosis . . . 69

4 Computational modelling and simulation of cardiac electrophysiology 71
4.1 Modelling action potentials . . . 71
4.1.1 Hodgkin–Huxley formulation of ionic currents . . . 72
4.1.2 Action potential model choice . . . 74
4.1.3 The ToR-ORd human ventricular action potential model . . . 75
4.1.4 Populations of models . . . 77
4.2 Modelling cardiac electrical wavefront propagation . . . 77
4.2.1 Monodomain model . . . 78
4.2.2 The MonoAlg3D simulator . . . 79
4.2.3 Multiscale modelling and simulation of cardiac electrophysiology . . . 79
4.3 Tuning conduction velocity: spatial discretisation . . . 83
4.4 Modelling ionic remodelling in HCM . . . 84
4.5 Modelling acute myocardial ischaemia . . . 86
4.5.1 Modelling ischaemic action potentials . . . 86
4.5.2 Modelling regional acute myocardial ischaemia . . . 88
4.6 Measuring arrhythmic risk . . . 89

5 Interplay between cellular ionic remodelling and acute myocardial ischaemia in HCM 91
5.1 Introduction . . . 91
5.2 Methods . . . 92
5.2.1 Creation of control and HCM populations of AP models . . . 92
5.2.2 Simulation of ischaemic conditions . . . 93
5.2.3 Measurements of effective refractory period . . . 93
5.2.4 Patch-clamp validation . . . 94
5.3 Results . . . 94
5.3.1 Abnormal response to ischaemia in HCM-remodelled cells . . . 94
5.4 Discussion . . . 100
5.5 Conclusions . . . 100
5.6 Limitations . . . 101

6 Electrophysiological mechanisms of ischaemia-induced arrhythmias in HCM 103
6.1 Introduction . . . 103
6.2 Methods . . . 104
6.2.1 HCM tissue and biventricular models with ischaemia and fibrosis . . . 104
6.2.2 Pacing protocol . . . 105
6.2.3 Perfusion imaging . . . 106
6.3 Results . . . 106
6.3.1 Re-entry emerges earlier in the onset of ischaemia in HCM tissue . . . 106
6.3.2 Multiple mechanisms of in-tissue ischaemia-fibrosis interaction . . . 110
6.3.3 Clinically informed ischaemia and fibrosis distributions . . . 113
6.3.4 Transmural extent of ischaemia modulates arrhythmic risk in HCM ventricles . . . 115
6.3.5 Multiple mechanisms of ischaemia-fibrosis interaction in HCM ventricles . . . 117
6.4 Discussion . . . 119
6.5 Conclusions . . . 121
6.6 Limitations . . . 121

7 Electrophysiological mechanisms underlying T wave pseudonormalisation on stress ECGs in HCM 123
7.1 Introduction . . . 123
7.2 Methods . . . 125

7.2.1 HCM biventricular models with regional and global K^+ accumulation . . . 125
7.2.2 ECG analysis . . . 126
7.3 Results . . . 127
7.3.1 Septal and apical HCM phenotype baseline models with regional ionic remodelling 127
7.3.2 Effects of serum vs. regional K^+ on T wave abnormalities . . . 130
7.3.3 Effects of pacing rate vs. regional K^+ on T wave abnormalities . . . 139
7.4 Discussion . . . 142
7.5 Conclusions . . . 144
7.6 Limitations . . . 144

8 Effects of ranolazine on the arrhythmic substrate in HCM 145
8.1 Introduction . . . 145
8.2 Methods . . . 146
8.2.1 HCM tissue and biventricular models . . . 146
8.2.2 Pacing protocol . . . 147
8.2.3 Modelling effects of ranolazine . . . 147
8.2.4 Simulated ECG analysis . . . 147
8.2.5 Clinical ECGs of HCM patients pre- and post-ranolazine . . . 147
8.3 Results . . . 148
8.3.1 Baseline HCM electrophysiological phenotypes . . . 148
8.3.2 Baseline HCM arrhythmic risk . . . 150
8.3.3 Ranolazine effect on HCM electrophysiology . . . 153
8.3.4 Ranolazine effect on arrhythmic risk . . . 157
8.3.5 Effects of pacing rate . . . 161
8.4 Discussion . . . 162
8.5 Conclusions . . . 165
8.6 Limitations . . . 166

9 Conclusions and future directions 169
9.1 Key findings . . . 169
9.2 Future directions . . . 172
9.3 General limitations . . . 174
9.4 Conclusions . . . 175

10 References 177

A Appendix 225

CHAPTER 1

Introduction

This chapter introduces the heart disease hypertrophic cardiomyopathy (HCM) and the key knowledge gaps considered in the scope of this thesis, in relation to arrhythmic risk predictions, the diagnosis of ischaemia, and pharmacologic antiarrhythmic therapies. The aims of the thesis and an outline of the thesis are further provided.

1.1 Background

HCM is one of the most common inherited heart diseases and a leading cause of sudden cardiac death (SCD) in the young. The majority of SCDs in HCM are caused by unexpected ventricular arrhythmias [268]. The first-line therapy for SCD prevention in HCM is the implantable cardioverter-defibrillator (ICD), which is a surgically implanted device effective at detecting and terminating ventricular arrhythmias [320]. However, 7–10 ICDs are implanted for every 1 patient that benefits from ICD termination of arrhythmia at 5 years of follow-up [224], each carrying the risks of surgery, device complications and inappropriate shocks [190]. There is therefore a strong calling to discern low from high-risk patients to better target ICD therapy, a goal that may be achieved through investigating the mechanisms that cause arrhythmias, and refining techniques to detect lethal arrhythmic substrates in HCM. There is further motivation to investigate the use of pharmacologic antiarrhythmic therapies in HCM, as alternatives to ICDs with lesser risks in the context of suboptimal SCD risk stratification.

Acute myocardial ischaemia is widely acknowledged as a key contributor to lethal arrhythmias in HCM [47], particularly in young patients [61, 113, 116, 122, 189, 307, 407], but the clinical assessment of ischaemia does not yet feature in SCD risk stratification [224], despite impaired myocardial perfusion affecting most patients [305]. Instead, SCD risk stratification remains primarily based on risk markers such as a prior malignant arrhythmia, unexplained syncope, and a family history of SCD. Although predictive of SCD [224], such risk markers are limited in part because most SCDs are the first presentation of HCM [377], and there is substantial phenotypic heterogeneity in disease expression even within the same family [400]. Despite myocardial ischaemia being characterised as a substrate for lethal arrhythmias in the general population, typically due to coronary artery disease, myocardial ischaemia in HCM is typically unrelated to coronary artery territories, instead colocalising with ventricular hypertrophy [143]. Myocardial ischaemia in HCM can still cause myocardial infarction [215, 383] and lethal arrhythmias [116, 122, 189, 307], through several pro-ischaemic mechanisms including small vessel disease, sarcomere energetic inefficiency, increased energy demand due to hypertrophy, reduced capillary density, excessive vascular compression, and obstruction of the left ventricular outflow tract (LVOT). With myocardial ischaemia being inducible by increases in myocardial workload [77, 307], a refined understanding of myocardial ischaemia could further elucidate the relationship between exercise and SCD, and refine the controversial exercise restrictions applied to HCM patients [14, 214, 376].

The arrhythmic substrate in HCM is further complicated by chronic electrophysiological abnormalities thought to be secondary to hypertrophy, where repolarisation of the ventricles after contraction is slowed, due to alterations in the subcellular ion channels that regulate the activity of cardiac cells [66]. This ionic remodelling is understood to promote abnormal cellular triggered electrical activity, but how it modulates clinically significant organ-scale arrhythmias is unknown, despite pro-arrhythmic hypertrophy-ischaemia interactions reported in the general population [381].

Myocardial fibrosis also contributes to lethal arrhythmias in HCM, with visible evidence of extensive fibrosis on cardiac magnetic resonance (CMR) recently being included as a risk factor [117, 224, 274, 378]. However, not only are fibrosis and ischaemia causally related [111, 299] and frequently overlapping on imaging [36], but studies investigating imaging of ischaemia and arrhythmias frequently do not control for fibrosis [176], and vice versa [105]. Mechanistic uncertainty therefore remains as to the

independent relative contributions of ischaemia and fibrosis to arrhythmias. The occurrence of SCDs in HCM patients with no known risk factors [139] may in part be explained by other substrates such as myocardial ischaemia and ionic remodelling, as both can emerge early in disease onset and may even precede hypertrophy [67, 138, 156, 160].

Not only is there possible confounding between arrhythmic substrates, but the diagnosis of myocardial ischaemia may also be adversely affected by ionic remodelling and fibrosis in HCM. With the stress electrocardiogram (ECG) detection of ischaemia being reliant on dynamic repolarisation abnormalities, the presence of abnormal repolarisation at baseline causes problems for the diagnostic criteria [222]. Abnormal repolarisation measures are the single most common baseline ECG abnormality in HCM, present in 80% of cases [25, 262], where both ionic remodelling and fibrosis are plausible contributors [201, 402]. During a stress ECG, a range of further repolarisation abnormalities can also develop [77], but non-specific stress ECG changes have limited prognostic value [54]. Therefore, it is important to discern pathological ischaemic changes from benign changes that occur with exercise. One such stress ECG finding of controversial clinical significance is where repolarisation abnormalities such as inverted T waves are transiently corrected during exercise (T wave pseudonormalisation) [77, 241]. Despite reported associations with transmural myocardial ischaemia in coronary artery disease cohorts [212], the mechanisms underlying T wave pseudonormalisation in HCM are unknown. Because transmural infarctions are sometimes identified at SCD autopsy [215], potential markers of transmural ischaemia are of clinical interest in HCM [106].

Functional causes of arrhythmias in HCM such as myocardial ischaemia and ionic remodelling are also of significant interest from a therapeutic standpoint. Unlike irreversible structural substrates like fibrosis, myocardial ischaemia and ionic remodelling may be amenable to pharmacologic interventions. Ranolazine is a late Na^+ blocking drug used for the control of angina in HCM, which can ameliorate slowed repolarisation [66, 250] and microvascular ischaemia [15]. Ranolazine has demonstrated efficacy in a randomised controlled trial at reducing the premature ventricular complex (PVC) burden in symptomatic, non-obstructive HCM patients [270], and real-world analysis has also identified a subgroup of responders for the relief of ventricular arrhythmias [15]. As potential mechanisms, *in vitro* data has shown that ranolazine, through correcting repolarisation and favourable effects on Ca^{2+} handling, reduces

the incidence of cellular triggers [66] and spontaneous contractions in a mouse HCM model [67]. However, the mechanisms by which ranolazine affects the whole-organ arrhythmic substrate (beyond cellular triggers) are unknown, despite the substrate being critically important for clinically significant arrhythmias such as ventricular tachycardia (VT).

In summary, the key knowledge gaps considered in the scope of this thesis are:

(i) How the electrophysiological effects of ischaemia manifest as altered repolarisation and refractoriness in cells affected by HCM ionic remodelling is unknown.

(ii) How ischaemia-induced arrhythmias are affected by the presence of other substrates such as HCM ionic remodelling and diffuse fibrosis is unknown.

(iii) How acute myocardial ischaemia manifests on ECGs in HCM with abnormal repolarisation at baseline is unknown.

(iv) The mechanisms by which ranolazine affects the arrhythmic substrate in HCM and clinically significant arrhythmias is unknown.

These major gaps in knowledge in part remain because human *in vivo* investigations of electrophysiological mechanisms are challenging, as invasive mapping protocols are not routinely performed in these high-risk patients. Therefore, in this thesis a multiscale human computational modelling and simulation approach is used in synergy with data from clinical perfusion imaging, clinical ECGs and human HCM cardiomyocyte patch-clamp experiments to investigate electrophysiological mechanisms related to ischaemia to aid the stratification of ischaemic arrhythmic risk, diagnosis of ischaemia and potential pharmacologic amelioration of arrhythmic risk in HCM.

1.2 Aims

The central aim of this thesis is to investigate electrophysiological mechanisms related to ionic remodelling and acute myocardial ischaemia in human HCM. The specific aims are to:

(i) Investigate the effects of acute myocardial ischaemia on human HCM-remodelled cardiomyocyte action potential (AP) biomarkers.

(ii) Investigate the electrophysiological mechanisms by which ischaemia interacts with other pathological features in human HCM tissue and ventricles (ionic remodelling and diffuse fibrosis) to modulate arrhythmic risk.

(iii) Investigate how regional/serum K^+ levels and heart rate affect T wave morphology and the diagnosis of ischaemia on stress ECGs in human HCM.

(iv) Investigate the effects of antianginal late Na^+ block (ranolazine) on arrhythmic risk in human HCM.

1.3 Outline

Chapter 2 introduces the cardiac electrophysiology concepts that are used throughout the thesis. Most importantly, this introduces the cardiomyocyte, the AP and derived biomarkers, alongside basic concepts in ventricular arrhythmogenesis.

Chapter 3 consists of a literature review of evidence related to ionic remodelling and myocardial ischaemia in HCM, underscoring the clinical significance of these disease factors and their possible role in lethal arrhythmic events.

Chapter 4 introduces the computational methods used in the multiscale modelling and simulation of cardiac electrophysiology, as applied in this thesis. This includes the modelling of ion channels from a subcellular scale and how these are combined to form a model of the human ventricular cardiomyocyte AP, up to the tissue and organ scales.

Chapter 5 presents the investigation of how the cellular response to acute myocardial ischaemia is affected

by the presence of ionic remodelling in HCM. The interactions identified between ionic remodelling and ischaemia are important in the following Chapters 6 and 7, as this cellular response underlies effects on arrhythmic risk and the ECG.

Chapter 6 presents the investigation of mechanisms underlying arrhythmias induced by acute myocardial ischaemia in HCM tissue and biventricular models, where ischaemic arrhythmic risk is significantly increased by the presence of ionic remodelling. The role of diffuse fibrosis in arrhythmogenesis during ischaemia is further investigated.

Chapter 7 presents the investigation of how ionic remodelling interacts with acute myocardial ischaemia on the stress ECG in HCM using biventricular models. Specifically, baseline repolarisation abnormalities on the ECG can be corrected, or "pseudonormalised", by myocardial ischaemia, giving rise to a transiently healthier-looking ECG despite the deleterious presence of ischaemia. The benign effects of exercise were further investigated (increased heart rate and serum K^+ accumulation), as disputed competing mechanisms underlying this phenomenon.

Chapter 8 presents the investigation of ranolazine, an anti-ischaemic drug with significant effects on HCM electrophysiology, as a potential pharmacologic antiarrhythmic therapy in HCM using tissue and biventricular models. ECG biomarkers associated with antiarrhythmic effects were further sought, to identify the HCM subgroups most likely to benefit.

Chapter 9 concludes with a summary of the thesis, a critical discussion of the investigations, the key conclusions made, and suggested future directions of research.

CHAPTER 2

Cardiac electrophysiology

This chapter introduces fundamental concepts in cardiac electrophysiology, from the scale of subcellular ionic currents up to the tissue and organ scales. The biomarkers used to quantify cardiac electrophysiology are further defined, both at the cellular level of electrical activity, and that measured from the whole heart by the ECG. The chapter finishes by summarising the electrophysiological effects arising from acute myocardial ischaemia and its role in ventricular arrhythmogenesis.

2.1 Gross cardiac anatomy, function and electrophysiology

The human heart (Fig. 2.1A) consists of four chambers bounded by a muscular wall, which consists of a layer lining the inside of the chambers (endocardium), a thick middle section (myocardium) and an outer layer (epicardium). The upper and lower chambers are called the atria and ventricles respectively, with a muscular septum dividing the left and right chambers. The heart pumps blood around the body.

Firstly, deoxygenated blood from the venae cavae fills the right atrium and is then pumped into the right ventricle (RV) by contraction of the right atrial myocardium, where flow is regulated by the tricuspid valve. Contraction of the RV myocardium pumps deoxygenated blood through the pulmonary artery, into the lungs. Oxygenated blood from the lungs fills the left atrium through the pulmonary veins and is then pumped into the left ventricle (LV) by contraction of the left atrial myocardium, where flow is

regulated by the mitral valve. Contraction of the thick LV myocardium pumps oxygenated blood through the aorta, which connects to a vast network of arteries that deliver oxygen to the entire body, including the heart itself through the coronary arteries. Deoxygenated blood returns to the right atrium through a network of veins, where the cardiac cycle repeats. Right and left atrial activity is synchronised, such that in the atrial cycle the contraction and relaxation phases are termed atrial systole and atrial diastole respectively. This is also true of the right and left ventricles, which simultaneously undergo ventricular systole, and ventricular diastole [50].

Myocardial contraction is mediated by the propagation of electrical signals. Macroscopically, the order in which regions of the myocardium contract is determined by pathways of the cardiac conduction system that stretch across much of the heart (Fig. 2.1B). Junctions couple the cardiac conduction system to the myocardium, where the electrical signal propagates through the myocardium to initiate contraction. The cardiac conduction system ensures that the myocardium across the ventricles is stimulated at approximately the same time, so that myocardial contraction is coordinated such that blood is pumped effectively [50].

During normal functioning, electrical stimulation of the heart begins at the sinoatrial node, which consists of pacemaker cells that can periodically generate electrical stimuli, even in the absence of the brain or nervous system. The signal then traverses the internodal path and Bachmann's bundle, diffusing into the atrial myocardium and causing atrial systole. Upon reaching the atrioventricular node, slow conduction within delays propagation, ensuring that the atria have fully contracted before ventricular contraction. The delayed signal propagates to the bundle of His contained in the interventricular septum, which splits into left and right branches. Purkinje fibres carry the signal to the ventricular endocardium via Purkinje-myocardium junctions, from which the impulse propagates through the ventricular myocardium to cause ventricular systole [50]. This normal periodic pattern of electrical activity originating from the sinoatrial node is termed sinus rhythm.

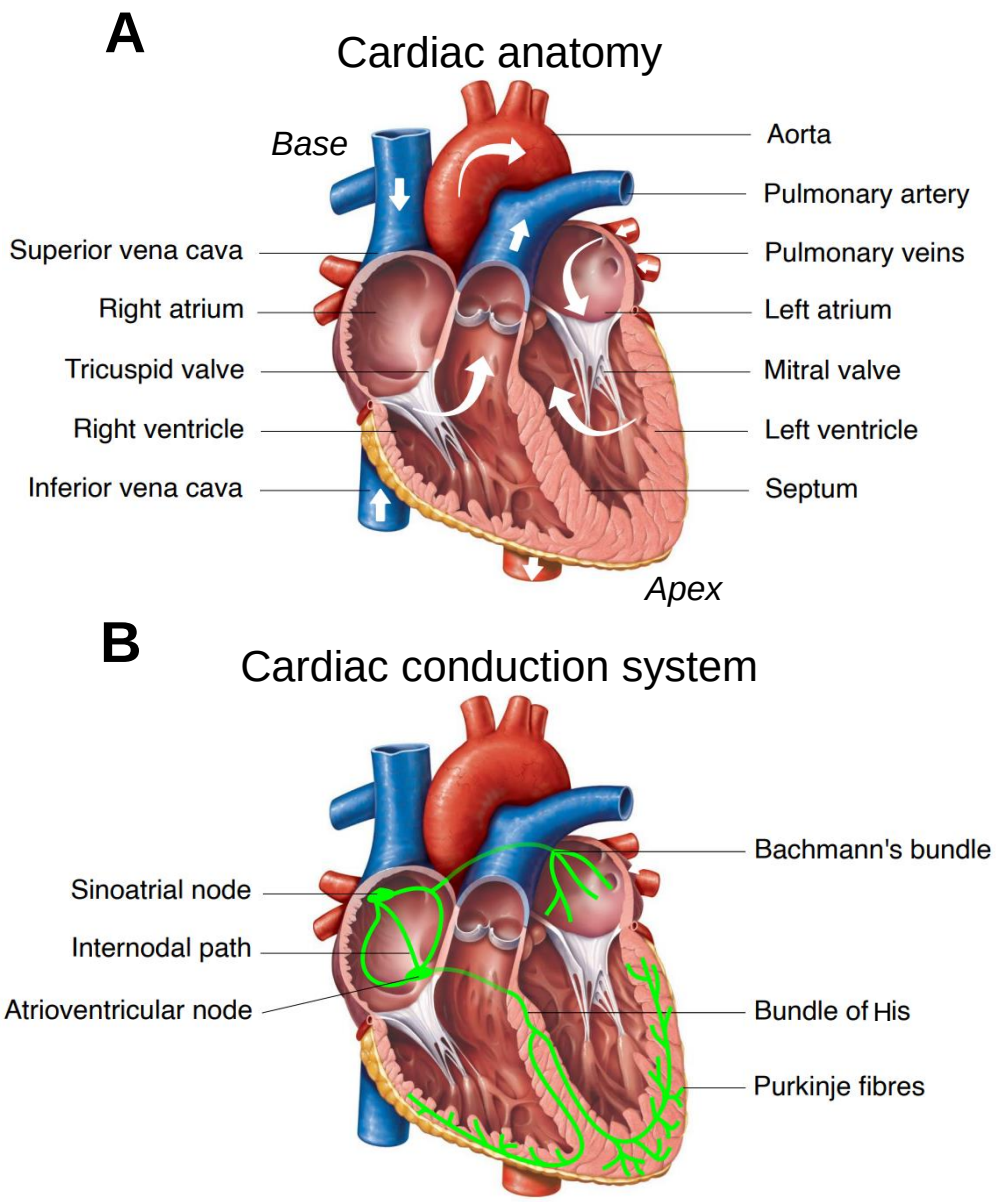


Figure 2.1: The human heart. (A) Gross cardiac anatomy and function, where white arrows denote the direction of blood movement. (B) The cardiac conduction system, where conduction pathways are denoted in green [50]. Adapted under non-commercial license [58].

2.2 Fine cardiac structure and electrophysiology

2.2.1 Cardiomyocytes

The myocardium consists of many cardiac muscle cells called cardiomyocytes, which are ellipsoidally cylindrical in shape, being around 100 μm in length and 20 μm in diameter [86, 316]. Cardiomyocytes synchronously contract and relax in response to electrical stimulation, to produce systole and diastole.

Outside of the cardiomyocyte, a matrix of collagen provides the structural rigidity to enable force transmission during myocardial contraction [136]. There are also fibroblasts, immune cells and vascular cells, all of which are critical for growth, repair and immune response of the myocardium [104].

2.2.2 Ion channels, pumps and exchangers

Cardiomyocytes are surrounded by an electrically insulating cell membrane, which separates the cardiomyocyte interior (intracellular space) from the exterior (extracellular space). The repeated changes in cardiomyocyte contractile state are caused by the transfer of ions between intracellular and extracellular space, as well as between neighbouring cardiomyocytes. The main ions involved are sodium (Na^+), calcium (Ca^{2+}) and potassium (K^+) ions. They typically have intracellular and extracellular concentrations of around $[Na^+]_i = 15$ mM and $[Na^+]_e = 140$ mM, $[K^+]_i = 150$ mM and $[K^+]_e = 5$ mM, and $[Ca^{2+}]_i = 15$ mM and $[Ca^{2+}]_e = 10^{-4}$ mM, respectively [236].

At the cardiomyocyte membrane, ions can only move through ion channels, pumps and exchangers. Ion channels form a pore, through which an electrical current of ions can flow passively along the electrochemical gradient. The permeability of ion channels is often gated, such that the activity of each channel varies in time within each contraction-relaxation cycle. The majority of ion channels are gated by voltage, but some channels are gated by chemical messengers (ligand-dependent gating) or tension (mechanosensitive gating). Ion channels are typically ion-specific, most of which correspond to either Na^+, Ca^{2+} or K^+ ions [118]. Ion pumps, unlike ion channels, transport ions in the opposite direction to electrochemical gradients by consuming energy. Ion pumps use a minimum of two gates timed such that they do not simultaneously open, shielding ions from the electrochemical gradient in a biological

airlock. Finally, ion exchangers act upon multiple ion types, exchanging the inward transport of one ion type for the outward transport of another [107].

2.2.3 Action potentials

The potential difference between the interior and exterior surfaces of the cardiomyocyte, called the membrane potential (V_m), is a useful summary of cardiomyocyte electrical activity. When a cardiomyocyte is electrically stimulated, it undergoes a characteristic excursion in membrane potential with time (Fig. 2.2A), called an action potential (AP). Typical cardiomyocyte AP morphology can be described as having phases [60]:

- **Phase 4: Resting.** The cardiomyocyte is in a steady state, held at a resting membrane potential (RMP) of around -90 mV by the Na^+/K^+ pump current (I_{NaK}) and inward rectifier current (I_{K1}).
- **Phase 0: Depolarisation.** Upon electrical stimulation, a rapid influx of Na^+ depolarises the cardiomyocyte to a peak membrane potential through the activation of the fast Na^+ current (I_{Na}).
- **Phase 1: Notch.** Rapid depolarisation ceases due to the inactivation of I_{Na}. There is slight repolarisation due to the extrusion of K^+ through the transient outward current (I_{to}), alongside the exchange of Na^+ and Ca^{2+} through the Na^+/Ca^{2+} exchange current (I_{NCX}).
- **Phase 2: Plateau.** There is an approximate equilibrium between inward Ca^{2+} through the L-type Ca^{2+} current (I_{CaL}) and outward K^+ through the slow delayed rectifying potassium current (I_{Ks}), which is further affected by I_{NCX}.
- **Phase 3: Repolarisation.** Inactivation of I_{CaL}, alongside extrusion of K^+ through the inward rectifier current (I_{K1}) and rapidly delayed rectifier current (I_{Kr}), leads to repolarisation and a return to the resting phase. Although a small contribution in healthy cells, repolarisation is also affected by a sustained influx of Na^+ ions through the late component of the Na^+ current (I_{NaL}). Under conditions of adenosine triphosphate (ATP) depletion, the opening of ATP-sensitive K^+ current (I_{KATP}) may also contribute to this repolarisation phase.

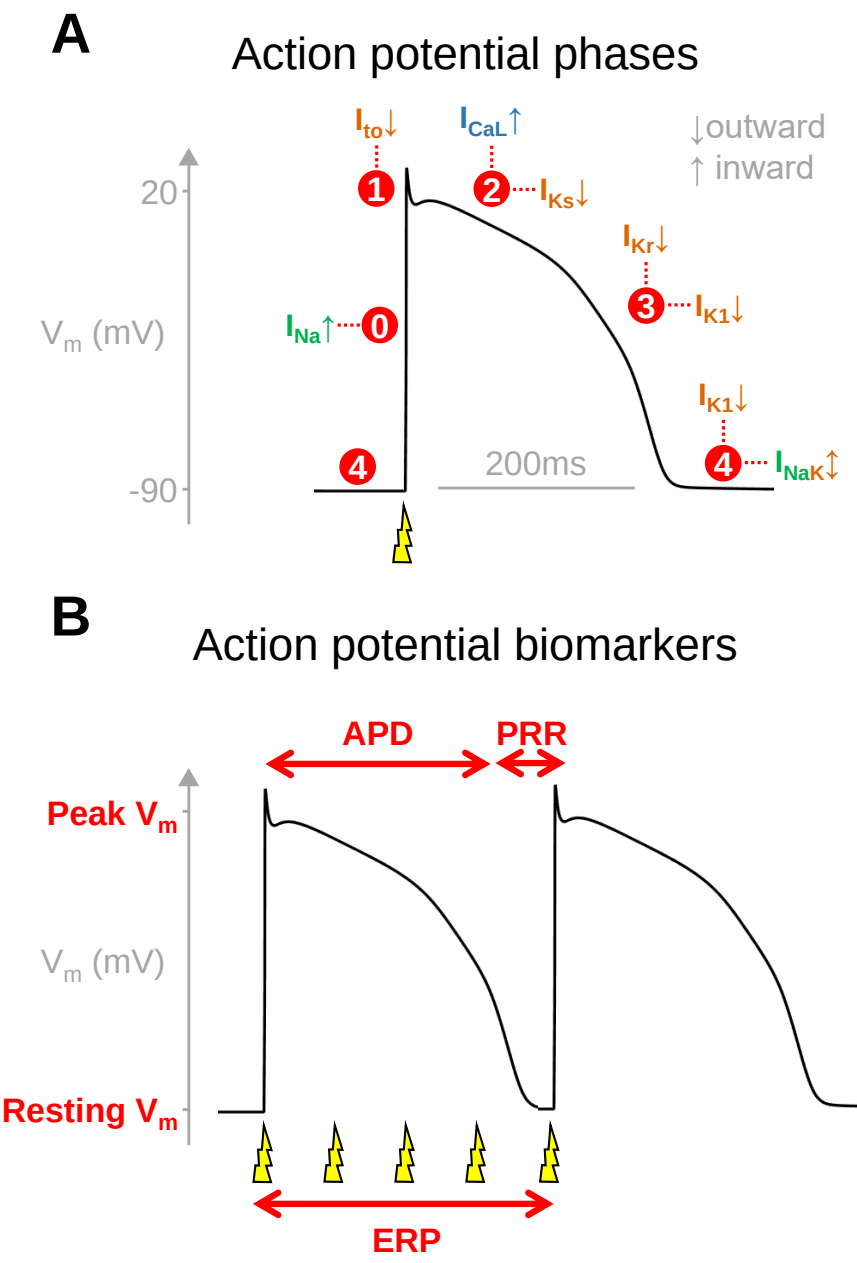


Figure 2.2: The action potential. (A) Representative AP morphology of a human ventricular cardiomyocyte, where phases 0-4 are denoted alongside the key ionic currents and pumps associated with each phase. (B) AP biomarkers including the action potential duration (APD), effective refractory period (ERP), post-repolarisation refractoriness (PRR), peak V_m and resting membrane potential (RMP). Yellow symbols denote external electrical stimulation of the cardiomyocyte, where stimulation can only elicit a further AP once the ERP has expired.

Measurements derived from the AP and AP propagation (Fig. 2.2B) are useful for explaining the mechanisms underlying cardiac arrhythmia. Features of the AP affect electrical conduction (or can even block conduction) at the organ scale. In this thesis, the effective refractory period (ERP), action potential duration (APD) and conduction velocity (CV) are the most frequently used biomarkers.

In the context of ventricular arrhythmias, the ERP is among the most important biomarkers. Not only is the ERP a critical factor for cardiac arrhythmias in animal experimental setups and computational modelling [361], but invasive clinical measurements of ERP can be used to predict life-threatening arrhythmias in some cardiac patients [312]. The ERP is defined as the time following AP initiation for which further stimulation (at a given stimulus amplitude) is unable to elicit a further impulse that propagates through tissue [144]. At the scale of single cells, this is loosely adjacent to the time following AP initiation for which a further AP cannot be initiated.

Under normal conditions, the ERP is approximately the same as the APD [345], where the APD is defined as the time taken following AP initiation for cellular repolarisation. The APD is typically measured at some threshold of repolarisation, almost always 90%, where APD90 corresponds to the time taken to reach 90% of the repolarisation from the peak to the RMP. In this thesis, APD was used synonymously with APD90, unless otherwise indicated as APDXX where the threshold of repolarisation is XX%. The APD is primarily affected by the currents I_{Kr}, I_{K1} and I_{NaL} which are involved in phase 3. Experimental works frequently use measures of APD as correlates of arrhythmia inducibility [386], as a surrogate for ERP. This is due to the relative ease of measuring the APD, as compared to the premature stimulus protocols required to measure ERP. Clinically, the APD is also a more accessible measure because noninvasive surrogates of the APD exist (see later the QT interval in section 2.3), whereas the ERP requires an invasive electrophysiological study. However, under ischaemic conditions, the ERP and APD may be affected in different ways [345], such that measures like post-repolarisation refractoriness (PRR) (calculated as ERP − APD) are relevant.

The CV (velocity of AP wavefront propagation in myocardial tissue) is also an important biomarker in the context of arrhythmias. Although also a tissue-level measurement, CV is significantly affected by I_{Na} availability, and has AP correlates such as the AP upstroke velocity (the rate of change of V_m with time

during phase 0, $\frac{dV_m}{dt}$) [269]. Of note, the CV in ventricular myocardium is anisotropic as a consequence of the fibre structure (see later Fig. 2.3A).

It is further notable that AP biomarkers vary in time as a consequence of changing conditions in the heart, including variation in intracellular/extracellular ion concentrations, beta-adrenergic stimulation and pacing rate. Pacing rate is one such condition that can be non-invasively measured and has important electrophysiological implications. The CV, APD and ERP typically decrease as pacing rate is increased, in part due to rate dependence of ion channel gating (see later Fig. 2.3B) [93, 240].

2.2.4 Ca^{2+} subsystem

There are further subcellular processes that control the movement of Ca^{2+} between the cytoplasm and sarcoplasmic reticulum, which is a large reserve of Ca^{2+} separate from the cytoplasm inside the cardiomyocyte. The concentration of Ca^{2+} regulates the contraction of the cell, which is termed excitation-contraction coupling. Entry of Ca^{2+} from the extracellular space stimulates the release of Ca^{2+} from the sarcoplasmic reticulum, which is termed calcium-induced calcium release [94]. Ca^{2+} ions then bind to proteins on myofilaments, stimulating myofilaments to slide over one another. The net effect of this movement of myofilaments is contraction of the cardiomyocyte. Contraction is ceased when Ca^{2+} is extruded from the cell, as through the Ca^{2+} pump current (I_{pCa}) and I_{NCX}, or readmitted to the sarcoplasmic reticulum through the sarcoendoplasmic reticulum Ca^{2+} ATPase (SERCA) pump.

The cytoplasmic Ca^{2+} concentration (the time course of which, over a contraction-relaxation cycle, is termed the Ca^{2+} transient) is a property of the cardiomyocyte that is particularly useful when considering mechanisms related to contraction or Ca^{2+}-induced cellular triggers. As with the AP, Ca^{2+} transient biomarkers can also be defined, including the time to peak Ca^{2+} concentration and the time for Ca^{2+} concentration to decay.

2.2.5 Cardiomyocyte-cardiomyocyte coupling

When the myocardium is stimulated by the cardiac conduction system at a Purkinje-myocardium junction, the electrical stimulus propagates from that point throughout the myocardium, because each ventricular cardiomyocyte is connected to around 10 other cardiomyocytes in a side-to-side, end-to-end,

or somewhere-in-between configuration [316]. Gap junctions form a bridge between cardiomyocytes of a few nanometers in length, across which ions can diffuse as electrochemical gradients are induced by a cardiomyocyte undergoing an AP [310, 330]. If there is sufficient diffusion of ions, partial depolarisation of the neighbouring cardiomyocyte will induce an AP in that cardiomyocyte too, such that the AP propagates.

Due to the cylindrical shape of cardiomyocytes, alongside the subcellular distribution of gap junctions, the myocardium is structurally and electrically anisotropic, such that the speed of AP propagation is direction-dependent [84]. The myocardium is sometimes described as having a fibre-like structure, where a longitudinal axis is defined along the length of the cardiomyocyte (or average of a group of cardiomyocytes), with perpendicular transmural and transverse axes (Fig. 2.3A), where conduction is fastest along the longitudinal axis [348].

2.2.6 Myocardial heterogeneities

In addition to being anisotropic, the myocardium is spatially heterogeneous in structure and electrophysiology. For example, average fibre orientation changes significantly across the ventricular wall, varying over a 120° range from epicardium to endocardium as measured in dogs (Fig. 2.3A) [344]. The APD also varies across the ventricular wall, with cardiomyocytes closer to the endocardium having the longest APD, and those closer to the epicardium having the shortest APD (Fig. 2.3B), as measured in human LV tissue samples [114]. Noninvasive measurements in humans have also shown that APDs in the apical myocardium may be 40 ms shorter than those in the basal myocardium [301], and that APDs in the LV myocardium may be 10–30 ms longer than that in the RV myocardium [33, 301]. These electrophysiological heterogeneities are explained by regional differences in ion channel expression. For example, expression of I_{to} and I_{Ks} have been measured to vary between cardiomyocytes extracted from the basal and apical myocardium in dogs [347].

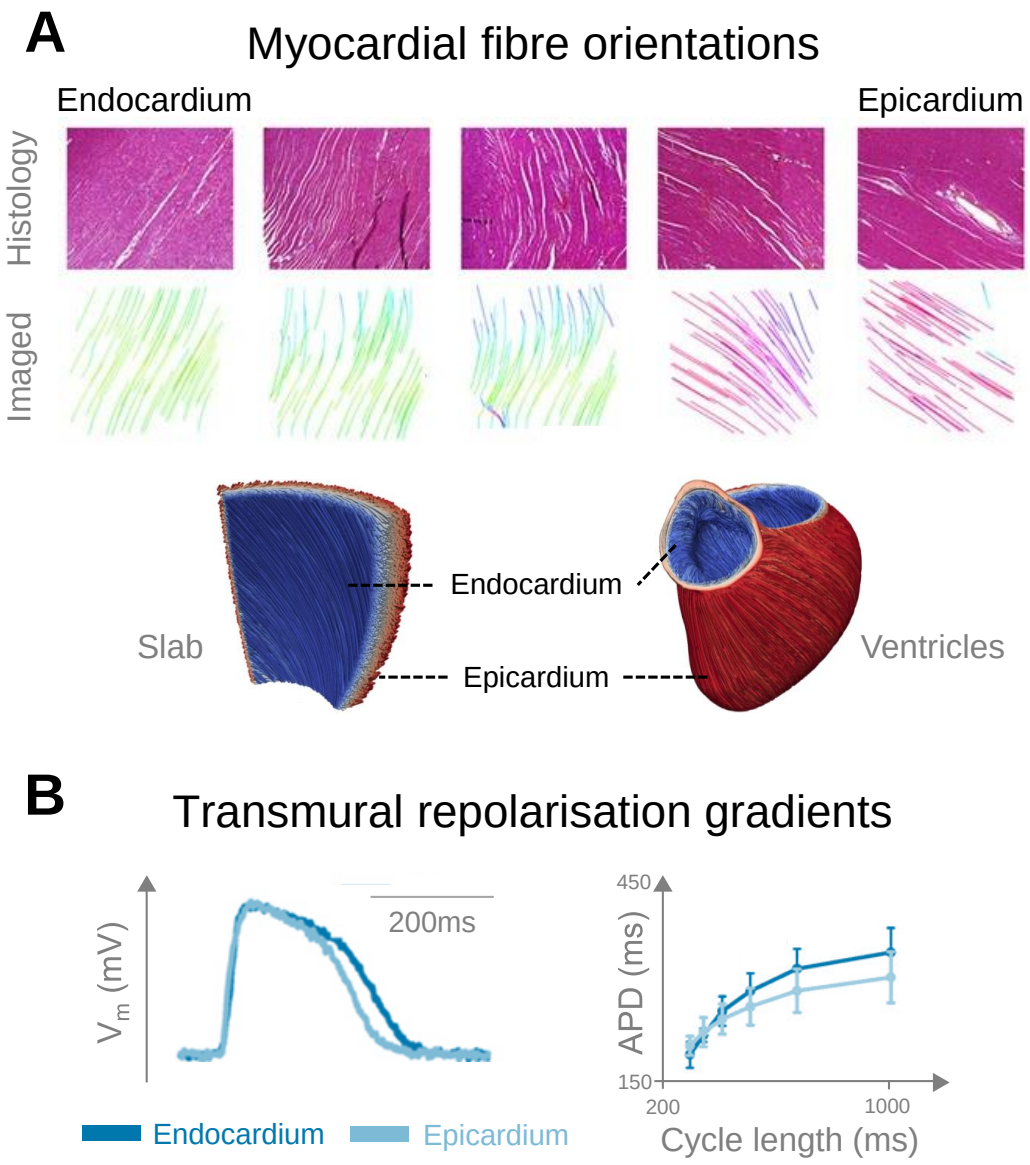


Figure 2.3: (A) Myocardial fibre orientations across the ventricular wall, as measured in sheep using histology and imaging. This is further illustrated at the tissue slab and organ scale. (B) APDs across the ventricular wall, as measured in sheep. Adapted under Creative Commons license [4, 227, 277].

2.3 Electrocardiograms

2.3.1 Recording an ECG

The ECG is a noninvasive measure of electrical activity in the heart, recorded via electrodes which are placed at various positions on the surface of the subject (Fig. 2.4A). Standard clinical practice is to measure a 12-lead ECG (Fig. 2.4B), derived from signals recorded at 10 electrodes. There are 4 electrodes called limb electrodes, placed at the left arm (LA), right arm (RA), left leg (LL) and right leg (RL), where the RL electrode is only used to control noise, rather than in the computation of leads. The 6 remaining electrodes are called precordial electrodes V1–V6, placed on the chest of the subject.

There are 3 bipolar limb leads (I, II and III), which are computed from the LA, RA and LL electrodes as:

(i) $\mathrm{I} = \mathrm{LA} - \mathrm{RA}$

(ii) $\mathrm{II} = \mathrm{LL} - \mathrm{RA}$

(iii) $\mathrm{III} = \mathrm{LL} - \mathrm{LA}$

There are 3 augmented unipolar limb leads measured relative to the Wilson central terminal potential, calculated as $\mathrm{V_w} = \frac{1}{3}(\mathrm{RA} + \mathrm{LA} + \mathrm{LL})$, which are computed from the LA, RA and LL electrodes as:

(iv) $\mathrm{aVR} = \frac{3}{2}(\mathrm{RA} - \mathrm{V_w})$

(v) $\mathrm{aVL} = \frac{3}{2}(\mathrm{LA} - \mathrm{V_w})$

(vi) $\mathrm{aVF} = \frac{3}{2}\,(\mathrm{LL} - \mathrm{V_w})$

Finally, there are 6 unipolar precordial leads V1–V6 measured relative to $\mathrm{V_w}$ which are computed from electrodes V1–V6 by subtracting $\mathrm{V_w}$ from each respective electrode.

During a heartbeat, each ECG lead measures a characteristic excursion in electrical potential, which consists of a series of waves corresponding to stages of the cardiac cycle (Fig. 2.4C). The first wave is the P wave, which is a small deflection (< 0.25 mV) recorded as the atria depolarise. Subsequent repolarisation of the atria is usually not visible, as it is low amplitude and masked by the other waveforms.

The next wave is the QRS complex, which is typically the largest deflection ($>$ 0.5–1.0 mV), recorded as the ventricles depolarise. Due to the shape of the ventricles and cardiac conduction system, the predominant direction of the depolarising wavefront changes relative to the electrodes at different stages of ventricular depolarisation. The Q wave is recorded during depolarisation of the septum, which occurs from the LV side to the side of the RV. The R wave is recorded during the bulk of ventricular depolarisation, where wavefronts travel from the base to the apex of the ventricles, and into the thick LV from endocardium to epicardium. The S wave is recorded at the end of ventricular depolarisation, where wavefronts travel towards the base of the ventricles to stimulate the remaining myocardium. The relative contributions of the Q, R and S waves to the QRS complex are lead-dependent, because different leads are more or less aligned with the base-apex and LV-RV directions. Usually, the final wave is the T wave, a deflection of intermediate amplitude ($<$ 0.5–1.0 mV), recorded as the ventricles repolarise. Under healthy conditions, the T wave is typically an upright deflection except in leads aVR, III and V1 [321]. Inverted T waves are usually otherwise pathological, indicating a non-specific cardiac disease. Sometimes, a distinct deflection after the T wave is measurable, called the U wave, but its cause is unknown [168].

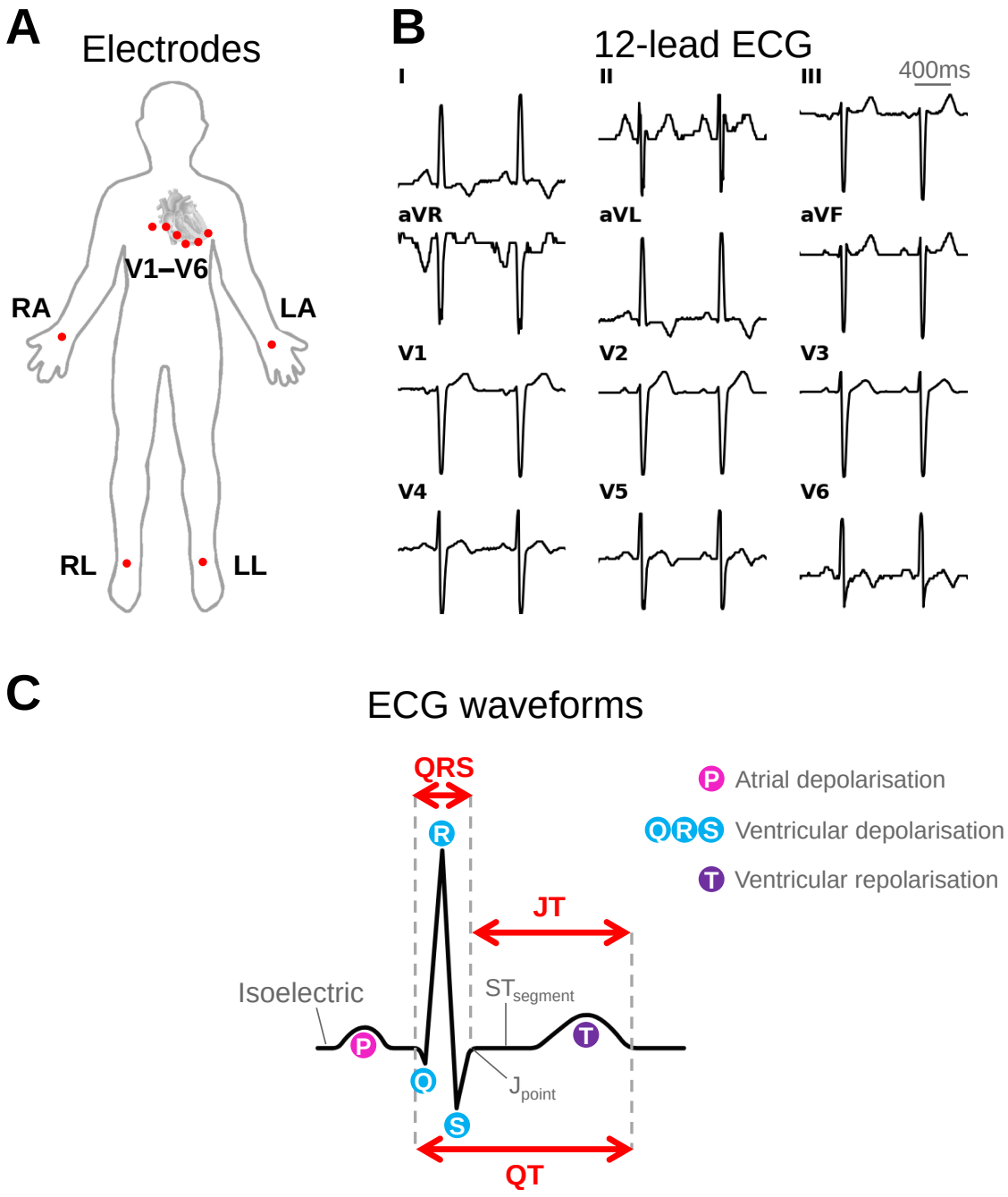


Figure 2.4: Basics of the ECG. (A) Positions of the 10 electrodes used to record a clinical 12-lead ECG. (B) Example clinical 12-lead ECG. (C) ECG waveforms nomenclature. Key waveforms are the P wave (atrial depolarisation), QRS complex (ventricular depolarisation) and the T wave (ventricular repolarisation). Frequently used ECG biomarkers including the QRS duration, JT interval and QT interval are denoted. Adapted under non-commercial license [57].

2.3.2 Biomarkers of the ECG

Measurements derived from the ECG (Fig. 2.4C) are useful for identifying cardiac disease, including abnormalities of ventricular depolarisation (QRS complex) and repolarisation (T wave). In this thesis, the QT interval, JT interval, QRS duration, ST segment potential and RR interval are the most frequently used biomarkers. The RR interval (time elapsed between consecutive R peaks) is used as a measurement of the pacing cycle length.

The QT interval is defined as the time elapsed from the onset of the Q wave until the end of the T wave (Fig. 2.4C). Similarly, the JT interval is defined as the time elapsed from the J point until the end of the T wave, where the J point is the point at which the QRS complex meets the ST segment (corresponding to the end of depolarisation and beginning of repolarisation). Therefore, whereas the QT interval comprises the time for both ventricular depolarisation and repolarisation, the JT interval comprises only the time between the end of ventricular depolarisation and the end of ventricular repolarisation.

Because both the QT and JT intervals include the time taken for ventricular repolarisation (essentially the APD), and the APD is strongly dependent on pacing rate as shown previously in Fig. 2.3B, they are usually rate-corrected to the QT_c and JT_c intervals, respectively [140]. This ensures that the QT or JT interval measured contains a useful metric of ventricular repolarisation, rather than being susceptible to fluctuations secondary to pacing rate variability. Various rate-correction formulae exist, each with relative strengths and weaknesses depending on the clinical purpose and patient group being studied [365]. Unlike the QT and JT intervals, the QRS duration (Q wave onset to S wave end) is much less affected by pacing rate. This is because the time for ventricular depolarisation is primarily determined by the cardiac conduction system, which is independent of myocardial CV rate dependence.

In clinical practice, it is conventional to calculate the QT_c interval from lead II, or lead V5 if it is infeasible in lead II [140]. However, the QT_c interval may vary depending on which lead of the 12-lead ECG is used. This variation among leads, which may reflect electrical heterogeneity in the ventricles, is sometimes quantified as the QT_c dispersion, calculated as the difference between the maximum and minimum QT_c intervals among the 12 leads. JT_c dispersion is similarly calculated as the difference between the maximum and minimum JT_c intervals among the 12 leads. Although such measures of

dispersion may be associated with cardiac pathology, there are significant methodological difficulties in their measurement. Where the ECG is abnormal, such as in HCM, the end of the T wave may not be easily identifiable, such that many leads may be excluded from the dispersion calculation. This, amongst other limitations, leads to $> 30\%$ relative measurement error [317].

The ST segment comprises the region between the end of the QRS complex and beginning of the T wave (corresponding to the plateau phase of the AP). Elevation or depression of the ST segment from the isoelectric line, measured at the J point, is a further useful biomarker in the context of myocardial ischaemia.

Typical ranges of these biomarkers are 350–460 ms for the QT_c interval [306], 240–380 ms for the JT_c interval [242], 70–100 ms for the QRS duration [303], and ≤ 50 ms for QT_c dispersion [317]. The ST segment potential is typically ≤ 0.1 mV from the isoelectric line, but thresholds for abnormality are dependent on the lead and patient demographic (see later section 2.4.4) [373].

2.4 Electrophysiological effects of acute myocardial ischaemia

2.4.1 Acute myocardial ischaemia

Acute myocardial ischaemia occurs when the blood supplied to the myocardium is suddenly insufficient to meet its homeostatic demands. The effects of ischaemia on the myocardium are considered reversible initially (stage 1, in the first 30 minutes), but at later times irreversible tissue damage occurs (stage 2) [42]. During the reversible stage, two stages of ventricular arrhythmias are reported experimentally at 2–10 minutes (stage 1a) and 12–30 minutes (stage 1b) of myocardial ischaemia [162, 339]. Half of ischaemic SCDs in the general population are estimated to occur during stage 1 [85]. In HCM, lethal arrhythmias induced by ischaemia are reported to occur suddenly and without symptomatic forewarning, first appearing as a loss of consciousness and sometimes during increased myocardial workload [113, 122, 307]. As these reports are consistent with stage 1a arrhythmias, this thesis focuses on the effects of myocardial ischaemia in the early reversible stage.

2.4.2 Ischaemic action potentials

In the myocardium affected by ischaemia, there are electrophysiological changes including effects on AP morphology, refractoriness and electrical conduction (Fig. 2.5A). Ischaemic changes in AP biomarkers are characterised by decreased CV [247, 348], decreased RMP negativity [150, 247], and decreased APD alongside prolonged ERP, giving rise to PRR [70, 345]. AP upstroke slowing may also slow the CV [174].

The main causes of these acute electrophysiological changes are considered to be combined hyperkalaemia (increased K^+ concentration in extracellular space), hypoxia (ATP depletion) and acidosis (decreased pH) [22, 174, 247]. Increases in extracellular K^+ are ubiquitous among experimental studies of acute myocardial ischaemia [43]. In the in situ pig, which is considered to be a good animal model due to pigs' many similarities with humans (including vasculature), extracellular K^+ concentrations are reported to peak at 7–9 mM (from a baseline of 5 mM) in affected myocardium during 3–10 minutes of initial left anterior descending (LAD) coronary artery occlusion [102]. Similar timescales of K^+ accumulation are reported in other pig studies [133, 339]. ATP depletion is similarly common among experimental studies, with 20–40% decreases in ATP concentrations reported at up to 10 minutes of myocardial ischaemia [21, 209, 302, 375, 392]. Acidosis is also reported, with pH reaching 6.4 (from baseline of 7.4) at 10 minutes of myocardial ischaemia in pigs [102, 133].

It is notable that, in evaluating the timescales and peak severities of ischaemic changes in experimental setups, the exact findings are dependent on the species (often vascular and electrophysiological differences exist), the ischaemia induction protocol (partial vs. total occlusion and which artery was affected), the thickness of tissue preparations or affected myocardial region, and even the occurrence or number of repeated occlusions [22, 43, 102]. This is in combination with the in-study intersubject heterogeneity in the response to ischaemia and the time-dependent nature of ischaemia progression. This is further exemplified by variable reports in timing of stage 1a arrhythmias even in the same species (e.g. 2–10 minutes [339] vs. 10–15 minutes [71]). Therefore, a universal time course of ischaemic electrophysiological changes is not well defined. In the context of SCD, it is more relevant to note that the arrhythmias recorded earliest during ischaemic onset occur with alongside changes like hyperkalaemia, acidosis, RMP changes and conduction delay, well before cell-to-cell decoupling [339].

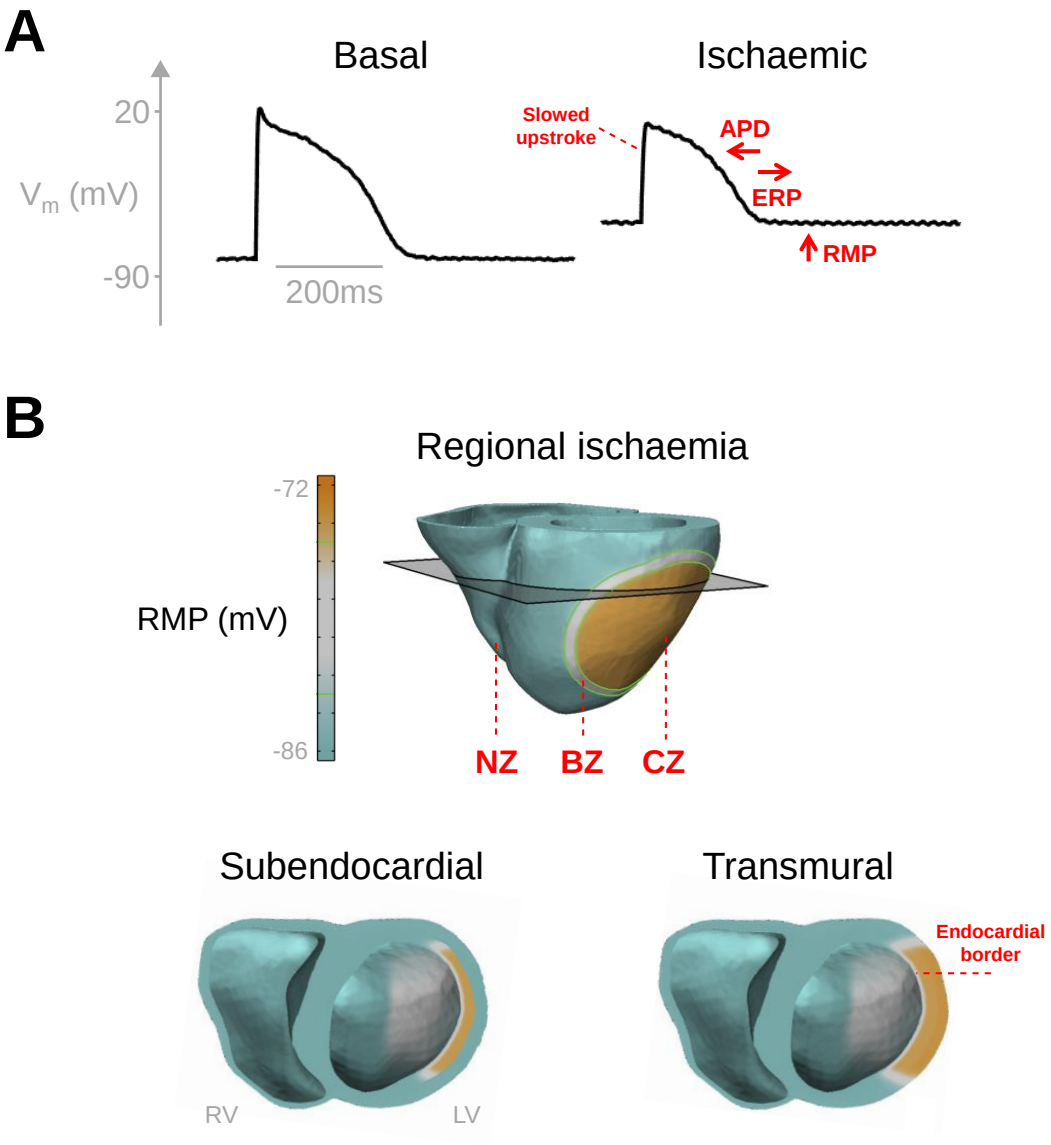


Figure 2.5: (A) Effects of ischaemia on the AP. Traces correspond to measurements made in RV cardiomyocytes from undiseased human donor hearts, where ischaemia consisted of hyperkalaemia, hypoxia and acidosis. Experimental data provided by Prof. András Varró, University of Szeged. (B) Schematic of regional acute myocardial ischaemia in the human ventricles, illustrating the normal zone (NZ), border zone (BZ), core zone (CZ) and endocardial perfusion layer alongside variable ischaemic transmurality. Adapted under Creative Commons license [92].

Effects arising from increased extracellular K^+ are in part due to the effects of K^+ on RMP [334], where the RMP becomes less negative because of the reduced K^+ concentration gradient across the cell membrane, such that less work per unit charge is required for the transmembrane K^+ movement. Due to the voltage-gating of I_{Na}, the AP upstroke is slowed as there is limited I_{Na} availability with reduced RMP negativity, which contributes to slowed CV [334]. Also, extracellular K^+ elevation decreases the cellular APD, by increasing I_{K1} and I_{Kr}.

Hypoxia is also responsible for APD shortening, due to activity of I_{KATP} following ATP depletion. Activity of I_{KATP} early in the onset of ischaemia is evidenced by findings that I_{KATP} blockade with glibenclamide can attenuate K^+ accumulation, APD50 shortening and ischaemic ECG abnormalities at up to 10 minutes of myocardial ischaemia [146, 182, 243, 369, 379, 389]. Hypoxia may also contribute to RMP elevation and subsequent CV slowing by starving I_{NaK} of the ATP it needs to function [247].

Acidosis is reported to impair I_{Na} and I_{CaL} [141, 391], which leads to further impairment of CV in ischaemic myocardium [334].

2.4.3 Regional acute myocardial ischaemia

Acute myocardial ischaemia typically affects only a region of the ventricular myocardium, confined to the perfusion bed of an affected coronary artery (or branch thereof). Therefore, ischaemic APs develop in the affected myocardium, called the core zone (CZ), yet APs remain unaffected in myocardium remote from the ischaemia, called the normal zone (NZ) (Fig. 2.5B). Experimental measurements in regionally ischaemic dog and pig ventricles also describe the existence of a transitional region between the normal zone (NZ) and core zone (CZ), where APs gradually change from normal to ischaemic [128, 149], due to gradients in local blood flow and metabolites. This transitional region of around 1 cm is called the border zone (BZ). At the endocardium, APs are also less affected by ischaemia, because blood from within the ventricular cavity perfuses an endocardial border of around 0.1 cm [380]. A further important consideration is that the transmurality of the ischaemic myocardium varies, in some cases only affecting the subendocardium (subendocardial ischaemia), to in other cases affecting the full width of the ventricular wall (transmural ischaemia), as illustrated in Fig. 2.5B.

2.4.4 Effects on the ECG

With acute myocardial ischaemia reducing the amplitude and plateau phase of the AP, shortening the APD and elevating RMP (section 2.4.2), the ECG manifestations of these electrophysiological changes are frequently used to diagnose ischaemia [373]. From section 2.3, the parts of the ECG corresponding to these AP phases would be the ST segment, T wave and isoelectric line (or TQ segment). Moreover, due to its regional effects, it might be expected to affect only a subset of leads.

Indeed clinically, it is the ST segment that is the primary ECG biomarker used to diagnose myocardial ischaemia. Thresholds of ST segment deflections are defined based on the given lead and patient demographic to maximise diagnostic accuracy [164, 373]. Of note, because the TQ segment is always zeroed in clinical ECGs, any depression/elevation of the TQ segment is transferred to depression/elevation of the ST segment [68]. This is in contrast to experimental setups which can discern pure ST segment changes from pure TQ segment changes, which may better reflect the specific AP-related mechanisms [172, 339]. Therefore, the clinical diagnosis of ischaemia based on the ST segment contains RMP-related shifting of the isoelectric line in addition to true changes to the ST segment. Finally, the T wave associates of myocardial ischaemia are inversion of T waves or the development of hyperacute T waves, reflecting ischaemic changes in repolarisation gradients [164].

Although the earliest manifestations of ischaemia can appear in the T waves and ST segment, and the ECG is widely used, the diagnostic performance is suboptimal. A systematic review estimates that the standard 12-lead ECG has a 43% sensitivity and 94% specificity for the identification of ischaemia or infarct in acute coronary syndrome [188]. Although relatively specific in this estimate, ST segment abnormalities can also be a manifestation of benign early repolarisation or other pathologies like pericarditis [68]. In the context of HCM, diagnosis may be particularly challenging because hypertrophy can also manifest as such ST-T repolarisation abnormalities [222]. Sometimes, a stress ECG is performed to detect inducible ischaemia, where the ECG is recorded during exercise or pharmacologically-induced stress.

2.5 Ventricular arrhythmias

A ventricular arrhythmia is an abnormal heart rhythm that originates from the ventricles.

2.5.1 Cellular arrhythmias

Ventricular arrhythmias may emerge in part due to AP abnormalities described at the single cell scale. These include delayed afterdepolarisations and early afterdepolarisations, as illustrated in Fig. 2.6A. A delayed afterdepolarisation is thought to result from spontaneous diastolic Ca^{2+} release from the sarcoplasmic reticulum due to increased load, causing partial depolarisation via I_{NCX} after AP repolarisation has completed. Conversely, an early afterdepolarisation is thought to result from reactivation of I_{CaL} during phases 2–3 of the AP, leading to abnormal transient depolarisation during the repolarisation phase [325]. If enough cardiomyocytes in a region undergo an afterdepolarisation, and to a sufficient threshold of depolarisation, this can trigger an ectopic AP that propagates and causes a premature heart beat.

2.5.2 Types of ventricular arrhythmias

Ventricular arrhythmias are often diagnosed on the ECG. There are various types of ventricular arrhythmias, including (Fig. 2.6B):

(i) Premature ventricular complex (PVC), an abnormal beat occurring before the next sinus rhythm beat is expected, often with an abnormal QRS complex.

(ii) PVC couplets, consisting of 2 consecutive PVCs without a normal heart beat between.

(iii) Ventricular tachycardia (VT), consisting of ≥ 3 consecutive beats at a rate of > 100 bpm.

(iv) Ventricular fibrillation (VF), consisting of chaotic irregular deflections at a rate of 150–500 bpm without identifiable QRS complexes or T waves.

VT and VF are considered clinically significant arrhythmias, particularly as VT can degenerate into VF, and VF causes SCD [267]. Atrial arrhythmias like atrial fibrillation (AF) also exist, but filtering properties of the atrioventricular node prevent AF spreading to the ventricles.

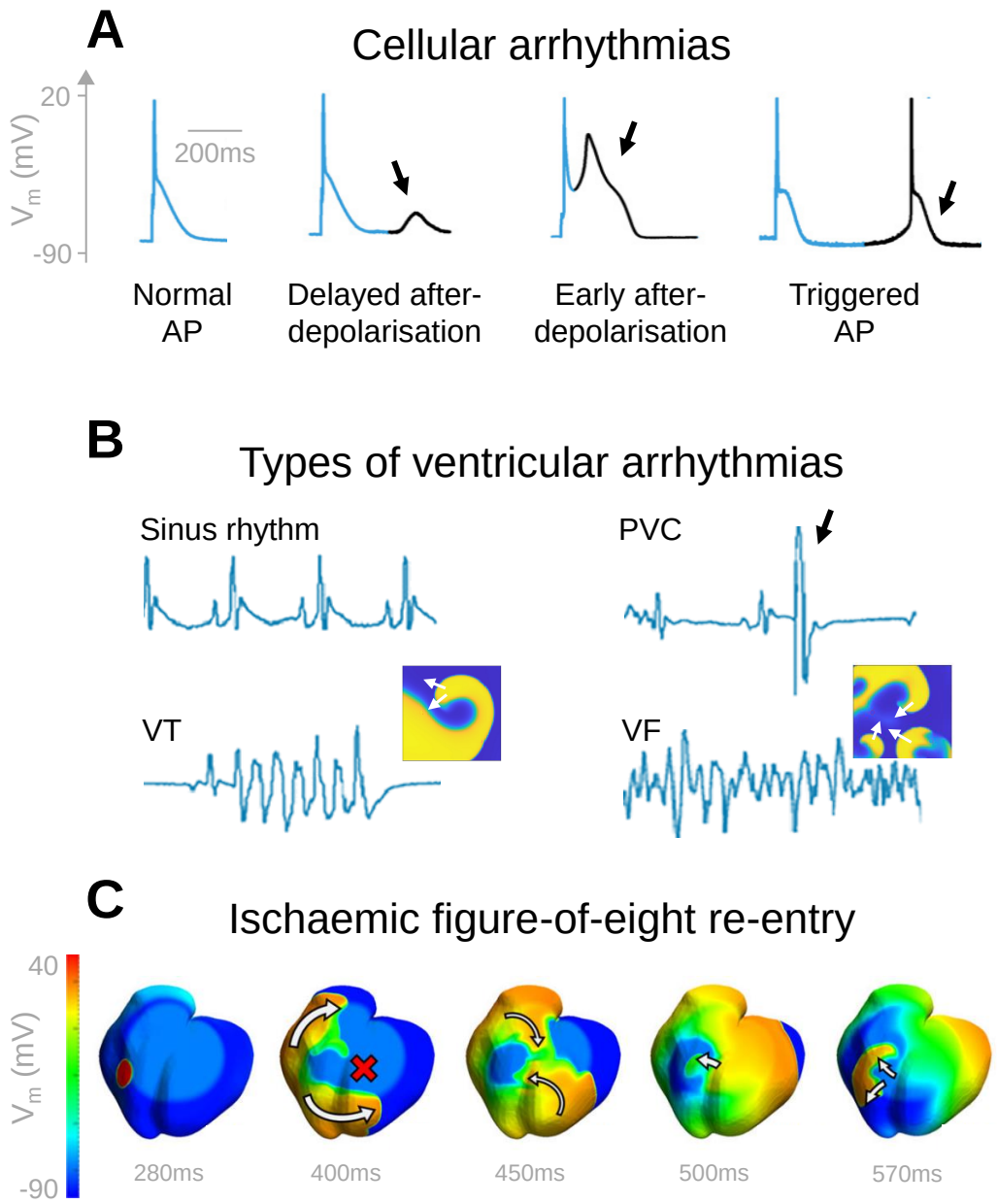


Figure 2.6: (A) Examples of delayed and early afterdepolarisations, which can trigger premature APs. (B) Example ECGs of ventricular arrhythmias in rats, including a premature ventricular complex (PVC), and episodes of ventricular tachycardia (VT) and ventricular fibrillation (VF). In-tissue wavefronts associated with VT and VF are also illustrated. (C) Schematic of the figure-of-eight re-entry mechanism that occurs during myocardial ischaemia. Adapted under Creative Commons license [124, 229, 325, 405].

2.5.3 Mechanisms of ventricular arrhythmias

The induction of a clinically significant arrhythmia is thought to require the combination of an arrhythmic substrate (a proarrhythmic existing tissue condition) and a trigger (typically a premature, ectopic electrical stimulus) [73]. In this context, the cellular afterdepolarisations shown in Fig. 2.6A are thought to act as a trigger for VT and VF [267]. Yet, PVCs are common, occurring around every 10 minutes in HCM, in contrast to VT and VF which are disproportionally rare [3]. In the general population, PVCs are even considered to be benign [210]. Therefore, there is significant interest in the transient pathophysiological factors (including myocardial ischaemia) that modulate arrhythmic substrates, which allow PVCs to occasionally initiate VT and VF [267].

Experimental measurements in pig and dog hearts have characterised how ventricular arrhythmias occur during acute myocardial ischaemia [71, 147, 148, 151]. Premature beats are reported to emerge from the NZ directly adjacent to the BZ, inducing VT through figure-of-eight re-entry [148]. This is illustrated in Fig. 2.6C. Such activation patterns are possible because of the electrophysiological heterogeneity that is present during acute myocardial ischaemia (Fig. 2.5B), where the ERP in the CZ can be prolonged relative to the NZ. When a premature stimulus occurs, prolonged refractoriness in the CZ leads to regional conduction block. During the time it takes for the ectopic wavefront to advance around the CZ, it begins to recover excitability, such that it can be stimulated by the ectopic wavefront in a retrograde fashion. If the NZ recovers excitability in time, this retrograde propagation can lead to a complete re-entrant cycle and a further premature beat (or even multiple beats, if this pattern of activation is sustained).

There are various other forms of ventricular arrhythmias associated with specific electrophysiological mechanisms. For example, torsades de pointes is a type of VT caused by a prolongation of the QT interval (delayed AP repolarisation). Moreover, arrhythmic substrates are not only functional (like myocardial ischaemia and ionic remodelling), but structural remodelling like myocardial fibrosis is also known to play a role in arrhythmogenesis [105].

CHAPTER 3

Literature review of myocardial ischaemia and ionic remodelling in HCM

This chapter details the inherited heart disease hypertrophic cardiomyopathy (HCM) and its most notorious adverse outcome: arrhythmias leading to sudden cardiac death. In the previous chapter, it was shown how cellular abnormalities and acute myocardial ischaemia can cause ventricular arrhythmias. These functional disease factors are hypothesised to play a key role in arrhythmogenesis in HCM, hence this chapter reviews the clinical and experimental evidence related to myocardial ischaemia and ionic remodelling in HCM.

3.1 Hypertrophic cardiomyopathy

3.1.1 General background

HCM is characterised by unexplained myocardial thickening of the LV (Fig. 3.1), affecting 0.2–0.5% of the population [328], making it one of the most common inheritable heart diseases. The clinical diagnosis of HCM is made on the basis of LV wall thickness being ≥ 15 mm in the absence of abnormal loading conditions (such as hypertension) [14, 97, 274]. The typical phenotype (80% of patients) is characterised by more prominent hypertrophy of the septum, but in a minority of patients the hypertrophy is mostly apical [221, 278].

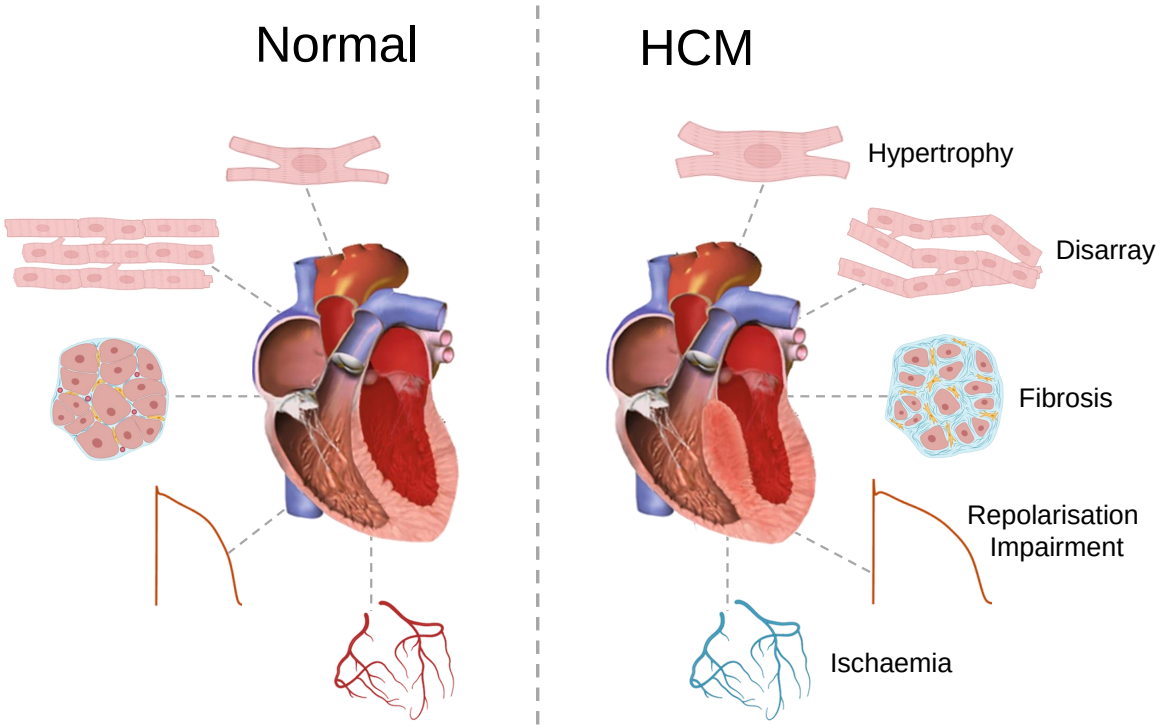


Figure 3.1: The HCM heart with hypertrophy of the interventricular septum (right), as compared to a normal heart (left) [75]. HCM myocardium is affected by cardiomyocyte hypertrophy, myofibre disarray (misalignment of cardiomyocytes), fibrosis, slowed repolarisation and ischaemia (blood supply-demand mismatch). Adapted under Creative Commons license [263].

HCM is an inherited disease associated with more than 1400 causal variants in more than 12 genes [211, 218], although causal variants in only 2 sarcomere genes (the beta-myosin heavy chain and myosin binding protein C genes) account for around 1/2 of all HCM cases [211]. Genotype-phenotype correlation in HCM is weak, such that the variability in expression, penetrance and prognosis of HCM cannot be explained with genotype alone [193]. Genetic testing is therefore limited to diagnostic applications such as the cascade testing of relatives of HCM patients [274].

3.1.2 Causes of mortality in HCM

HCM is a significant cause of excess mortality [195], therefore the prevention of excess mortality is a key challenge in its clinical management. The typical HCM-specific causes of mortality are [195, 219]:

(i) SCD, which is the main driver of excess mortality in the young ($<$ 35 years), but affects patients into midlife and beyond.

(ii) Heart failure, which tends to occur in midlife and beyond.

(iii) Stroke associated with AF, which is more frequent in elderly patients.

3.1.3 Sudden cardiac death

At present, SCD is estimated to occur in 0.3% of HCM patients per year [1, 231]. However, the estimated incidence of SCD varies, with lower estimates in unselected cohorts [377], and higher estimates in some selected populations with a prior clinical diagnosis of HCM [8, 195, 326]. HCM is one of the leading causes of SCD in young athletes [289].

SCDs in HCM are caused by lethal arrhythmias. Most frequently, this involves sinus rhythm being interrupted by a PVC, which is followed by VT that degenerates into VF [267].

3.1.4 Prevention of sudden cardiac death

Effective SCD prevention requires that an effective intervention is used in HCM patients that are identified as susceptible to SCD. This is first limited by the finding that around 70% of SCDs in HCM occur in previously undiagnosed individuals [377], yet population screening for HCM is not advised [74]. Therefore, clinical efforts to prevent SCD at present are focused on risk stratification among the diagnosed to target antiarrhythmic therapy.

Antiarrhythmic therapy

There is no randomised, controlled evidence to support the use of antiarrhythmic drugs for SCD prevention in HCM [97, 274]. Instead, the ICD is the first-line therapy for SCD prevention in HCM, which is a surgically implanted device that is effective at detecting and terminating ventricular arrhythmias

[320]. As there are penalties associated with ICD use, including surgical risks, device complications and inappropriate shocks [190], one of the main clinical challenges in HCM is SCD risk stratification to target ICD implantation.

Risk stratification

Clinical guidelines for SCD risk stratification and ICD decision making are geographically heterogeneous [14, 97, 274], but in general the factors used to estimate SCD risk in adults with HCM include [224, 266]:

(i) non-sustained VT

(ii) unexplained syncope

(iii) a family history of SCD

(iv) maximum LV wall thickness

(v) LVOT obstruction

(vi) age

(vii) LV apical aneurysm

(viii) late gadolinium enhancement (LGE)

(ix) left atrial diameter

(x) LV ejection fraction

(xi) abnormal blood pressure response to exercise

Notably, despite the genetic origins of HCM, no studies have demonstrated an independent prognostic role for genotype variants in SCD risk stratification, so genotype is not used in ICD decision making [14]. It is also notable that historically, SCD risk stratification has almost always been validated in midlife HCM cohorts [224], yet age is an important factor in SCD incidence [195] and SCD risk markers differ by age [232]. Age-dependence of the SCD substrate is also evident at SCD autopsy [367] and during arrhythmias recorded on ICD ECGs [267]. Therefore, there have been recent developments in SCD risk stratification in paediatric HCM [261], but further work is needed to improve the age disparity in risk stratification and understanding of the SCD substrate.

Even in the prospective validation of SCD risk models for adult HCM, it is estimated that 7–10 ICDs are inserted for every 1 patient that benefits from ICD termination of arrhythmia at 5 years of follow-up [224] (or even up to 30 ICDs in another analysis [8]), despite improvements in mortality rates over time

[195]. This is in part because HCM is relatively common [328], yet SCD event rates are low [1], which results in overuse of ICDs in the context of suboptimal risk stratification. This may be exacerbated by the geographic differences in clinical guidelines, which use either the quantitative estimation of individual SCD risk at 5 years of follow-up (European [14, 97, 266]), or the presence of any (binary) major risk marker (US [224, 274]), to guide ICD implantation. It remains the case that there are no randomised trials to validate either strategy [97]. Finally, it is possible that societal, economic and cultural factors contribute to heterogeneously interpreted guidelines [97]. For example, ICDs are used at twice the rate in US vs. non-US sites without differences in SCD rates [254].

Exercise restriction

As recently as 2011, clinical consensus was to disqualify athletes with HCM from competitive sports [112, 213, 284], based on reported links between high intensity exercise and SCD [214]. Clinical consensus has since evolved to have a case-by-case discussion of the risks, where the informed patient takes partial responsibility for the decision to compete [97, 274]. However, this reflects uncertainty in the evidence associating SCD and exercise [14], and the role of exercise restrictions in HCM is a subject of ongoing controversy [376]. The most recent clinical consensus is to allow some low-risk individuals to engage in competitive sport after expert evaluation [14]. However, techniques to predict which patients may be put at risk specifically by exercise are limited.

Unknowns in the substrate for sudden cardiac death

There is a strong calling to understand the basic mechanisms leading to SCD, to supplement traditional risk factors [286]. Ventricular arrhythmogenesis in HCM is thought to be contributed to by myocardial fibrosis, fibre disarray, microvascular ischaemia and an abnormal cellular substrate (including remodelling in ion channels and the Ca^{2+} subsystem) [286]. Although there has been progress in elucidating the role of fibrosis in SCD risk (through LGE-CMR) [105, 224], myocardial ischaemia, and slowed repolarisation secondary to ionic remodelling [66], are absent from risk stratification models and the related mechanisms remain poorly understood. Therefore, the following sections detail the experimental and clinical evidence of myocardial ischaemia and ionic remodelling in HCM, to motivate the mechanistic investigations of these disease factors.

3.2 Myocardial ischaemia

3.2.1 Imaging of ischaemia in HCM

Perfusion measurements are commonly used as a surrogate of ischaemia, as integrated measures of flow through both the epicardial coronary arteries and the microcirculation. Regional perfusion defects are characteristic of the HCM phenotype and present as regions of impaired myocardial blood flow (MBF) at rest or during exercise/pharmacologically induced hyperaemia (Fig. 3.2).

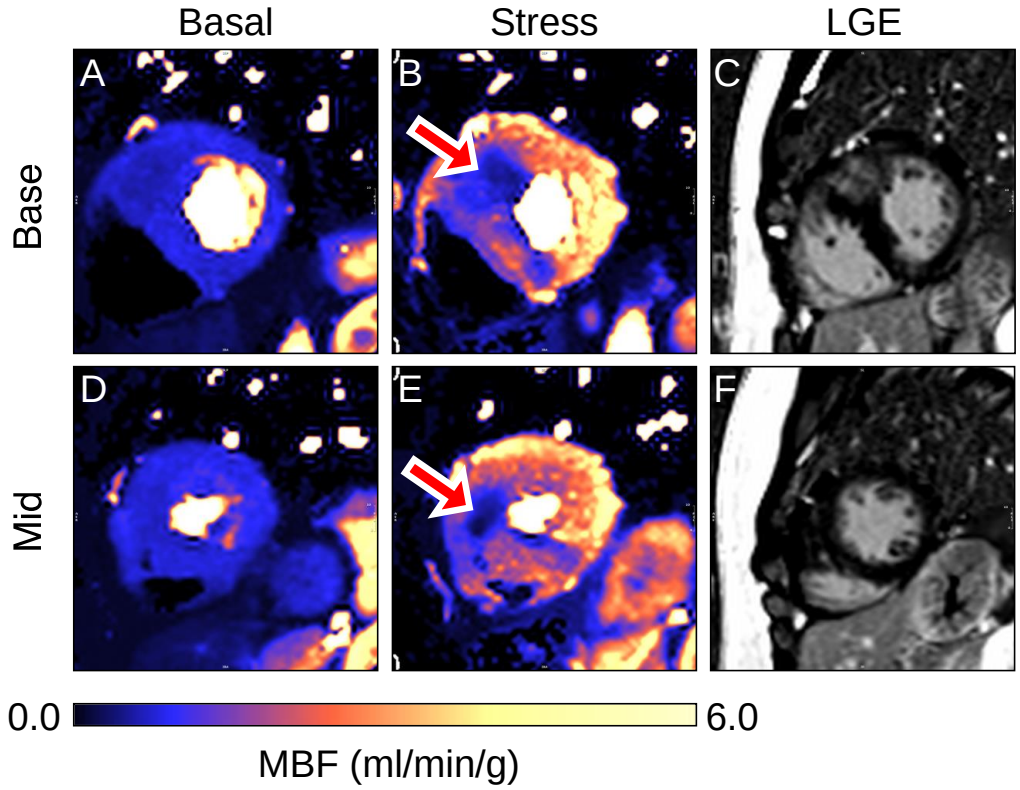


Figure 3.2: Stress perfusion defects in HCM on perfusion CMR. (A, D) Basal and (B, E) adenosine-stress MBF on perfusion CMR in the (A, B) base and (D, E) mid LV slices of a 40 year-old woman with sarcomeric causal variant positive HCM, showing stress perfusion impairment (denoted with arrows) in the maximally hypertrophied anterior wall and septum. (C, F) LGE in the same patient for the base and mid LV slices, respectively, showing dense focal enhancement in the hypertrophied anteroseptum.

Perfusion impairment is commonly inferred from a reduced ratio of hyperaemic MBF to rest MBF, termed the myocardial perfusion reserve (MPR) or myocardial perfusion reserve index (MPRI), and is generally considered an acceptable surrogate for ischaemia [222]. Table 3.1 summarises the non-invasive imaging studies that have assessed the presence of perfusion defects in HCM patients, through CMR, echocardiography and nuclear imaging. However, not all imaging modalities are equally accurate. Perfusion defects on Th-201 scintigraphy, for example, correlate poorly with acidosis [96].

Since the last review of imaging techniques for myocardial ischaemia in HCM in 2009 [222], ischaemia assessment with CMR has been widely adopted. Perfusion CMR boasts MBF quantification at high resolution, without radiation exposure, and has proven high sensitivity for coronary artery disease diagnosis in the general population [126]. The capability of CMR to measure multiple modalities further enables the assessment of ischaemic and fibrotic burden in quick succession (see later Table 3.2). Moreover, as ischaemia results from an imbalance between oxygen supply and demand, modalities such as blood oxygen level dependent (BOLD) CMR that is sensitive to myocardial oxygenation can provide further insight to oxygen supply and demand in HCM [163].

Across the perfusion imaging studies in Table 3.1, ischaemia is frequently identified in HCM patients, with the largest perfusion CMR study to date identifying inducible perfusion defects in 84% of their cohort [305]. Because perfusion defects were typically identified on visual assessment, often the severity of impairment was omitted. However, quantitative assessments have identified a subset of 21–31% of patients in whom regional perfusion can fall during vasodilator stress [36, 143], a finding suggestive of severe microvascular dysfunction.

Ref	Year	Imaging modality	N HCM+/−	Summary of findings
[264]	1987	Th-201 emission CT	72 / 0	57% any, 24% fixed, 33% reversible
[88]	1989	Scintigraphy	28 / 0	39% any
[362]	1989	Th-201 emission CT	29 / 0	3% fixed, 52% stress
[349]	1993	Th-201 emission CT	82 / 0	33% fixed, 39% reversible
[87]	1993	Scintigraphy	23 / 0	78% any
[336]	1996	Scintigraphy	17 / 0	71% any
[95]	1996	Scintigraphy	94 / 0	20% fixed, 21% reversible
[397]	1998	Scintigraphy	105 / 0	69% any, 30% fixed, 60% reversible
[385]	1998	Th-201 emission CT	216 / 0	40% any, 25% fixed, 22% reversible
[311]	2004	SPECT	101 / 0	54% any, 28% fixed, 41% reversible
[235]	2008	CMR	37 / 0	46% rest
[72]	2008	Echo	68 / 74	46% CFR < 2
[245]	2010	SPECT + MCE	33 / 23	100% any (MCE), 0% any (SPECT)
[28]	2012	PET	33 / 0	72% reversible
[29]	2013	PET	47 / 0	72% any
[360]	2013	CMR	86 / 0	57% any
[370]	2014	CMR	33 / 0	87% any
[143]	2014	CMR	35 / 0	31% MPR < 1
[288]	2015	CMR + Echo	148 / 0	7% any
[145]	2015	CMR	12 / 9	18% rest, 73% stress
[51]	2015	CMR	80 / 0	30% rest
[54]	2016	Echo	706 / 0	38% CFVR ≤ 2
[371]	2016	CMR	30 / 0	60% stress
[130]	2018	CMR	13 / 0	0% rest, 54% stress
[36]	2019	CMR	101 / 30	79% any
[299]	2019	CMR	35 / 0	71% MPRI < 1.4
[169]	2020	CMR	115 / 0	42% stress
[208]	2020	CMR	105 / 0	45% MPRI ≤ 2
[305]	2021	CMR	449 / 0	84% stress
[138]	2021	CMR	50 / 28	20% any
[407]	2021	SPECT	91 / 0	77% any, 24% fixed, 53% reversible
[5]	2021	CMR	75 / 0	91% any

Table 3.1: Studies reporting prevalence of perfusion defects among HCM patients. Perfusion defects were mostly identified by visual assessment, and in some cases assessed quantitatively with perfusion reserve/flow measurements [54, 72, 143, 208, 299]. Studies reporting the prevalence of perfusion defects on visual assessment identified perfusion defects occurring at rest, stress, exclusively stress (reversible), and both at rest and stress (fixed). N HCM+/−: numbers of HCM patients and non-HCM controls; CT: computed tomography; SPECT: single-photon emission computed tomography; CMR: cardiac magnetic resonance; PET: positron emission tomography; MCE: myocardial contrast echocardiography; CFR: coronary flow reserve; CFVR: coronary flow velocity reserve; MPR: myocardial perfusion reserve; MPRI:

myocardial perfusion reserve index.

3.2.2 Pathophysiological mechanisms of ischaemia in HCM

Small vessel disease

Structural abnormalities in the small blood vessels that supply the myocardium are a common finding in the histology of HCM hearts [19, 179]. As many as 56–83% of HCM patients have small vessel disease to some degree [183, 217, 220, 246]. The abnormalities typically include marked thickening of the vessel walls, luminal narrowing of small intramural coronary arteries [215] and increased arterial stiffness [26]. The luminal area of arterioles, as a percentage of total vascular area, has been measured to be 13–30% lower in HCM patients than in controls [178, 322, 351], with 14% of small vessels in one study having an external diameter:lumen ratio ≥ 3 (normally < 2.5) [366]. Other studies found small vessel disease in 92% of myocardial specimens taken from 57 HCM patients [103], and that the HCM myocardium had 30$\times$ more abnormal intramural coronary arteries per section on average than controls [220]. The degree of small vessel disease may be particularly severe in patients with heart failure [111].

Reduced density of small vessels

Numerous studies have measured the density of small vessels in hypertrophied HCM septal/LV tissue samples and have found this to be 21–44% lower than in control patients [26, 120, 154, 178, 256, 322, 403]. With no convincing association with genotype [120], reductions in small vessel density may be linked to hypertrophy in HCM and are more severe in end-stage disease patients, such as those undergoing heart transplantation, than in patients referred for myectomy [256]. The reported association between reduced small vessel density and perfusion reserve blunting suggests that this is another cause of ischaemia [322].

Left ventricular outflow tract obstruction

LVOT obstruction is a hallmark feature of HCM and is defined as a peak LVOT pressure gradient ≥ 30 mmHg. LVOT obstruction may be present at rest (in up to 51% of HCM patients [208, 221, 223, 331]) or develop during exercise (in 33–62% [223, 331]). Severe obstruction (≥ 50 mmHg) may be seen

in up to 20% of patients [54]. Even in the absence of hypertrophy, LVOT obstruction may be present due to systolic motion of the anterior mitral valve leaflet towards the LVOT [283]. This typically results from lengthening of the anterior mitral valve leaflet, abnormal chordal-mitral valve attachment or bifid papillary muscle hypermobility [283].

LVOT obstruction is associated with reduced perfusion reserve [54, 72, 208, 353] particularly in the LAD artery which supplies the anterior wall and septum [184, 353], reduced hyperaemic MBF [173], reduced endo-epicardial hyperaemic MBF ratio [340], reduced perfusion upslope (a measure of contrast agent wash-in time) [384] and an additional hemodynamic forward deceleration wave in systole [304]. These associations may be explained by coronary hypoperfusion and increased oxygen demand, as greater myocardial work is required to overcome the obstruction.

Despite these reported associations, other studies have found no relationship between LVOT obstruction and ischaemia, and infarction has been reported in non-obstructive HCM [189], confirming the role of other mechanisms including microvascular dysfunction [5, 29, 47, 288, 407].

Diastolic and systolic effects

Diastolic dysfunction, which is one consequence of sarcomeric causal variants, is an early feature of HCM in many patients [192, 295]. With myocardial blood flow greatest during diastole, constrained diastole results in impaired perfusion [225]. In a study by Raphael et al., invasive measurements of coronary pressure and flow showed that diastolic dysfunction in HCM led to impaired decompression of the microcirculation [304], and these effects could be exacerbated by exercise [291]. During systole, hypertrophy causes excessive compression of intramyocardial blood vessels, leading to abnormal coronary haemodynamic forces [304], which can manifest as systolic flow reversal in septal perforator arteries of HCM patients [6, 132, 184, 358] even in the absence of LVOT obstruction [304].

Myocardial bridging

Another potential mechanism of perfusion impairment among HCM patients is myocardial bridging, which is when a segment of a coronary artery tunnels through the myocardium rather than over it. This is seen in 23–41% of HCM patients compared to 5–7% of the general population [20, 332]. Multiple

case reports highlight bridging as a possible cause of ischaemia [271, 292, 318, 395], however surgical correction of myocardial bridging remains controversial [185, 234].

Genetic and metabolic factors

In multiple studies of genotyped HCM patients, vasodilator stress BOLD CMR has detected impaired myocardial oxygenation even in pre-hypertrophic carriers of sarcomeric causal variants, despite preserved perfusion [119, 163, 300]. One possible explanation for this dissociation in oxygenation and perfusion often observed in the early phase of the disease is that myocardial oxygen demand may be increased even in the absence of hypertrophy [2, 142, 356, 368]. In line with this, experimental non-hypertrophic murine models of sarcomeric causal variants have demonstrated increased oxygen expenditure arising from energetic inefficiency associated with sarcomeric causal variants [199]. In HCM patients with overt hypertrophy, the degree of stress oxygenation may be as severe as that seen in severe aortic stenosis [206, 300].

3.2.3 Relationships between markers of disease severity and ischaemia

Myocardial hypertrophy and ischaemia

The greater the degree of hypertrophy (quantified as wall thickness or LV mass), the greater the degree of perfusion impairment (typically quantified as rest or hyperaemic MBF, perfusion reserve, flow velocity, or as the presence of visual defects). This has been reported both at a segmental level [36, 51, 110, 123, 137, 143, 145, 163, 173, 179, 208, 245, 290, 360, 384, 396] and in HCM patients on average [5, 6, 12, 28, 169, 173, 264, 293, 340, 353, 358, 385]. In addition to reductions in capillary density [120], hypertrophy was frequently associated with enhanced luminal narrowing of small vessels [178, 183, 351, 366]. A further macroscopic explanation is that the increase in muscle mass characteristic of HCM is inadequately supplied by the major coronary arteries, which have reduced luminal volume per unit myocardial mass [165, 171, 327]. Heterogeneous flow among major coronary arteries secondary to variable regional demand is a further consequence of hypertrophy [179, 184, 327, 353].

Although perfusion defects are overall more prevalent in cohorts with hypertrophy (Table 3.1), 20% of HCM sarcomeric causal variant carriers without hypertrophy may still have perfusion defects [138], and

even in hypertrophic cohorts, 30–40% of patients may have perfusion defects in segments with only mild hypertrophy [79, 88]. When compared to controls, even non-hypertrophied segments in HCM have reduced perfusion reserve on average [36].

Segmental and transmural distribution of ischaemia

Two studies reported perfusion defects [370] or the presence of an exercise wall motion abnormality (WMA) [288] to be most frequently septal, which is consistent with the septum and anterior LV wall being the most frequently hypertrophied regions in HCM [221]. In another cohort, the septum and inferior segments were most affected by perfusion defects [110]. Perfusion defects have also been reported as primarily located in the septum in prehypertrophic HCM sarcomeric causal variant carriers [138], which may be explained by small vessel disease reported as mostly affecting the septum in histological analyses [103, 220]. However, Villa et al. reported a more diffuse burden of hypoperfusion in a cohort without severe hypertrophy [371], consistent with the widespread distribution of small vessel disease in a different histological analysis by Varnava et al. [366].

There are also conflicting reports on the segmental distribution of perfusion defects in single positron emission computed tomography (SPECT) imaging studies [125, 132, 311, 385], which may be due to partial volume effects, given the wall thickness-dependent sensitivity of SPECT imaging. Indeed, positron emission tomography (PET) studies, which have similar problems with partial volume effects due to its low resolution, sometimes report similar impairment in MBF between the septum and LV free wall [47, 173, 197], with two exceptions [29, 198].

Perfusion impairment in HCM is predominantly subendocardial [36, 79, 110, 138, 143, 173, 197, 290, 305, 340, 360], although transmural hypoperfusion has also been reported [36, 123].

Myocardial fibrosis and ischaemia

Repeated episodes of ischaemia have been implicated in fibrosis accumulation and extensive scarring in HCM [19, 215]. A longitudinal study of HCM patients with combined LGE to assess fibrosis burden and stress perfusion imaging found that patients with impaired perfusion reserve had a greater increase in LGE mass over time [299]. Indeed, multiple histopathological studies have shown that the presence of

diseased small intramural coronary arteries and reductions in microvascular density are topographically correlated with the presence of fibrosis [19, 103, 111, 220, 246, 355], with one exception [366]. This was similarly reported among patients [351], with Kwon et al. reporting that the presence of small vessel disease is independently associated with 14× increased risk of myocardial scarring [183]. The association with replacement fibrosis appears primarily in end-stage HCM [103]. However, whereas ischaemia is predominantly subendocardial in HCM [36, 79, 110, 138, 143, 173, 197, 290, 305, 340, 360], fibrosis is predominantly mid-wall in HCM [32, 53, 83, 108, 137, 145, 215, 337, 343]. This transmural dissociation has been reported directly on imaging [145, 360]. Segment-wise associations between fibrosis and ischaemia have also been reported on imaging in HCM (Table 3.2), however it remains to be seen whether this is due to the confounding effect of disease severity reflected by wall thickness [143], or due to difficulties in discerning regions of ischaemia and fibrosis [371].

Imaging studies that did not perform epi-endocardial segmentation, but controlled for wall thickness, found independent associations between perfusion impairment and either LGE or extracellular volume [110, 137, 145, 208]. One study with epi-endocardial segmentation and control for wall thickness reported an independent association between LGE and hyperaemic MBF [36], but two smaller similar studies found that either this association was lost after controlling for wall thickness [143], or the differences in perfusion with/without LGE were modest [79]. Patient-wise analyses typically found ischaemia-fibrosis associations [12, 29, 99, 288, 305, 354, 360, 371, 407], with reported exceptions [169, 304].

Collectively, these findings suggest colocalization of pathology (microvascular dysfunction and fibrosis) and the potential for ischaemia to promote the fibrosis phenotype. However, it is possible that imaging difficulties in discerning regions of fibrosis and hypoperfusion could overestimate the fibrosis-ischaemia association [371]. Furthermore, assessment of LGE alone can miss any association between interstitial fibrosis and small vessel disease [103] and in this regard, it is worth considering the study in which ischaemia was independently associated with extracellular volume, but not LGE [208].

Ref Modality	N HCM+/−	Epi-endo segmented	Relevant comorbidities	Summary of findings
[36] CMR	101 / 30	Yes	CAD (0%) DM (17%)	LGE associated with reduced hyperaemic MBF^{M}
[360] CMR	100 / 0	Yes	CAD (5%) DM (10%)	LGE transmurally dissociated from hyperaemic MBF impairment^{U}
[290] CMR	35 / 14	Yes	CAD (N/A) DM (0%)	LGE associated with reduced hyperaemic MBF^{U}
[143] CMR	35 / 0	Yes	CAD (0%) DM (0%)	LGE associated with reduced MPRI, rest and hyperaemic MBF^{U+M-}
[79] CMR	20 / 10	Yes	CAD (0%) DM (N/A)	LGE associated with reduced MPR, hyperaemic MBF^{M}, unclear if statistically significant
[208] CMR	105 / 0	No	CAD (0%) DM (11%)	ECV, not LGE, associated with MPRI $< 2^{M}$ LGE associated with reduced MPRI^{U}
[110] CMR	75 / 0	No	CAD (N/A) DM (N/A)	LGE, ECV, T1 and T2 associated with stress perfusion defects^{M}
[10] CMR	55 / 0	No	CAD (0%) DM (N/A)	ECV, LGE and T1 associated with hypoxia^{U}
[396] CMR	47 / 21	No	CAD (0%) DM (0%)	LGE associated with increased time to perfusion peak^{U}
[343] PET	34 / 0	No	CAD (N/A) DM (N/A)	LGE associated with reduced hyperaemic MBF, particularly if visually transmural LGE^{U}
[163] CMR	37 / 31	No	CAD (N/A) DM (N/A)	LGE associated with reduced MPRI^{U}
[137] CMR	22 / 13	No	CAD (N/A) DM (N/A)	LGE associated with lower maximum perfusion upslopes^{M}
[145] CMR	12 / 9	No	CAD (N/A) DM (N/A) All <30 years	LGE associated with lower stress/rest ratio of maximum perfusion upslopes^{M}
[29] PET	47 / 0	N/A	CAD (N/A) DM (11%)	Delayed enhancement visually coincided with stress perfusion defects^{U}
[159] Scinti-graphy	6 / 0	N/A	CAD (0%) DM (N/A)	LGE visually coincided with stress perfusion defects^{U}

Table 3.2: Imaging studies in which segment-wise associations between ischaemia and fibrosis have been analysed. Epi-endo segmented refers to whether imaged LV segments were further divided into epicardial and endocardial subsegments. ^{U}Association does not control for wall thickness; ^{M}Association controls for wall thickness; $^{U+M-}$Association is lost when controlling for wall thickness. N HCM+/−: numbers of HCM patients and non-HCM controls; CAD: coronary artery disease; DM: diabetes mellitus; CMR: cardiac magnetic resonance; PET: positron emission tomography; LGE: late gadolinium enhancement; MBF: myocardial blood flow; MPRI: myocardial perfusion reserve index; MPR: myocardial perfusion

reserve; ECV: extracellular volume.

Extracellular matrix expansion in myocardial regions remote from microvascular dysfunction has been suggested to be triggered by pro-hypertrophic transforming growth factor beta signalling secondary to the sarcomeric causal variant [352]. This non-ischaemic aetiology of fibrosis would support the findings of other studies where fibrosis can be seen in hearts with normal perfusion [29, 299].

3.2.4 Clinical manifestations of myocardial ischaemia in HCM

The main clinical manifestations of myocardial ischaemia in HCM patients are angina and dyspnoea [15, 37, 72, 170, 349], alongside dynamic changes on exercise/vasodilator-induced stress ECG testing [95, 187]. Perfusion abnormalities may also be present in the absence of symptoms [12, 95, 169, 208, 264, 311, 385], so the relationship between pathology and symptoms may not always be consistent. Of interest, post-mortem studies of HCM patient hearts have noted a relative absence of historical symptoms among individuals with transmural infarction [215]. This confirms the potential for ischaemia to be silent, possibly through small fibre neuropathy reducing afferent pain signal detection. Mildly abnormal troponin levels are also common among HCM patients, reported in 74% [115], and likely represent myocyte injury or necrosis thought to be exacerbated by myocardial ischaemia.

3.2.5 Mechanisms of myocardial ischaemia progression in HCM

Figure 3.3 summarises the likely progression of factors affecting oxygen supply and demand in HCM. Early in development, ATP depletion arising from the sarcomeric causal variant likely causes stress oxygenation impairment [119, 163], and could contribute to phenotype development through SERCA ATP starvation, Ca^{2+} accumulation and hypertrophy via Ca^{2+} signalling [17]. The cause of subsequent metabolic abnormalities in HCM is unclear [158, 329, 368]. Small vessel disease, present even in those less than 1 year of age [220], could emerge during embryonic development driven by sarcomeric causal variants [273], and is proposed to be one of the earliest factors in the cascade of events related to ischaemia [222]. Pre-hypertrophic diastolic dysfunction secondary to the sarcomeric causal variant [192, 295] could contribute by limiting the time for myocardial relaxation, leading to increased rest MBF

[225], which could promote vascular remodelling through increased shear stress. However, perfusion impairment reported in the absence of diastolic dysfunction [123] suggests that diastolic dysfunction is not the only contributor. Early perfusion defects seen on stress imaging of HCM patients may occur due to the microscopic steal phenomenon secondary to small vessel disease, or due to an abnormal vasomotor response of diseased myocardium to pharmacologically induced vasodilation [36].

As cells become hypertrophied, either to compensate for cells lost through ischaemia-induced fibrosis or other pathological processes, ischaemia is further promoted by local reductions in small vessel density [120], greater energetic demands, increased extravascular compression, and LVOT obstruction. Post-hypertrophy diastolic dysfunction (possibly exacerbated by ionic remodelling in hypertrophied segments [64]) may be a key contributor to ischaemia as the diastole-specific perfusion reserve is more strongly correlated with wall thickness than the time-averaged perfusion reserve [179]. Moreover, the increased oxygen demand of hypertrophy leads to resting vasodilation, giving rise to 'maxed out' vasodilation at rest [138, 143, 184, 340, 398] and explains why perfusion defects are more prevalent in cohorts with hypertrophy [305] than those without [138].

With disease progression, the ischaemic threshold is incrementally lowered, such that acute episodes of ischaemia are inducible despite non-stenotic epicardial coronary arteries. In some HCM patients, transient increases in energetic demands, such as during AF-induced increases in ventricular pacing [189] or during exercise [122], are sufficient to trigger an ischaemic episode, which can precipitate lethal ventricular arrhythmias.

In patients with the most severe small vessel disease and insufficient capillary density, ischaemia leads to gross macroscopic transmural scarring [103, 108, 111, 222, 256], which contributes amongst other factors (mitral regurgitation [305]) to the 2–16% subset of HCM patients that progress to end-stage disease [272, 406]. Myocyte death eventually leads to total replacement of myocardial regions with fibrosis, such that affected regions are devoid of myocytes that could hypertrophy, leading to wall thinning, LV stiffening and systolic dysfunction [252, 299, 305]. In this stage, LVOT gradients are resolved at the peril of reduced ejection fraction.

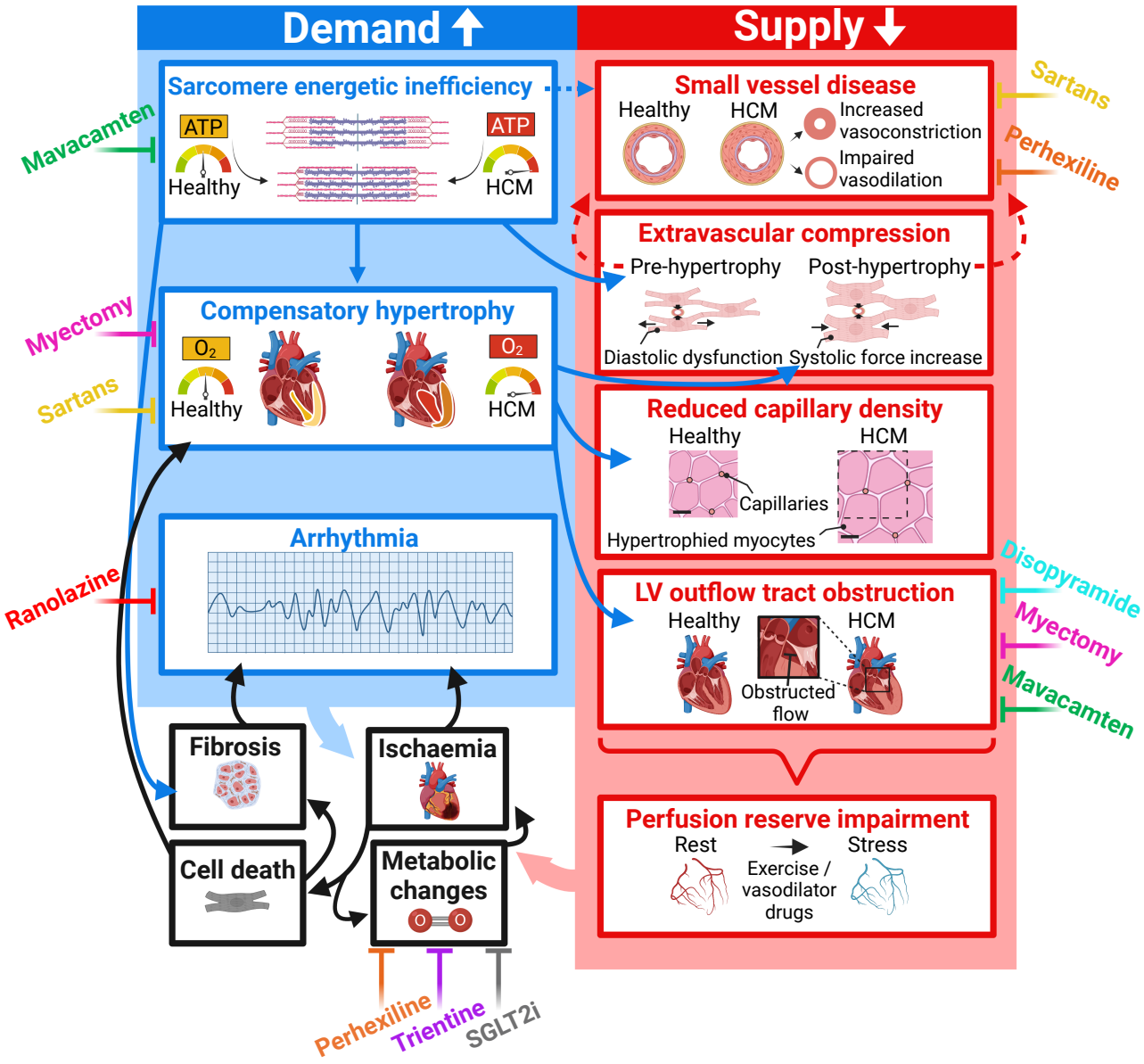


Figure 3.3: Mechanisms involved in progression of ischaemia in HCM [75]. Disease factors in HCM constrain myocardial blood supply and increase energetic demands. Possible relationships between pro-ischaemic disease factors are denoted by arrows, alongside potential anti-ischaemic therapies [225].

3.2.6 Prognostic value of myocardial ischaemia in HCM

Composite endpoints

The studies in Table 3.3 have analysed the association of ischaemia in HCM with adverse events using composite endpoints, where non-arrhythmic events such as heart failure or all-cause death were included. Although many studies found hypoperfusion to be associated with adverse outcomes on multivariate analysis [46, 47, 54, 72, 159, 187], they did not assess focal fibrosis burden, which is an independent predictor of mortality in HCM [105]. In the study that did account for fibrosis confounding, exercise WMAs were an independent predictor of cardiac events – not visual assessment of perfusion defects on CMR [288]. Although WMAs are not specific for myocardial ischaemia, a strong association between perfusion defects and WMAs has been reported [288]. In the largest study to date, exercise WMAs were substantiated as a possible risk factor in HCM, particularly when considered alongside non-invasive quantitative perfusion reserve measurements [54].

Overall, the studies in Table 3.3 demonstrate that quantitative assessment of ischaemia identifies a subgroup of HCM patients at high risk of adverse outcomes, with the hyperaemic MBF threshold on PET optimally associated with outcomes estimated as 1.1–1.35 ml/min/g [46, 47, 272]. There is mixed evidence from studies of visual perfusion assessment, suggesting that further studies may benefit from quantitative perfusion analysis.

The prognostic value of other pathophysiological mechanisms, such as myocardial bridging, is debatable. Although bridging has been shown to predict poorer prognosis in one paediatric cohort [393], this association was not consistent elsewhere [244]. Furthermore, Sorajja et al. did not observe an association between bridging and poor outcomes in adult HCM patients [342].

Ref Year	N HCM+/−	Ischaemia measure	Follow-up (years)	Summary of findings
[257] 1996	62 / 0	SPECT metabolic impairment score ≥ 30 vs. < 30	3 ± 1	11× risk of death^{U}
[187] 1997	79 / 0	ST segment depression on dipyridamole ECG	6 ± 1	6× risk of cardiac events^{U} Independent predictor of cardiac events^{M*}
[385] 1998	216 / 0	Fixed perfusion defect(s) on SPECT	3 ± 2	Unrelated to HCM-related death^{M*} 2× risk of historical syncope / ventricular fibrillation^{U}
[47] 2003	51 / 12	Lowest tertile of hyperaemic MBF on PET	8 ± 2	10× risk of cardiac death^{M*} 20× risk of unfavourable outcome^{M*}
[311] 2004	101 / 0	Fixed perfusion defect(s) on SPECT	6 ± 3	Unrelated to cardiac death^{U} 3-4× risk of severe complications^{U}
[72] 2008	68 / 74	Perfusion reserve < 2 on echo	2 ± 1	4× risk of cardiac events^{M*}
[159] 2011	55 / 0	Anterior junction stress score > 2 on scintigraphy	6	8× risk of cardiac events^{M*}
[207] 2013	35 / 0	LAD perfusion < 2 on Doppler catheter	9	3-6× risk of cardiac events^{U}
[288] 2014	148 / 0	Perfusion defects and exercise WMAs on CMR + echo	7 ± 2	Perfusion defect(s) associated with 5× risk of cardiac events^{U+M-} Exercise WMAs associated with 400× risk of cardiac events^{M}
[54] 2016	706 / 0	Perfusion reserve < 2 and WMAs on echo	4 [2, 6]	5× risk of cardiac events^{M*}
[46] 2016	100 / 0	Lowest tertile of hyperaemic MBF on PET	4 ± 2	7× risk of unfavourable outcome^{M*}
[407] 2021	91 / 0	Perfusion defect(s) on SPECT	8 [4, 11]	3× risk of cardiac events^{U}

Table 3.3: Studies that investigated the association between ischaemia and prognosis in HCM patients, where composite endpoints were used. Follow-up durations given as mean or median, with variability given as ± standard deviation or [lower quartile, upper quartile], where available. ^{U}Univariate analysis; ^{M}Multivariate analysis controlling for fibrosis; ^{M*}Multivariate analysis not controlling for fibrosis. N HCM+/−: numbers of HCM patients and non-HCM controls; SPECT: single-photon emission computed tomography; MBF: myocardial blood flow; PET: positron emission tomography; LAD: left anterior descending; WMA: wall motion abnormality; CMR: cardiac magnetic resonance.

Arrhythmia and sudden cardiac death

Acute myocardial ischaemia (in the absence of epicardial coronary stenoses) may be an important cause of fatal arrhythmias and SCD in HCM [191, 293, 298, 387], as multiple case reports describe arrhythmias precipitated by acute myocardial ischaemia in young patients [122, 189, 307]. In a postmortem study of 19 young ($\leq$ 35 years) SCD victims with HCM, 11 had physical evidence of acute-subacute myocardial ischaemia (coagulative necrosis, neutrophilic infiltrate, myocytolisis, granulation tissue healing, infarction) in the septal myocardium [19]. Multiple foci of transmural infarction have also been reported in some deceased HCM patients, despite having normal epicardial coronary arteries [215].

Numerous studies (Table 3.4) have analysed the association between ischaemia and arrhythmia in HCM. Many studies accounted for confounding by fibrosis and found independent associations between ischaemia measurements and arrhythmia [5, 51, 169, 198]. The specific association was variable across studies, and it is unclear the extent to which differences in imaging modality, protocol and cohort may have contributed to this variety. Importantly, however, there is some suggestion that measurements of MBF heterogeneity predict arrhythmic risk [198, 203], motivating further study of regional perfusion quantification. There is further evidence from echocardiographic and scintigraphic studies that ischaemia is associated with syncopal episodes in HCM [87, 88].

Ref Year	N HCM+/−	Age (years)	Ischaemia measure	Summary of findings
[196] 1997	84 / 0	43 ± 12	Perfusion reserve / transmural MBF gradients on PET	Unrelated to syncope or non-sustained VT on Holter^{U}
[323] 2009	95 / 0	41 ± 15	Lower hyperaemic MBF on PET	Associated with history of AF^{M*}
[12] 2011	62 / 35	47 ± 16	Lower rest MBF on CMR	Associated with non-sustained VT on Holter^{U}
[51] 2015	80 / 0	50 ± 18	Rest perfusion defects on CMR	Associated with non-sustained VT on Holter^{M}
[198] 2018	133 / 0	50 ± 15	High hyperaemic MBF heterogeneity on PET	4× risk of VT on ICD electrogram/Holter^{M}
[293] 2019	104 / 0	58 ± 15	Lower perfusion on angiography	Associated with paroxysmal supra-VT and VT on Holter^{U}
[203] 2020	25 / 0	57 ± 13	Decreased hyperaemic endo/epicardial MBF ratio on PET	Associated with non-sustained VT on ICD electrogram^{U}
[169] 2020	115 / 0	52 ± 11	Perfusion defect(s) on CMR	6× risk of non-sustained VT on Holter^{M}
[407] 2021	91 / 0	14 [10, 16]	Perfusion defect(s) on SPECT	Associated with non-sustained VT on follow-up^{U}
[176] 2021	32 / 0	62 ± 16	Reduced perfusion upslope on CMR	Associated with VT on Holter^{U}
[5] 2021	75 / 0	55 ± 15	Perfusion defect(s) on CMR	2× risk of supra-VT on Holter, but not VT^{M}

Table 3.4: Studies that investigated the association between ischaemia and arrhythmia in HCM patients. Ages given as mean or median, with variability given as ± standard deviation or [lower quartile, upper quartile], where available. ^{U}Univariate analysis; ^{M}Multivariate analysis controlling for fibrosis; ^{M*}Multivariate analysis not controlling for fibrosis. N HCM+/−: numbers of HCM patients and non-HCM controls; MBF: myocardial blood flow; PET: positon emission tomography; VT: ventricular tachycardia; CMR: cardiac magnetic resonance; SPECT: single-photon emission computed tomography; ICD: implantable cardioverter-defibrillator.

Heart failure

Some studies report an association between ischaemia and heart failure. Hamada et al. used Th-201 scintigraphy to study 48 HCM patients and found that development of heart failure was associated with

perfusion impairment [125]. Similarly, Olivotto et al. used stress PET in 51 HCM patients and found that adverse LV remodelling and systolic dysfunction were predicted by quantitative assessment of perfusion [272]. SPECT imaging of 65 HCM patients also found an association between metabolic impairment and heart failure [257]. Similarly, perfusion and LGE CMR of 62 HCM patients found that reduced MBF was the only independent predictor of functional status when LGE and hypertrophy were accounted for [12]. However, in the largest longitudinal perfusion CMR study to date of 449 HCM patients, perfusion defects on visual assessment were unable to predict heart failure [305]. LGE progression may instead be a more prominent factor in the development of heart failure as an independent association has been reported [299].

Confounding by coexisting pathology

In evaluating the independent prognostic contributions of perfusion defects and presence of LGE, not only are perfusion defects confounded by presence of LGE due to the possibly causal link between ischaemia and fibrosis in HCM [299], but some perfusion defects correspond to sites of LGE [169]. It is therefore unclear whether SCDs in HCM are caused by (i) primary ventricular arrhythmia related to fibrosis [105], or (ii) secondary ventricular arrhythmia during ischaemia [51]. Simultaneous echo and perfusion CMR in 148 HCM patients showed that cardiac event rates were highest when both LGE and exercise WMAs were observed [288], hence both factors may contribute to increased risk. This is further supported by the finding that both fixed and reversible perfusion defects have prognostic value [407], as perfusion abnormalities present at rest are thought to represent severe fibrosis [51]. Ischaemia may be particularly relevant to the cases of juvenile SCDs in which replacement fibrosis is absent [111].

As a possible cause of ischaemia, LVOT obstruction is already recognised as a risk factor for SCD in adults [98] and children [260]. Finally, further confounding may arise from AF due to its association with ischaemia [323].

Exercise

Myocardial ischaemia in HCM is relevant in the context of evolving clinical guidelines on exercise restrictions. If SCD is related to exercise [377], then ischaemia is a plausible arrhythmic substrate through

exercise-induced ischaemia [308], latent LVOT obstruction [331] and reduced diastolic filling time [291] during increased workload. Measurements derived from stress perfusion imaging could contribute to decisions made with patients on exercise, although at present there is limited clinical evidence that this would be useful.

Of note, two meta-analyses have shown that SCDs in young HCM patients are 75% more common in athletes than non-athletes [78, 363]. Age appears to be a factor in the association between exercise and SCD in HCM [90], with Weissler-Snir et al. reporting 80% of HCM-related SCDs in those $\leq$ 20 years old being related to exercise, compared to $<$ 5% of those $>$ 20 [377]. Interestingly, a study of 1380 HCM patients showed that, on multivariate analysis, only non-sustained VT induced by exercise was associated with SCD – not non-sustained VT generally [113]. In this analysis, 21% of patients with exercise-induced non-sustained VT had preceding ST depression, and most were $<$ 40 years of age. There are other varying reports of SCD-predictive measures derived from exercise [59, 204, 308], including the ventilation-to-CO2 slope and anaerobic threshold during exercise, all of which could indicate propensity for underlying myocardial ischaemia on cardiopulmonary exercise testing.

3.3 Ionic remodelling

Ionic remodelling refers to chronic changes in subcellular ion channel kinetics or expression, which can have effects on the AP, electrical propagation, and subcellular Ca^{2+} handling.

3.3.1 Experimental evidence

Whereas there is over 35 years of evidence of myocardial ischaemia on imaging in HCM (seen previously in Table 3.1), ionic remodelling in human HCM cardiomyocytes was first directly measured in 2013 by Coppini et al. [66]. These patch-clamp experiments, performed on human septal samples from HCM patients undergoing surgical myectomy for relief of LVOT obstruction, showed that HCM-remodelled cells have increased I_{NaL} activity, impaired repolarising K^+ channels, and altered subcellular Ca^{2+} handling. These changes manifested in the hypertrophied HCM cardiomyocytes as increased APD, altered APD pacing rate dependence, an increased incidence of early and delayed afterdepolarisations, and an abnormal response to beta-adrenergic stimulation [62]. There is further evidence from a mouse model of HCM that

I_{NaL} is upregulated at 1 month of age, suggesting that ionic remodelling may be an early development in the disease [67].

3.3.2 ECG evidence

Because measurements of subcellular ion channels require *in vitro* experimentation, and human samples are scarce, evidence of abnormal repolarisation in HCM is far more abundant as measured non-invasively on the ECG.

Slowed repolarisation may be reflected in the QT_c interval, as prolonged QT_c ($>$ 480 ms) occurs in as many as 1 in 8 HCM patients, which is more than twenty-fold that in the general healthy population [155]. Of note, slowed activation contributes equally to slowed repolarisation in causing prolonged QT_c in HCM, as the QRS duration and JT_c interval are both 34 ms longer on average in HCM patients with $QT_c > 480$ ms [155]. Therefore, QT_c interval prolongation is not specific to slowed repolarisation in HCM. The more repolarisation-specific JT_c interval, although likely a better index of slowed repolarisation, is not widely used clinically and thus it is scarcely reported in HCM. As such, both the QT_c and JT_c intervals offer some insight as to the role of slowed repolarisation of HCM. It is further notable that prolongation of QT_c and JT_c intervals in HCM may be heterogeneous among leads, as reflected by measurements of QT_c and JT_c dispersion of up to 150 ms [394].

Another possible manifestation of ionic remodelling on the ECG in HCM is the presence of pathological T wave inversions, particularly where T wave inversion is unexplained by other factors (such as being secondary to abnormal depolarisation) [200]. In previous computational modelling of HCM, it was shown that apex-to-base repolarisation gradients (secondary to ionic remodelling in regions of hypertrophy) may in part explain T wave inversions in HCM [201].

Finally, ionic remodelling in HCM may manifest as dynamic repolarisation abnormalities. During exercise, the QT_c interval is reported to abnormally increase in HCM [62], which is mechanistically explained by an abnormal response of HCM-remodelled cardiomyocytes to beta-adrenergic simulation [89]. There is further increased 24-hour variability in T wave morphology, which could be attributed to interactions between ionic remodelling and circadian or pacing rate effects [202].

3.3.3 Spatial distribution of ionic remodelling

It is notable that, whereas the spatial distribution of perfusion (as a surrogate for myocardial ischaemia) may be imaged with high-resolution pixel-wise perfusion CMR, significant uncertainty remains as to the spatial distribution of ionic remodelling in HCM. Human HCM samples originate only from the parts of the hypertrophied septum being surgically removed [66], and measures to extract spatial repolarisation information from the 12-lead ECG remain limited [317, 372]. Even using novel techniques such as electrocardiographic imaging (ECGI), where spatial electrophysiological data is derived from hundreds or thousands of vest-worn unipolar electrodes, repolarisation duration is still only characterised at the epicardial surface, missing the septum entirely. Nonetheless, even at the epicardium, repolarisation has been measured with ECGI as more spatially heterogeneous than in controls [157].

In the *in vitro* experiments, slowed repolarisation was independent of the sarcomeric causal variant, suggesting that ionic remodelling may be a downstream effect of hypertrophic remodelling in HCM [66]. This notion is consistent with reports in which QT_c was associated with maximum LV wall thickness [155], and associations between JT_c dispersion and LV wall thickness heterogeneity [319]. Of note, however, one study reports prolonged QT_c in HCM patients with a particular sarcomeric causal variant even in the absence of LV hypertrophy [156]. Finally, a spatially heterogeneous pattern of ionic remodelling is expected to contribute to T wave inversions in HCM [201].

3.3.4 Prognosis

Several studies have analysed associations between ECG measures of repolarisation and prognosis in HCM (Table 3.5). Variability between the associations reported may in part be due to differences between adult vs. childhood HCM cohorts [262, 393] and selected vs. unselected cohorts [216].

Ref Year	N HCM+/−	Follow-up (years)	Summary of findings
[34] 1993	26 / 13	N/A	QT_c and QT_c dispersion associated with ventricular arrhythmias^U
[393] 1998	99 / 0	5	QT_c dispersion associated with mortality^U
[394] 2001	46 / 0	4 ± 3	QT_c dispersion and JT_c dispersion associated with SCD^U
[216] 2001	254 / 69	8 ± 6	QT_c and QT_c dispersion unrelated to SCD^U
[275] 2010	116 / 78	10	QT_c and pathological T wave inversion associated with cardiac arrest^U
[23] 2013	164 / 0	6 ± 4	QT_c associated with ventricular arrhythmias^M
[82] 2015	195 / 0	6 [3, 9]	QT_c associated with ventricular arrhythmias^M
[25] 2016	1004 / 0	7 ± 7	QT_c associated with adverse cardiac events^M
[205] 2017	221 / 0	4 [2, 9]	QT_c dispersion associated with SCD^M
[121] 2020	127 / 0	6 ± 2	Abnormal repolarisation associated with ventricular arrhythmias^M
[404] 2022	149 / 0	3 [2, 6]	QT_c associated with ventricular arrhythmias^M
[262] 2022	356 / 0	4 [2, 8]	QT_c and pathological T wave inversion unrelated to ventricular arrhythmias^M

Table 3.5: Studies that investigated the association between abnormal ECG repolarisation and prognosis in HCM patients. Follow-up durations given as mean or median, with variability given as ± standard deviation or [lower quartile, upper quartile], where available. ^{U}Univariate analysis; ^{M}Multivariate analysis. N HCM+/−: numbers of HCM patients and non-HCM controls; SCD: sudden cardiac death.

Of note, some studies report an incremental improvement in SCD risk stratification by supplementing conventional risk factors with ECG repolarisation metrics [82, 121, 205, 404]. In one study, a composite ECG risk scoring system was devised for use in childhood HCM, based on various ECG metrics [275]. External validation of this composite ECG risk score found it comparable to the performance of clinical guidelines for childhood HCM [262]. Interestingly, close monitoring of individual HCM patients in one small study found that VF tended to occur only beyond a critical threshold of QT_c dispersion [239].

CHAPTER 4

Computational modelling and simulation of cardiac electrophysiology

This chapter introduces the computational techniques used to simulate cardiac electrophysiology throughout the thesis. This includes the mathematical modelling of subcellular ionic currents, which are combined to form the model of cardiomyocyte electrophysiology. The coupling of these models in space with diffusion equations is then described, later used to simulate electrical propagation at the tissue and organ scales in the MonoAlg3D simulator. Finally, following the review of myocardial ischaemia and ionic remodelling in HCM in the previous chapter, this chapter explains how these functional disease factors were modelled.

4.1 Modelling action potentials

Cardiac electrophysiological behaviour can be simulated by modelling the ion channels, pumps and exchangers that control ion movement across the cardiomyocyte membrane. These can be combined into a model of the cardiomyocyte AP capable of reproducing real AP behaviours, such as pacing rate dependence of the APD, cellular refractoriness, the response to drugs, and subcellular Ca^{2+} handling. Ionic currents in cardiomyocyte electrophysiology models are most frequently formulated using the approach developed by Hodgkin and Huxley [9], as described next.

4.1.1 Hodgkin–Huxley formulation of ionic currents

The original Hodgkin–Huxley model is an early model of squid nerve cell electrophysiology [135]. Although naively far from the human ventricular cardiomyocyte, this Hodgkin–Huxley formulation provided a mathematical formalism of ionic currents extensible to other excitable media, including cardiac muscle. Within a decade of its inception in 1952, the Hodgkin–Huxley formulation had been applied by Prof. Denis Noble at Oxford to model the APs of cardiac pacemaker and Purkinje cells [258, 259], and it remains the main formulation used in modern cardiac AP models [357].

The original Hodgkin–Huxley model expressed the movement of ions in and out of the squid nerve cell as three ionic current densities: I_{Na} (flow of Na^+), I_K (flow of K^+) and I_l (pooled flow of other ions). For each of these ionic current densities, they modelled the changes in ion channel permeability that occur during the AP, where permeability changes to allow ions to passively flow along electrochemical gradients. They expressed the current density $I_i(t)$ at time t for each type of ion i as

$$I_i = g_i(V_m - E_i) \tag{4.1}$$

where g_i is the conductance of ion channel i, $V_m(t)$ is the transmembrane potential, and E_i is the equilibrium or Nerst potential of ion type i [135]. The equilibrium potential is the ion-dependent membrane potential at which there is no net flow of that particular ion type. Although Hodgkin and Huxley take E_i to be constants, these can in general be calculated as

$$E_i = \frac{RT}{zF}\ln\left(\frac{[i]_e}{[i]_i}\right) \tag{4.2}$$

where R is the molar gas constant, T is temperature, z is ion valence, F is the Faraday constant, and $[i]_e$ and $[i]_i$ are the extracellular and intracellular concentrations of ion i respectively.

Unlike that of an ohmic resistor (for which $V = IR$), ion channels typically have a non-linear I/V relationship. For example, rectifier channels have an asymmetric I/V relationship that allows only unidirectional ion flow [118]. In general, the form of conductance g_i is assumed based on the ion channel

gating mechanism observed and is optimised to best fit the experimental data, typically varying in time t and with V_m. For example, for the movement of Na^+ across the squid nerve cell membrane, experiments motivated g_{Na} to be assumed proportional to the number of internal membrane sites occupied by three activating molecules but that are not blocked by an inactivating molecule. This motivated a form of g_{Na} that is dependent on gating variables m and h for activation and inactivation molecules, respectively. This was expressed as

$$g_{\mathrm{Na}} = \bar{g}_{\mathrm{Na}} m^3 h \tag{4.3}$$

where $\bar{g}_{\mathrm{Na}}$ is the maximal Na^+ conductance, m is the proportion of activating molecules *inside* the membrane and h is the proportion of inactivating molecules *outside* the membrane. The movement of activating and inactivating molecule types are described by differential equations given by

$$\frac{dp}{dt} = \alpha_p(1-p) - \beta_p p, \tag{4.4}$$

for $p \in [m, h]$, where α_p and β_p are molecule-specific rates of transfer across the cell membrane. The general form of transfer rates used in Hodgkin–Huxley models is given by

$$\alpha(V) = \frac{a + bV_m}{c + ge^{\frac{V_m+d}{f}}} \tag{4.5}$$

where the parameters (a, b, c, d, f, g) can be experimentally derived for the given gating mechanism [255]. In many cases, including in the Hodgkin–Huxley model, many of these parameters reduce to zero. Of note, most AP models based on the Hodgkin–Huxley formalism model the closure of the fast component of the Na^+ current as the product of two inactivation gates with different kinetics, commonly denoted as h and j.

With the transfer of activating and inactivating molecules well described, g_i encapsulates the variation of ion channel permeability for each ion type i, giving rise to realistic behaviour of each ionic current density I_i. The total current density attributable to ion channels across the cell membrane is therefore $\sum_i I_i$. The total current density across the cell membrane must also include a capacitative current, because the cell membrane acts as a capacitor by electrically insulating intracellular and extracellular

space. The total membrane current density can therefore be expressed as

$$I = C_m \frac{dV_m}{dt} + \sum_i I_i \tag{4.6}$$

where C_m is the capacitance per unit area of the cell membrane.

As an alternative to the Hodgkin–Huxley formulation of ionic currents, the Markov model formulation (characterised by stochastic transitions between a finite set of states) is also sometimes used. Notably however, comparative simulations of ventricular APs using Hodgkin–Huxley and Markov model formulations have shown that AP biomarkers are almost identical between the two approaches [40]. The Hodgkin–Huxley formulation is typically preferred over the Markov model formulation due to its reduced computational complexity, particularly for resource-intensive tasks such as organ-scale simulations.

4.1.2 Action potential model choice

A recent review describes over 60 major mathematical models of cardiomyocyte electrophysiology [9], formulated to model cardiomyocytes of different species (from rabbits to humans), variable cell type (from atrial to ventricular, and even cells of the fast conduction system), and with variable biophysical detail and experimental validation. The optimal AP model to use depends upon the given application and hypothesis. In this thesis, which aims to investigate electrophysiological disease mechanisms in human HCM ventricles, the applicable AP models were initially narrowed to the < 10 human ventricular cardiomyocyte AP models [9, 357].

Then, two crucial considerations were: (1) that the AP model contains all the (validated) behaviours relevant to each research question, and (2) that the AP model is of sufficient computational simplicity for simulations to be feasible across a parameter space considered satisfactory for the given investigation. Therefore, the optimal AP model was considered to be one of sufficient biophysical detail that retains all of the relevant validated AP behaviours. However, predicting a priori the optimal relevant biophysically-detailed AP model is challenging, especially for an investigative study of mechanisms. Nonetheless, the use of an AP model validated for investigations of HCM ionic remodelling and acute ischaemic effects were clear minimum requirements for this thesis. In practice, the human ventricular Tomek et

al. (ToR-ORd) AP model [357], as an extension of the O'Hara–Rudy (ORd) model [265], was used throughout. This is justified next in section 4.1.3.

4.1.3 The ToR-ORd human ventricular action potential model

The ToR-ORd AP model describes the movement of ions between cellular subspaces and in/out of the cardiomyocyte via 19 currents/fluxes each described by a Hodgkin–Huxley, or Markov model formulation (Fig. 4.1) [357].

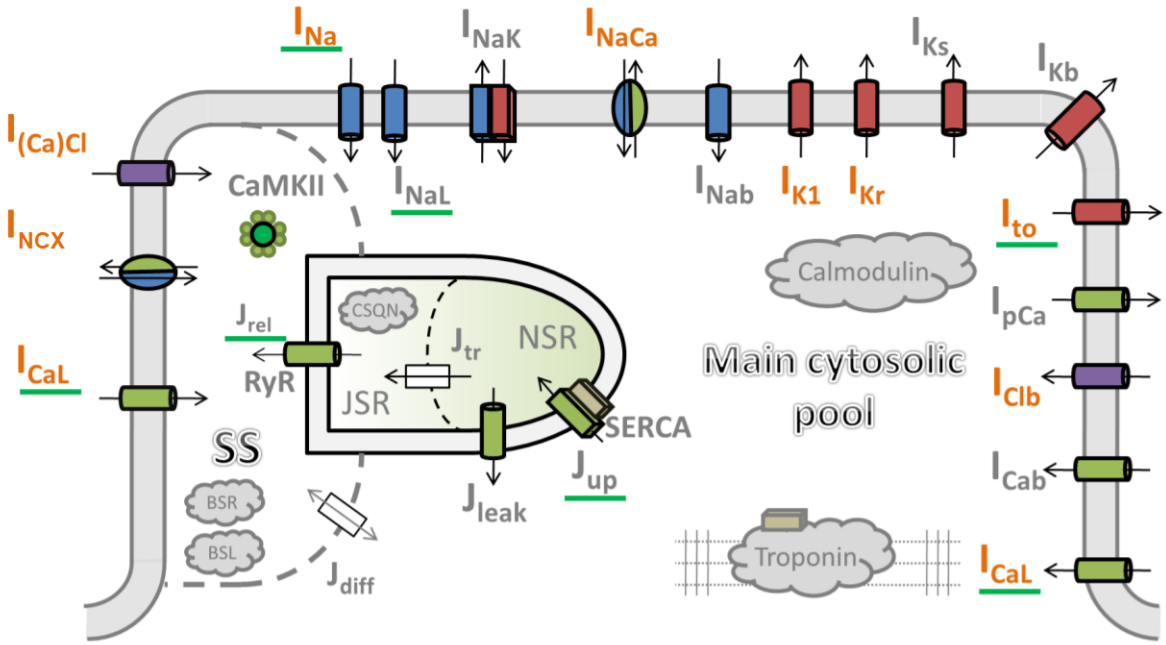


Figure 4.1: The ToR-ORd cardiomyocyte model. The model is divided into: the main cytosolic space, the junctional subspace (SS), the junctional sarcoplasmic reticulum (JSR) and the network sarcoplasmic reticulum (NSR). The currents between extracellular and the main cytosolic space are the: early and late Na^+ currents I_{Na} and I_{NaL}; Na^+/K^+ pump I_{NaK}; sarcolemmal component of the Na^+/ Ca^{2+} exchange current I_{NCX}; background Na^+, Ca^{2+}, K^+ and Cl^- currents I_{Nab}, I_{Cab}, I_{IKb} and I_{ClB}; inward rectifier K^+ current I_{K1}; rapidly delayed rectifier K^+ current I_{Kr}; slow delayed rectifier K^+ current I_{Ks}; transient outward K^+ current I_{to}; sarcolemmal Ca^{2+} pump I_{pCa}; and the sarcolemmal component of the L-type Ca^{2+} current I_{CaL}. The currents between extracellular and junctional subspace are the: Ca^{2+}-sensitive Cl^- current $I_{(Ca)Cl}$ alongside the junctional components of I_{NCX} and I_{CaL}. Diffusion between the junctional subspace and the main cytosolic space is mediated by the diffusion flux J_{diff}. Fluxes transiting the

sarcoplasmic reticulum are the: ryanodine receptor Ca^{2+} release flux J_{rel} from the JSR into the SS; Ca^{2+} uptake via the SERCA pump J_{up}, and Ca^{2+} leak flux J_{leak} between the cytosolic space and the NSR. Adapted under Creative Commons license [357].

The ToR-ORd model was chosen because of its:

(i) Validation of the HCM slowed repolarisation phenotype secondary to ionic remodelling [89], modelled in Chapters 5–8.

(ii) Validation of hyperkalaemia-induced postrepolarisation refractoriness during ischaemia, in addition to its model predecessor being selected as highly suitable for ischaemia simulations in a previous sensitivity analysis [91], relevant for the modelling of ischaemia in Chapters 5–7. Of particular relevance to this thesis, the former ORd model required *ah-hoc* modifications to support AP propagation under ischaemic insults.

(iii) Validation of drug blocks and drug safety predictions, relevant for the modelling of ranolazine in Chapter 8.

(iv) Calibration to human myocardial CV, relevant to simulations of ventricular arrhythmias in Chapters 6 and 8.

(v) Validation of APD pacing rate dependence, relevant for simulations of stress (exercise) ECGs in Chapter 7.

(vi) Validation of human QRS durations and QT intervals in ECG simulations, relevant for ECG investigations in Chapters 7 and 8.

The ToR-ORd AP model is also calibrated or validated in relation to various other criteria, in addition to being the latest generation in the evolution of human ventricular cardiomyocyte AP models [357]. Further to its extensive validation, it is capable of simulating important cellular arrhythmic triggers such as early afterdepolarisations (seen previously in Fig. 2.6A), and different cell types of the ventricular myocardium including endocardial and epicardial types (seen previously in Fig. 2.3B).

4.1.4 Populations of models

The ToR-ORd model describes average behaviour of the human ventricular cardiomyocyte AP. However, in section 2.3 it was established that there is a large range of ECG biomarkers considered normal. Typical QT_c and JT_c intervals (as surrogates for the cellular APD) have a $>$ 100 ms range, yet ventricular APDs are on average around 300 ms, illustrating the significant electrophysiological relative variability in healthy humans. *In vitro* human cellular recordings of APD also exhibit substantial relative variability in the same studies, as well as in other AP biomarkers [31, 253]. This is particularly important in the context of ventricular arrhythmias and SCD, as these events may be fine-tuned and rare, rather than the average behaviour. For example, drugs with known proarrhythmic risks have $<$ 1% incidence of such adverse effects [390].

The populations of models methodology involves repeating a simulation protocol for a broad range of model parameters that are representative of real electrophysiological population variability [30]. Populations of AP models are usually constructed in 2 steps: (1) ionic current conductances g_i are randomly varied within some $\pm$ X% of their baseline model values to create a pool of candidate AP models, then (2) candidate AP models are added to the final population if all their AP biomarkers are within experimentally recorded ranges [253]. In this way, electrophysiological variability is assumed to be predominantly determined by variability in maximal ionic conductances, rather than in kinetics.

In addition to explaining intersubject electrophysiological variability [30], the approach has already demonstrated applications in preclinical drug cardiotoxicity assessment [281], with increasing interest from drug regulatory authorities. Also of relevance to this thesis, populations of AP models with HCM ionic remodelling have been used to investigate ionic profiles associated with cellular arrhythmias [282] and variability in the response to beta-adrenergic stimulation in HCM [89].

4.2 Modelling cardiac electrical wavefront propagation

The arrhythmic substrate is a crucial component of clinically significant arrhythmias, as previously explained in section 2.5. Yet, study of the arrhythmic substrate in humans *in vivo* is not routinely performed due to its invasiveness. Study of arrhythmia mechanisms in humans is often confined to the

cell scale [66], with substrate-level mechanisms typically confined to animal models [148, 386]. The offering made by the computational approach in this thesis is the increased feasibility of mechanistic investigations of *human* cardiac electrophysiology at the *organ* scale. For this to be realised, modelling of electrical conduction and electrophysiological heterogeneity is required.

Cardiac electrical wavefront propagation can be described with reaction-diffusion equations, where the cellular AP described by ionic currents across intracellular and extracellular space (reaction) is coupled in a spatial domain allowing electrical activity to propagate (diffusion). In other words, the membrane potential $V_m(t)$ in section 4.1.1 becomes $V_m(\vec{x}, t)$, where $\vec{x}$ is a position in the spatial domain. This assumes a continuum approach, where differential equations are solved in spatially discretised units representative of a group of cardiomyocytes. In this thesis, the monodomain model is used.

4.2.1 Monodomain model

The monodomain model is a reaction-diffusion partial differential equation (PDE), where the transmembrane current density from Eq. (4.6) is coupled to a diffusion term, which approximates the diffusion of ions in space. This formulation assumes that intracellular and extracellular conductivity ratios are the same, and that Ohm's law applies [7]. The monodomain equation is given by

$$\frac{\lambda}{1+\lambda}\nabla \cdot (\sigma_i \nabla V_m) = \chi \left(C_m \frac{\partial V_m}{\partial t} + \sum_i I_i \right), \tag{4.7}$$

where V_m is the membrane potential, σ_i is the intracellular conductivity tensor, C_m is the membrane capacitance, I_i is ionic current i, χ is the surface-to-volume ratio of the cell, and λ is the ratio between intracellular and extracellular conductivities $\lambda = \frac{\sigma_i}{\sigma_e}$. The monodomain equation was solved with no-flux boundary conditions, such that current did not flow into/out of the spatial domain, imposed by

$$\hat{n} \cdot (\sigma_i \nabla V_m) = 0 \tag{4.8}$$

at the surface boundary of the spatial domain, where $\hat{n}$ is the surface normal. Simulations of organ-scale electrical wavefront propagation have shown excellent agreement between ventricular activation times derived from the monodomain model and more detailed alternative diffusion modelling methodology (see

also the bidomain model [7, 294]). The monodomain model was therefore used in this thesis as it is less computationally complex to solve than the bidomain alternative, and behaviours requiring a more detailed bidomain model (such as defibrillation) were not considered in this work.

4.2.2 The MonoAlg3D simulator

MonoAlg3D is the open-source scientific computing software used in this thesis to solve the 3D monodomain equation [315]. Briefly, the reaction (a system of non-linear ordinary differential equations (ODEs), here encoding the ToR-ORd AP model) and diffusion (a linear parabolic PDE) components of the monodomain model are split using Godunov operator splitting, and solved separately in discrete time steps in a spatial domain discretised using the finite volume method (as hexahedral volumes) [315].

The use of MonoAlg3D was motivated by its optimisation for use on graphics processing units (GPUs), which significantly accelerates runtime, permitting simulation studies of a larger scale. MonoAlg3D also supports adaptive timestepping in the solving of ODEs, which attenuates the computational complexity of solving the ToR-ORd AP model.

4.2.3 Multiscale modelling and simulation of cardiac electrophysiology

Multiscale modelling and simulation of cardiac electrophysiology involves integrating models of various biological organisation across spatial scales (from subcellular ion channels, to the cardiomyocyte AP, to the tissue and organ scales) to investigate the electrical activity of the heart (Fig. 4.2).

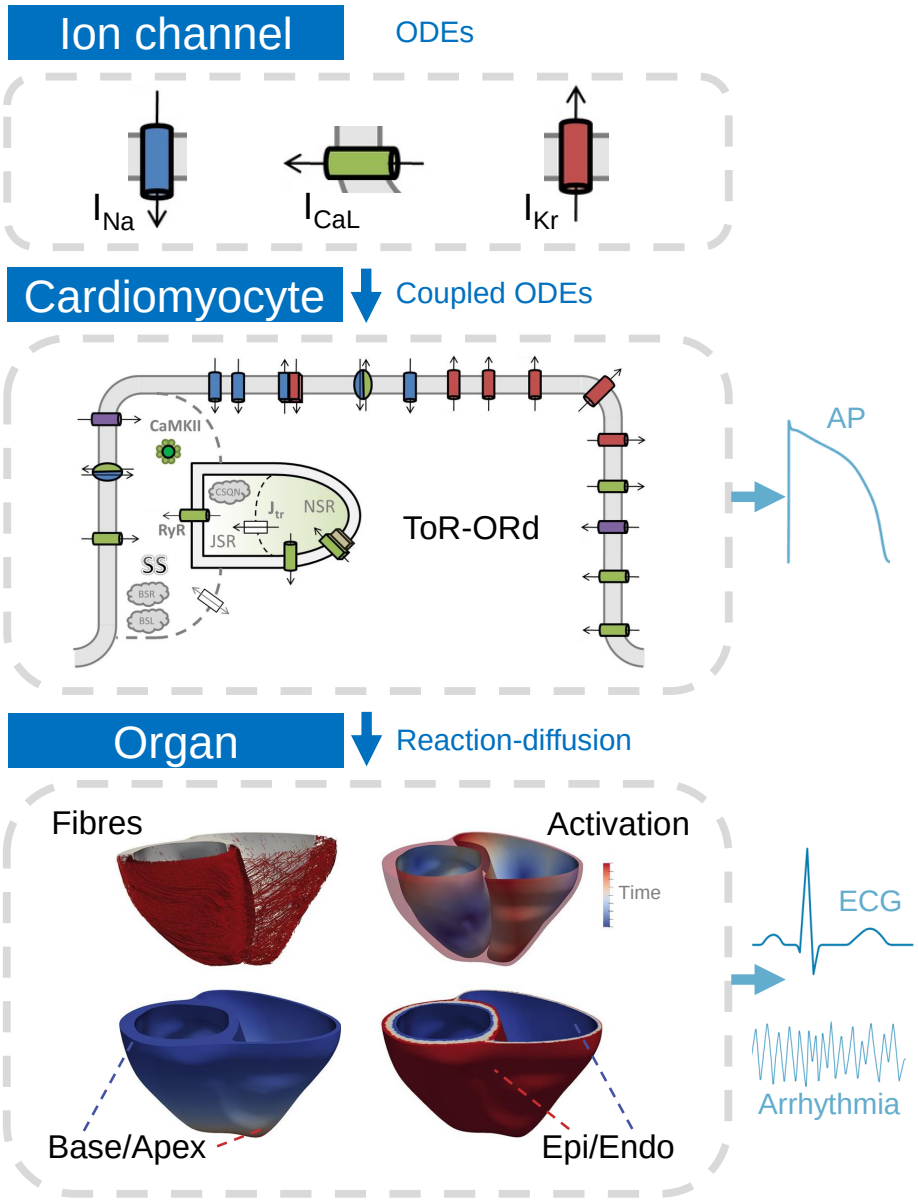


Figure 4.2: Multiscale modelling and simulation of cardiac electrophysiology [75]. Major ionic currents are described with ODEs, which are coupled together to form a model of the ventricular cardiomyocyte AP. AP models are solved on a spatially discretised volume (a mesh) with a diffusion term, to model myocardial AP propagation. At the organ scale, biventricular models are anatomically detailed with fibres (locally describing the orientation of preferential conduction), endocardial activation sequences (approximating the sequence of stimulation by the Purkinje fibres), apex-to-base APD gradients, and endocardial/epicardial cell types. Adapted under Creative Commons license [357, 374].

The cell, cable, tissue and organ scales

The spatially discretised volume on which the monodomain equation is solved is termed the mesh, which is formed of hexahedral volumes in MonoAlg3D. Although the overall aim of this thesis is to investigate realistic human arrhythmia dynamics and ECG biomarkers, there are advantages to simulating cardiac electrophysiology in spatial domains of variable complexity (not just at the organ scale). There is always a careful balance to be struck between the physiological accuracy required for a given research question and the computational complexity of the involved simulations. In increasing complexity order, spatial domains considered in this thesis include:

(i) The single cell (0D), which can be used to measure simple AP biomarkers such as the APD and the incidence of cellular arrhythmic triggers (Fig. 2.6A) under various conditions, without any electrical propagation.

(ii) The cable domain (1D), which consists of volumes coupled along a single axis where electrical propagation is possible. Direct measurements of the ERP and CV can be made in the cable domain, which are not possible in single cells unless surrogate biomarkers are used.

(iii) The tissue domain (2D), a 1 layer thick slab, where it is possible to simulate how more complex behaviours like re-entrant wavefronts emerge from tissue heterogeneities (Fig. 2.6B).

(iv) The biventricular domain (3D), an anatomically detailed volume representative of the human ventricles, which can be used to investigate arrhythmia mechanisms in a physiologically accurate environment (Fig. 2.6C). Realistic human ECGs can be derived from biventricular simulations, which can be used for both validation purposes and to investigate effects on ECG biomarkers.

Due to the large number of mesh elements, simulations of arrhythmia dynamics in the biventricular domain require significant amounts of computational resources, such that limited simulations are feasible, which often precludes a thorough analysis of parameter sensitivity. Therefore, the tissue domain can be used to investigate arrhythmia mechanisms across a wider parameter space (and include features like populations of AP models), to supplement the biventricular simulations.

Modelling organ-scale anatomical and electrophysiological detail

The specific modelling methods used in the organ-scale simulations of this thesis are now described. Existing biventricular meshes derived from CMR scans were used, as constructed in previous work [201]. This included one mesh derived from an HCM patient with septal hypertrophy, and another mesh from an HCM patient with apical hypertrophy.

These meshes included heterogeneous fibre orientations modelled by defining local longitudinal, transverse, and transmural directions using rule-based methods, as in previous works [41, 201], with anisotropic conductivity $\sigma_{\text{longitudinal}} > \sigma_{\text{transverse}} \approx \sigma_{\text{transmural}}$ [348]. The exact conductivities were tuned to human CV measurements [348] (see later section 4.3).

A realistic human ventricular activation sequence was used to periodically electrically stimulate the meshes, as developed in previous work [41, 201]. Briefly, the activation sequence begins at 7 sites on the endocardium, identified as the earliest points of activation resulting from the human fast conduction system. Each mesh element on the endocardial surface was prescribed a stimulus time proportional to its distance to its closest point of the 7 sites, as computed with Dijkstra's algorithm. Therefore, the entire endocardium was prescriptively activated over a period of around 70 ms, which then propagated into the myocardium via reaction-diffusion. ECGs derived from simulations using such activation sequences had realistic human-like QRS complexes [41].

Transmural APD gradients were retrieved through using the endocardial and epicardial cell types as defined in the ToR-ORd model [357]. In the meshes, the inner 70% of transmural width was defined as endocardial and the outer 30% as epicardial cells, as in previous biventricular modelling, to retrieve ECGs with T waves of appropriate polarity, magnitude and duration [65].

Apex-to-base APD gradients were also retrieved by rescaling the maximal I_{Ks} conductance for each mesh element by an (exponential) scaling factor in distance from a point defined at the apex, in the range 0.2–5, as in previous work [201]. The maximal I_{Ks} conductance scaling factor was smallest at the base (0.2×) and greatest in the apex (5×), such as to reproduce the experimentally reported shorter APDs at the apex [301].

Data availability

The meshes (tissue and biventricular), modified MonoAlg3D source code and configuration file templates required to reproduce the simulations described in this thesis are available online (DOI: 10.5287/ora-exzbr0nny).

4.3 Tuning conduction velocity: spatial discretisation

The ToR-ORd AP model was developed to be able to produce myocardial CV that is consistent with human experimental measurements of around 65 cm/s [357]. To ensure that this benchmark was met in the MonoAlg3D framework, longitudinal, transverse and transmural conductivities were tuned in cable simulations to human experimental measurements [348]. A key consideration in tuning the CV was that the CV is sensitive to the spatial discretisation scheme (dx), whereas AP properties such as the AP are mostly insensitive to dx [55]. Therefore, dx was considered simultaneously with the CV. In practice, the conductivities $\sigma_{\text{longitudinal}} = 2.52$ mS/cm and $\sigma_{\text{transverse}} = \sigma_{\text{transmural}} = 1.57$ mS/cm were used, to produce agreement with human CV measurements without excessive error in CV for the chosen dx (Fig. 4.3).

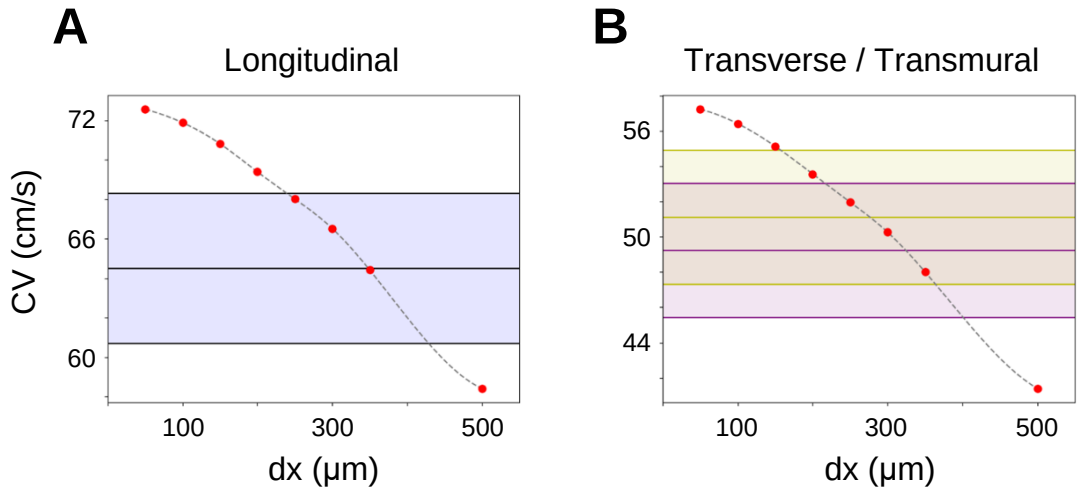


Figure 4.3: Myocardial conduction velocity (CV) vs. spatial resolution (dx) in the (A) longitudinal and (B) transverse/transmural directions for the chosen conductivity parameters, for dx = [50, 100, 150, 200, 250, 300, 350, 500] μm. Highlighted regions in CV correspond to human experimental measurements of

CV (mean ± SEM) along the longitudinal (blue), transverse (purple) and transmural (yellow) directions [348].

The spatial discretisation dx was required to be (1) sufficiently resolved to preclude artefactual wavebreak and erroneous re-entry dynamics, (2) able to produce human CV, (3) sufficiently resolved to discern endocardial from epicardial cells in anatomical reconstructions of the human ventricles (minimum wall thickness can reach 1–2 mm [134]), and (4) sufficiently coarse to curtail simulation runtime complexity.

These requirements are in general dependent on the computational modelling and simulation framework used, and there is not a universally prescribed dx, such that the recommendation by Clayton et al. is that solutions for a given investigation are compared for agreement across spatial resolutions [55]. Therefore, subsets of both arrhythmic risk and ECG investigations were repeated for a range of dx (see later Appendix Figs. A.6 & A.18). Notably, measures of arrhythmic risk across populations of AP models were similar across spatial resolutions even up to dx = 500 μm. Although re-entrant wavefronts were delayed at coarser dx reflecting reduced CV, re-entry dynamics were similar and artefactual break-up was not observed. This is in-line with the use of adaptive meshing up to dx = 400 μm in the benchmarking of MonoAlg3D [315], and similar spiral wave evolution in a uniform mesh with dx = 400 μm in another simulation study (even though wavefronts were more jagged) [180]. Spatial resolutions of dx $>$ 400 μm were not used in arrhythmic risk studies to avoid excessive CV error.

4.4 Modelling ionic remodelling in HCM

The ionic remodelling and associated slowed repolarisation in HCM (seen before in section 3.3) has been computationally modelled in previous works. These studies applied rescaling of various AP model parameters to replicate the HCM electrophysiological phenotype [89, 282], based on *in vitro* human HCM voltage clamp, protein expression, and mRNA expression data [66]. The specific changes made are detailed in Table 4.1.

Parameter	Symbol	Effect of HCM remodelling on parameter
Cell volume	V	+90%
Troponin-Ca^{2+} affinity	K_{TRPN}	-50%
Late Na^{+} conductance	g_{NaL}	+165%
Background Na^{+} conductance	g_{Nab}	+165%
Inward K^{+} rectifier conductance	g_{K1}	-30%
Rapidly delayed K^{+} rectifier conductance	g_{Kr}	-45%
Slow delayed K^{+} rectifier conductance	g_{Ks}	-45%
Transient outward K^{+} conductance	g_{to}	-70%
Na^{+}/Ca^{2+} exchange conductance	g_{NCX}	+30%
Na^{+}/K^{+} pump conductance	g_{NaK}	-30%
Ca^{2+} release conductance	g_{rel}	-20%
Ca^{2+} reuptake conductance	g_{up}	-35%
L-type Ca^{2+} conductance	g_{CaL}	+10%
Fast voltage-dependent L-type Ca^{2+} time constant	T_{ff}	+35%
Slow voltage-dependent L-type Ca^{2+} time constant	T_{fs}	+20%
Fast Ca^{2+}-dependent L-type Ca^{2+} time constant	T_{fcaf}	+35%
Slow Ca^{2+}-dependent L-type Ca^{2+} time constant	T_{fcas}	+20%
Ca^{2+} voltage gating shift	K_{jca}	+15

Table 4.1: Parameters modelled as affected by HCM remodelling, as used in previous HCM investigations [66, 89, 282].

Simulated APs with slowed repolarisation, secondary to the ionic remodelling, are illustrated in Fig. 4.4, as in previous work by Passini et al. [282]. The HCM AP models were validated against experimental measurements of biomarkers including APD50, APD90, $\frac{dV_m}{dt}$, Peak V_m, RMP and Ca^{2+} transient biomarkers. Of note, the work by Passini et al. used the ORd AP model (the predecessor to the ToR-ORd AP model); however, this model of HCM ionic remodelling has been further investigated and validated using the ToR-ORd AP model in other work [89]. Therefore, the formulation of ionic remodelling in HCM described in Table 4.1 is used throughout this thesis.

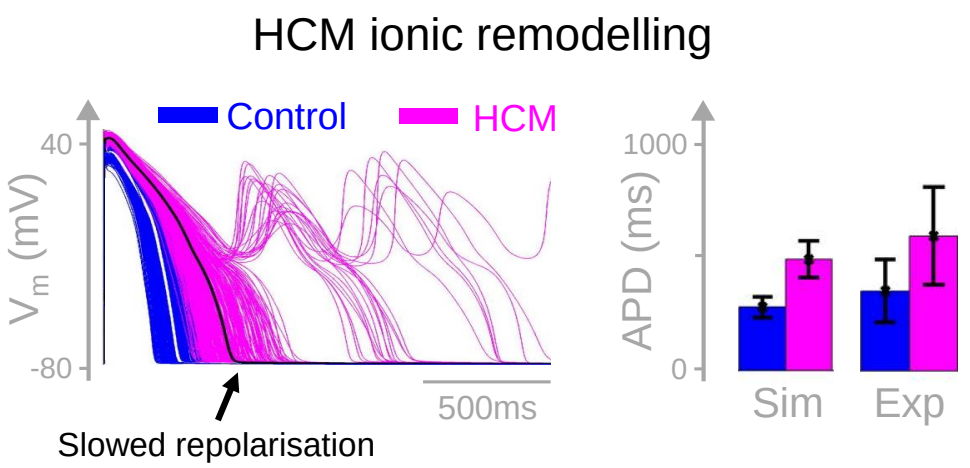


Figure 4.4: Simulated AP populations with HCM ionic remodelling, as in work by Passini et al. [282]. Simulated (Sim) AP biomarkers, including the APD, were validated against human HCM *in vitro* measurements (Exp) [66]. Adapted under Creative Commons license [282].

4.5 Modelling acute myocardial ischaemia

4.5.1 Modelling ischaemic action potentials

In section 2.4.2, the effects of acute stage 1a myocardial ischaemia on the AP and the key factors involved (hyperkalaemia, hypoxia, and acidosis) were described. These effects have been computationally modelled in numerous previous works [45, 92, 228, 309]. The acute ischaemic effects considered throughout this thesis and their origins are now introduced.

Hypoxic activation of I_{KATP} was modelled using a formulation previously developed in agreement with experimental data under healthy and diseased conditions [238], originally formulated to reproduce hypoxic APD decreases [333]. This model of I_{KATP} is given by

$$I_{\mathrm{KATP}} = f_{\mathrm{KATP}}\, g_{\mathrm{KATP}} b \left(\frac{[K^+]_e}{[K^+]_{eN}} \right)^{0.24} (V_m - E_K) \tag{4.9}$$

where f_{KATP} is the fraction of activated channels, $g_{KATP} = 4.3195$ mS/μF is the channel conductance,

$[K^+]_e$ is the extracellular K^+ concentration, $[K^+]_{eN} = 5$ mM is the basal extracellular K^+ concentration, V_m is the membrane potential, and E_K is the K^+ equilibrium potential. The dependence on magnesium ions and molecules MgADP/MgATP that was previously introduced [238] has been simplified to a constant scaling factor $b = 0.01538$ in this form [91, 315].

The degree of I_{KATP} activation in computational electrophysiology models has been investigated in correspondence to experimental measurements of ischaemic APD decreases [91] and dominant frequency behaviour during VF [56]. These analyses found reasonable agreement with experimental recordings for activation fractions equivalent to $f_{KATP} = [0.0, 0.038, 0.075, 0.11, 0.15]$ and $f_{KATP} = [0.0030, 0.023, 0.35]$, where differences in maximal channel conductance have been adjusted for. Of note, these analyses considered I_{KATP} activation with concomitant hyperkalaemia of up to $[K^+]_e = 9$ mM [56, 91], like the degree of ischaemic K^+ accumulation reported experimentally [102]. Downregulation of I_{Na} and I_{CaL} (typically -25%) is considered to be representative of acidosis [309, 334]. Combined hyperkalaemia, hypoxia and acidosis in this form (or similar) is almost ubiquitous among studies in which the electrophysiological effects of acute myocardial ischaemia are computationally modelled [45, 92, 228, 229, 309, 334]. Therefore, and as further reinforced by the experimental evidence related to ischaemia previously described in section 2.4.2, in this thesis ischaemia considered parameters of $[K^+]_e$ in 4–9 mM, f_{KATP} in 0–0.20, and acidosis as a 25% downregulation of I_{Na} and I_{CaL}. Acidosis was kept fixed because its relative contribution to ischaemic AP changes is considered small relative to that of hyperkalaemia and hypoxia, both in simulation [56] and experimental studies [174]. Indeed, a previous computational sensitivity analysis of ischaemia modelled acidosis as a fixed effect [91].

A preliminary sensitivity analysis of how hyperkalaemia and hypoxia affect key AP biomarkers (CV, APD, and PRR) in the ToR-ORd AP model was conducted (Fig. 4.5). The sensitivity analysis shown in Fig. 4.5 was derived from simulations in a 5 cm long cable using the baseline endocardial ToR-ORd AP model.

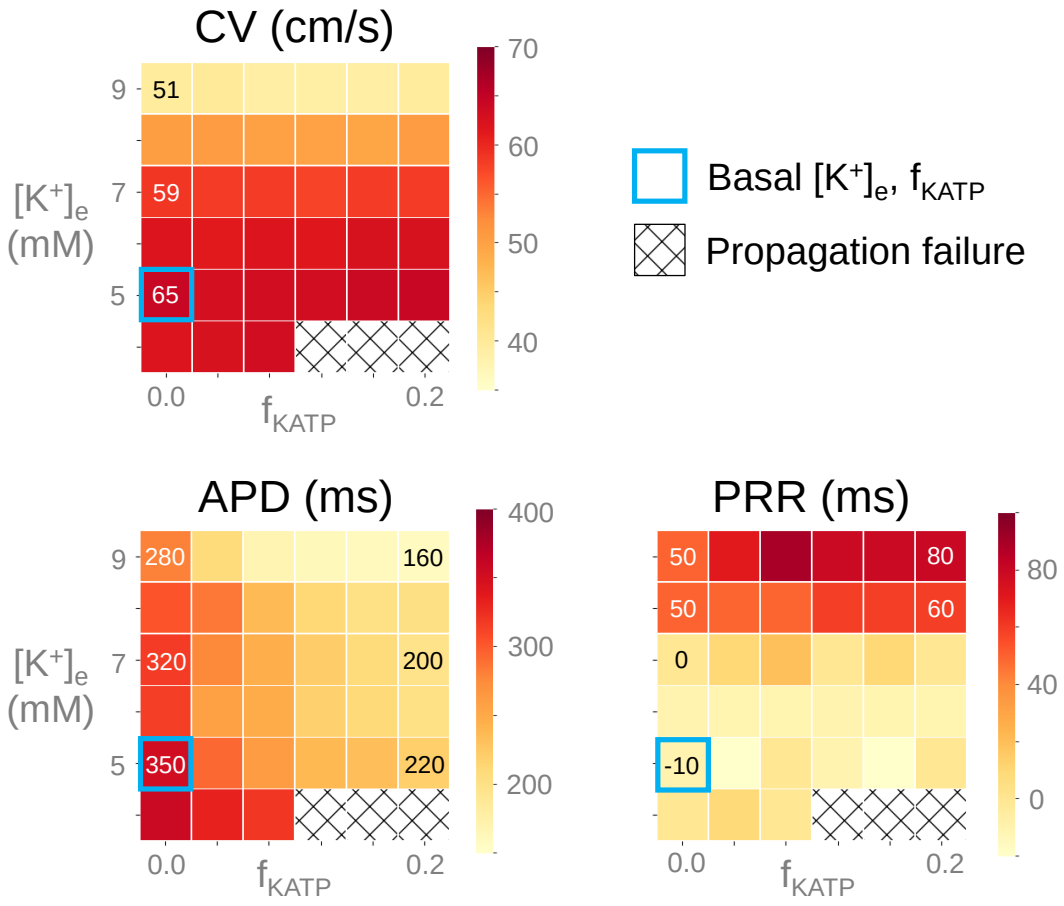


Figure 4.5: Effects of hyperkalaemia (parameterised with $[K^+]_e$) and hypoxia (parameterised with f_{KATP}) on CV, APD and PRR in the ToR-ORd AP model, as measured in cable simulations.

Figure 4.5 shows how decreases in CV in the model are primarily due to hyperkalaemia, decreasing from 65 cm/s at basal $[K^+]_e = 5$ mM to 51 cm/s at $[K^+]_e = 9$ mM, similar to ischaemic CV decreases reported experimentally in humans [348]. The APD was decreased by both hyperkalaemia and hypoxia, and PRR developed, consistent with experimental measurements of APD and PRR in humans [345]. Of note, PRR was primarily determined by the degree of hyperkalaemia, but was enhanced by hypoxia.

4.5.2 Modelling regional acute myocardial ischaemia

Regional acute myocardial ischaemia was modelled in tissue and biventricular domains including (i) the CZ, subjected to the full severity of hyperkalaemia, hypoxia and acidosis; (ii) the BZ, a 0.5 cm wide

region over which the severity of hyperkalaemia, hypoxia and acidosis decreased as a linear function of distance from the CZ edge to the NZ; and (iii) an endocardial border of 0.06 cm in width, unaffected by ischaemia (Fig. 2.5B) [92, 228].

4.6 Measuring arrhythmic risk

The arrhythmic risk associated with a given substrate can be measured in tissue and biventricular simulations by attempting to induce arrhythmia, using a particular sequence of electrical stimulation termed an S1-S2 protocol [92, 228].

This typically involves initially stimulating the mesh with a normal sinus rhythm beat (S1), followed by a premature, ectopic stimulus (S2). The S1-S2 protocol is often repeated for a range of S1-S2 time intervals. For a given arrhythmic substrate, the range of S1-S2 time intervals (or coupling intervals) at which arrhythmia is inducible (termed the vulnerable window), and the type and duration of the resulting arrhythmias, gauges arrhythmic risk. An example of an arrhythmia following the application of S2 is shown in Fig. 2.6C.

The specific S1-S2 pacing protocols used throughout the thesis are now described. S1 refers to the human physiological ventricular activation sequence in biventricular simulations as described in section 4.2, or a planar wavefront applied to an edge of the square domain in tissue simulations. S2 refers to a circular/spherical stimulus of radius 0.5 cm applied at points later defined in Chapters 6 and 8.

Models were initialised with AP model state vectors extracted from single cell simulations after 100 S1 beats. After AP model stabilisation, the S1-S2 protocol consisted of 2 S1 beats at a 1 Hz pacing rate (unless otherwise indicated) followed by S2 at a given S1-S2 time interval. In-tissue experiments were repeated for a range of S1-S2 intervals, varied in 5 ms increments in the range [ERP_0 - T_0, ERP_1 + T_1], where ERP_0 is the ERP of the unaffected myocardium, and ERP_1 is the longer ERP of the ischaemic and/or HCM-remodelled myocardium. Safety margins T_0 and T_1 were set to ensure that (1) ectopic propagation failed at the minimum S1-S2 interval, and that (2) conduction was no longer blocked in the ischaemic and/or HCM-remodelled region at the maximum S1-S2 interval. In some AP models, the range of S1-S2 intervals was extended to ensure that a minimum of 10 S1-S2 coupling intervals were

simulated. In biventricular models, a minimum of 10 S1-S2 intervals were considered, varied in 5 ms increments following the minimum S1-S2 interval for which S2 propagated. In non-ischaemic simulations (such as those in Chapter 8), the APD was used as a surrogate for ERP in defining the S1-S2 interval ranges.

On analysis, arrhythmic risk simulation outputs were classified as either (1) the ectopic failed to propagate; (2) the ectopic propagated but no re-entry occurred (PVC); (3) a single re-entry occurred (PVC couplets); or (4) multiple cycles of re-entry occurred (VT).

Separate from arrhythmic risk, S1-S2 protocols can also be applied to single cells and cable simulations to measure the ERP, by identifying the earliest premature S2 beat for which re-excitation is possible (Fig. 2.2B).

CHAPTER 5

Interplay between cellular ionic remodelling and acute myocardial ischaemia in HCM

This chapter investigates how AP biomarkers are affected by acute myocardial ischaemia in HCM cardiomyocytes with ionic remodelling. This involved the construction of control and HCM populations of AP models, which were then subjected to ischaemia.

5.1 Introduction

The changes in AP biomarkers that occur during acute myocardial ischaemia have been well characterised in healthy cardiomyocytes [91, 345, 348]. However, despite the high incidence of perfusion impairment in HCM (Table 3.1), and extensive ionic remodelling [66], ischaemic electrophysiological changes in HCM have not yet been explored.

Therefore, this thesis chapter aimed to investigate the effects of acute myocardial ischaemia on human HCM-remodelled cardiomyocyte AP biomarkers, focusing on the ERP (as an important determinant of arrhythmic risk) and the APD (due to its manifestation on the ECG). It was hypothesised that the ERP and APD would be modulated by combinations of chronic ionic remodelling and acute myocardial ischaemia in HCM.

5.2 Methods

5.2.1 Creation of control and HCM populations of AP models

The population of models methodology (seen previously in section 4.1.4) was used to create a population of healthy cardiomyocyte models with variability in AP morphology, as typically observed experimentally [31]. 1000 candidate models were generated by randomising the 11 main conductances (g_{CaL}, g_{Na}, g_{to}, g_{NaL}, g_{Kr}, g_{Ks}, g_{K1}, g_{NCX}, g_{NaK}, g_{rel} and g_{up}) within $\pm$50% of their original values using Latin hypercube sampling, with the ToR-ORd ventricular endocardial cardiomyocyte AP model used as a baseline (previously justified in section 4.1.2) [357]. Each candidate model was simulated for 100 beats at 1 Hz pacing rate, and AP and Ca^{2+} transient biomarkers were measured. Models were excluded from the population if any biomarker fell outside of experimentally observed ranges (Table 5.1), resulting in 228 remaining AP models which formed the control AP population. By applying the model of HCM ionic remodelling previously shown in Table 4.1 to each control model, the analogue population of 228 HCM AP models was created [282].

Biomarker	Units	Minimum	Maximum	Ref
APD40	ms	84.9	323.6	[31]
APD50	ms	106.6	349.4	[31]
APD90	ms	178.1	442.7	[31]
APD90 - APD40	ms	61.2	153.0	[31]
Resting V_m	mV	-94.4	-78.5	[31]
Peak V_m	mV	7.3	39.6	[31]
Peak V_m - Resting V_m	mV	92.0	130.0	[282]
Peak Ca^{2+} - Resting Ca^{2+}	nM	230.0	530.0	[282]
Ca^{2+} 50% decay time	ms	90.0	375.0	[282]
Ca^{2+} 90% decay time	ms	200.0	750.0	[282]
Ca^{2+} peak time	ms	40.0	70.0	[282]

Table 5.1: AP and Ca^{2+} transient biomarker ranges used to calibrate the control population of models. APDXX: action potential duration measured at XX% of repolarisation from the peak to resting membrane potential.

5.2.2 Simulation of ischaemic conditions

The populations of control and HCM human AP models were identically subjected to the individual and combined effects of stage 1a acute myocardial ischaemia (hyperkalaemia, hypoxia and acidosis), as previously described in section 4.5.1. AP models were paced for 100 beats with a 1 Hz pacing rate, then AP biomarkers including the APD and ERP were measured.

5.2.3 Measurements of effective refractory period

Because the APD is no longer a reliable surrogate measure of the ERP under ischaemic conditions [345], direct measurements of the ERP were made. ERPs of each AP model were measured in both cellular and cable domains. Cellular ERP measurements were used as estimates of refractoriness to be later used in tissue arrhythmia induction simulations. Cable ERP measurements were used as final measurements of ERP, as reported in the results and figures.

Cellular effective refractory periods

The ERP of each AP model was measured using an S1-S2 protocol (previously introduced in section 4.6) in single cells, where S1 and S2 both refer to electrical stimulation applied to the cell. The S1-S2 interval was varied in 10 ms increments up to the cycle length, then the cellular ERP was defined as the S1-S2 interval for which S2 induced an AP of maximally prolonged upstroke.

Cable effective refractory periods

The ERP of each AP model was measured using an S1-S2 protocol (previously introduced in section 4.6) in a cable of length 5.5 cm, where S1 and S2 both refer to electrical stimulation at one end of the cable. The S1-S2 interval was varied in 10 ms increments up to the cycle length, then the cable ERP was defined as the maximum S1-S2 time interval for which excitation (defined as a membrane potential $>$ -40 mV) of the cable centre point did not occur.

5.2.4 Patch-clamp validation

Briefly, viable single myocytes (n = 12) were obtained from septal samples from HCM patients (N = 5) who underwent septal myectomy and were compared to control myocytes (n = 7) from non-failing non-hypertrophic aortic stenosis patients (N = 3) with bulging septa who underwent myectomy. Of note, these control cells had slightly longer basal APD than totally healthy myocytes. APs were measured in these myocytes at pacing rates of 0.2 Hz and 0.5 Hz, for extracellular K^+ concentrations of $[K^+]_e = 5$ mM and $[K^+]_e = 9$ mM. The studies were approved by the local Ethics Committee and written informed consent was obtained from all participants. See Appendix section A.1.1. for full patch-clamp experimental methods. All patch-clamp experimental data was provided by Dr. Raffaele Coppini, University of Florence. In patch-clamp experiments, the relationship between basal APD and the hyperkalaemic change in APD was assessed using the MATLAB `corrcoef()` function. Hyperkalaemic simulations were repeated at a 0.5 Hz pacing rate to facilitate comparisons with patch-clamp experiments.

5.3 Results

5.3.1 Abnormal response to ischaemia in HCM-remodelled cells

The populations of human AP models (228 control paired to 228 HCM) under basal conditions are shown in Fig. 5.1A. Consistent with experimental evidence [66], the HCM AP models were characterised by markedly prolonged AP and increased ERP, as shown in Fig. 5.1B. Hyperkalaemia caused APD decreases, post-repolarisation refractoriness, and made RMP less negative in both populations (Fig. 5.1C), as is typical of hyperkalaemia [91]. APD shortening also occurred in both populations when subjected to hypoxia (Fig. 5.1D).

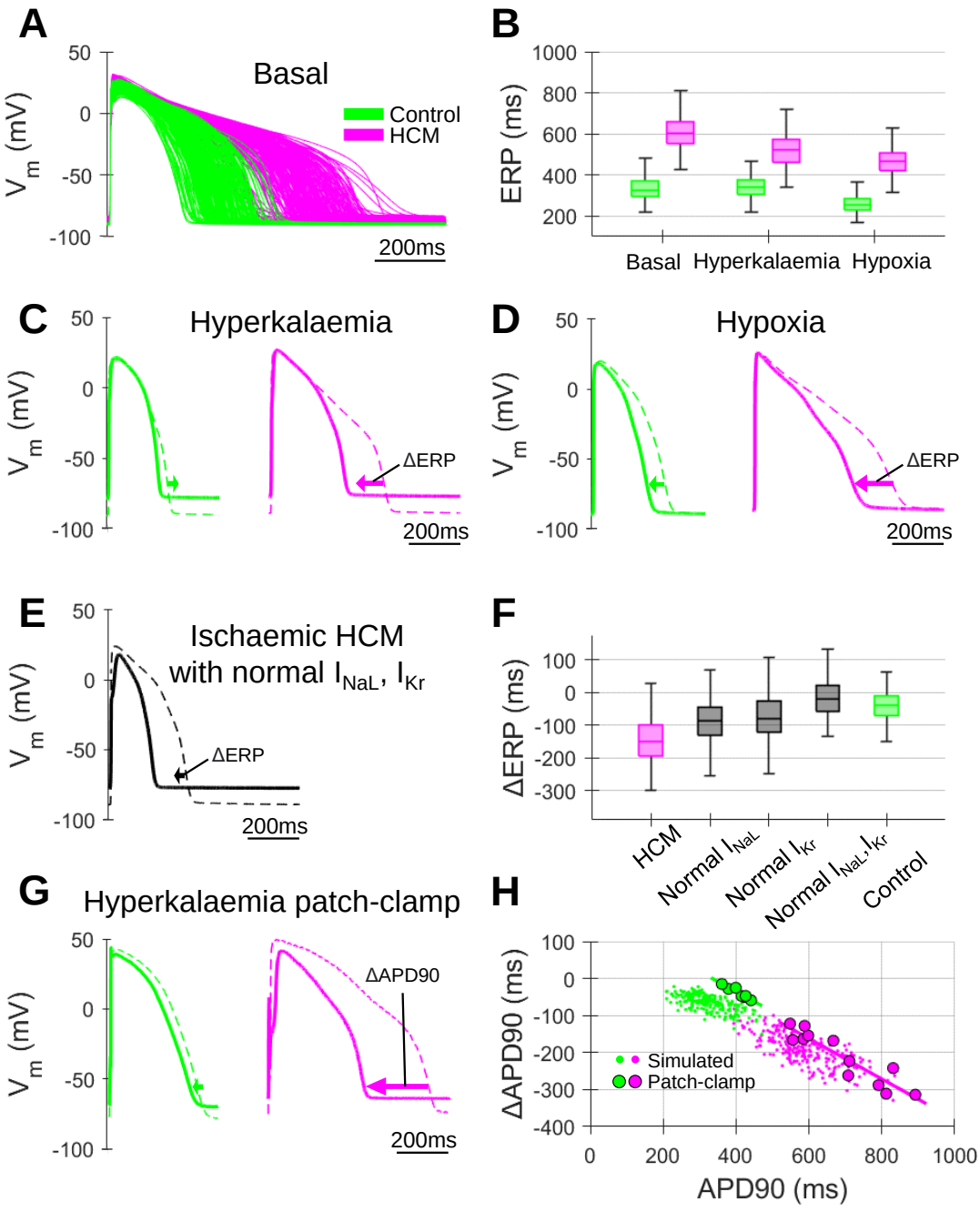


Figure 5.1: Cellular HCM response to ischaemia. (A) Simulated populations of non-ischaemic control (n=228) and HCM (n=228) human AP models. (B) ERPs among the populations under basal, hyperkalaemic ($[K^+]_e = 8$ mM) and hypoxic ($f_{KATP} = 0.09$) conditions, showing abnormal hyperkalaemic and enhanced hypoxic ERP shortening in HCM. (C) Representative simulated AP traces during hyperkalaemia ($[K^+]_e = 8$ mM) (solid) compared to basal conditions (dashed). Arrows

denote change in ERP due to hyperkalaemia. (D) Representative simulated AP traces during hypoxia ($f_{KATP} = 0.09$) (solid) compared to basal conditions (dashed). Arrows denote change in ERP due to hypoxia. (E) Representative simulated AP traces with HCM remodelling except in I_{NaL} and I_{Kr} during ischaemia (hyperkalaemia, hypoxia and acidosis) (solid) compared to basal conditions (dashed). Arrow denotes change in ERP due to hyperkalaemia. (F) The difference in ERP during ischaemia with respect to basal conditions (ΔERP) among populations with full HCM ionic remodelling, HCM except I_{NaL} upregulation, HCM except I_{Kr} downregulation, HCM except both I_{NaL} and I_{Kr} remodelling, and control electrophysiology. (G) Representative patch-clamp human AP traces during hyperkalaemia ($[K^+]_e = 9$ mM) (solid) compared to basal conditions (dashed) paced at 0.5 Hz (n = 12 HCM cells from N = 5 patients; n = 7 control cells from N = 3 patients). (H) The difference in APD90 during hyperkalaemia ($[K^+]_e = 9$ mM) with respect to basal conditions (ΔAPD90) vs. basal APD90 in patch-clamp experiments, compared to the simulated AP models paced at 0.5 Hz. Patch-clamp experiments confirmed the relationship between basal APD and hyperkalaemic APD decreases in control and HCM (both $p < 0.001$).

However, marked differences were observed in the response of ERP to ischaemia between control and HCM AP models. In control models, ERP increased slightly during hyperkalaemia from 330 $\pm$ 60 ms to 340 $\pm$ 50 ms, while instead significantly decreased in HCM models from 600 $\pm$ 80 ms to 520 $\pm$ 80 ms (Figs. 5.1B & 5.1C). In control models, ERP decreased during hypoxia to 260 $\pm$ 40 ms whereas it decreased by a larger extent in HCM models to 460 $\pm$ 60 ms (Figs. 5.1B & 5.1D). Components of the HCM ionic remodelling were selectively removed to identify the cause of these abnormalities, which showed that remodelling of I_{NaL} and I_{Kr} was responsible for the abnormal ERP response to ischaemia in HCM cells (Figs. 5.1E & 5.1F).

The degree of hyperkalaemic AP shortening in HCM (Fig. 5.1C) underlying the hyperkalaemic ERP decreases predicted by the simulation study was experimentally confirmed in patch-clamp experiments of human HCM cardiomyocytes (Figs. 5.1G & 5.1H). An increase in extracellular K^+ concentration from $[K^+]_e = 5$ mM to $[K^+]_e = 9$ mM led to an APD decrease of 210 $\pm$ 70 ms experimentally in human HCM cardiomyocytes, comparable to the decrease of 200 $\pm$ 40 ms identified in simulations. In patch-clamp

experiments, longer basal APDs were associated with greater hyperkalaemic APD shortening in control and HCM ($p < 0.001$ both) (Fig. 5.1H). Although the control cells were from aortic stenosis patients with slightly longer basal APDs than simulated control myocytes, the degree of hyperkalaemic APD shortening was consistent between simulations and patch-clamp experiments.

The ionic mechanisms of I_{NaL} and I_{Kr} responsible for the abnormal APD and ERP response to myocardial ischaemia in HCM are now described. Hyperkalaemic reductions in the APD occurred secondary to decreased I_{NaL} magnitude (Figs. 5.2A & 5.2B), which was caused by a reduced maximal open channel probability imposed by the voltage-dependence of I_{NaL} inactivation gating in the presence of ischaemic RMP elevation (Fig. 5.2C). As ionic remodelling in HCM was characterised by upregulation of I_{NaL} channels [66], I_{NaL} impairment by hyperkalaemia was magnified in HCM, leading to a large ischaemic reduction in this sustained inward current and therefore enhanced APD shortening. Similarly, I_{Kr} was significantly downregulated by ionic remodelling in HCM [66]. Systematically removing this component of HCM ionic remodelling (i.e., increasing I_{Kr}) therefore increased the magnitude of total repolarisation current, shortening APD and bringing it closer to that of control cardiomyocytes. Changes in APD associated with I_{Kr} downregulation under ischaemia were however due to interactions between I_{Kr} and I_{K1}, where combined prolongation of the plateau phase due to HCM remodelling in I_{Kr} and the effect of $[K^+]_e$ on I_{K1} voltage-dependence led to an enhanced hyperkalaemic repolarisation response, in agreement with experimental findings in rabbit ventricular cardiomyocytes [129].

In contrast to the important interactions identified between HCM ionic remodelling and hyperkalaemia and hypoxia, acidosis had similar effects (and of a small magnitude) in both control and HCM populations. Specifically, acidosis alone scarcely affected ERPs in control (330 ± 60 vs. 330 ± 60 ms; acidosis vs. baseline) and HCM (590 ± 80 vs. 600 ± 80 ms) AP models (Fig. 5.3). The main consequence of acidosis was reduced CV in control (57 ± 6 vs. 63 ± 6 cm/s; acidosis vs. baseline) and HCM (56 ± 5 vs. 62 ± 6 cm/s). This 10% reduction in CV was expected based on previous computational modelling of acidosis [334].

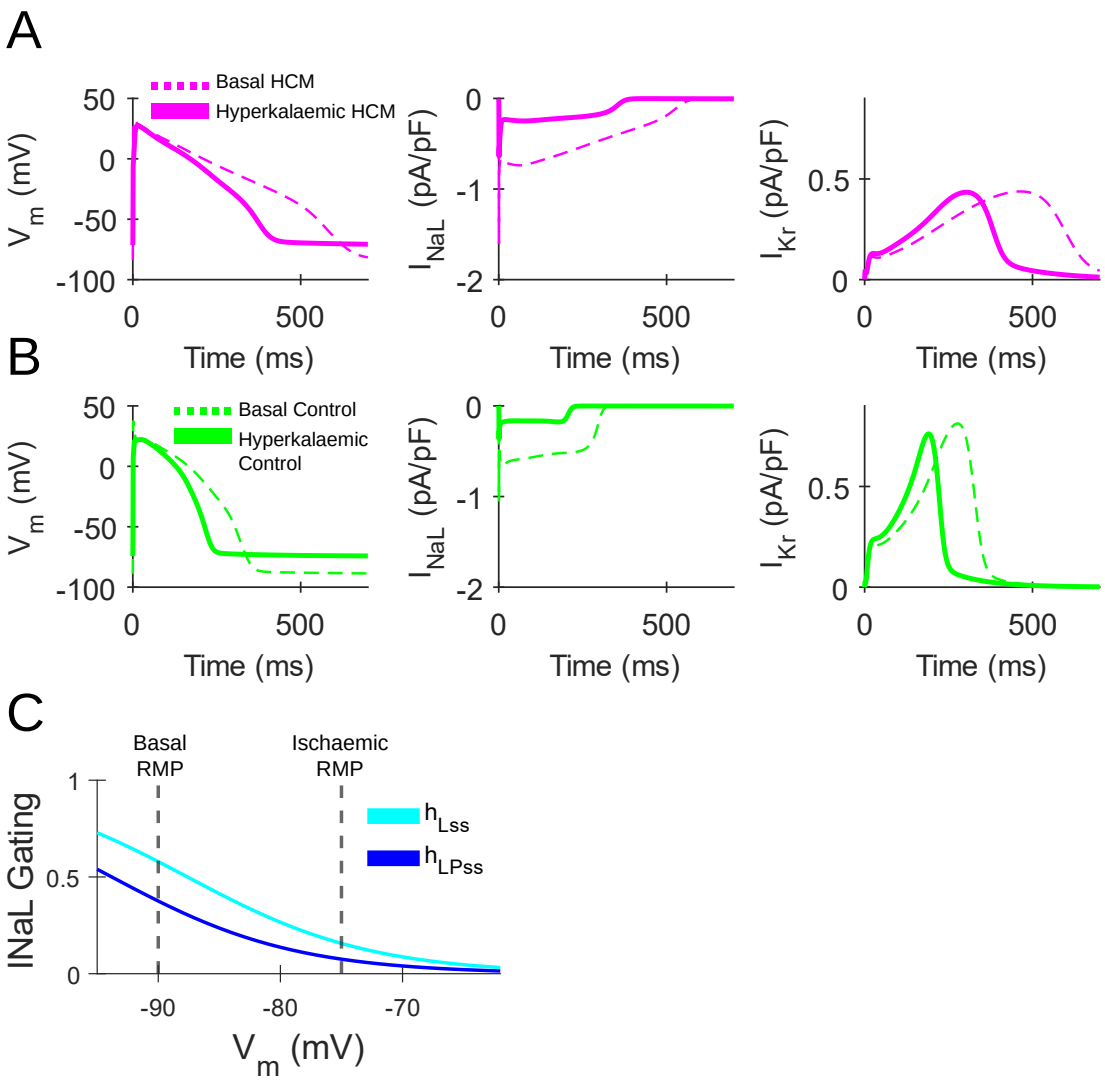


Figure 5.2: Remodelling of I_{NaL} and I_{Kr} channels underlies abnormal response of HCM cardiomyocytes to ischaemia. Representative AP traces (left), I_{NaL} (middle) and I_{Kr} (right) under basal (dashed line) and hyperkalaemic ($[K^+]_e$ = 9 mM) (solid line) conditions, for (A) HCM-remodelled cardiomyocytes, and (B) control cardiomyocytes. (C) Non-phosphorylated (h_{Lss}) and phosphorylated (h_{LPss}) inactivation gating steady states of I_{NaL}, where there was significant impairment during ischaemic RMP elevation compared with basal RMP (dashed, vertical lines).

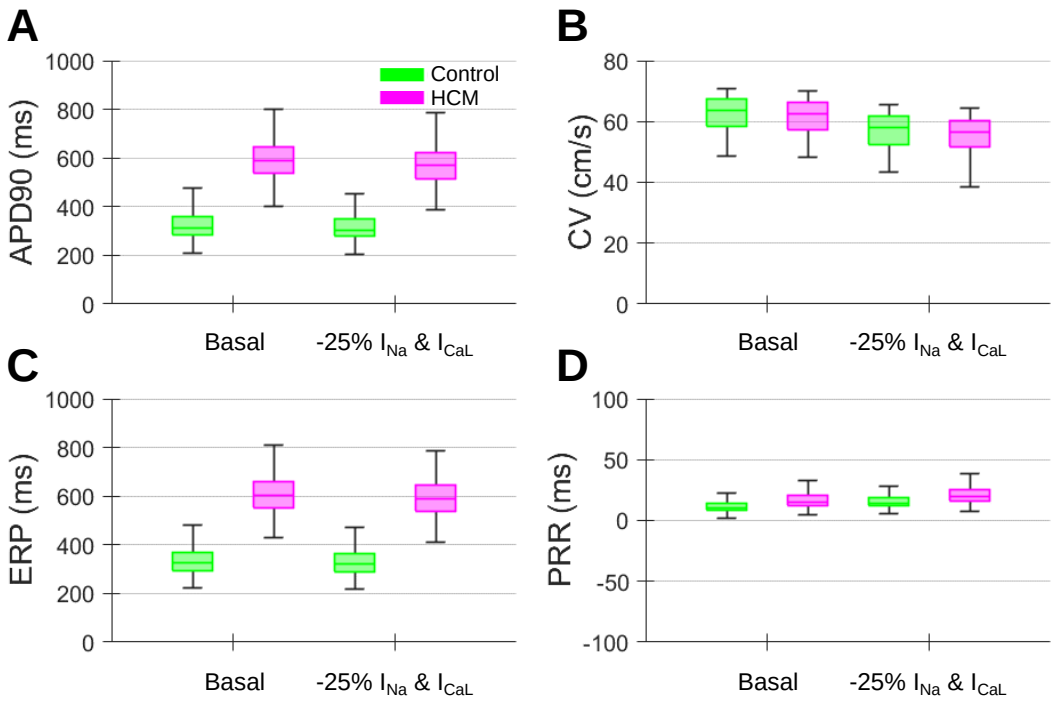


Figure 5.3: Effects of acidotic impairment of I_{Na} and I_{CaL} on AP biomarkers. (A) APD, (B) CV, (C) ERP and (D) PRR for control and HCM populations of models subjected to basal conditions and acidosis (-25% I_{Na} & I_{CaL}).

Effects on Ca^{2+} transient biomarkers are further shown in Appendix Fig. A.1, where myocardial ischaemia led to similar changes in both populations. Of note, Ca^{2+} transient durations in HCM remained prolonged at 570 $\pm$ 30 ms compared to controls at 440 $\pm$ 50 ms during ischaemia. This contrasts with the significant ischaemic APD decreases observed in HCM models, which may have implications for cellular arrhythmias in HCM. The sensitivity of AP biomarkers to additional ischaemic effects in I_{NaK}, I_{NaL} and I_{NCX} was also investigated in Appendix Fig. A.2, showing that these additional ischaemic changes had small effects on AP biomarkers.

5.4 Discussion

The principal finding of the study reported in this thesis chapter is that, during ischaemia, there was a reduction of the ERP and enhanced APD shortening in human HCM cardiomyocytes, when compared with control cardiomyocytes.

Ischaemic ERP shortening in HCM due to chronic ionic remodelling has not been well documented in previous works. However, hyperkalaemic reductions in ERP under conditions of I_{Kr} block [18] (a component of HCM ionic remodelling) have been reported, as opposed to increases in ERP with normal electrophysiology [345]. In the present simulation study, ischaemic ERP shortening in HCM always occurred concomitantly with enhanced APD shortening (Appendix Fig. A.7). Indeed, both enhanced ischaemic ERP [131, 175] and APD [22, 131, 175, 369] shortening, and APD dispersion [382], have been reported in various hypertrophied animal models. Interestingly, one study instead reported enhanced ischaemic ERP prolongation in hypertrophied rats [22]. These accentuated responses to ischaemia may in part be explained by faster K^+ accumulation in regions of hypertrophy [369]; however, the results presented in this chapter identified enhanced ischaemic ERP and APD responses even with the same increase in $[K^+]_e$. Although distinct from HCM, LV hypertrophy often manifests prolonged APD at baseline [381], and the ischaemic repolarisation response is markedly aggravated in these patients [313], which may reflect the enhanced cellular response identified in this thesis chapter. The concomitant ischaemic changes to refractoriness may have implications for arrhythmic risk in HCM.

5.5 Conclusions

Cardiac electrophysiology simulation studies and their subsequent validation via patch-clamp experiments in human ventricular cardiomyocytes identified that ionic remodelling in HCM causes an accentuated repolarisation response and opposite ERP response to acute myocardial ischaemia, as compared to non-remodelled cells. The electrophysiological interactions identified between ionic remodelling and acute myocardial ischaemia are later relevant to ischaemic arrhythmic risk (Chapter 6) and the ECG diagnosis of ischaemia (Chapter 7) in HCM.

5.6 Limitations

General computational limitations are detailed in section 9.3. Of particular relevance to this chapter, ectopy and alternans related to Ca^{2+} handling are further expected to be modulated by ischaemic impairment of the SERCA and sarcolemmal Ca^{2+} pumps, despite negligible effects on AP biomarkers (Appendix Fig. A.8).

CHAPTER 6

Electrophysiological mechanisms of ischaemia-induced arrhythmias in HCM

As shown in the previous chapter, electrophysiological interactions between HCM ionic remodelling and acute myocardial ischaemia determine cellular refractoriness, which is an important factor in arrhythmogenesis. This chapter therefore investigates how the presence of HCM ionic remodelling affects arrhythmic risk during an acute ischaemic episode, in both tissue and biventricular models.

6.1 Introduction

The significant independent contributions to ERP made by HCM ionic remodelling and myocardial ischaemia shown in Chapter 5 mean that refractoriness gradients may be variably enhanced in HCM, depending on the presence and spatial distribution of ionic remodelling and transient ischaemia. However, despite being shown to promote cellular triggers [66, 282], the implications that HCM ionic remodelling may have for substrate arrhythmic risk during ischaemia remains unknown. Moreover, with structural remodelling frequently identified in regions of perfusion impairment (as shown previously in Table 3.2), the further contribution of fibrosis to ischaemic arrhythmic risk is also unknown.

This chapter aimed to investigate the electrophysiological mechanisms by which ischaemia interacts with other pathological features in human HCM tissue and ventricles (ionic remodelling and diffuse fibrosis) to modulate arrhythmic risk. It was hypothesised that, because gradients of refractoriness

are common precursors of conduction block and subsequent re-entry in myocardial ischaemia [228], increased refractoriness heterogeneity secondary to chronic ionic remodelling in hypertrophied regions would increase vulnerability to conduction block and hence arrhythmic risk. It was further hypothesised that exacerbation of ischaemic conduction delay by diffuse fibrosis would be proarrhythmic during myocardial ischaemia in HCM.

6.2 Methods

To test the hypothesis that HCM ionic remodelling increases arrhythmic risk during ischaemia, scenarios were considered where (i) regional acute myocardial ischaemia colocalises with HCM ionic remodelling, and (ii) regional acute myocardial ischaemia occurs under control electrophysiology. To test the hypothesis that fibrosis modulates arrhythmic risk during ischaemia in HCM, simulation studies were conducted where (iii) regional acute myocardial ischaemia colocalises with HCM ionic remodelling and diffuse fibrosis, which were compared with scenario (i).

6.2.1 HCM tissue and biventricular models with ischaemia and fibrosis

Representative human biventricular models of septal HCM were used, alongside tissue HCM models, as described in section 4.2. Simulations in tissue were repeated using 50 different AP models randomly sampled from the AP populations from section 5.2.1, to account for inter-subject variability in disease expression. All simulations used a spatial discretisation of 250 μm or 300 μm.

Ischaemia

Acute myocardial ischaemia in tissue and biventricular models was modelled as the combined effects of hyperkalaemia, hypoxia, and acidosis, as previously described in section 4.5.1. In tissue simulations, a hyperkalaemia/hypoxia sensitivity analysis was performed rather than explicitly modelling different time points in acute ischaemia [45], because there may be differences in K^+ accumulation rate in HCM [369] and whether widespread impairment of K^+ channels extends to I_{KATP} channels is unknown [66]. The degree of acidosis was fixed in the sensitivity analysis because it had negligible effects on refractoriness and identical effects on CV between control and HCM AP models (Fig. 5.3).

Regional acute myocardial ischaemia was modelled as a circular/spherical region with a diameter of 5 cm (including CZ and BZ as previously described in section 4.5.2) [92, 100, 101, 228], consistent with reported concentric perfusion defects in HCM [169], which are frequently $>$ 3 cm in extent [349]. In 3D, both subendocardial and transmural ischaemia were modelled as reported clinically (previously described in section 3.2.3), where subendocardial and transmural ischaemia were considered to affect 50% and 100% of the LV wall transmurally, respectively. Subendocardial and transmural ischaemia corresponded to 11% and 33% of LV volume affected respectively, comparable to the reported 2–35% LV range of perfusion defect sizes reported in HCM [245].

HCM ionic remodelling

HCM ionic remodelling, as detailed in Table 4.1, was modelled following section 3.3.3. HCM ionic remodelling was modelled as a concentric circular affected region in tissue models, and a spherical region affecting the full transmural width of septal hypertrophy in the HCM biventricular mesh.

Fibrosis

Myocardial fibrosis was modelled by setting a fraction of mesh elements as non-conductive and unexcitable, assigned stochastically using a uniform probability density function. Arrhythmic risk in fibrotic HCM tissue was measured for 10%, 20%, and 30% fibrotic densities, for 10 randomised distributions at each value. Arrhythmic risk in fibrotic human HCM ventricles was measured at 30% fibrotic density, for one randomised distribution.

6.2.2 Pacing protocol

Arrhythmic risk was quantified using the S1-S2 protocol previously described in section 4.6, with S2 always applied in the lateral BZ of the ischaemic region, approximating ischaemic experiments in which premature beats emerged from the NZ directly adjacent to the BZ [148]. In tissue models, S2 was applied mid-BZ proximal to the side of S1. In biventricular models, to account for the non-planar S1 activation, experiments were repeated for 6 different S2 positions to sufficiently cover the ischaemic BZ in the apico-basal and anterior-posterior planes, applied endocardially mid-BZ and equispaced around the region of ischaemia.

6.2.3 Perfusion imaging

To inform the region of the HCM biventricular model affected by myocardial ischaemia, LV segment-wise clinical perfusion imaging data was used. Twenty-eight HCM patients (Appendix Table A.1) were prospectively enrolled from the inherited cardiac conditions clinic at the John Radcliffe Hospital in Oxford, United Kingdom. All participants provided informed written consent. The CMR study was approved by the National Research Ethics Committee (REC ref 12/LO/1979).

After appropriate clinical screening, HCM patients underwent adenosine vasodilator stress CMR imaging at 3 Tesla (Trio, Siemens Healthcare, Erlangen, Germany). The CMR protocol included adenosine vasodilator stress and rest first-pass perfusion imaging to assess for perfusion abnormalities. Adenosine vasodilator stress perfusion was performed at a standard 140 mcg/kg/min, and in non-responders was up titrated as previously described [300]. For perfusion analysis, MPRI was measured from stress and rest signal intensity curves as previously described [299]. All perfusion imaging data was provided by Prof. Betty Raman, University of Oxford. T-tests were applied to compare MPRI measurements in each LV segment between patients with and without a history of VT using the `scipy.stats` Python library.

6.3 Results

6.3.1 Re-entry emerges earlier in the onset of ischaemia in HCM tissue

Arrhythmic risk studies were performed for 900 in-tissue scenarios, spread across 50 human control and HCM AP models randomly sampled from the populations, for 9 parameter combinations of hyperkalaemia and hypoxia. This consisted of ectopic S1-S2 protocols applied to tissue models of acute regional myocardial ischaemia (Fig. 6.1A) for a range of coupling intervals, totalling 28,040 simulations of re-entry inducibility. Analysis of the arrhythmic risk studies highlighted that ischaemia-induced re-entry can emerge at a much lesser ischaemic extent under conditions of HCM ionic remodelling than in non-diseased myocardium.

The summary statistics of arrhythmic risk in Fig. 6.1B show that only 0–2% of control models enabled re-entry at low hyperkalaemic extent ($[K^+]_e = 7$ mM), compared to 66–100% of models affected by HCM

ionic remodelling. Moreover, the range of S1-S2 time intervals at which re-entry occurred (the vulnerable window) at low hyperkalaemic extent was also markedly greater in HCM, ranging between 12.5–29.4 ms compared to 0–0.1 ms in controls. These considerations also held at an intermediate hyperkalaemic extent ($[K^+]_e = 8$ mM). Ischaemia in control tissue models only became relatively pro-arrhythmic at a high hyperkalaemic extent ($[K^+]_e = 9$ mM), for which the HCM-remodelled region failed to support retrograde propagation.

Differences in re-entry inducibility are explained by differences in ERP between ischaemic control and HCM tissue (Fig. 5.1B), and the dependence that figure-of-eight re-entry has on ERP gradients. Figure-of-eight re-entry requires that (i) S2 propagates in the NZ; (ii) S2 is blocked at the CZ; (iii) retrograde propagation occurs in the CZ; and (iv) retrograde propagation can re-excite the NZ.

Conditions (i) and (ii) approximately require that $ERP_{CZ} > ERP_{NZ}$, a condition which was already satisfied by the regional HCM ionic remodelling without ischaemia (Figs. 5.1B & 6.1C). The contribution of ischaemia to arrhythmic risk in 2D HCM models was that, through shortening of ERP_{CZ} and CV, conditions (iii) and (iv) were satisfied in an ischaemic region of realistic size. Conversely, in control models, the condition that $ERP_{CZ} > ERP_{NZ}$ required a threshold extent of hyperkalaemia above which the ERP is prolonged (and above which this outweighs hypoxic ERP shortening). Specifically, at $[K^+]_e = 7$ mM there were sufficient reductions in the CV and ERP_{CZ} to enable re-entry in HCM models, whereas in control models ERP_{CZ} was only sufficiently prolonged beyond a threshold $[K^+]_e = 8$ mM.

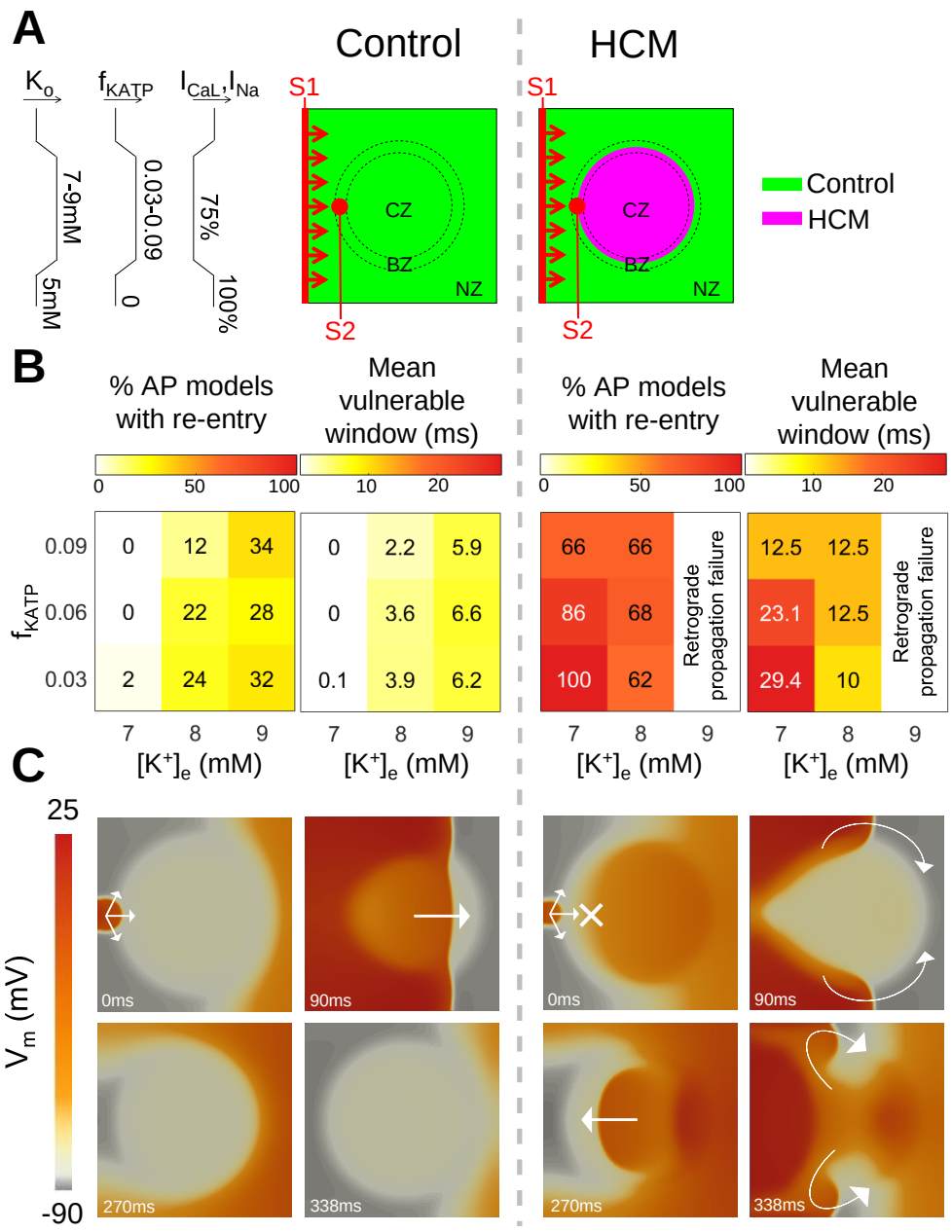


Figure 6.1: In-tissue characterisation of HCM ischaemic arrhythmic risk. (A) Schematics of in-tissue acute myocardial ischaemia domains, with control electrophysiology (left) and regional HCM electrophysiology (right), for which arrhythmic risk was measured in 50 randomly sampled AP models. Domains consisted of a CZ subjected uniformly to the full extent of ischaemia, a BZ where ischaemic parameters ($[K^+]_e$, f_{KATP}, and I_{CaL}, I_{Na} inhibition) were linearly varied towards baseline values away from the CZ (left hand side diagrams), and the NZ unaffected by ischaemia. The positions of sinus rhythm activation (S1) and the ectopic stimulus (S2) are denoted. (B) Summary statistics of arrhythmic

risk over the hypoxia/hyperkalaemia parameter space for the 50 AP models in tissue, as characterised using ectopic S1-S2 pacing protocols. (C) Representative in-tissue simulations at $[K^+]_e = 7$ mM, $f_{KATP} = 0.06$ following application of S2 demonstrate how conduction block was infrequent in ischaemic control myocardium (left), but common in ischaemic HCM myocardium (right) due to ionic remodelling. Subsequent re-entries occurred in HCM. The circular ischaemic region has visibly a less negative RMP. Arrows and crosses indicate direction of wavefront propagation and locations of conduction block, respectively. Time elapsed (ms) following S2 is denoted in each frame.

It is notable that, although arrhythmic risk decreased as ischaemia progressed from mild to severe extents of hyperkalaemia and hypoxia in HCM models (Fig. 6.1B), arrhythmic risk for $[K^+]_e = 7$–8 mM was significantly greater than that under non-ischaemic conditions (where only 16% of models enabled re-entry). Even under control electrophysiology, a decrease in arrhythmic risk for progression to severe ischaemic parameters is frequently observed in computational models [45, 100], and the high arrhythmic risk occurring at an intermediate degree of ischaemia [45] may also apply to HCM. This is because for hyperkalaemia with $[K^+]_e > 10$ mM total conduction block often occurs [334]. Indeed, the failure of re-entries to emerge in HCM tissue models at high hyperkalaemic extent ($[K^+]_e = 9$ mM) was typically caused by retrograde propagation failure. Ionic remodelling in HCM includes I_{NaK} impairment [282], which made the RMP even less negative and constrained I_{Na} availability for AP propagation (Fig. 6.2). Retrograde propagation typically involved thin wavefronts that were unable to overcome this effect.

The dependence of arrhythmic risk during myocardial ischaemia on the extent of regional HCM ionic remodelling was further analysed in Appendix Fig. A.3. These findings suggest that, in the early stages of HCM, arrhythmic risk may increase as ionic remodelling develops, but that in the later stages marked ERP prolongation may preclude re-entries. The sensitivity of in-tissue arrhythmic risk to additional ischaemic effects in I_{NaK}, I_{NaL} and I_{NCX} was investigated in Appendix Fig. A.4, showing that these components had minor consequences for arrhythmic risk. In a subset of in-tissue simulations, sensitivity of the in-tissue arrhythmic risk to hypoxic BZ width and spatial resolution was investigated in Appendix Figs. A.5 & A.6 respectively, showing only modest sensitivity to these factors.

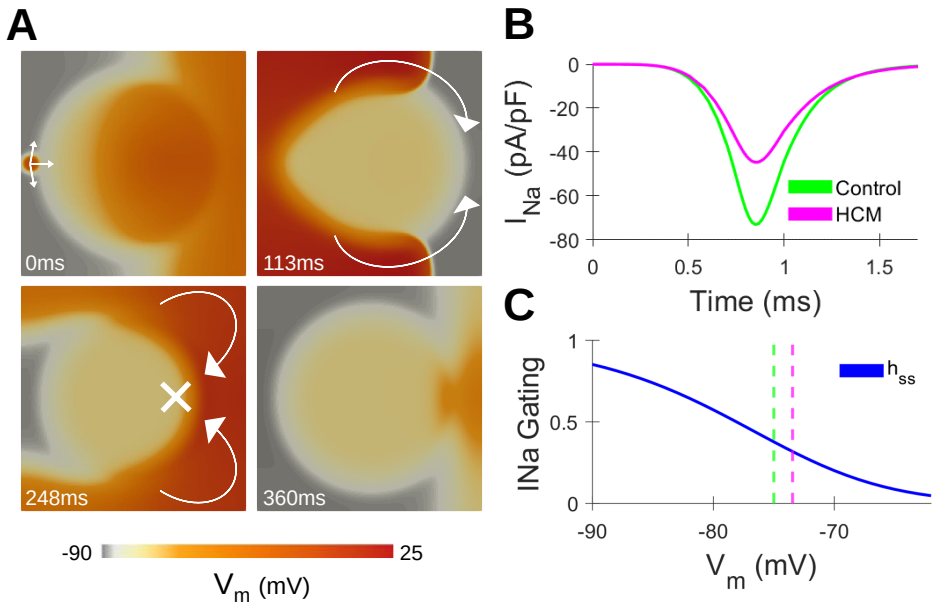


Figure 6.2: Mechanisms of retrograde propagation failure in HCM tissue at severe hyperkalaemic extent. (A) Retrograde propagation failure occurred in most HCM tissue models with $[K^+]_e = 9$ mM, precluding re-entry. The time elapsed (ms) following S2 is denoted in each frame. (B) I_{Na} availability at $[K^+]_e = 9$ mM was significantly impaired, especially so in HCM models. (C) I_{Na} impairment was contributed to by reduced negativity of the RMP in HCM models (magenta, dashed) compared to control models (green, dashed). HCM models had impairment of I_{NaK} function, further reducing the negativity of RMP and decreasing the steady state inactivation gating of I_{Na}.

6.3.2 Multiple mechanisms of in-tissue ischaemia-fibrosis interaction

Arrhythmic risk modulation by ischaemia-fibrosis interactions was investigated for 450 HCM tissue scenarios, spread across 15 human HCM AP models, for the 3 fibrotic extents in [10, 20, 30]%, where randomised distributions of fibrosis were sampled 10 times at each fibrotic density. Ectopic stimulus protocols were applied to tissue models of acute regional myocardial ischaemia with diffuse fibrosis, for a range of coupling intervals totalling 16,950 simulations of re-entry inducibility. Informed by the results on ischaemic burden in HCM, episodes of ischaemia were simulated using the hyperkalaemia and hypoxia

parameters $[K^+]_e = 7$ mM and $f_{KATP} = 0.06$. The 15 human HCM AP models were chosen from the HCM population such as to include a set of AP models exhibiting variability in arrhythmic risk in the prior non-fibrotic scenarios. Specifically, no re-entry vs. induced re-entry emerged in 8 and 7 AP models, respectively, in the non-fibrotic case.

Analysis of in-tissue arrhythmic risk simulations identified that mechanisms of ischaemia-fibrosis interaction are strongly dependent on the underlying electrophysiology. Among some AP models, fibrosis had a net antiarrhythmic effect by interrupting retrograde propagation through slowing or impairing conduction in the CZ. In the example shown in Fig. 6.3A, retrograde propagation was able to complete with no fibrosis (0%) or mild fibrotic infiltration (10%), but with further impaired conduction from greater fibrosis content (20%), total conduction block occurred. In other AP models, fibrosis had a pro-arrhythmic effect by delaying CZ conduction enough for timely NZ recovery. In the example shown in Fig. 6.3B, retrograde propagation with no fibrosis (0%) or mild fibrotic infiltration (10%) allowed re-excitation of the CZ shortly after the ectopic stimulus. With greater fibrosis content (20%), CZ conduction was impaired such that retrograde propagation was delayed enough for the NZ to recover excitability, which allowed re-entry.

Some patterns of fibrosis enabled re-entrant wavefronts to emerge asymmetrically, such that they interacted with the wavetail of previous re-entrant cycles, promoting sustained break-up (Fig. 6.3C). In this case, clockwise propagation was blocked by a refractory wavetail, whilst anticlockwise propagation persisted. This formed a stable rotor anchored to the ischaemic-fibrotic region. These results suggest that breaking the symmetry of figure-of-eight re-entries is one mechanism by which fibrosis increases arrhythmia sustainability in HCM. The circuit length of a single asymmetric rotor is greater than that of each of two symmetric re-entries in a figure-of-eight, hence they are less easily interrupted by fluctuations in cycle-to-cycle activation and ERP.

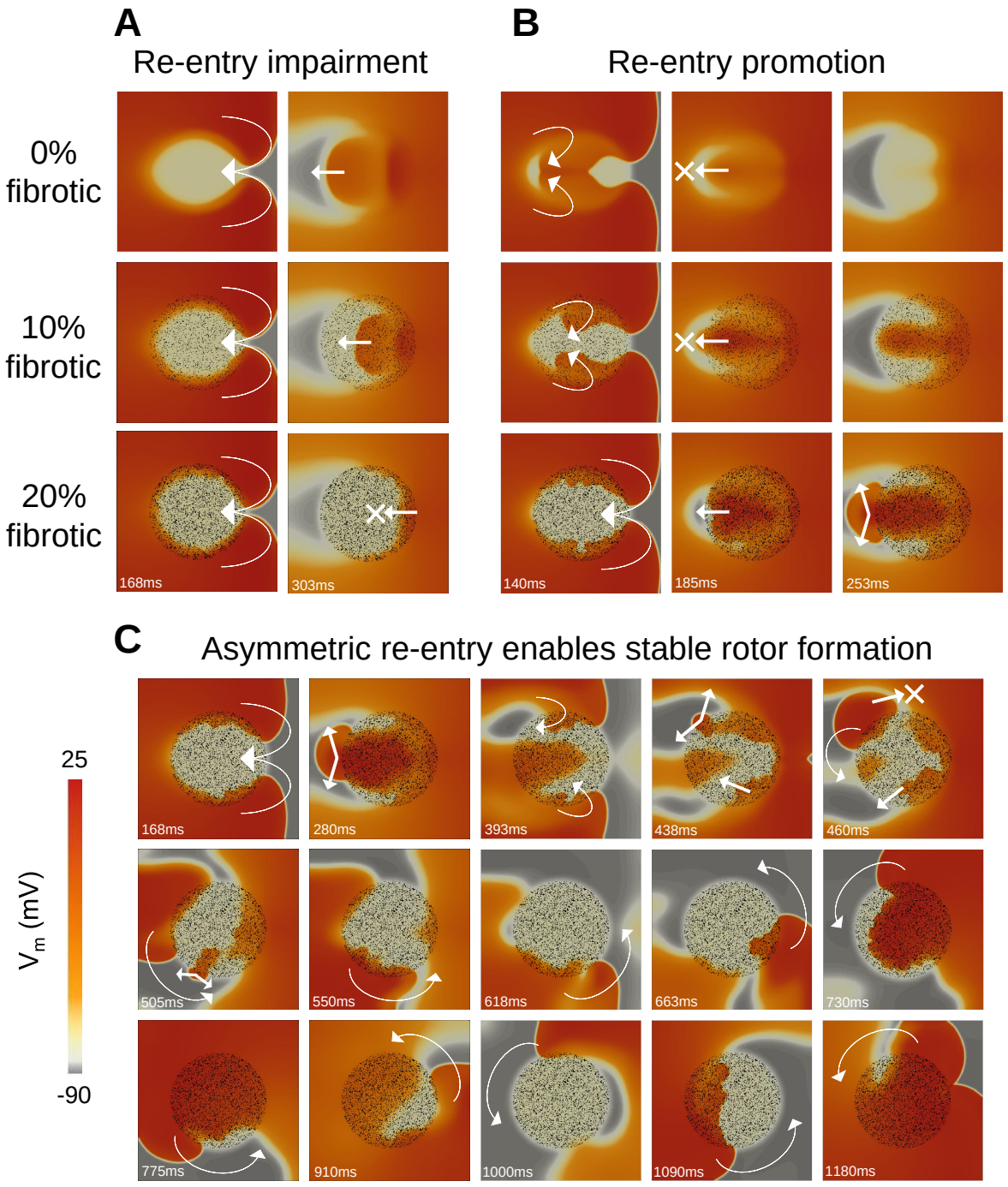


Figure 6.3: Diffuse fibrosis modulated arrhythmic risk during ischaemia in HCM. Representative in-tissue simulations following application of S2 demonstrate how the presence of diffuse fibrosis affected re-entry inducibility in ischaemic HCM myocardium, through three different mechanisms. Conduction impairment at increased fibrosis density led to (A) retrograde propagation block at the CZ, preventing re-entrant cycles, or (B) retrograde propagation delay at the CZ, enabling re-entrant cycles by allowing NZ to

recover excitability. (C) The fibrotic microstructure led to asymmetric retrograde propagation, such that the re-entrant wavefront interacted with the refractory wavetail and formed a stable rotor, anchored to the ischaemic-fibrotic region. Arrows and crosses indicate direction of wavefront propagation and locations of conduction block, respectively. Time elapsed (ms) following S2 is denoted in each frame.

AP models in which fibrosis increased arrhythmic risk during ischaemia tended to have a higher Na^+ conductance and lower ERP in the ischemic core zone of affected HCM myocardium. This is because, with higher Na^+ conductance, fibrosis delayed conduction but was unable to block retrograde propagation entirely. In these models, the ERP in the CZ was too low to block conduction long enough for ERP in the external NZ to recover excitability (Fig. 6.3B) unless fibrosis was present to delay retrograde propagation. When fibrosis promoted re-entry, it was more likely to be sustained because ERP in the CZ was short in these cases. These findings suggest that fibrosis may play a pro-arrhythmic role in less diseased HCM states (lesser degree of ionic remodelling and healthy conduction), but antiarrhythmic in more diseased states (greater ionic remodelling and impaired conduction). Interactions between the density of fibrosis and the ERP during hypoxia have been explored in previous computational modelling [314] and the present study shows that similar effects may be relevant in HCM due to further ERP modulation by ionic remodelling.

6.3.3 Clinically informed ischaemia and fibrosis distributions

Biventricular simulations of acute myocardial ischaemia in HCM were informed by segmental mid-slice LV measurements of MPRI from N = 28 HCM sarcomeric causal variant carriers with LV hypertrophy, acquired with stress perfusion CMR imaging.

In this cohort, hypertrophy was primarily septal (Fig. 6.4A), whereas the distribution of severe perfusion impairment (MPRI < 1) was highly variable (Fig. 6.4B), reflecting diffuse small vessel disease in HCM. Although a diffuse phenomenon, the most frequently affected segment with severe MPRI impairment was anteroseptal (Fig. 6.4B). Patients with VT had lower inferoseptal MPRI compared to those without (0.8 ± 0.2 vs. 1.3 ± 0.4, $p < 0.01$), as in Fig. 6.4C. As ionic remodelling and LGE in HCM are hypertrophy-associated [66, 201], combinations of ionic remodelling, ischaemia and fibrosis are most

likely to occur in the septum, hence all combinations of disease factors were modelled as septal.

Modelling ischaemia as septal is reinforced by the evidence that septal ischaemia in HCM is particularly common in previous works [138, 287, 370]. Specifically, visual examples of large perfusion defects involving the septum of HCM patients can be seen in these other studies [130, 138], like that shown in Fig. 6.4D. Finally, hypoperfusion and hypertrophy are associated (section 3.2.3), further motivating the inclusion of ischaemia in the hypertrophied septum of the anatomical model of human HCM ventricles.

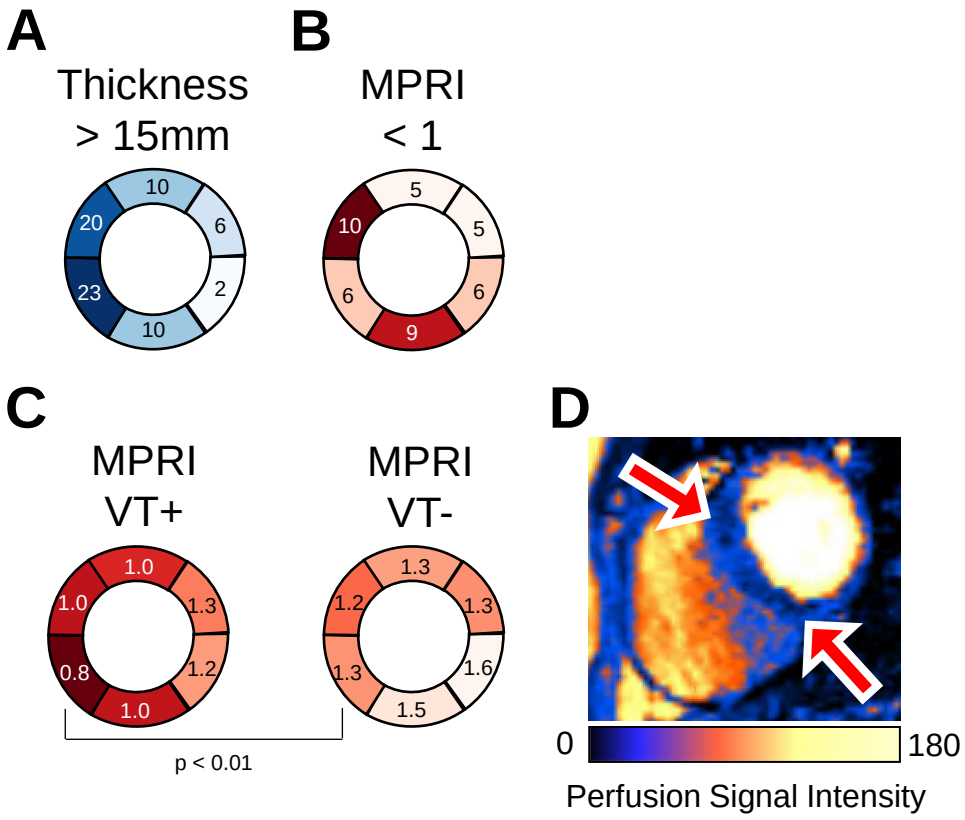


Figure 6.4: Clinical perfusion imaging data from HCM patients (N = 28). (A) Number of segments with wall thickness > 15 mm, demonstrating predominant septal involvement of hypertrophy. (B) Number of segments with MPRI < 1, showing that perfusion impairment is diffuse in HCM. (C) Comparison of MPRI between patients with and without a history of VT (N = 5, 23 respectively), where an association was observed between inferoseptal perfusion impairment and VT ($p < 0.01$). (D) Colour perfusion scan showing large septal perfusion defects (denoted by arrows) in an HCM patient.

6.3.4 Transmural extent of ischaemia modulates arrhythmic risk in HCM ventricles

Arrhythmic risk simulations in human ventricles were conducted in 9 scenarios, spread across subendocardial and transmural ischaemia for control and HCM electrophysiology. Transmurally ischaemic HCM scenarios were further simulated under the effects of mid-wall and transmural fibrosis. Ectopic stimulus protocols were applied to these ventricular scenarios for 6 ectopic positions at 10 S1-S2 coupling intervals, for a total of 540 simulations of re-entry inducibility.

Extending upon the in-tissue investigations in Fig. 6.1, arrhythmia inducibility studies in anatomical reconstructions of the human HCM ventricles identified the transmural extent of ischaemia as a key determinant of arrhythmia sustainability. Vulnerable windows to re-entry in subendocardially and transmurally ischaemic HCM biventricular models are shown in Fig. 6.5A, showing how non-sustained and sustained re-entries may be induced with appropriately timed S1-S2 coupling intervals, for 6 ectopic stimulus positions around the BZ. Multiple cycles of re-entry only emerged for transmural ischaemia, whereas only single re-entries were observed in subendocardial ischaemia. This is because slowed repolarisation in the region of HCM ionic remodelling unaffected by subendocardial ischaemia (RV side of septum) typically interrupted further re-entrant cycles (Fig. 6.5B), whereas transmural ischaemia led to ERP shortening in this region that enabled further excitation and re-entry formation (Fig. 6.5C). Conversely, subendocardial ischaemia manifested a greater inducibility of single re-entries. This is because the slow repolarising non-ischaemic segment with ionic remodelling adjacent to the ischaemic subendocardium caused conduction block to occur at a wider range of S1-S2 coupling intervals. However, the region with ionic remodelling was unable to sustain re-entry due to its long ERP. This exemplifies competing effects of increased ERP on arrhythmic risk in HCM ventricles (further explored in Appendix Fig. A.3).

Moreover, comparisons of arrhythmic risk simulations in ischaemic HCM ventricles with control ventricles identified that at a mild ischaemic extent ($[K^+]_e = 7$ mM and $f_{KATP} = 0.06$), arrhythmia was only inducible in ventricles affected by HCM ionic remodelling. This corroborates the in-tissue findings, because again ERP was not prolonged sufficiently by ischaemia to produce conduction block unless ionic remodelling was present, even in the biventricular models.

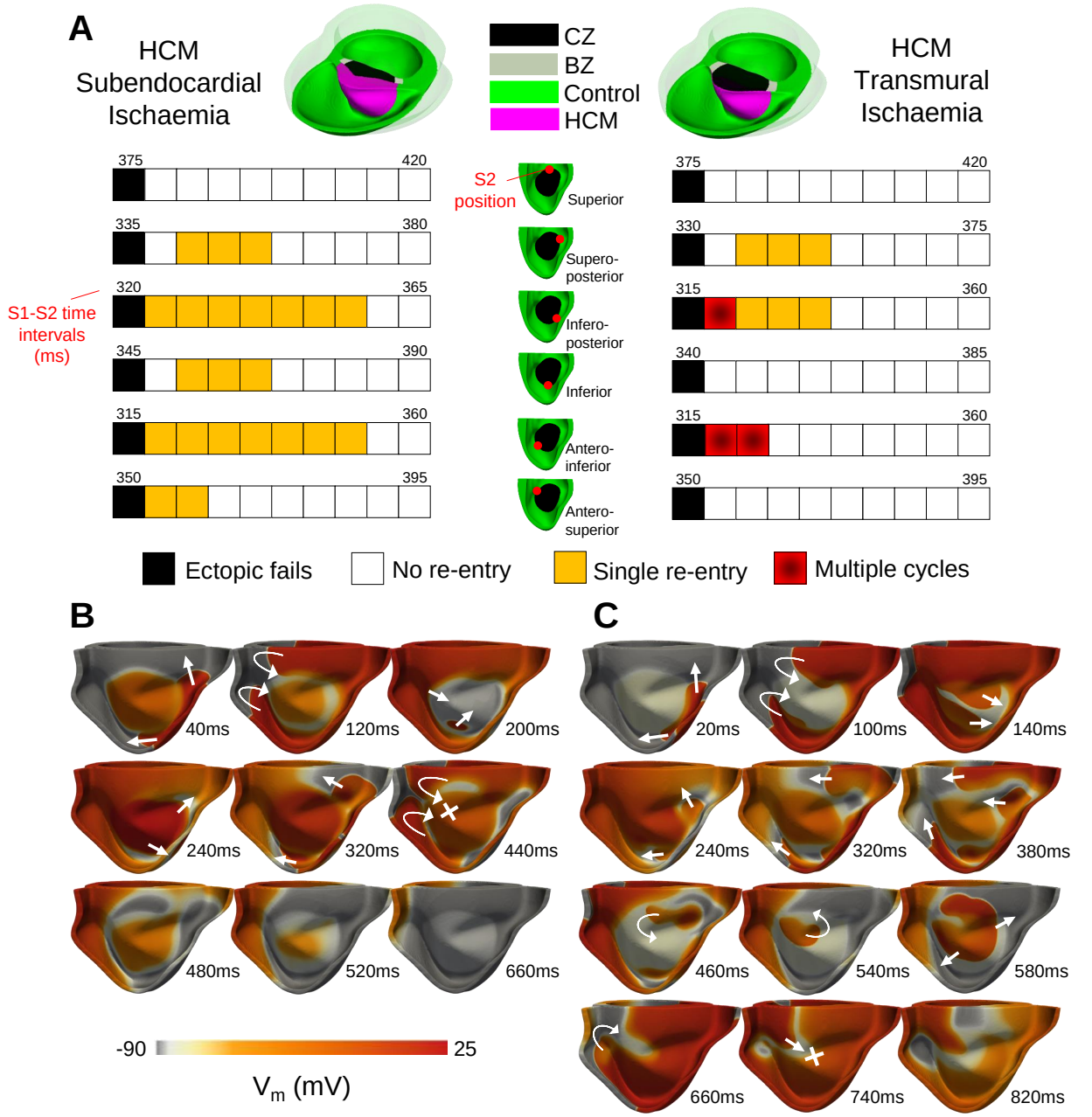


Figure 6.5: Transmural extent of ischaemia modulated arrhythmic risk in HCM. (A) Outcomes (either ectopic failure, no re-entry induced, single re-entry, or multiple cycles of re-entry) of the S1-S2 pacing protocol applied to the ischaemic biventricular HCM mesh, for the range of S1-S2 time intervals tested, with the minimum and maximum S1-S2 time denoted for each of the 6 ectopic positions. Subendocardial ischaemia (left) enabled wider windows of vulnerability to single re-entries, whereas transmural ischaemia (right) promoted increasingly sustained arrhythmia in HCM. At this low extent of ischaemia, re-entry

was only inducible with regional HCM ionic remodelling. (B) Representative single cycle of re-entry in subendocardial ischaemia following the application of S2, compared with (C) multiple cycles of re-entry in transmural ischaemia, as viewed from the RV cavity. Arrows and crosses indicate direction of wavefront propagation and locations of conduction block, respectively. Time elapsed (ms) following S2 is denoted in each frame.

6.3.5 Multiple mechanisms of ischaemia-fibrosis interaction in HCM ventricles

The dependence of fibrosis-ischaemia interaction on the underlying HCM cellular electrophysiology, as identified in tissue (Fig. 6.3), is further exemplified in the transmurally ischaemic HCM ventricles (Figs. 6.6A & 6.6B), where arrhythmic risk was investigated with contributions from mid-wall and transmural fibrosis in HCM ventricles. To facilitate comparison with non-fibrotic simulations, Fig. 6.6A uses the same AP model used in Fig. 6.5. To compare with the ischaemia-fibrosis interactions identified in tissue, Fig. 6.6B uses the same AP model as in Fig. 6.3C. To characterise the effect of increasing transmural extents of fibrosis, diffuse fibrosis was simulated in mid-wall and transmural distributions.

In the first scenario (Fig. 6.6A), both mid-wall and transmural fibrosis were sufficient to interrupt the multiple cycles of re-entry that were previously possible in the non-fibrotic case (Fig. 6.5A). This was possible through the blocking of repeated retrograde excitation, as illustrated earlier in Fig. 6.3A. Fibrosis may therefore not always increase arrhythmic risk; failure to sustain early re-excitation in the affected region can be protective. Interestingly, transmural septal fibrosis (Fig. 6.6A, right-hand side) increased vulnerability to single re-entries through promoting conduction block at a wider range of S1-S2 coupling intervals, in agreement with Fig. 6.3B.

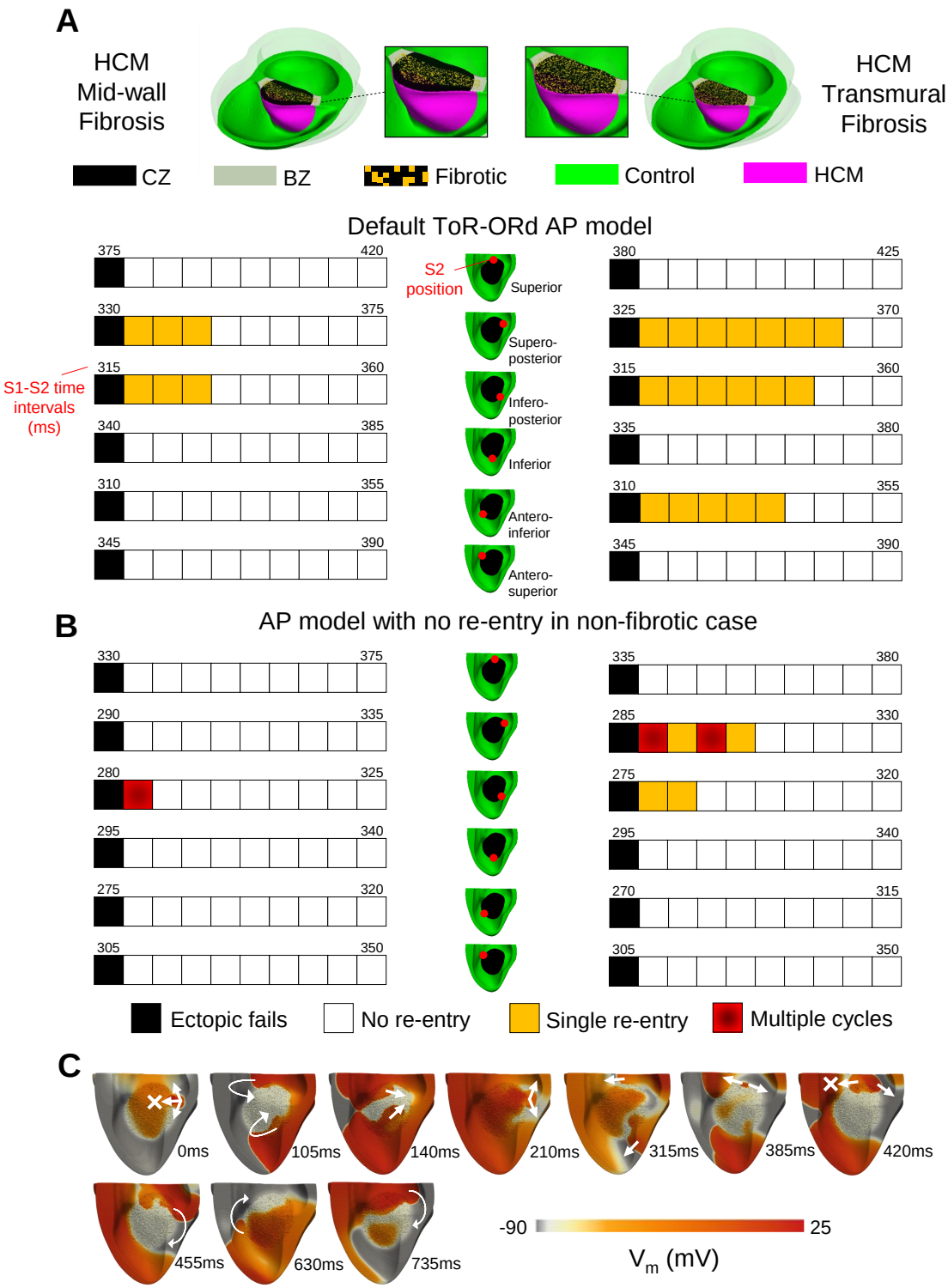


Figure 6.6: Effect of fibrosis on arrhythmic risk during ischaemia was electrophysiology-dependent in HCM. Outcomes (either ectopic failure, no re-entry induced, single re-entry, or multiple cycles of re-entry) of the S1-S2 pacing protocol applied to the transmurally ischaemic biventricular HCM mesh

with mid-wall (left) and transmural (right) diffuse fibrosis, for the range of S1-S2 time intervals tested, with the minimum and maximum S1-S2 time denoted for each of the 6 ectopic positions. (A) When using the default ToR-ORd AP model, multiple re-entrant cycles that were previously possible in the non-fibrotic case were interrupted by both mid-wall and transmural fibrosis by bidirectional conduction block. (B) In an alternative AP model from the populations, for which re-entry was not inducible under non-fibrotic conditions, mid-wall and transmural fibrosis enabled sustained re-entries to be induced by delaying conduction. (C) Representative sustained re-entry formation following the application of S2 for the alternative AP model in the transmurally ischaemic and fibrotic biventricular HCM mesh, where fibrosis forced a re-entry to emerge asymmetrically, which set up a large sustained rotor anchored to the diseased myocardium. Arrows and crosses indicate direction of wavefront propagation and locations of conduction block, respectively. Time elapsed (ms) following S2 is denoted in each frame.

For the alternative AP model (Fig. 6.6B), for which arrhythmia was not inducible without diffuse fibrosis in either tissue (Fig. 6.3C) or ventricular simulations, sustained rotors became possible for both mid-wall and transmural fibrosis. As in Fig. 6.3B, fibrosis had the effect of delaying retrograde propagation in 3D. However, the distribution of fibrosis affected the axis along which conduction was delayed, such that sustained re-entries were enabled for ectopic stimuli at different positions for mid-wall and transmural fibrosis (Fig. 6.6B). Sustained rotors were initiated by asymmetry in the retrograde propagation during re-entry caused by the fibrotic microstructure, leading to one side of the figure-of-eight re-entry being blocked by the refractory wavetail, such that a rotor formed around the ischaemic-fibrotic region (Fig. 6.6C). As observed before in tissue (Fig. 6.3C), this larger configuration of re-entry did not self-terminate, because its long circuit length facilitated an excitable gap that rendered the arrhythmia insensitive to cycle-to-cycle fluctuations in ERP.

6.4 Discussion

Prevention of SCD remains a key challenge in the management of HCM patients, complicated by a limited understanding of SCD causal mechanisms. This thesis chapter sought to investigate how ionic remodelling and fibrosis can interact with ischaemia in HCM to modulate arrhythmic risk. The principal

findings of the study reported in this thesis chapter are that (i) ionic remodelling in HCM enabled re-entry to emerge at a less severe extent of ischaemia; (ii) an increased transmural extent of ischaemia enabled increased arrhythmia sustainability in HCM; and (iii) there were multiple electrophysiology-dependent mechanisms of fibrosis-ischaemia interaction, including the propensity for fibrosis to change figure-of-eight re-entries into more stable patterns of re-entry.

The association of LV hypertrophy with an increased risk of arrhythmias [381], and reports that HCM patients with electrocardiographic abnormalities in the ST complex (evidence of ionic remodelling) have an increased risk of arrhythmias [121], may be partially explained by hypertrophy-ischaemia interactions. In one study, canines with LV hypertrophy had a higher rate of SCD during ischaemia compared to their non-hypertrophic counterparts [177]. Moreover, in rats undergoing ischaemia, VF susceptibility may be increased in those with LV hypertrophy, particularly when the ischaemia and hypertrophy coincide [335]. In the present simulation study, electrophysiological interactions between hypertrophy-associated ionic remodelling and ischaemia increased arrhythmia susceptibility early in ischaemic onset. This is relevant because the severity of demand ischaemia may be self-limiting through dyspnoea and angina in HCM, and ATP levels may be better maintained in demand ischaemia [181]. Of clinical importance, arrhythmic risk contributions from ionic remodelling in HCM motivates investigation of pharmacologic amelioration of ionic remodelling, through K^+ channel enhancement or late Na^+ block. Ranolazine has already shown effect in reducing ectopy burden in HCM [270], and this antiarrhythmic effect may extend to the arrhythmic substrate. Aside from the ionic remodelling, it is notable that LV hypertrophy may directly modulate arrhythmic risk through mechanisms akin to the critical mass hypothesis [127], and the contribution of this factor relative to the ionic remodelling may be of interest for further study.

Simulations of acute myocardial ischaemia in non-HCM ventricles have demonstrated that multiple re-entrant cycles are more inducible in transmural than subendocardial ischaemia [228], a finding reinforced by the present study with HCM ionic remodelling at a lesser extent of ischaemia. The pro-arrhythmic interactions that occur when transmural ischaemia affects HCM-remodelled myocardium may in part explain why adults with both HCM and epicardial coronary artery disease have rates of death that significantly exceed those of patients with just epicardial coronary artery disease [341].

In previous work that investigated interactions between hypoxia and fibrosis, a deleterious interaction was observed in which hypoxic ERP reductions enabled micro-anatomical re-entries to form in fibrotic myocardium [314]. However, the present study identified that under conditions of full ischaemia, the net effect on ERP was dependent on the balance of hyperkalaemic and hypoxic severity. When considering hyperkalaemia (and the ionic remodelling in HCM), regional ERP increases were possible. Although ERP increases further precluded micro-anatomical re-entries in the fibrotic simulations, it was identified that in the onset of ischaemia the increase in ERP heterogeneity instead enabled figure-of-eight re-entries around the affected region. Moreover, in the present study the impact of fibrosis on arrhythmic risk was critically dependent on its density and fast Na^+ channel availability, where conduction impairment was initially proarrhythmic but became antiarrhythmic as tissue became unexcitable. This effect, identified in previous modelling [38], is therefore also relevant in HCM. A further finding is that diffuse fibrosis was able to change re-entry patterns by inducing asymmetric retrograde propagation, breaking the symmetry of figure-of-eight patterns and leading to stable rotor formation.

6.5 Conclusions

In tissue and biventricular models, potential deleterious interactions were identified between myocardial ischaemia, ionic remodelling and diffuse fibrosis. Such mechanisms may be relevant to the occurrence of lethal arrhythmias in patients with mild HCM phenotypic expression, such as in juvenile patients [61] with no replacement fibrosis [111] and limited hypertrophic remodelling [367].

6.6 Limitations

General computational limitations are detailed in section 9.3. Of particular relevance to this chapter, the region of ischaemia simulated was informed by mid-slice LV perfusion reserve measurements only. Moreover, other types and distributions of fibrosis may also be present in HCM, which may harbour different interactions with ischaemia. Myocardial fibrosis was modelled as non-conductive and unexcitable mesh elements, thus whether the mechanisms identified in the present study are affected by electrotonic fibroblast-myocyte coupling was not investigated.

CHAPTER 7

Electrophysiological mechanisms underlying T wave pseudonormalisation on stress ECGs in HCM

As shown in the previous chapter, ionic remodelling and acute myocardial ischaemia can form a high-risk arrhythmic substrate in the HCM ventricles, consistent with clinical reports of poorer prognosis. This chapter investigates how myocardial ischaemia may be better detected on the stress ECG in HCM, to identify the arrhythmic substrate before a potentially lethal arrhythmia is induced.

7.1 Introduction

Although evidence of perfusion impairment is sometimes associated with poorer prognosis and arrhythmias in HCM (Tables 3.3 & 3.4), perfusion imaging is not used in clinical SCD risk stratification for HCM [14, 97, 274]. This may in part be because perfusion imaging is sensitive only to myocardial blood supply, and perfusion is frequently only visually assessed rather than quantified. Whether acute myocardial ischaemia is actually inducible, such that significant electrophysiological changes occur (section 2.4.2) and form arrhythmic substrates, might better be detected with the ECG. Indeed, arrhythmias in HCM are sometimes preceded by ischaemic ECG findings like ST segment changes [113, 307].

With myocardial ischaemia in HCM being inducible by increases in myocardial workload [61, 307],

the stress ECG may be used to identify inducible ischaemia. However, ECG detection of ischaemia is suboptimal in general (section 2.4.4), and especially so in HCM where ECG repolarisation is usually already abnormal at baseline [222]. Moreover, as myocardial ischaemia is not the only possible change that occurs during the stress ECG, exercise-associated increases in pacing rate and serum K^+ concentration must also be considered [408]. Notably, the presence of HCM ionic remodelling changes how the pacing rate [66] and K^+ concentration affects repolarisation (Chapter 5). In this chapter, $[K^+]$ will refer to the K^+ concentration in the extracellular space.

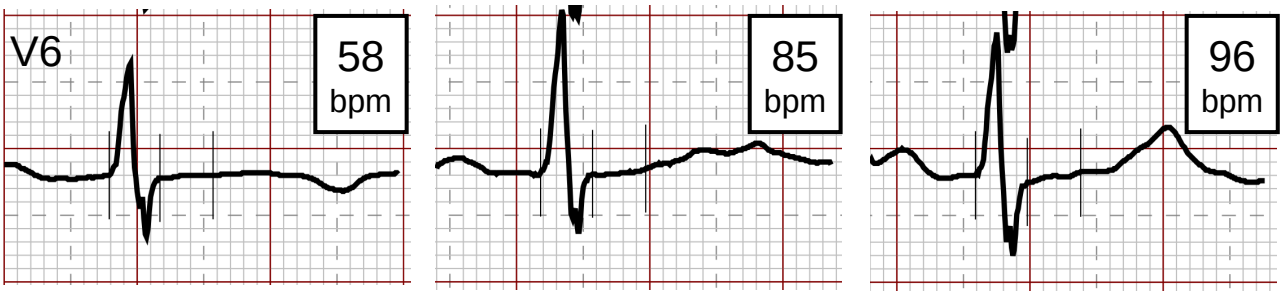


Figure 7.1: Stress ECG T wave pseudonormalisation in HCM. At rest, a 53 year old man with HCM presents with an inverted T wave in lead V6 (left). During cardiopulmonary exercise testing (central and right panels), T wave polarity is corrected. Stress ECG data was provided by Dr. Matteo Beltrami, Careggi University Hospital, Florence.

With slowed repolarisation secondary to regional ionic remodelling manifesting as T wave inversion in HCM [201], and myocardial ischaemia correcting slowed repolarisation (Chapter 5), this chapter sought to investigate the role of myocardial ischaemia in T wave pseudonormalisation, which can occur on stress ECGs (Fig. 7.1). Specifically, the aim was to investigate how regional/serum $[K^+]$ and increases in heart rate affect T wave polarity and the diagnosis of acute myocardial ischaemia on stress ECGs in human HCM. It was hypothesised that T wave pseudonormalisation occurs primarily in HCM due to an accentuated repolarisation response of the remodelled myocardium to ischaemic effects such as regional $[K^+]$ increases, while exercise-induced serum $[K^+]$ increases and pacing frequency contribute to

this phenomenon to a lesser extent.

7.2 Methods

To test the hypothesis that stress T wave pseudonormalisation occurs due to acute myocardial ischaemia, exercise serum $[K^+]$ increases, and/or increased pacing frequency, biventricular HCM models were subjected to (i) regionally ischaemic $[K^+]$ increases, (ii) global $[K^+]$ increases, and (iii) increased pacing frequency.

7.2.1 HCM biventricular models with regional and global K^+ accumulation

Representative human biventricular models of septal and apical HCM were used, as T wave pseudonormalisation has been reported in both septal obstructive [77] and apical HCM patients [16, 161]. All simulations used a spatial discretisation of 500 μm. In pacing frequency investigations, basic cycle lengths in [1000, 700, 600, 500, 400] ms were used.

HCM ionic remodelling

HCM ionic remodelling, as detailed in Table 4.1, was modelled following section 3.3.3. Gradients of HCM electrophysiological remodelling were therefore identically applied to the endocardial surfaces of the hypertrophied regions in both the septal and apical HCM models, with the affected region defined by the intersection of a 4 cm diameter sphere with the mesh. To characterise inter-subject variability in T wave pseudonormalisation, human HCM biventricular simulations were repeated for 10 human AP models selected from the population in section 5.2.1. 10 HCM-remodelled APs were selected to have APD in the range 420–600 ms as reported experimentally [66], varied in 20 ms increments to consider a range of electrophysiological disease severity.

K^+ accumulation

Regions affected by ischaemic $[K^+]$ increases were modelled as circular/spherical with a diameter of 5 cm (including CZ and BZ as previously described in section 4.5.2) [92, 100, 101, 228], consistent with reported concentric perfusion defects in HCM [169], which are frequently $>$ 3 cm in extent [349]. The

region affected by ischaemic $[K^+]$ increases in the biventricular models was chosen to engulf the most hypertrophied region associated with the greatest electrophysiological remodelling, as this configuration was hypothesised to be most likely to cause T wave pseudonormalisation. Regionally ischaemic $[K^+]$ increases were therefore included in the region of septal hypertrophy in septal HCM models, and in the region of apical hypertrophy in the apical HCM models. Indeed, septal and apical infarctions have been reported in HCM [189, 237], and perfusion defects are more prevalent in hypertrophied segments [110].

Serum $[K^+]$ increases such as those during exercise were modelled by affecting the entire human HCM biventricular myocardium identically [408]. The effects of regional and serum K^+ accumulation were investigated for $[K^+]$ in 4–9 mM, consistent with healthy $[K^+]$ ranges and those estimated to occur during stage 1a of human cardiac ischaemia [56, 167], as previously detailed in section 4.5.1.

7.2.2 ECG analysis

The following ECG biomarkers were computed for each lead: QT interval, amplitudes of inverted T wave components, and ST segment changes from baseline. The maximum QT interval across the 12-lead ECG (max QT) was further used as an index of the longest ventricular repolarisation time. Baseline was considered to be with $[K^+]$ of 5 mM at 1 Hz pacing.

7.3 Results

7.3.1 Septal and apical HCM phenotype baseline models with regional ionic remodelling

The 10 human ventricular electrophysiological profiles used in the biventricular simulations of this chapter are shown in Fig. 7.2A, where HCM electrophysiological remodelling was characterised by significant AP prolongation. This resulted in prolonged max QT interval under baseline conditions proportional to the degree of electrophysiological remodelling (Fig. 7.2B), when regional remodelling was included in the septal (Fig. 7.2C) and apical (Fig. 7.2D) human biventricular HCM models. The gradients of HCM ionic remodelling correspond to a linear gradient in rescaled ionic conductances from the baseline AP model up to the maximally remodelled tissue, which corresponds to the rescaling of ionic conductances listed in Table 4.1. The regional ionic remodelling caused heterogeneous repolarisation times in the septal (Fig. 7.2E) and apical (Fig. 7.2F) models. These repolarisation gradients manifested as morphological T wave abnormalities, which were less widespread among leads in simulations of the septal hypertrophy phenotype (4–5 affected: I, aVR, aVL, V5 and V6 as in Fig. 7.3) than the apical hypertrophy phenotype (7–8 affected: I, II, III, aVR, aVL, aVF, V5 and V6 as in Fig. 7.4), as reported clinically [279]. Representative T wave inversions are shown for lead V6 in the septal model (Fig. 7.2G) and for lead V5 in the apical model (Fig. 7.2H).

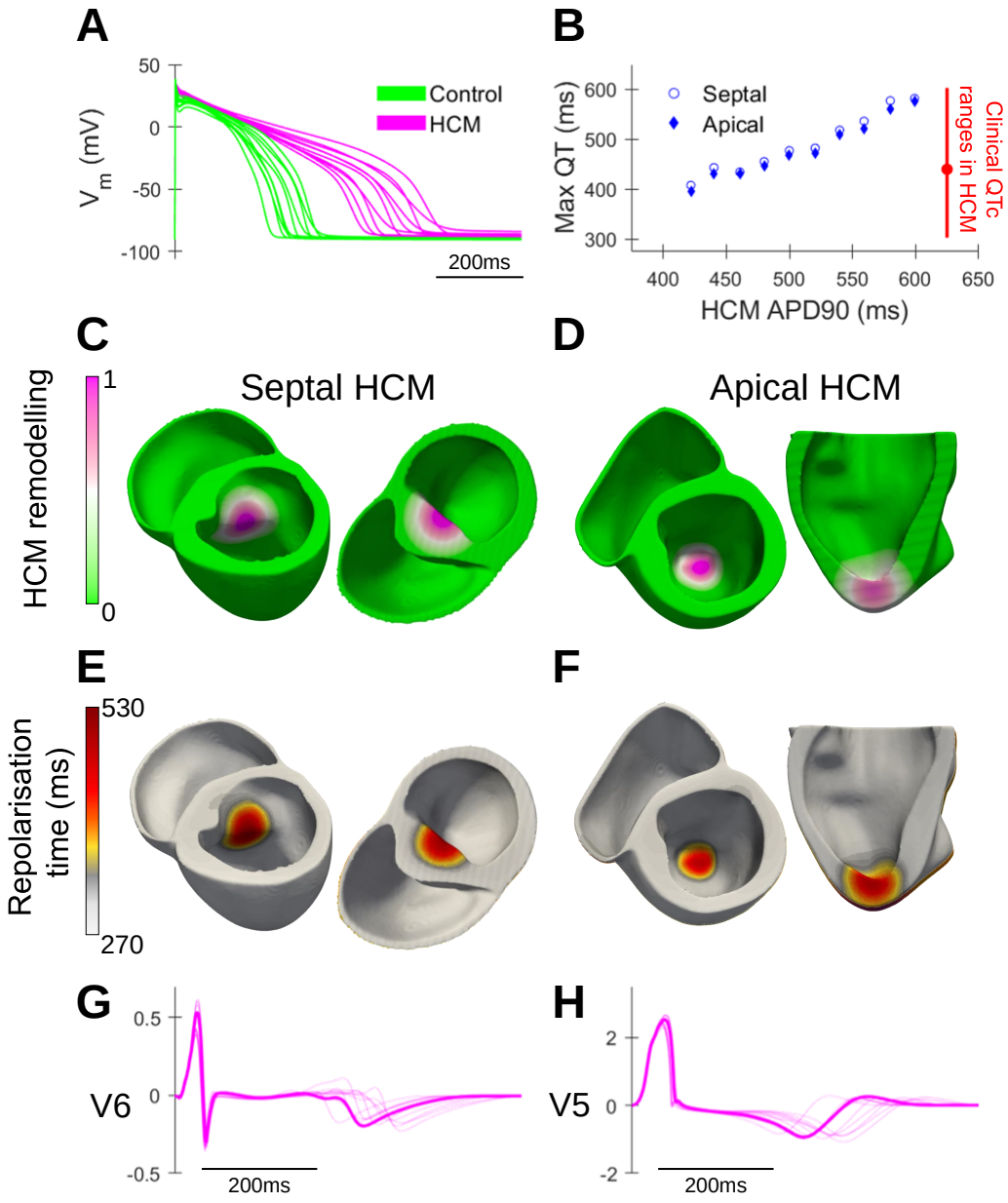


Figure 7.2: Construction of septal and apical human HCM biventricular models. (A) Cellular AP traces for the 10 electrophysiological profiles used in biventricular simulations, where each human control AP model is paired with its HCM-remodelled counterpart. (B) Max QT interval measured from ECGs derived from the biventricular simulations against the cellular APD of each respective biventricular simulation, compared to clinical QT_c ranges in HCM [155]. (C, D) Distribution of HCM electrophysiological remodelling imposed in biventricular simulations for septal and apical HCM phenotypes, respectively. (E, F) Repolarisation time maps, reflecting the HCM ionic remodelling for septal and apical phenotypes,

respectively. (G, H) ECGs from biventricular HCM simulations, showing characteristic T wave inversions in lead V6 in septal (G), and lead V5 in apical (H) hypertrophy patterns. All results presented at 1 Hz pacing.

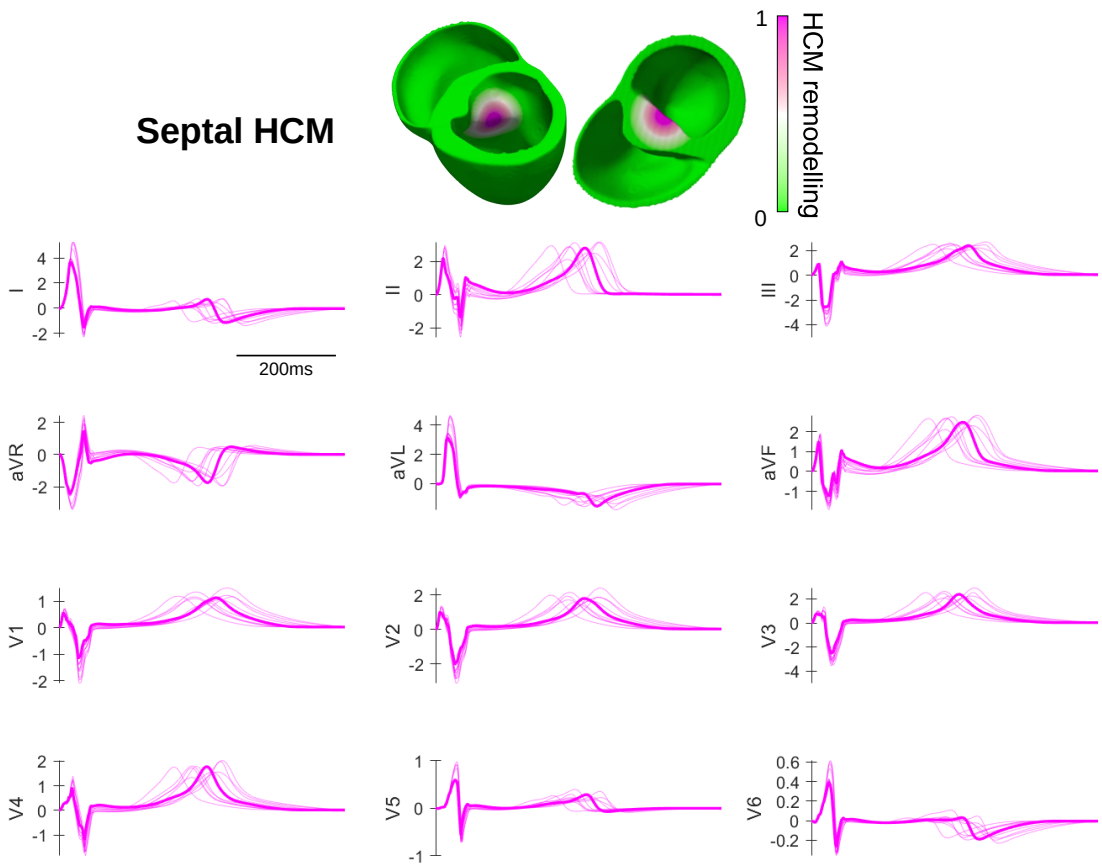


Figure 7.3: 12-lead ECGs derived from baseline septal HCM models (n = 10).

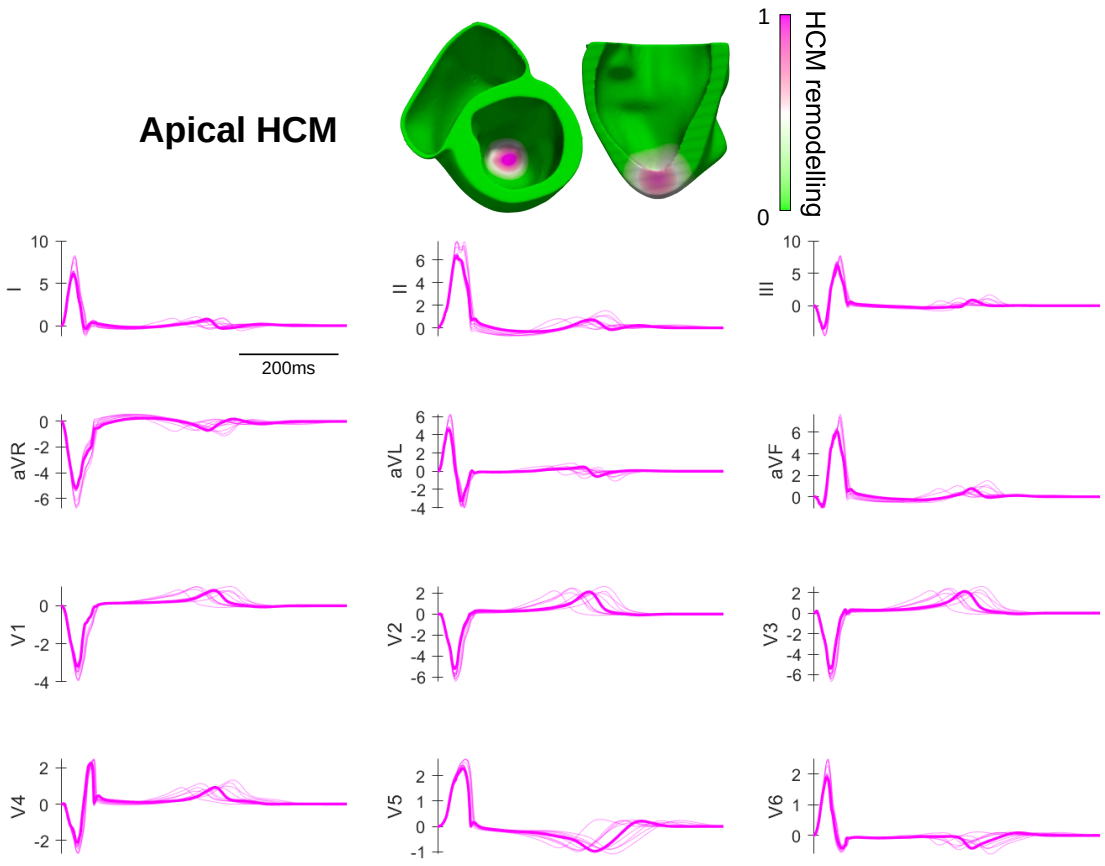


Figure 7.4: 12-lead ECGs derived from baseline apical HCM models (n = 10).

7.3.2 Effects of serum vs. regional K^+ on T wave abnormalities

Figure 7.5 shows how, in septal HCM models, the effects of global serum [K^+] increases (uniformly elevated [K^+] throughout the entire ventricles) on the ECG were different to those arising from regionally ischaemic [K^+] increases (elevated [K^+] affecting only the region of septal hypertrophy and ionic remodelling). Representative lead V6 traces are shown for increases in serum [K^+] (Fig. 7.5A) and regional [K^+] (Fig. 7.5B), where significant changes to T wave morphology and QT interval are visible.

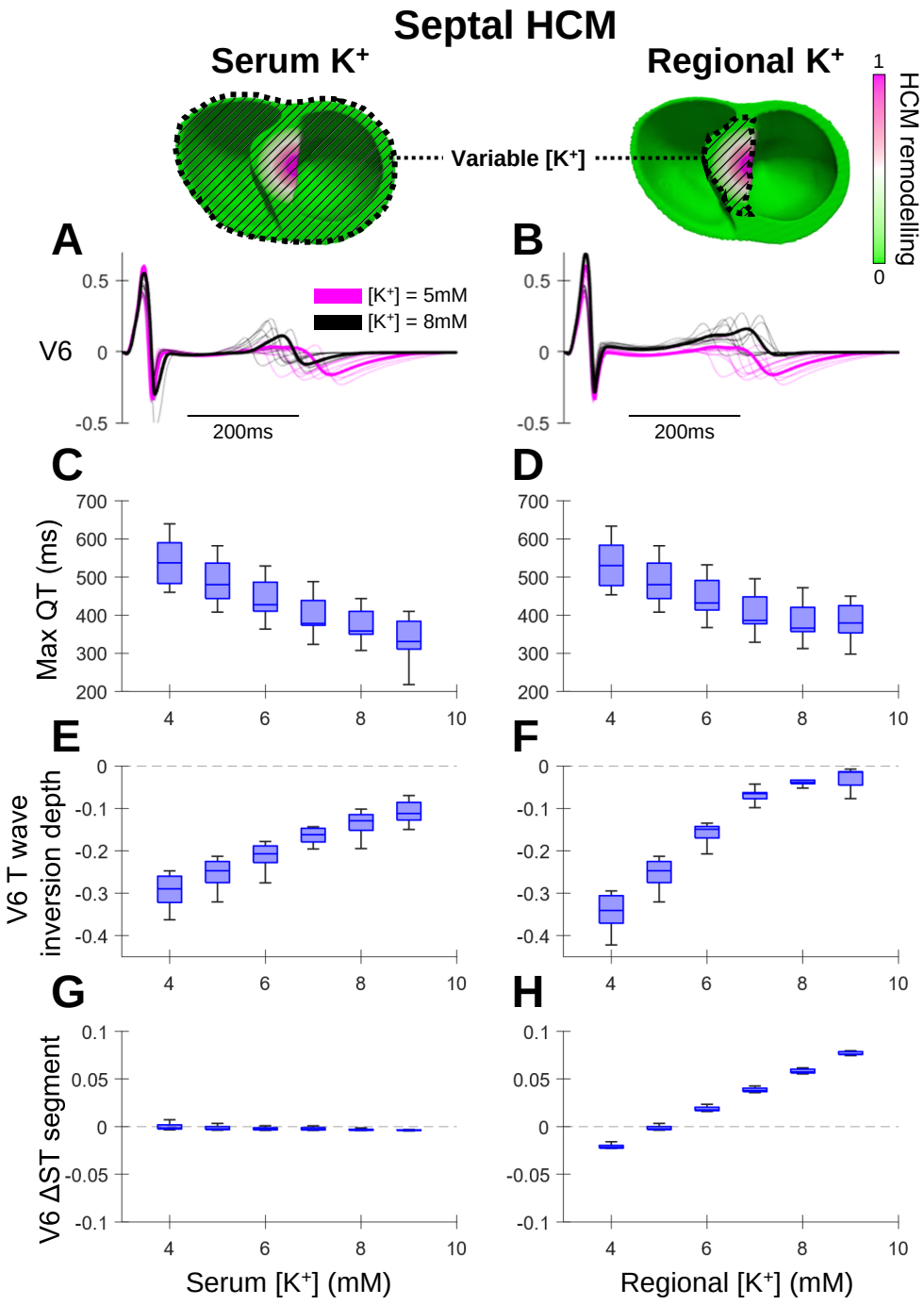


Figure 7.5: Comparisons of the effect of increased serum [K^+] vs. increased regional [K^+] on ECG biomarkers in septal HCM. (A, B) Representative lead V6 traces, showing that T wave morphology was modulated (but not totally pseudonormalised) by serum [K^+] (A), while full T wave pseudonormalisation occurred due to ischaemia-induced regional [K^+] increases (B). (C, D) Max QT interval, (E, F) lead V6 T wave inversion depth, and (G, H) lead V6 ST segment changes, plotted against serum [K^+] and

regional $[K^+]$, respectively. All results presented at 1 Hz pacing.

For mild $[K^+]$ changes (4–7 mM), max QT interval was similarly decreased for both serum and regional $[K^+]$ increases (Figs. 7.5C & 7.5D), reflecting stark $[K^+]$-induced reductions in APD in the HCM-remodelled region in both cases (Appendix Fig. A.9). For severe $[K^+]$ increases (8–9 mM), when induced regionally by ischaemia, the APD was reduced to that of, or less than, the APD of the normal myocardium, which prevented further QT interval shortening (Appendix Fig. A.10). The QT interval was instead determined by the rest of myocardium modelled as unaffected by HCM remodelling and ischaemia. For severe serum $[K^+]$ increases, the QT interval continued to decrease as the myocardium unaffected by HCM remodelling was now also affected by $[K^+]$-induced reductions in APD. A further discriminant between serum and regional $[K^+]$ increases was that QT dispersion was decreased by regional $[K^+]$ increases more-so than by serum $[K^+]$ (Appendix Fig. A.11).

Differences between serum and regional $[K^+]$ increases were also observed in lead V6 T wave morphology (Figs. 7.5E & 7.5F), with ischaemia-induced regional $[K^+]$ increases causing a greater correction to T wave inversion per unit of extracellular $[K^+]$ elevation than increases in global serum $[K^+]$. While the negative component of the T wave was almost entirely corrected in all models for elevated regional $[K^+]$ of 8–9 mM (Fig. 7.5F), a negative biphasic component remained in all models if subjected to serum $[K^+]$ increases (Fig. 7.5E).

Whereas serum $[K^+]$ did not affect the ST segment (Fig. 7.5G), regional $[K^+]$ increases manifested as ST elevation proportional to the degree of $[K^+]$ increase (Fig. 7.5H), as is common for transmural ischaemia. In comparing Fig. 7.5F and Fig. 7.5H, it is notable that the magnitude of ST segment changes associated with ischaemia-induced regional $[K^+]$ increases was significantly smaller than that of changes to the T wave amplitude. This highlights that T wave pseudonormalisation may be the only perceptible ECG abnormality associated with myocardial ischaemia during stress ECG testing, particularly earlier in the onset of acute ischaemia.

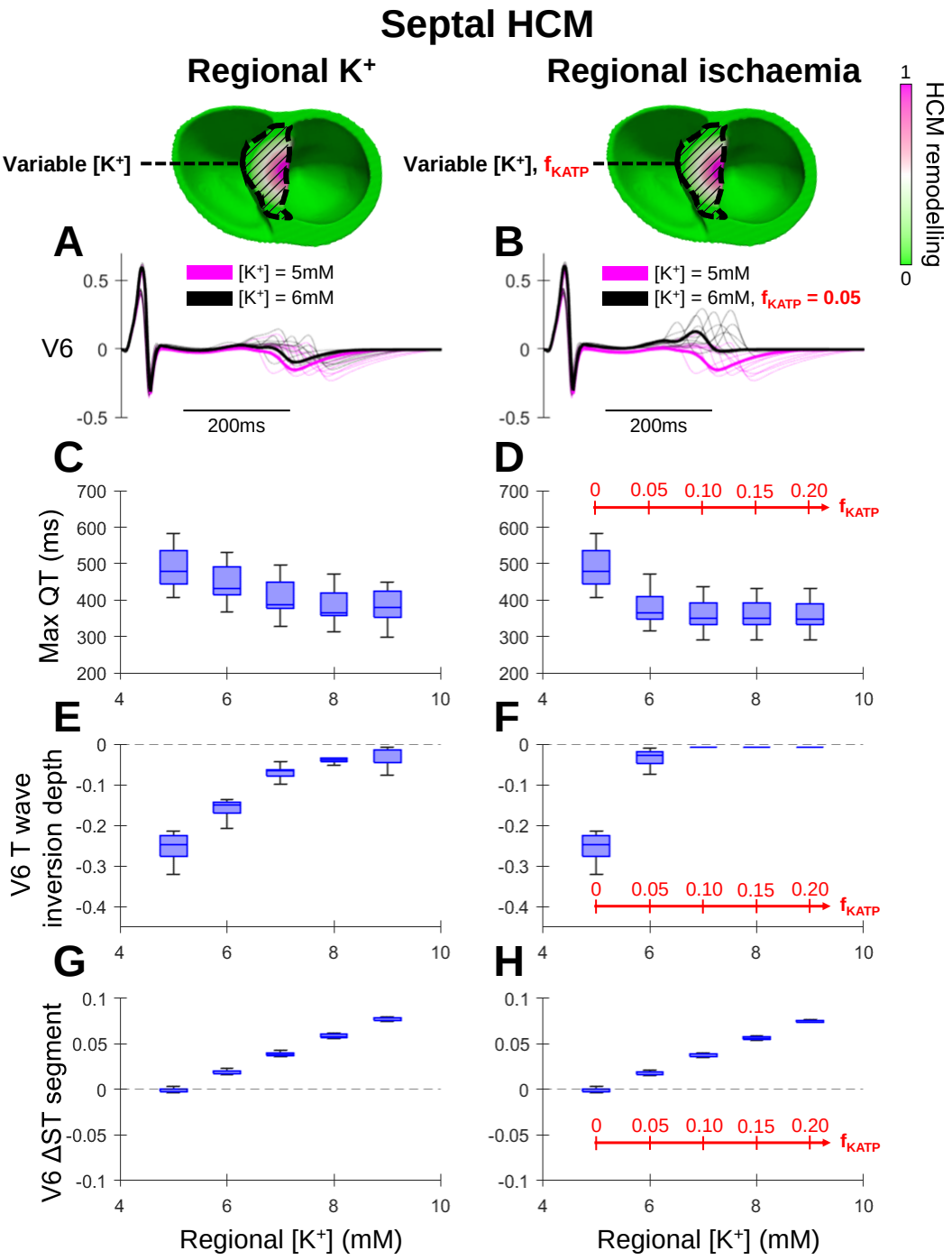


Figure 7.6: Comparisons of the effect of increased regional $[K^+]$ vs. regional $[K^+]$ increases and I_{KATP} activation on ECG biomarkers in septal HCM. (A, B) Representative lead V6 traces, showing that T wave pseudonormalisation occurred at a milder $[K^+]$ increase when I_{KATP} activation was also considered. (C, D) Max QT interval, (E, F) lead V6 T wave inversion depth, and (G, H) lead V6 ST segment changes,

plotted against regional [K^+] and regional [K^+] with a fraction f_{KATP} of KATP channels activated, respectively. All results presented at 1 Hz pacing.

When considering the other major metabolic and molecular components of acute myocardial ischaemia on top of regional [K^+] increases, such as acidosis and activation of I_{KATP} [92, 167, 228], pseudonormalisation of the T wave was accentuated (Fig. 7.6).

Furthermore, T wave pseudonormalisation occurred in proportion to the degree of colocalisation between regional [K^+] increases and ionic remodelling, even with fast pacing (Fig. 7.7), and T wave pseudonormalisation similarly occurred when a more complex regional distribution of [K^+] elevation was considered (Appendix Fig. A.12).

Of interest, at the largest extent of global serum K^+ concentrations tested ([K^+] = 9 mM), some models in the virtual cohort exhibited impaired conduction and the propagation of severely stunted APs (Appendix Fig. A.13). The regions with stunted APs propagated slowly and more heterogeneously (leading to stark QRS prolongation), alongside rapid repolarisation (as stunted APs did not reach full depolarisation). Consequently, T wave peak amplitudes and terminal points were not easily discernible, and such instances were excluded from the analysis of T wave inversion. This occurred because at [K^+] = 9 mM, the RMP of -74.9 $\pm$ 0.2 mV was significantly less negative than at basal conditions of -90.0 $\pm$ 0.4 mV, which constrained I_{Na} availability during the AP upstroke phase. Indeed, models without discernible T waves were characterised by lower I_{Na} maximal conductances of 9.1 $\pm$ 2.5 vs. 14.5 $\pm$ 0.7 ms/µF in models with discernible T waves. The aforementioned effects were also responsible for the increased range of max QT intervals observed with increasing [K^+] = 8 mM to [K^+] = 9 mM (310–440 vs. 220–410 ms respectively) in the remaining virtual models (Fig. 7.5C).

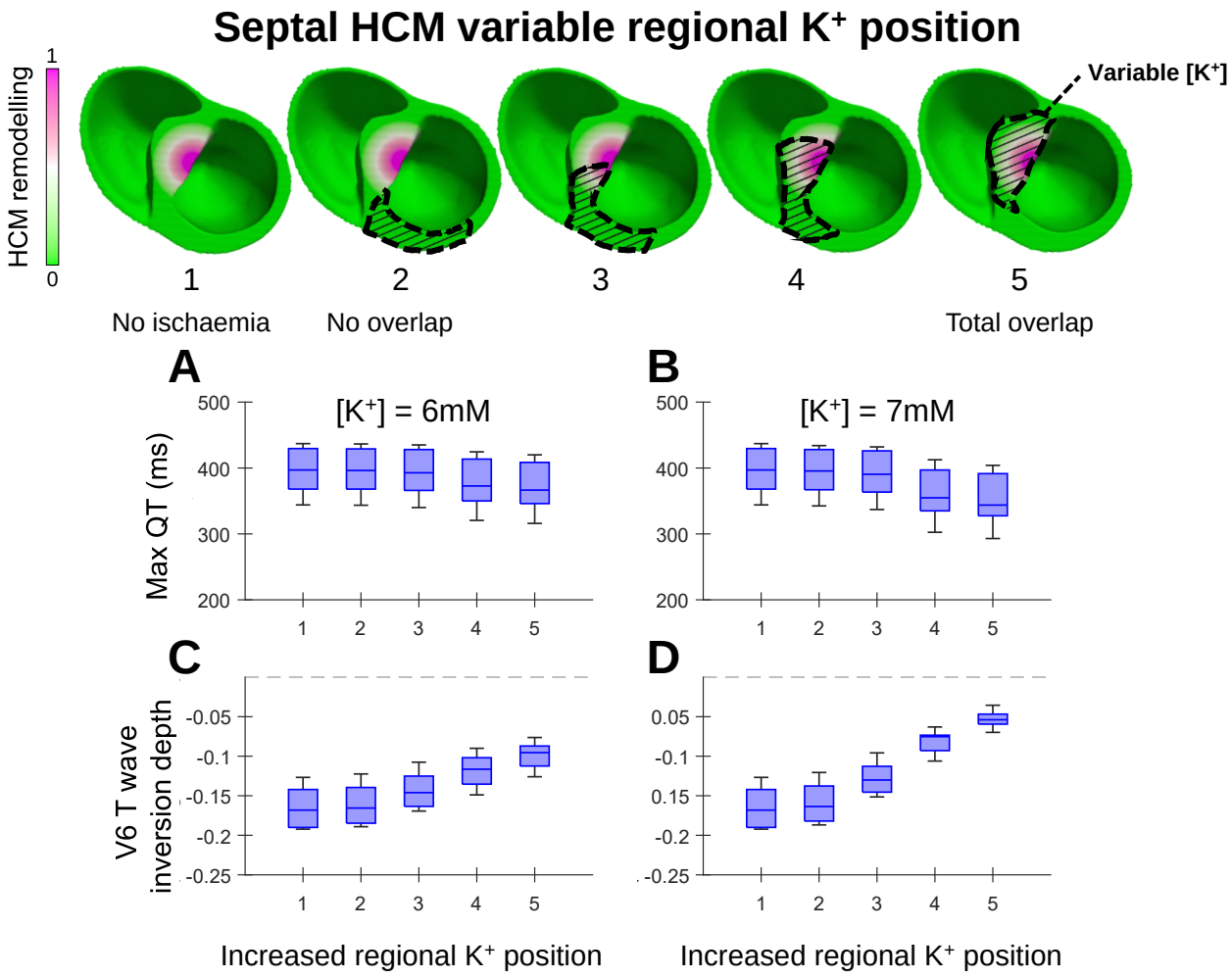


Figure 7.7: Effects of variable positioning of regional $[K^+]$ increases on ECG biomarkers in septal HCM. (A, B) Max QT interval with regional $[K^+] = 6$ mM and 7 mM, respectively, for the 5 considered scenarios of ischaemia/HCM-remodelling overlap. (C, D) Lead V6 T wave inversion depth with regional $[K^+] = 6$ mM and 7 mM, respectively, for the 5 considered scenarios. All results presented at 2 Hz pacing.

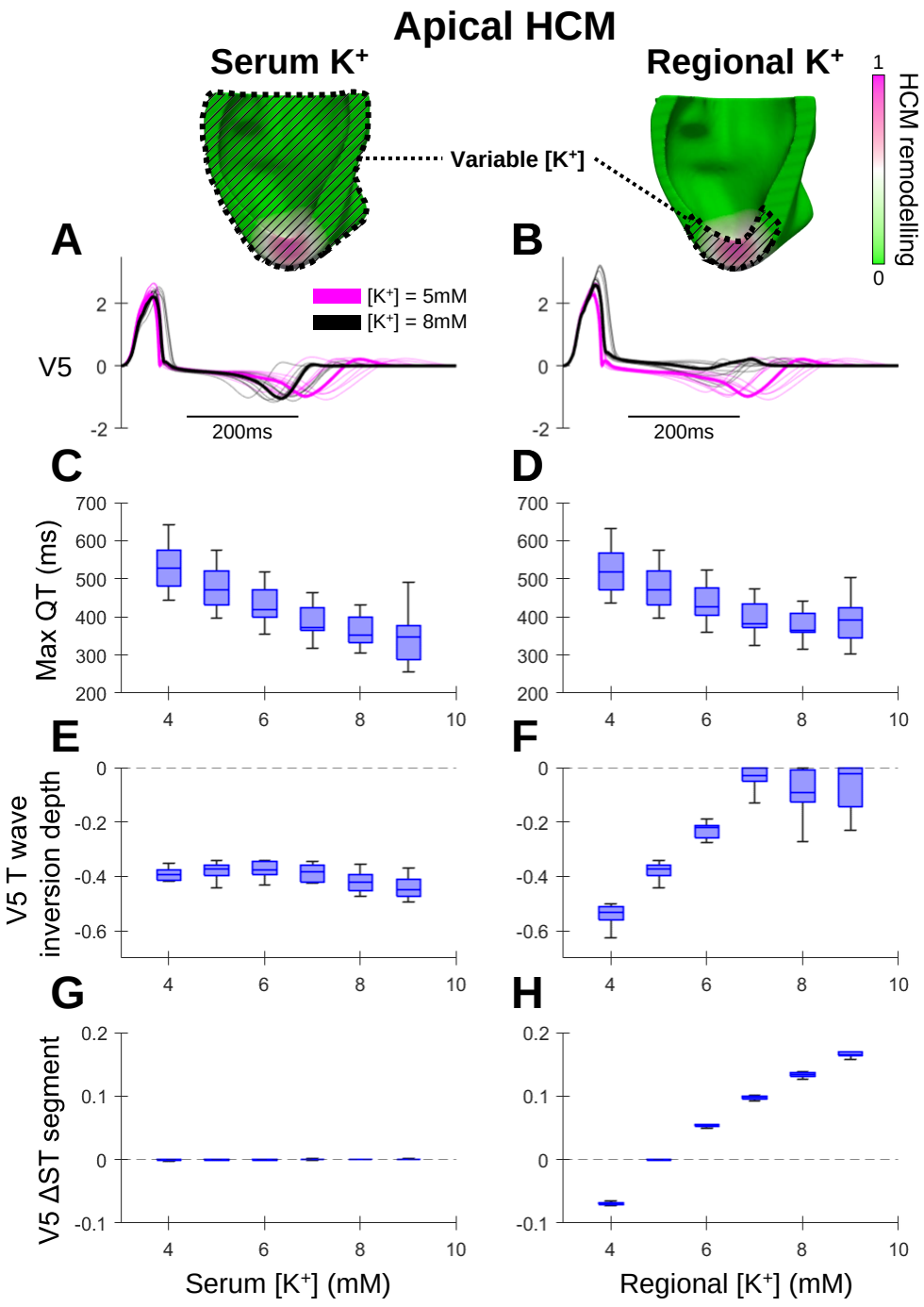


Figure 7.8: Comparisons of the effect of increased serum [K^+] vs. increased regional [K^+] on ECG biomarkers in apical HCM. (A, B) Representative lead V5 traces, showing that T wave morphology was modulated (but not pseudonormalised) by serum [K^+] (A), while full T wave pseudonormalisation occurred due to ischemia-induced regional [K^+] increases (B). (C, D) Max QT interval, (E, F) lead V5

T wave inversion depth, and (G, H) lead V5 ST segment changes, plotted against serum $[K^+]$ and regional $[K^+]$ changes, respectively. All results presented at 1 Hz pacing.

Overall, a similar behaviour was observed for apical HCM models (Fig. 7.8) in the dependence of max QT interval and ST segment elevation on global serum $[K^+]$ increases (uniformly elevated $[K^+]$ throughout the entire ventricles) and regionally ischaemic $[K^+]$ increases (elevated $[K^+]$ affecting only the region of apical hypertrophy and ionic remodelling). However, while T wave inversion was slightly corrected by global serum $[K^+]$ increases in septal HCM models (Fig. 7.5E), serum $[K^+]$ increases left T wave inversions largely unaffected in apical HCM models (Fig. 7.8E).

The increased capacity for ischaemia-induced regional $[K^+]$ increases to cause T wave pseudonormalisation compared to exercise-induced global serum $[K^+]$ increases is explained in Fig. 7.9. Under basal conditions, T wave inversions manifested due to repolarisation gradients, caused by slowed repolarisation in the region of hypertrophy (Fig. 7.9A). As serum $[K^+]$ was elevated, repolarisation times in the hypertrophic remodelled region were reduced, but repolarisation in remote myocardial regions was also accelerated, such that repolarisation gradients persisted (Fig. 7.9B). When $[K^+]$ increase was confined to the HCM-remodelled region, the regionally prolonged repolarisation time was reduced without affecting much of the remote myocardium, such that the baseline repolarisation gradients were counteracted, leading to T wave pseudonormalisation (Fig. 7.9C). It is also of note that the upper range of serum $[K^+]$ considered corresponds to global cardiac ischaemia [56, 167] while only a much lesser serum $[K^+]$ increase typically occurs during exercise [408], thus further minimising the possibility of ascribing T wave pseudonormalisation effects to exercise-induced increases in serum $[K^+]$.

When septal and apical models had multiple concurrent regions of $[K^+]$ elevation, T wave pseudonormalisation occurred similarly as in the case of a single region (Appendices A.14 & A.15), but the second region of $[K^+]$ elevation made secondary contributions such as enhanced ST segment elevation (Appendix Fig. A.16) or new T wave notching in other leads (Appendix Fig. A.17). Finally, similar T wave pseudonormalisation occurred when finer spatial discretisations were used (Appendix Fig. A.18).

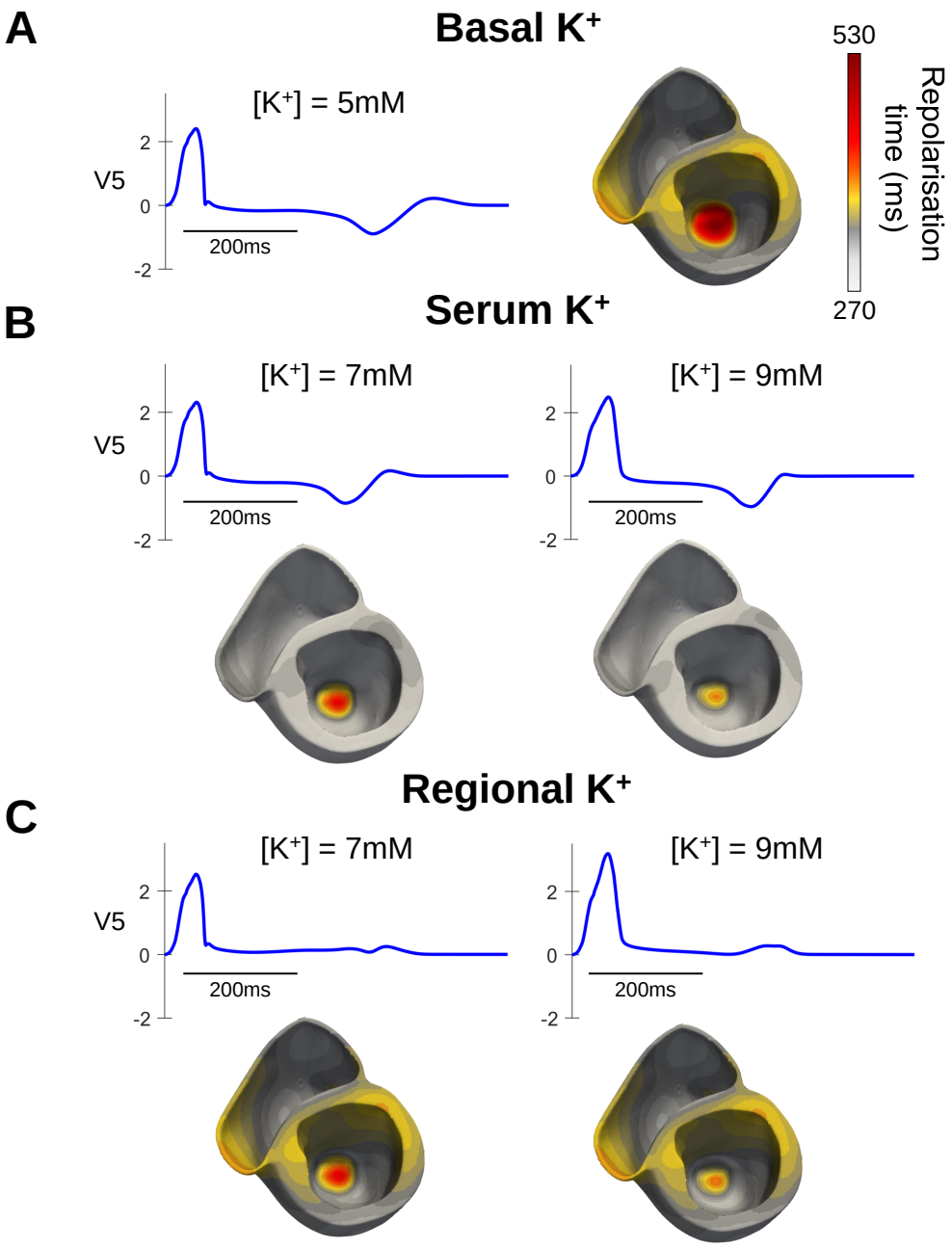


Figure 7.9: Mechanism for T wave pseudonormalisation preferentially occurring due to ischaemia-induced regional $[K^+]$ increases vs. exercise-induced global serum $[K^+]$ increases. (A) Under basal $[K^+]$ conditions, lead V5 T wave inversion (left), characteristic of apical HCM, occurred due to apico-basal repolarisation gradients (right). (B) During serum $[K^+]$ increases, T wave inversions persisted because APs were shortened in both the region of HCM remodelling and the remote myocardium, preserving apico-basal repolarisation gradients. (C) During regional $[K^+]$ increases, T waves became

pseudonormalised because APs were shortened only in the region of HCM remodelling, correcting abnormal baseline repolarisation gradients.

7.3.3 Effects of pacing rate vs. regional K^+ on T wave abnormalities

Comparisons between the effects of increased pacing rate and regionally ischaemic [K^+] increases on the ECG are shown in Fig. 7.10 for septal HCM models in the virtual cohort. For both increased pacing rate and regional [K^+] increases, significant changes to T wave morphology and max QT interval are visible (Figs. 7.10A & 7.10B).

Substantial reductions to the max QT interval occurred at increased pacing rates due to APD rate dependence (Fig. 7.10C). The max QT interval continued to decrease at high pacing rates, contrary to the levelling off behaviour seen for high regional [K^+] (Fig. 7.10D), for the same reasons as with the comparison to serum [K^+] (APD of the HCM-remodelled region reducing to that of the HCM of the non-remodelled myocardium like that shown in Appendix Fig. A.10).

Substantial but incomplete correction of T wave inversion was observed only at the highest pacing rates representative of vigorous exercise (Fig. 7.10E), due to enhanced APD rate-dependence of the HCM-remodelled myocardium [66], leading to partial correction of abnormal repolarisation gradients. Full T wave correction was however not observed, unlike for regional [K^+] increases (Fig. 7.10F). The comparisons between serum and regional [K^+] in Fig. 7.5 at 1 Hz were similar at 2 Hz pacing (Appendix Fig. A.19). For the apical HCM models, as before under serum [K^+] increases, increases of the pacing rate did not significantly affect T wave inversion depth (Fig. 7.11).

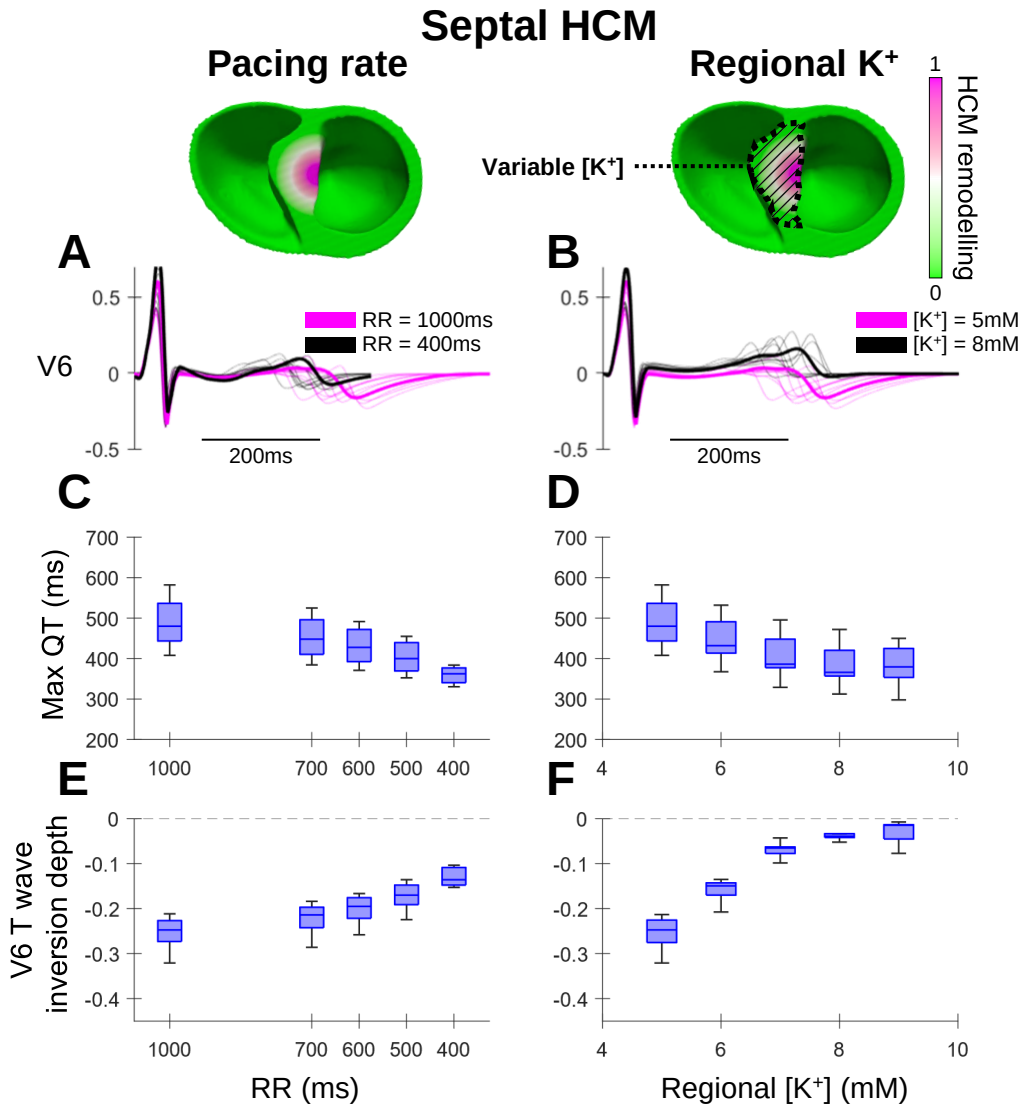


Figure 7.10: Comparisons of the effects of increased pacing rate vs. regional $[K^+]$ increases on ECG biomarkers in septal HCM. (A, B) Representative lead V6 traces, showing that T wave morphology was modulated (but not totally pseudonormalised) by fast pacing (A), and that full T wave pseudonormalisation occurred due to regional $[K^+]$ increases (B). (C, D) Max QT interval, and (E, F) lead V6 T wave inversion depth plotted against RR interval and regional $[K^+]$, respectively.

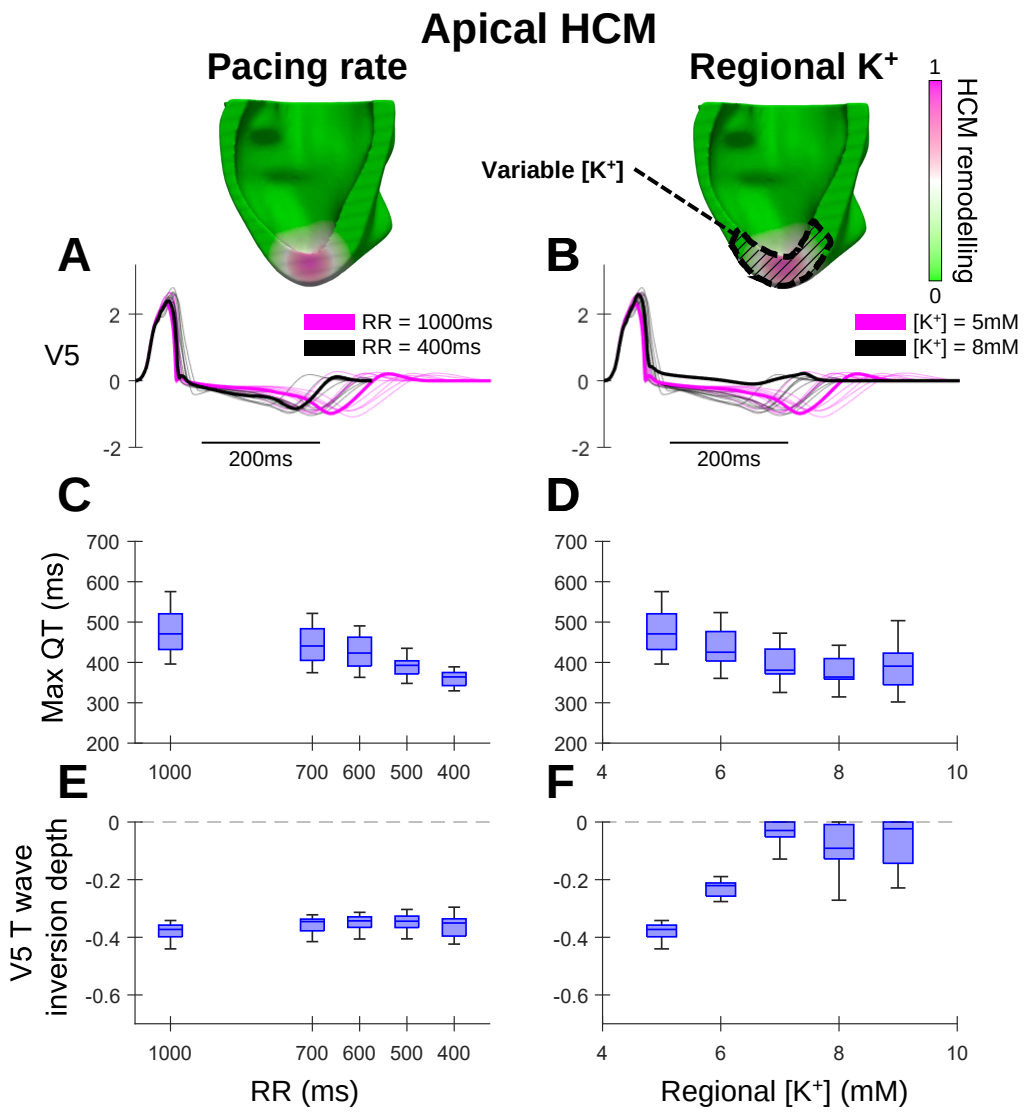


Figure 7.11: Comparisons of the effect of increased pacing rate vs. regional $[K^+]$ on ECG biomarkers in apical HCM. (A, B) Representative lead V5 traces, showing that (A) T wave polarity was largely unaffected by fast pacing, and (B) correction to T wave polarity occurred due to regional $[K^+]$ increases. (C, D) Max QT interval and (E, F) lead V5 T wave inversion depth plotted against (C, E) RR interval and (D, F) regional $[K^+]$.

7.4 Discussion

The principal findings of the study presented in this thesis chapter are that (i) acute regional myocardial ischaemia caused T wave pseudonormalisation in HCM when it colocalised with the remodelled myocardium; (ii) ischaemic T wave pseudonormalisation in HCM models preceded or occurred in the absence of significant ST segment changes; (iii) serum $[K^+]$ modulated the depth of inverted T waves, but T wave polarity was more sensitive to regional $[K^+]$ accumulation; and (iv) increased pacing rates during exercise modulated inverted T wave amplitudes and caused partial pseudonormalisation.

The finding that acute myocardial ischaemia can normalise inverted T waves is consistent with some early reports in cohorts with high rates of ischaemic heart disease, in which deficits on perfusion imaging [212] or significant new WMAs [186] were associated with pseudonormalisation, particularly for massive transmural deficits [230]. Similarly, severe stenosis of the LAD artery has also been linked to transient T wave pseudonormalisation in apical HCM patients [16], and the frequency of stress T wave pseudonormalisation is similar to that of other markers of severe ischaemia such as ST elevation [77]. The present study suggests that this is explained by ischaemic $[K^+]$ increases in a sizable extent of the HCM-remodelled myocardium, which attenuates baseline repolarisation gradients in HCM and corrects T wave polarity. This is mostly consistent with the electrophysiological basis of T wave pseudonormalisation formerly hypothesised by Simon et al. [338], who speculated that it could be explained by the superposition of acute ischaemic effects on myocardial cells (AP shortening) upon chronic disease effects (AP prolongation). This study presents computational evidence of these mechanisms, otherwise inviable to achieve *in vivo* in this high-risk cohort of patients. This ischaemic aetiology may also explain T wave pseudonormalisation reported in HCM during exercise [77, 161] or under administration of sodium nitroprusside [359] or dobutamine [161], as exercise and pharmacologically induced vasodilation are widely reported to induce regional perfusion impairment in HCM [187]. More broadly, the findings of the present study may be related to reports that ECGs with baseline repolarisation abnormalities have a limited range in which to become more abnormal during myocardial ischaemia [313].

For T wave pseudonormalisation induced by myocardial ischaemia, these changes occur 10–30 seconds before frank ST elevation [230], which may be explained in the present study by the finding that T wave

inversion depth was more sensitive than ST elevation to $[K^+]$ increases. Given that exercise-induced ischaemia may be self-limiting in HCM through dyspnoea and angina (as the genesis is due to chronic microvascular dysfunction rather than acute epicardial coronary occlusion), electrophysiological changes preceding frank ST elevation may be increasingly relevant. For example, consideration of subthreshold ST segment changes could augment the diagnosis of myocardial ischaemia if accompanied by changes in T wave polarity [230]. A further discriminant of ischaemic T wave pseudonormalisation from benign causes is that with ischaemia progression the QT interval is expected to stop decreasing, as APs in the ischaemic myocardium become shorter than those in the unaffected myocardium, such that the QT interval is dominated by the unaffected myocardium.

Stress T wave pseudonormalisation has also been reported in non-HCM patients without evidence of myocardial ischaemia [186, 194]. Independent of the exact cause, it is contingent on differential APD responses between the HCM-remodelled and non-remodelled myocardium. Multiple benign causes have been hypothesised, including tachycardia-induced decreases in ventricular repolarisation gradients and sympathetic stimulation [13]. However, there is now evidence that the sympathetic response of APD in diseased HCM myocardium is abnormal, such that repolarisation gradients are likely to be enhanced under sympathetic stimulation rather than corrected [62]. Conversely, rate-dependent repolarisation gradients were shown in the present study to contribute to pseudonormalisation due to accentuated APD rate dependence in diseased HCM cells [66], consistent with the association between heart rate and T wave inversion depth observed in apical HCM [202]. As a further potential contributor, the present study investigated how the accentuated $[K^+]$ dependence in diseased HCM cells manifests as T wave changes during exercise-induced serum $[K^+]$ increases. In the scenarios tested, serum $[K^+]$ had the potential to modulate T wave inversion magnitude, but only approached pseudonormalisation during severe global hyperkalaemia. Physiological exercise serum $[K^+]$ increases alone did not lead to full T wave pseudonormalisation in the present study, but may in part explain the difficulty of diagnosing ischaemia on the ECG in HCM [222]. The enhanced dependence of repolarisation in HCM-remodelled myocardium on $[K^+]$ can lead to enhanced T wave morphological changes under benign serum $[K^+]$ increases. A further important consideration is that the T wave response to serum $[K^+]$ increases differed between the septal and apical HCM models, suggesting that there is strong dependence on the ventricular anatomy

and regions affected by electrophysiological remodelling.

7.5 Conclusions

Altogether, these results support the hypothesis of the present study, which was that T wave pseudonormalisation may primarily be caused by regionally ischaemic $[K^+]$ increases in HCM, with secondary contributions from exercise-induced serum $[K^+]$ and pacing rate increases. T wave pseudonormalisation was always more sensitive to regional $[K^+]$ than serum (global) $[K^+]$ increases, and in apical models serum $[K^+]$ or fast pacing did not correct T wave polarities, suggesting that added anatomical constraints apply to non-ischaemic T wave pseudonormalisation. The present study explains the clinically challenging diagnosis of ischaemia on stress ECG in HCM [222], as T wave changes may be multifactorial in origin, with contributions from both ischaemia and benign exercise factors. Finally, the present study motivates further investigation of subthreshold ST segment changes in combination with T wave pseudonormalisation as criteria for diagnosing ischaemia on stress ECG in HCM.

7.6 Limitations

General computational limitations are detailed in section 9.3. Of particular relevance to this chapter, the effects of $[K^+]$ were explored in two configurations: regional and global. Whether there is hypertrophy-associated heterogeneity in $[K^+]$ increases in the ventricles accompanying exercise-induced serum $[K^+]$ increases is unknown [369]. The present study also focused on transmurally ischaemic $[K^+]$ accumulation and associated ST elevation, however subendocardial ischaemia and associated ST depression are a more common finding on stress ECGs in HCM [77]. Therefore, future work may consider how subendocardial insults modulate inverted T waves in HCM. A further consideration is that T wave inversion at baseline can also be caused by fibrosis, and the mechanisms identified in the present study would not apply to such cases. Furthermore, sudden relief of chronic disease and subsequent correction of repolarisation due to other effects, metabolic or otherwise, cannot be ruled out [359] as a cause of T wave pseudonormalisation. Finally, ECG abnormalities other than the T wave (resting ST elevation) have also been reported to normalise in some HCM patients [166].

CHAPTER 8

Effects of ranolazine on the arrhythmic substrate in HCM

The previous chapters investigated how HCM ionic remodelling modulates ischaemic arrhythmic risk and the ECG manifestation of ischaemia. In this chapter, the use of an anti-ischaemic drug (ranolazine) is investigated as a possible antiarrhythmic agent, in relation to its additional effects of correcting slowed repolarisation in HCM.

8.1 Introduction

Ranolazine is a drug that is approved for the treatment of chronic angina, which is reported to be effective at relieving microvascular ischaemia in HCM [15]. *In vitro* experiments on human HCM cardiomyocytes with ionic remodelling showed that ranolazine, through blocking I_{NaL}, can also correct slowed repolarisation [66]. Ranolazine is further reported to have antiarrhythmic effects in a subgroup of HCM patients [15, 270], but the underlying mechanisms are not fully understood.

This thesis chapter therefore sought to investigate the effects of ranolazine-induced I_{NaL} block on the arrhythmic substrate in HCM. As APD heterogeneity mediated by I_{NaL} has been shown to form a substrate for VT in animal models [386], it was hypothesised that correction of prolonged APDs by ranolazine [66, 67] would reduce refractoriness heterogeneity and the risk of VT. It was further hypothesised that the severity of ionic remodelling would modulate antiarrhythmic effects of ranolazine, and that there may be ECG biomarkers associated with the maximally benefiting HCM subgroups.

8.2 Methods

To test the hypothesis that ranolazine may be antiarrhythmic in HCM, tissue and biventricular scenarios were considered with (i) regional HCM ionic remodelling, and compared to those with (ii) regional HCM ionic remodelling and globally applied ionic effects of ranolazine.

8.2.1 HCM tissue and biventricular models

Representative human biventricular models of septal HCM were used, alongside tissue HCM models. Simulations in tissue were repeated using 50 different AP models randomly sampled from the AP populations from section 5.2.1 to account for inter-subject variability in disease expression. All simulations used a spatial discretisation of 350 μm or 400 μm.

HCM ionic remodelling

HCM ionic remodelling, as detailed in Table 4.1, was modelled in three different severities: moderate – where only I_{NaL} was upregulated, as reported early in murine HCM [67]; severe – where all ionic remodelling components were included, but with K^+ channel remodelling at half-maximal severity; and extreme – where all ionic remodelling components were included at full severity [66]. This produced 3×50 HCM AP models (with moderate, severe and extreme degrees of ionic remodelling), paired to 50 control AP models.

HCM ionic remodelling was modelled following section 3.3.3. Ionic remodelling was therefore included in the domains as a circle/sphere of radius 1.0 cm subjected to maximal ionic remodelling, encircled by a border of radius 2.5 cm containing a linear gradient in rescaled ionic conductances from non-remodelled up to maximally remodelled tissue. In tissue, this was applied from the centre of the domain, whereas in biventricular simulations this was applied from the site of maximal LV endocardial septal hypertrophy. A subset of tissue simulations were repeated for a larger HCM-affected region (radius 1.5 cm encircled by a border of radius 3.0 cm).

8.2.2 Pacing protocol

Arrhythmic risk was quantified using the S1-S2 protocol previously described in section 4.6, with S2 always applied immediately outside of the HCM-remodelled border. S2 was applied proximal to the side of S1 in tissue models, and applied endocardially in an infero-posterior position in biventricular models. A subset of tissue arrhythmic risk simulations were repeated using an S1 cycle length of 700 ms.

8.2.3 Modelling effects of ranolazine

The model of ranolazine was derived from previous computational modelling of the drug [281] as informed by *in vitro* IC50 measurements [11, 76]. The IC50 for I_{Kr} was adjusted to produce agreement with human *in vitro* experiments at a concentration of 10 μM, where statistically insignificant APD changes of -30 $\pm$ 40 ms were reported in control cardiomyocytes compared to changes of -120 $\pm$ 70 ms in HCM cardiomyocytes paced at 1 Hz [66]. Ranolazine was modelled using IC50s of 5.9 μM, 77 μM and 30.2 μM for I_{NaL}, I_{Kr} and I_{Na}, respectively, such that I_{NaL} was predominantly blocked with secondary effects on I_{Kr} and I_{Na}.

As experimental models of ranolazine typically administer 10 μM as a therapeutic concentration [66, 67, 386], yet variable dosage is administered clinically, ranolazine concentrations of 3, 6 and 10 μM were considered. These concentrations approximately correspond to dosages of 500, 1000 and 1500 mg bid, respectively [152, 350], where up to 1000 mg bid is used clinically in HCM [270] and 1500 mg bid has been used in clinical trials [49].

8.2.4 Simulated ECG analysis

In ECGs derived from biventricular simulations, the QT interval and JT interval were computed for each lead. The maximum QT and maximum JT intervals across the 12-lead ECG (max QT and max JT) were further used as indices of the longest ventricular repolarisation time.

8.2.5 Clinical ECGs of HCM patients pre- and post-ranolazine

Patients with HCM treated with ranolazine between January 2010 and December 2020 were identified from the Careggi University Hospital Cardiomyopathy Unit [15]. Resting 12-lead ECGs recorded before

and after ranolazine initiation were available in N = 76 patients at a mean follow-up duration of 17 ± 15 months. 3 patients with alternans either pre- or post-ranolazine were excluded, alongside 1 patient in which the full 12-lead ECG was illegible. A control group consisting of N = 35 HCM patients not initiated on ranolazine with resting 12-lead ECGs on an initial and follow-up visit (25 ± 22 months) were also assembled, selected to exclude those on amiodarone or disopyramide.

Automated ECG delineation software [226] was used to identify points corresponding to the beginning and end of the QRS, and end of the T wave in all 12 leads for each patient. JT intervals were automatically computed and manually reviewed in all 12 leads. Individual leads were excluded in cases of (1) ambiguous T wave end points or (2) excessive noise. JT intervals were rate-corrected according to $JT_c = JT/RR^{0.5}$ [24]. Finally, only leads in the same patient measurable on both the initial and follow-up visit were considered in the analysis. All raw ECG data was provided by Dr. Matteo Beltrami, Careggi University Hospital Cardiomyopathy Unit, Florence.

8.3 Results

8.3.1 Baseline HCM electrophysiological phenotypes

The human ventricular AP models used in simulations are shown in Fig. 8.1A, where HCM ionic remodelling manifested as slowed repolarisation. The variable degrees of HCM remodelling imposed (moderate, severe and extreme) corresponded to the range of APD prolongation demonstrated in Figs. 8.1B & 8.1C. When ECGs were derived from biventricular simulations (Fig. 8.1D) with AP models corresponding to the [25, 50, 75]th APD percentiles of their respective HCM electrophysiological remodelling type, increasing degrees of remodelling were associated with increasingly prolonged max QT intervals (Fig. 8.1E). This was also reflected in simulated ECG measurements of QT dispersion of 10–40 ms, 40–70 ms, 110–140 ms and 170–200 ms for control, moderate, severe, and extreme HCM remodelling, respectively.

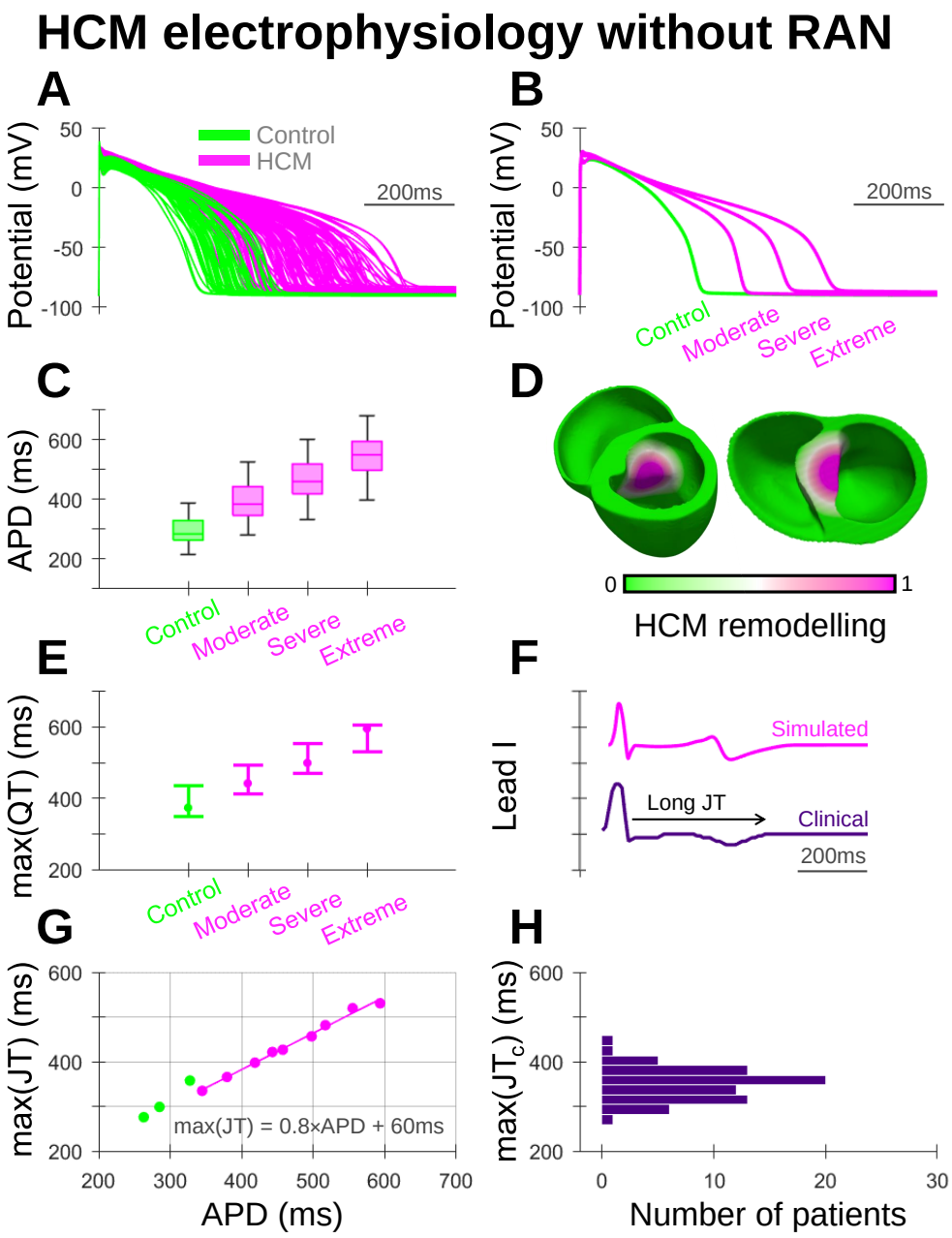


Figure 8.1: Electrophysiological remodelling in HCM. (A) Simulated populations of human ventricular endocardial AP models with non-remodelled electrophysiology (n = 50) paired with HCM-remodelled electrophysiology pooled across moderate, severe, and extreme models (n = 50 each). (B) Representative simulated endocardial AP traces. (C) APD distributions of control, moderate, severe, and extreme AP models showing increasing APD prolongation. (D) Human biventricular model with gradients of HCM electrophysiological remodelling in the region of septal hypertrophy, from which simulated

ECGs were derived for the various HCM remodelling severities. (E) Max QT intervals for the various electrophysiological phenotypes, where AP models corresponding to [25, 50, 75]th APD percentiles were used in biventricular simulations. (F) Example lead I ECG traces with prolonged JT intervals, simulated and clinically. (G) Max JT intervals derived from biventricular simulations, plotted against remodelled cellular APD. (H) Max JT_c intervals measured clinically among HCM patients (N = 72). All simulated results presented at 1 Hz pacing. RAN: ranolazine.

Clinically, as both delayed activation and repolarisation contribute to QT prolongation in HCM [155], JT intervals were derived from clinical and simulated ECGs (Fig. 8.1F) to isolate repolarisation effects (Figs. 8.1G & 8.1H). Among ECGs derived from biventricular simulations (Fig. 8.1G), the max JT interval increased with the APD of the HCM-remodelled region. The relationship between max JT and APD was fit according to $\max(JT) = 0.8 \times APD + 60$ ms, to allow relationships between in-tissue arrhythmic risk and APD to be related to the APD. Cellular APD was only partially translated into regional APDs and JT intervals in the biventricular model due to electrotonic coupling effects. Simulated max JT intervals were measured between 280–360 ms in controls, and in HCM 340–420 ms, 400–480 ms and 460–530 ms with moderate, severe and extreme remodelling, respectively. Among clinical ECGs (Fig. 8.1H), 64% of patients had max $JT_c > 340$ ms (akin to simulations with moderate remodelling), with 6% having max $JT_c > 400$ ms (akin to simulations with severe remodelling), similar to JT_c measurements made in another HCM study population [394].

8.3.2 Baseline HCM arrhythmic risk

Arrhythmic risk at baseline (Fig. 8.2) was quantified for 300 in-tissue scenarios, spread across 150 HCM AP models, and medium-sized and large HCM-remodelled regions (Figs. 8.2A & 8.2B). Ectopic S1-S2 protocols applied to these in-tissue scenarios totalled 16,988 simulations of re-entry inducibility including 543 PVC couplets and 216 VT episodes.

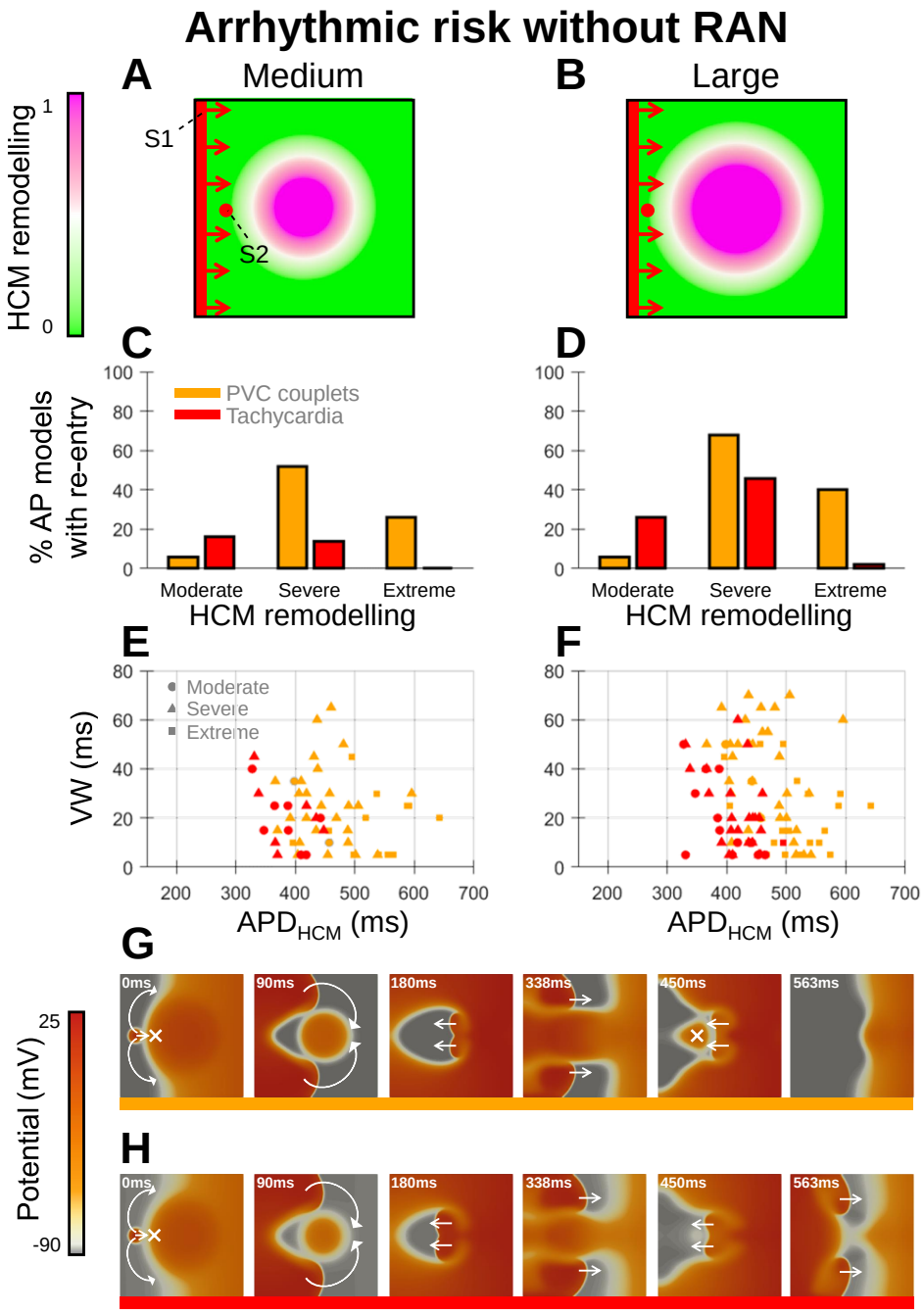


Figure 8.2: Arrhythmic risk in tissue HCM models without ranolazine. (A, B) Tissue domains used to simulate heterogeneous repolarisation for (A) medium-sized and (B) large regions affected by HCM remodelling. (C, D) Percentage of AP models vulnerable to the induction of re-entries (PVC couplets or VT) for moderate, severe, and extreme degrees of HCM remodelling, corresponding to the (C) medium-

sized and (D) large affected regions. (E, F) Re-entry vulnerable window width vs. HCM-remodelled APD for each AP model that had PVC couplets or VT, corresponding to the (E) medium-sized and (F) large affected regions. Plots are pooled across moderate (circles), severe (triangles) and extreme (squares) degrees of HCM remodelling. Orange symbols denote PVC couplets, while those in red denote VT formation. (G, H) Representative tissue simulations after the application of S2, showing the induction of (G) PVC couplets, and (H) VT (where multiple re-entrant cycles occur). Arrows and crosses denote directions of wavefront propagation and conduction block, respectively. Time elapsed following S2 is denoted in each frame. All results presented at 1 Hz pacing. RAN: ranolazine; VW: vulnerable window width.

Analysis of arrhythmic risk at baseline among the populations of AP models showed that re-entry inducibility was critically dependent on the degree of HCM remodelling (Figs 8.2C & 8.2D). Although re-entry was inducible in a subset of tissue models for all degrees of HCM remodelling, VT was almost only inducible with moderate-severe remodelling (14–46% of moderate-severe HCM AP models had VT) rather than extreme (0–2%). PVC couplets were observed most frequently among AP models with severe remodelling (52–68%), rather than moderate (6%) or extreme (26–40%). These results suggest that arrhythmic risk initially increases with progression of ionic remodelling in HCM, then may decline with more advanced ionic remodelling.

Analysis of AP biomarkers pooled across degrees of HCM remodelling yielded remodelled APD as a key determinant of PVC couplet and VT incidence (Figs. 8.2E & 8.2F). Compared to the full range of remodelled APDs (280–680 ms), PVC couplets only emerged in a subset (370–640 ms; orange symbols), and VT was inducible only for an even narrower range of APDs (330–490 ms; red symbols).

Mechanistically, this is explained by both PVC couplets and VT requiring a threshold extent of APD heterogeneity for unidirectional conduction block of S2 (not satisfied for remodelled APDs $<$ 330 ms), but VT imposing a further constraint on remodelled APDs for multiple cycles of re-entry to occur. Secondary to the APD, the HCM-remodelled ERP must satisfy $ERP < L/v$ for VT to occur (but not for PVC couplets), where L is the re-entrant circuit length and v is the conduction velocity. This

is shown in Fig. 8.2G, where a single re-entry (PVC couplet) occurred due to heterogeneous APDs that enabled conduction block, but further excitation was blocked by refractoriness in the remodelled myocardium ($ERP < L/v$ not satisfied). Conversely, in Fig. 8.2H, a shorter remodelled APD still enabled conduction block, but also sustained re-excitation ($ERP < L/v$ satisfied) such that VT was induced. This condition was responsible for the reduced incidence of VT in cases of extreme vs. severe remodelling, as the long ERP with extreme remodelling precluded multiple cycles of re-entry.

This condition was also responsible for the increased incidence of VT in the large vs. medium-sized HCM-remodelled region (Figs 8.2C & 8.2D), as an increased spatial extent of APD heterogeneity increased circuit length L, such that models with a greater ERP (secondary to larger APD) could now manifest VT. Indeed, VT occurred in models with remodelled APDs of 330–490 ms vs. 330–450 ms in the larger vs. medium-sized HCM-remodelled regions, respectively.

The reduced incidence of PVC couplets in cases of extreme vs. severe remodelling was attributed to the late S1-S2 coupling intervals required to allow the remodelled region to have recovered excitability post-S1. At these late S1-S2 coupling intervals, I_{Na} was increasingly recovered, such that CV of S2 wavefronts approached that of S1, impairing many re-entries. These expected behaviours constituted important validation of the framework, to enable the effects of ranolazine on arrhythmic risk to be subsequently investigated.

8.3.3 Ranolazine effect on HCM electrophysiology

Ranolazine, due to its predominant block of I_{NaL} (Fig. 8.3A), caused large APD decreases in HCM-remodelled cells, with modest effects in controls (Fig. 8.3B). This APD shortening being confined to HCM cells, without large changes in controls, was validated against that measured in patch-clamp experiments [66] (Fig. 8.3C). Specifically, 10 μM ranolazine led to APD changes of -120 $\pm$ 70 ms in n = 26 HCM cells from surgical myectomy samples from N = 11 HCM patients [66], compared to -90 $\pm$ 30 ms in simulated HCM cells. For controls, APD changes of -30 $\pm$ 40 ms occurred in n = 11 cells from N = 4 non-failing non-hypertrophic aortic stenosis patients, compared to -10 $\pm$ 10 ms in simulated control cells. Simulated changes in APD were similar across the different HCM remodelling severities (Fig. 8.3D), although slightly larger in cells with moderate remodelling due to the absence of K^+ channel

remodelling. When 10 μM ranolazine was applied to biventricular simulations with heterogeneous HCM remodelling (as shown before in Figs. 8.1D & 8.1E, where max JT intervals were initially prolonged), max JT intervals changed by median -70 ms (Figs. 8.3E & 8.3F), reflecting correction of impaired repolarisation by ranolazine. Examples of simulated 12-lead ECGs before and after 10 μM ranolazine are shown in (see later) Figs 8.4 & 8.5, for control and HCM models, respectively.

In the clinical ECGs, JT intervals were measurable on the initial and follow-up visit in 397 leads from 68 patients of 864 total possible leads in the ranolazine group, and 201 leads from 33 patients of 420 total possible leads in the no-ranolazine group. Decreases of the JT_c interval were observed under ranolazine in leads with longer JT_c at baseline (Fig. 8.3G), consistent with acceleration of repolarisation and abbreviation of the T wave (Fig. 8.3H). By comparing changes in JT_c intervals in the ranolazine and no-ranolazine groups (Fig. 8.3G), the effects of ranolazine on JT_c were estimated. At the lower drug concentration achieved clinically in most patients, JT_c intervals changed due to ranolazine by -10 to -15 ms in those with 360–380 ms basal JT_c, and -15 to -20 ms in those with 380–400 ms basal JT_c.

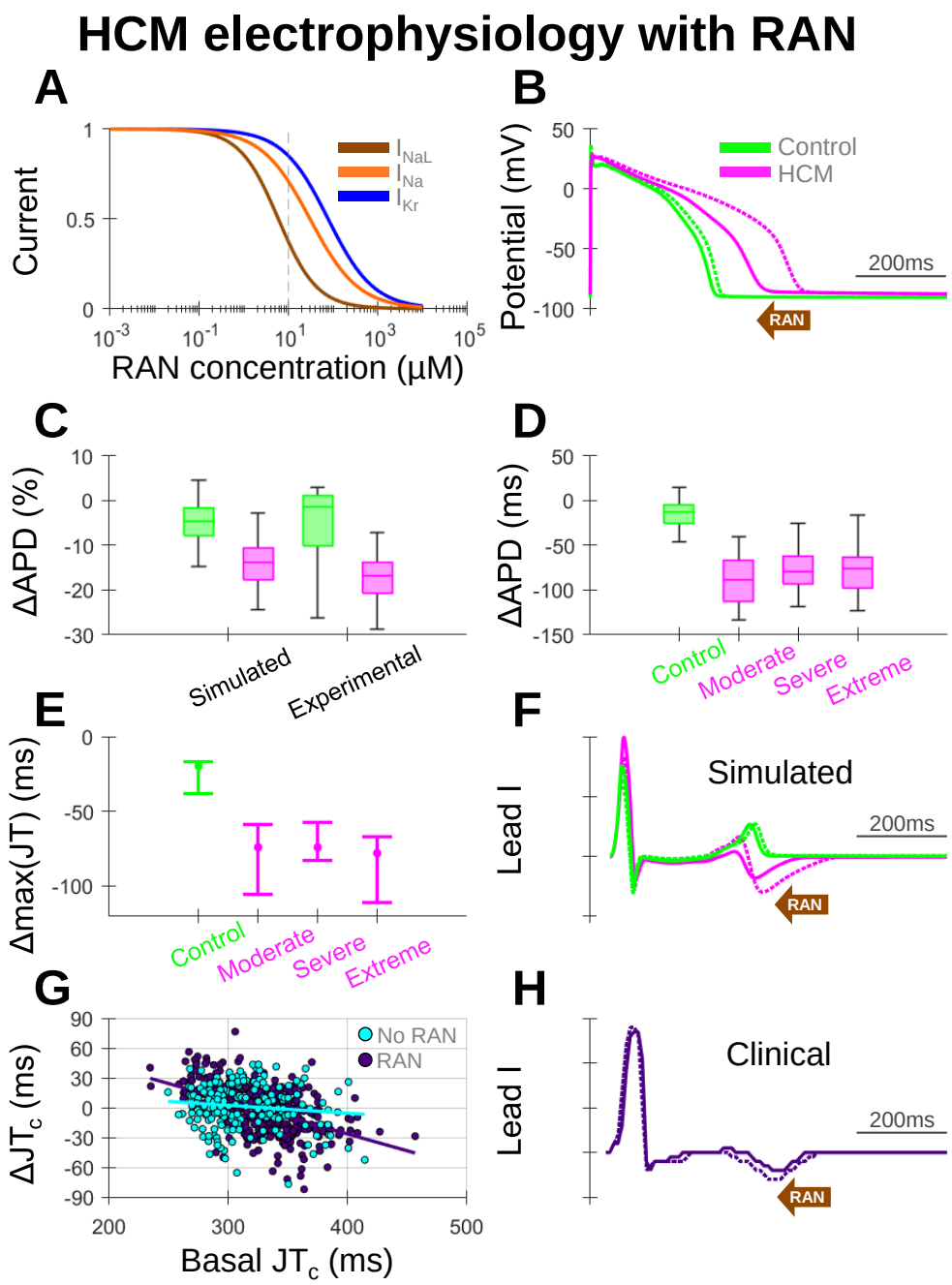


Figure 8.3: Effects of ranolazine on HCM electrophysiology. (A) Dose-response model of ranolazine, where I_{NaL} was primarily blocked with secondary effects on I_{Na} and I_{Kr}. (B) Representative simulated endocardial AP traces under 10 μM ranolazine (solid) compared with baseline (dashed), showing AP shortening predominantly in HCM. (C) Percentage changes in APD under 10 μM ranolazine in simulated and experimental setups [66]. (D) Simulated changes in APD under 10 μM ranolazine for control and

HCM AP phenotypes, where effects were similar for moderate, severe and extreme degrees of ionic remodelling. (E) Changes in max JT intervals under 10 μM ranolazine for the various electrophysiological phenotypes, where AP models corresponding to [25, 50, 75]th APD percentiles were used in biventricular simulations. (F) Representative simulated lead I traces under 10 μM ranolazine (solid) compared with baseline (dashed), showing JT shortening predominantly in HCM. (G) Change in clinical JT_c intervals on follow-up vs. JT_c at initial visit, as compared between those initiated with ranolazine (n = 397 leads from N = 68 HCM patients) and those without ranolazine (n = 201 leads from N = 33 HCM patients). (H) Example clinical lead I trace after ranolazine (solid) compared with baseline (dashed), showing shortening of the JT interval. All simulated results presented at 1 Hz pacing. RAN: ranolazine.

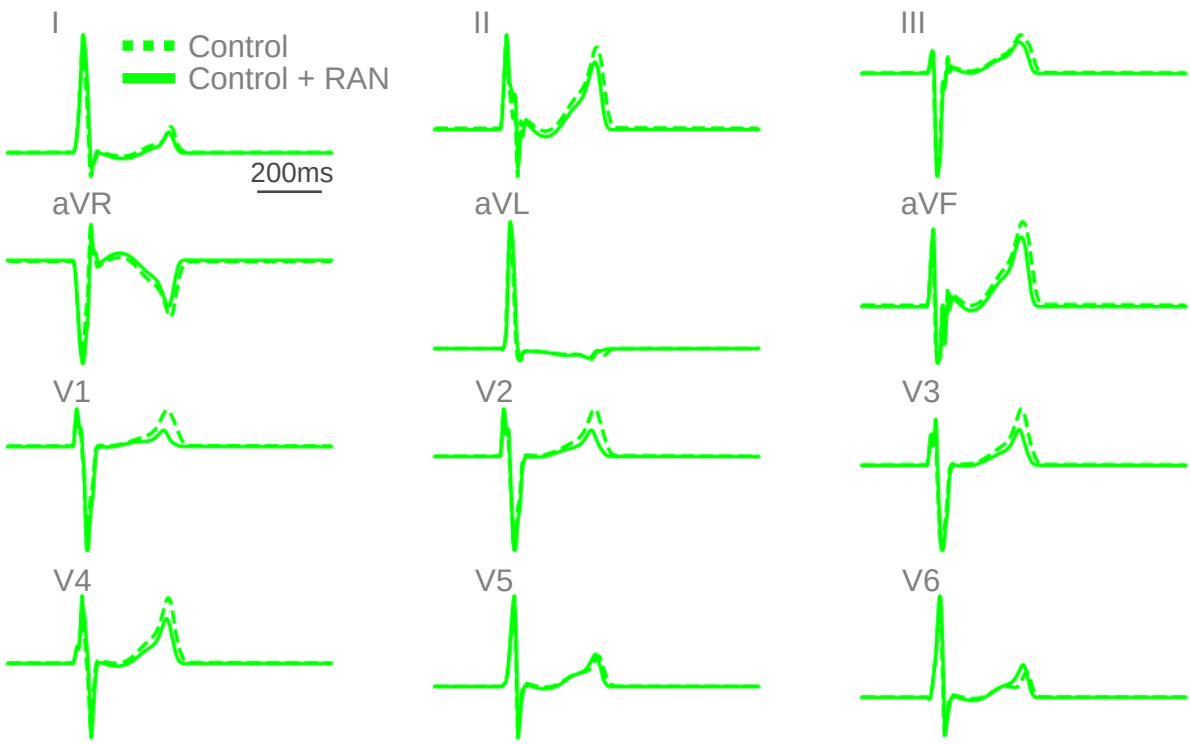


Figure 8.4: Representative simulated ECG without HCM ionic remodelling, before and after 10 μM ranolazine. RAN: ranolazine.

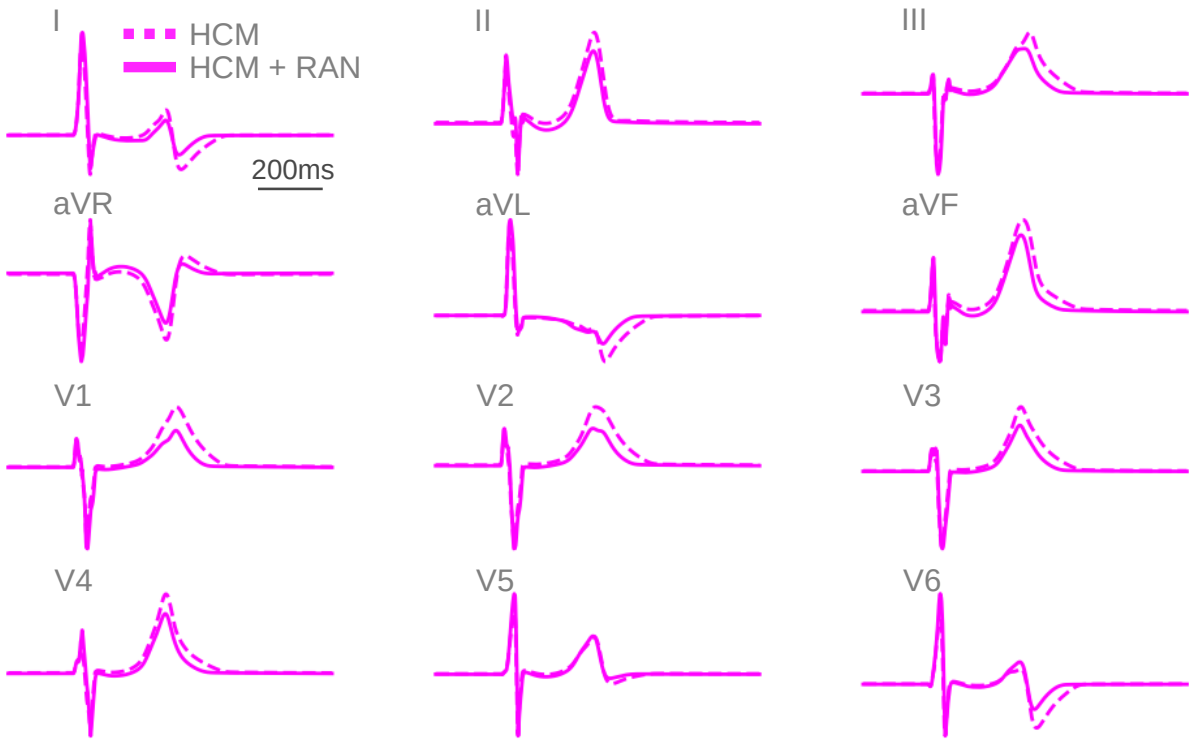


Figure 8.5: Representative simulated ECG with HCM ionic remodelling, before and after 10 μM ranolazine. RAN: ranolazine.

8.3.4 Ranolazine effect on arrhythmic risk

Arrhythmic risk with ranolazine (Fig. 8.6) was quantified for 600 in-tissue scenarios, spread across 150 HCM AP models, medium-sized and large HCM-remodelled regions, and three drug concentrations (3, 6, and 10 μM). Ectopic S1-S2 protocols applied to these in-tissue scenarios totalled 27,627 simulations of re-entry inducibility, including 1235 PVC couplets and 560 VT episodes.

At all drug concentrations, the effect of ranolazine on arrhythmic risk was critically dependent upon the degree of HCM remodelling, quantified as the HCM APD at baseline, for both the induction of PVC couplets (Fig. 8.6A) and VT (Fig. 8.6B). The inducibility of arrhythmias was decreased by ranolazine in models with a shorter baseline APD, but was increased in models with a longer baseline APD. These effects are related to the dependence of arrhythmic risk on remodelled APD, as presented for HCM

models at baseline (Figs. 8.2E & 8.2F), where PVC couplets and VT were maximally inducible for an intermediate range of APD prolongation. Ranolazine, which corrected prolonged APDs, pushed some models with moderate-severe remodelling out of this high-risk APD range, but pushed others with severe-extreme remodelling into the high-risk APD range.

Cutoff points in APD were therefore defined, where ranolazine could be beneficial in all models with APD $<$ cutoff, for the optimal net reduction in vulnerable window widths. Computed APD cutoffs were identical across HCM-remodelled region sizes and ranolazine concentrations. Of note, the APD cutoff for PVC couplet prevention (460 ms) was significantly greater than that for VT prevention (390 ms). This is explained by increased VT vulnerable window widths under ranolazine in many models, despite reduced PVC couplet vulnerable window widths (Fig. 8.6C, upper-left quadrant). The suitable APD cutoff for overall antiarrhythmic effect and safety was therefore 390 ms (equivalent to max JT $<$ 370 ms as in Fig. 8.1G).

Importantly, however, Figs. 8.6A–8.6C assumed the treatment of ranolazine in all models, independent of baseline arrhythmic risk. Although this was relevant for the safety of ranolazine as an antianginal, for antiarrhythmic purposes it is more relevant to confine the analysis to models with VT at baseline. Models with VT at baseline typically had lower APD anyway (Figs. 8.2E & 8.2F), such that 10 μM ranolazine applied only to models with VT reduced the total number of VT episodes from 216 to 129 (-40%), and PVC couplets from 543 to 378 (-30%), for analysis pooled over the medium-sized and large HCM-remodelled regions.

Following this strategy of applying ranolazine only to models with VT at baseline, reductions in VT occurred in a dose-dependent manner when analysed for the medium-sized HCM-remodelled region (Fig. 8.6D). Although the maximal reduction in VT was observed with 10 μM ranolazine (-90%), diminishing returns were observed with increasing ranolazine concentrations. Lower concentrations of 3 μM and 6 μM still resulted in comparable VT reductions (-50% and -70% respectively), such that clinical ranolazine dosages could have marked antiarrhythmic effects. For arrhythmic risk in the case of the larger HCM-remodelled region, reductions in VT with this strategy were modest (-20%) even under the maximal concentration of 10 μM ranolazine.

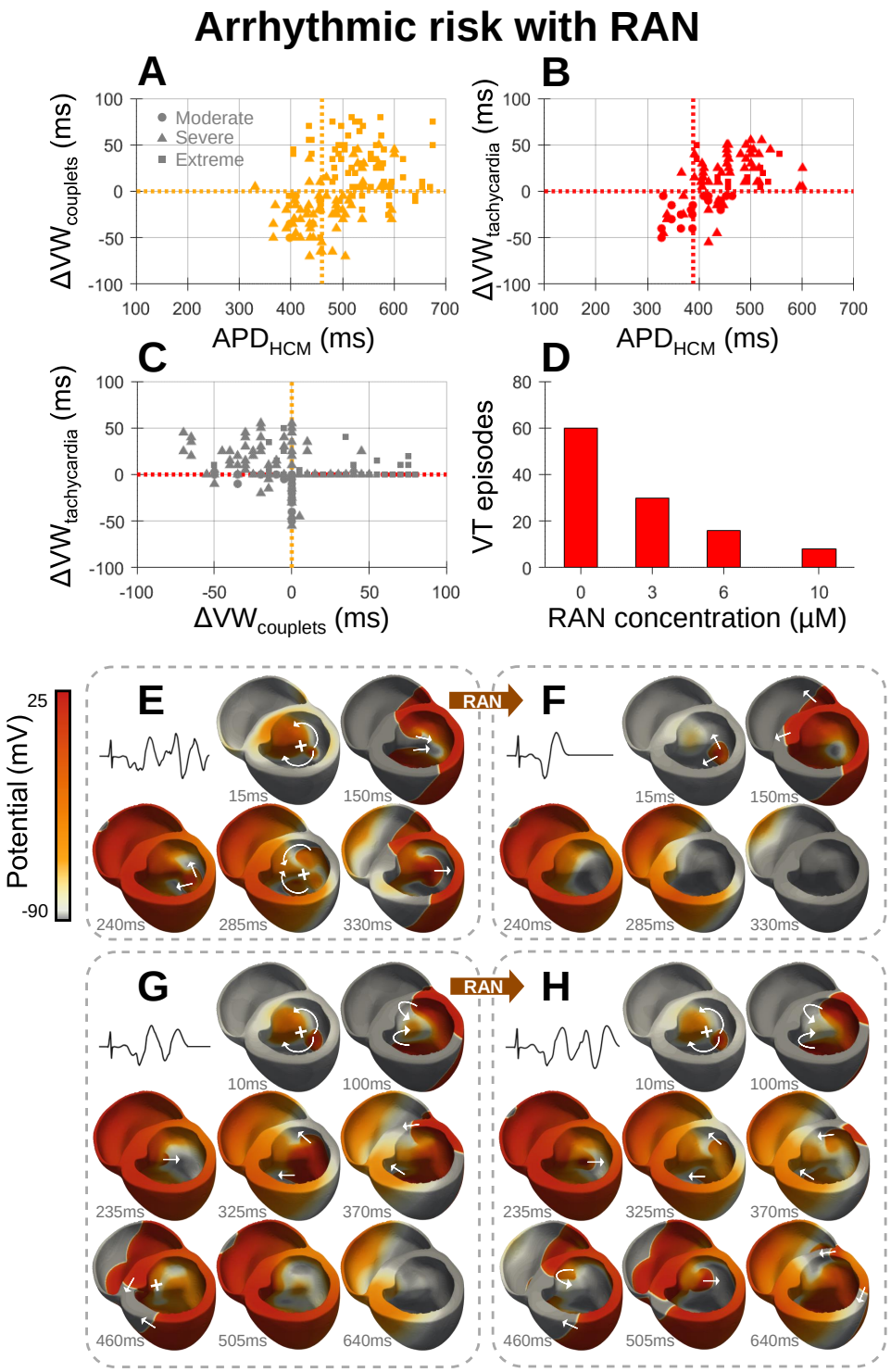


Figure 8.6: Effects of ranolazine on HCM arrhythmic risk. (A, B) The effect of 10 μM ranolazine on vulnerable window widths across tissue models, pooled for small and large HCM-remodelled regions and moderate-extreme degrees of remodelling, for (A) PVC couplets and (B) VT. Cutoff points in

APD for models in which ranolazine should be used (APD $<$ cutoff) for the optimal net reduction in vulnerable window widths are denoted (vertical, dashed). (C) Changes in VT vulnerable window widths plotted against changes in PVC couplet vulnerable window widths due to 10 μM ranolazine, showing that many models with a decreased incidence of PVC couplets under ranolazine had a concomitant increased incidence of VT. (D) Concentration-dependent effects of ranolazine on the number of VT episodes, when given to models with VT at baseline, as analysed for the medium-sized HCM-remodelled region. (E) Representative VT episode inducible at baseline which, (F) under 10 μM ranolazine, was not inducible due to homogenised repolarisation gradients that precluded conduction block and re-entry. (G) Representative PVC couplets inducible at baseline which, (H) under 10 μM ranolazine, manifested as VT due to the reduced APD and refractory period which enabled further re-entrant cycles to propagate that would otherwise have been blocked at baseline (460 ms frame). Arrows and crosses denote directions of wavefront propagation and conduction block, respectively. Time elapsed following S2 is denoted in each frame. All results presented at 1 Hz pacing. RAN: ranolazine; ΔVW: change undergone in vulnerable window width due to ranolazine.

Of note, when 10 μM ranolazine was applied only to models with VT at baseline, and APD $<$ 390 ms, the net effect on VT was improved for the larger HCM-remodelled region (from -20% to -40%), but slightly worsened for the medium-sized HCM-remodelled region (from -90% to -60%). This was also true at 3 μM and 6 μM (from -50% and -70% to -40% and -50%, respectively). This reduction in efficacy is explained by AP models which had reduced VT incidence under ranolazine with baseline APD $>$ 390 ms, which were not treated when applying the APD $<$ 390 ms cutoff.

The mechanism for antiarrhythmic ranolazine effects at low baseline APDs is shown in Figs. 8.6E & 8.6F. At baseline (Fig. 8.6E), gradients of repolarisation and refractoriness due to the HCM-remodelled region enabled conduction block following an ectopic stimulus, which then propagated retrogradely and re-entered multiple times (VT episode). When the same model was treated with 10 μM ranolazine (Fig. 8.6F), gradients of repolarisation and refractoriness were homogenised such that the ectopic stimulus propagated throughout the ventricles without conduction block or re-entry (a single PVC).

Conversely, the mechanism for proarrhythmic ranolazine effects at high baseline APDs is presented in Figs 8.6G & 8.6H. At baseline (Fig. 8.6G), a single re-entry occurred but subsequent cycles were blocked by prolonged refractoriness in the HCM-remodelled region (PVC couplets). When the same model was treated with 10 μM ranolazine (Fig. 8.6H), the initial single re-entry occurred almost identically, but later cycles now also conducted as ranolazine decreased refractoriness in the HCM-remodelled region (VT episode).

8.3.5 Effects of pacing rate

All the previous results considered ventricular pacing at 1 Hz. However, as cutoffs in APD (and the JT interval) were used to optimise ranolazine efficacy, and yet the JT interval is rate-dependent, the effect of pacing rate on the optimal APD/JT cutoff was considered. Arrhythmic risk was therefore further quantified at 1.5 Hz pacing for 300 in-tissue scenarios, spread across 150 HCM AP models for the medium-sized HCM-remodelled region, before and after 10 μM ranolazine.

When the effects of increasing pacing rate from 1 Hz to 1.5 Hz were analysed (Fig. 8.7), the optimal APD cutoff for VT prevention changed from 390 ms at 1 Hz pacing (Fig. 8.7A, as previously presented in Fig. 8.6B) to 350 ms at 1.5 Hz pacing (Fig. 8.7B), reflecting rate-dependent repolarisation gradients. The rate-dependent decrease in cutoff was compensated for by rate correction of the QT/JT interval, as when the 1.5 Hz vulnerable window analysis was repeated using model-specific APDs corresponding to 1 Hz, the 390 ms APD cutoff was preserved (Fig. 8.7C).

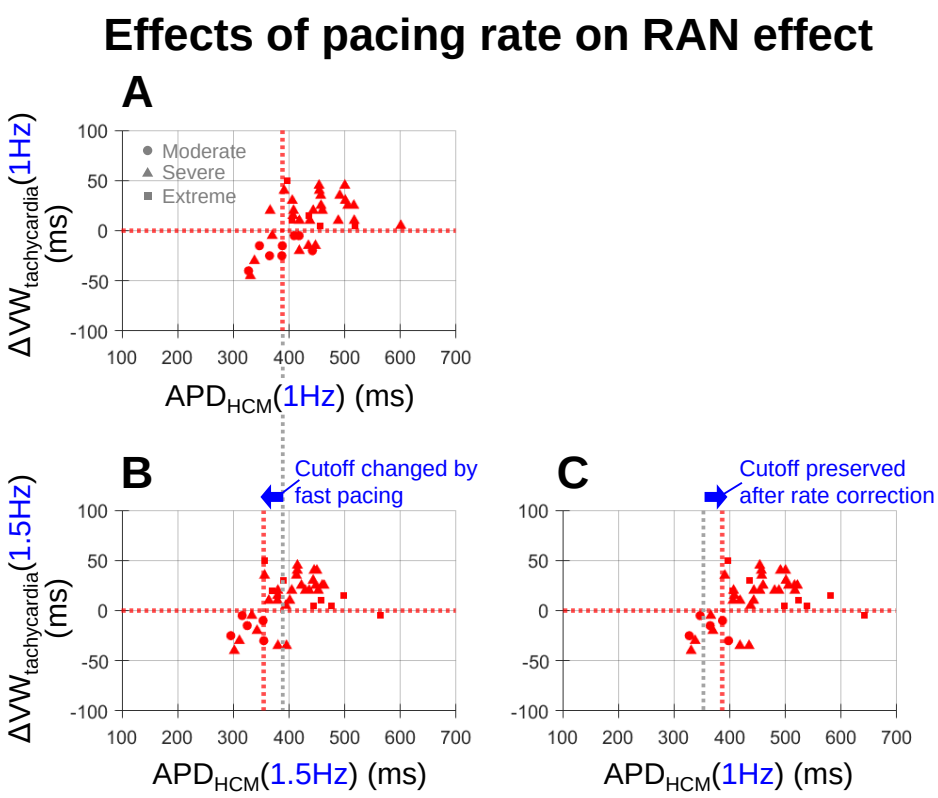


Figure 8.7: Effects of pacing rate on optimal APD cutoffs for ranolazine use. (A, B, C) The effect of 10 μM ranolazine on vulnerable window widths across tissue models with small HCM-remodelled regions, pooled for moderate-extreme degrees of remodelling, as measured at pacing rates of (A) 1 Hz and (B, C) 1.5 Hz. Cutoff points in APD for models in which ranolazine should be used (APD $<$ cutoff) for the optimal net reduction in vulnerable window widths are denoted (vertical, dashed). Optimal APD cutoffs decreased from (A) 390 ms at 1 Hz to (B) 350 ms at 1.5 Hz, but (C) rate-correction of APD to 1 Hz (analogous to using JT_c or QT_c) preserved the 390 ms APD cutoff. RAN: ranolazine; ΔVW: change undergone in vulnerable window width due to ranolazine.

8.4 Discussion

This thesis chapter aimed to exploit human multiscale modelling and simulation to investigate the electrophysiological mechanisms underlying the safety and antiarrhythmic efficacy of ranolazine in HCM, alongside ECG biomarkers associated with beneficial effects. The principal findings of the study reported

in this thesis chapter are that (i) ranolazine caused decreases of JT intervals in affected leads by accelerating repolarisation; (ii) ranolazine had optimal antiarrhythmic effects in models with moderately slowed repolarisation secondary to moderate ionic remodelling (max $JT_c < 370$ ms); and (iii) ranolazine increased risk of VT only in models with extreme severities of ionic remodelling.

Although clinical measurements of QT_c as measured in a single lead were unchanged by ranolazine on average in HCM [270], a subset of patients from a larger HCM cohort were reported to have decreased QT_c under another late Na^+ blocking drug, disopyramide [231]. The present study suggests that this is explained by decreases in the JT_c intervals of leads with longer baseline JT_c under late Na^+ block. It also suggests that impaired repolarisation and correction by late Na^+ block may be best observed on analysis of multiple leads, because JT and QT intervals were prolonged non-uniformly among simulated ECG leads, reflecting clinical reports of increased max JT_c and JT_c dispersion in HCM [319, 394]. Indeed, the effects of ranolazine varied among leads in the present study (Fig. 8.5), which is consistent with lead-dependent effects on the QT interval identified in previous computational modelling of combined late Na^+ and K^+ block with disopyramide in HCM [65]. This is explained by HCM ionic remodelling being heterogeneously distributed in the ventricles secondary to hypertrophy [201, 319]. The decrease in max JT of 70 ms identified in the present study under 10 μM ranolazine was consistent with QT_c decreases of 56 ms under ranolazine 1000 mg bid [52] or 10 ms per 1 μM [250] reported in congenital long QT (LQT) of type 3, where the gain-of-function late Na^+ mutations cause widespread repolarisation slowing. Late Na^+ block is also reported to reduce QT_c in LQT2 patients [27], which is relevant as in LQT2 slowed repolarisation is mediated by remodelling in both K^+ and late Na^+ channels, like in HCM [66]. QT_c decreases by late Na^+ block are lesser in LQT2 than LQT3 [388], which is also consistent with the present study in which HCM cells with late Na^+ and K^+ remodelling had lesser APD decreases induced by ranolazine than HCM cells with just remodelling in late Na^+.

Antiarrhythmic effects of ranolazine in HCM have been reported clinically, including a reduction in PVC burden in the randomised controlled trial of ranolazine [270] and the existence of a small real-world subgroup of responders in whom arrhythmic events did not recur after the introduction of ranolazine [15]. Moreover, in LQT3, decreases in QT_c with late Na^+ block were associated with reduced arrhythmic events [233], such that clinical guidelines recommend late Na^+ channel blockers [296]. There is therefore

a clinical precedent for the antiarrhythmic effects of ranolazine identified in the present study. However, whereas these simulated antiarrhythmic effects were entirely due to reductions in refractoriness gradients due to late Na^+ block, ranolazine is also an antianginal, so it is unclear whether clinical antiarrhythmic effects may also be attributed to reduced diastolic compression of the microcirculation and prevention of ischaemia. Indeed, in ischaemic non-HCM patients, ranolazine reduced the number and duration of ventricular arrhythmias in the RYPPLE trial [285], and ranolazine had antiarrhythmic effects in the first week of treatment in the MERLIN-TIMI trial [249, 324]. Antiarrhythmic effects like those in the present study are supported by clinical reports in patients without ischaemia [251]. This includes the RAID trial, where non-ischaemic patients were enrolled as well as ischaemic patients, and the efficacy in reducing ventricular arrhythmias was not significantly different between these subgroups [399]. Instead, low-to-moderate risk patients (no AF or other antiarrhythmic drug therapy) derived the most benefit. This might be explained by the presence of structural arrhythmic substrates in higher risk patients not amenable to ranolazine therapy. Indeed, all simulations in the present study considered only a functional rather than structural arrhythmic substrate, whereas fibrotic remodelling is common in HCM, which may explain why ranolazine does not in general prevent VT in HCM [15].

Ranolazine is considered safe for use in HCM [15] and proarrhythmic side effects are not evidenced clinically. Most patients have max $JT_c < 370$ ms (72% in the present study), where the present study predicts only antiarrhythmic effects. Moreover, despite the optimal JT cutoff of 370 ms, ranolazine only had a net proarrhythmic effect for JT cutoffs above 450–490 ms, which far exceeds JT_c intervals measured clinically. Clinical studies of ranolazine typically exclude HCM patients with $QT_c \geq 500$ ms anyway [270], who are more likely to have prolonged JT_c [155]. This is because ranolazine is contraindicated in patients with reduced repolarisation reserve at baseline, due to the risk of K^+ block inducing further QT_c prolongation and arrhythmias. Interestingly, the present study suggests that treatment of long QT HCM patients with ranolazine can also be proarrhythmic even when QT_c is decreased by late Na^+ block, due to increases in re-entry sustainability despite reduced repolarisation heterogeneity. Outside of HCM, there is randomised evidence that ranolazine 1000 mg bid may be proarrhythmic in some patient subgroups [399]. As a possible competing mechanism, it is notable that the incidence of early and delayed afterdepolarisations may also depend upon the degree of ionic remodelling [66], such that

proarrhythmic substrate effects of ranolazine at long JT intervals may be counteracted by antiarrhythmic action on cellular triggers.

The present study also motivates reconsideration of whether the QT_c interval is the optimal index for assessing the risk of drug-induced torsades de pointes in HCM. Both ventricular activation and repolarisation are profoundly delayed in HCM, to a degree that is heterogeneous among patients [155]. Although 17% of patients in the present study had lead II $QT_c \geq 480$ ms (close to other estimates [155]), 28% had max $JT_c \geq 370$ ms, and the overlap between these groups was suboptimal due to the presence of impaired activation (26% had mean QRS duration ≥ 150 ms). Some patients with $QT_c \geq 480$ ms may have a prolonged QRS duration with a normal repolarisation reserve, such that ranolazine could be used safely. Conversely, some patients with $QT_c < 480$ ms could have a normal QRS duration with reduced repolarisation reserve, in whom ranolazine may have torsades de pointes risk. Moreover, as prolonged QRS may be associated with fibrosis in HCM [280], prolonged QT_c in some patients may signify the presence of a structural substrate unamenable to ranolazine. Therefore, the applicability of ranolazine could better be assessed using the JT interval to eliminate the effects of activation delay, despite JT intervals being scarcely reported in HCM.

8.5 Conclusions

The antiarrhythmic efficacy of ranolazine may be critically dependent on the degree of ionic remodelling, spatial extent of the repolarisation heterogeneity, and HCM ionic remodelling pattern. The partial correction of heterogeneous repolarisation by ranolazine may be antiarrhythmic in most HCM patients (max $JT_c < 370$ ms) through the resolution of refractoriness gradients, susceptibility to conduction block and subsequent re-entrant VT. In the setting of severe-extreme slowed repolarisation, ranolazine can be proarrhythmic even when refractoriness gradients are partially ameliorated, through decreasing the maximum refractory period and increasing re-entry sustainability. This highlights the significant complexities involved in the pharmacologic modulation of functional arrhythmic substrates.

8.6 Limitations

General computational limitations are detailed in section 9.3. Of particular relevance to this chapter, the model of early ionic remodelling in HCM cells was assumed to be led by I_{NaL} as supported by murine experiments [67], but the relative contributions of I_{NaL} and I_{Kr} to slowed repolarisation in early human HCM is unknown, despite both contributing to remodelling in surgical myectomy patients [66].

The model of ranolazine was calibrated to the *in vitro* effects of ranolazine on human cardiomyocyte APDs [66], where control cells did not experience APD prolongation. However, some clinical studies in non-HCM patients have reported 5–14 ms QT_c prolongation under 1500 mg bid ranolazine [49]. Therefore, the possible risk of APD prolongation by ranolazine was not considered, although these effects are not evidenced in HCM. Ranolazine-induced APD prolongation in non-remodelled myocardium concomitant with APD decreases in HCM-remodelled myocardium may have implications for the arrhythmia mechanisms identified in the present study. Specifically, antiarrhythmic effects secondary to reductions in refractoriness gradients (Figs. 8.6E & 8.6F) may be enhanced by a further reduction in refractoriness gradients arising from APD prolongation in non-remodelled myocardium. Conversely, proarrhythmic effects secondary to reductions in the maximum ERP (Figs. 8.6G & 8.6H) were determined by ranolazine effects in the HCM-remodelled myocardium, and are unlikely to be affected by APD prolongation in non-remodelled myocardium.

It is further notable that human *in vivo* pharmacokinetic studies have shown that ranolazine is almost entirely metabolised, with 3 of the metabolites each being 30–40% as abundant as the parent compound and having variable effects on I_{NaL} and I_{Kr} [48, 153]. Historically, the calibration of computational ranolazine models to ex vivo experimental data has led to simulations with unphysiologically large APD/QT_c prolongation [248, 281], due to potent estimates of I_{Kr} block by the parent compound (IC50 = 12 μM). Much weaker I_{Kr} block by ranolazine metabolites has been reported (IC50s $>$ 50 μM) [48], which is closer to that used in the present study (IC50 = 77 μM). Further work may consider calibration of ranolazine I_{NaL} and I_{Kr} block using *in vivo* data in both healthy and HCM subjects, to refine representative IC50 estimates.

Moreover, although the present study identified decreases of the JT_c with ranolazine in some leads and this is consistent with the effects of disopyramide in HCM [231], measures such as JT_c dispersion were not addressed due to large numbers of lead exclusions [317]. Also, although both antiarrhythmic and proarrhythmic mechanisms of ranolazine observed in tissue were also demonstrated in biventricular simulations, future work may consider the relevance of other ECG biomarkers that are less well translated between tissue and biventricular simulations (e.g. T wave morphology).

Finally, as this work focused on investigating the effects of ranolazine on modulating the functional arrhythmic substrate in HCM, other possible structural arrhythmic substrates (diffuse and replacement fibrosis) were not modelled, which may limit ranolazine applicability.

CHAPTER 9

Conclusions and future directions

This chapter summarises the key findings of the investigations presented in Chapters 5–8, to motivate sensible future directions of research stemming from this thesis.

9.1 Key findings

This thesis set out to address the key knowledge gaps detailed in section 1.1 in relation to myocardial ischaemia in human HCM, through the thesis aims (i)–(iv) previously specified in section 1.2:

(i) Investigate the effects of acute myocardial ischaemia on human HCM-remodelled cardiomyocyte AP biomarkers.

(ii) Investigate the electrophysiological mechanisms by which ischaemia interacts with other pathological features in human HCM tissue and ventricles (ionic remodelling and diffuse fibrosis) to modulate arrhythmic risk.

(iii) Investigate how regional/serum K^+ levels and heart rate affect T wave morphology and the diagnosis of ischaemia on stress ECGs in human HCM.

(iv) Investigate the effects of antianginal late Na^+ block (ranolazine) on arrhythmic risk in human HCM.

To identify how cellular electrophysiology is affected by acute myocardial ischaemia in the setting of ionic

remodelling in HCM, the ToR-ORd human ventricular AP model was used alongside the populations of models approach. When subjected to ischaemia, HCM-remodelled cells had enhanced APD shortening and abnormal ERP shortening when compared to control cells, secondary to remodelling in I_{NaL} and I_{Kr}. These important computational predictions were further validated using collaborator human HCM patch-clamp experimental data, confirming the electrophysiological interactions between ionic remodelling and ischaemia. This agreement between computational predictions and subsequent experimental validation further reinforces the applicability of computational AP models to a range of human disease conditions, and supports the later thesis chapters.

To address how ischaemic arrhythmic risk is modulated by other pathological features in HCM, over 75,000 arrhythmia inducibility simulations were analysed in ischaemic tissue and ventricles affected by variations of concomitant ionic remodelling and diffuse fibrosis. In-tissue simulations conducted across a population of AP models and a range of hyperkalaemic/hypoxic severities demonstrated that, across a large parameter space, HCM ionic remodelling increases arrhythmic risk by increasing refractoriness gradients. Competing effects of diffuse fibrosis on arrhythmic risk was further shown, where further conduction delay by mild fibrosis was initially proarrhythmic, but was reversed in cases of severe fibrosis with total conduction block. In some cases, asymmetric conduction delay with fibrosis altered figure-of-eight re-entry patterns into stable rotors, increasing arrhythmia sustainability. Human biventricular simulations, as informed by typical distributions of hypoperfusion in HCM as seen on CMR scans, found that these in-tissue interactions between disease factors were preserved at the organ-scale. Furthermore, for characteristic subendocardial/transmural ischaemia and midwall/transmural fibrosis distributions, arrhythmic risk in biventricular simulations was shown to increase with increasingly transmural insults.

In relation to identifying HCM-specific stress ECG manifestations of acute myocardial ischaemia (T wave pseudonormalisation), simulated ECGs were derived from over 520 apical/septal HCM biventricular simulations affected by variations of ischaemic $[K^+]$ accumulation and/or exercise serum $[K^+]$ and pacing rate increases. These investigations demonstrated that the pseudonormalisation of inverted T waves can be an early sign of myocardial ischaemia in HCM, preceding significant changes to the ST segment. These investigations illustrated that ischaemic shortening of remodelled APDs may underlie T wave pseudonormalisation, providing an electrophysiological mechanism for this ECG phenomenon of

historically controversial clinical significance. By analysing regionally ischaemic simulations in comparison to those with benign exercise serum [K^+] and pacing rate increases, differential causes of T wave pseudonormalisation on the stress ECG were accounted for, explaining how both ischaemic and benign exercise changes can affect T waves in HCM. Therefore, further ECG biomarkers were proposed to better discern ischaemic from benign T wave pseudonormalisation, such as the consideration of subthreshold ST segment changes, the QT interval or QT dispersion.

Finally, to investigate the repurposing of an anti-ischaemic drug (ranolazine) as an antiarrhythmic in HCM, over 40,000 arrhythmia inducibility simulations were analysed in tissue and ventricles affected by variations of ionic remodelling and ranolazine concentrations. Simulations with ranolazine, as calibrated to collaborator human HCM patch-clamp experimental data and validated with clinical pre- and post-ranolazine ECGs, illustrated that amelioration of refractoriness gradients at clinically attainable drug concentrations may underlie its antiarrhythmic effects. These investigations underscore the general safety of ranolazine in HCM as an antianginal and illustrate its potential as an antiarrhythmic in patients with heterogeneous, moderately slowed repolarisation. Consistent with the clinical caution in treating patients with prolonged QT_c, possible proarrhythmic effects of ranolazine were also identified in cases of severe-extreme baseline prolonged JT_c in HCM models. Interestingly, these proarrhythmic effects were mediated by ranolazine-induced decreases in ERP, which is in contrast to the clinical belief that drug proarrhythmic risk arises primarily from further drug-induced QT_c prolongation (increases of ERP). These competing mechanisms related to the ERP and ERP heterogeneity are of significance to antiarrhythmic drug design and repurposing in general, and motivated the proposal to use the JT_c interval (rather than QT_c) to predict drug efficacy and/or cardiotoxicity in the setting of activation impairment such as in HCM.

Altogether, ionic remodelling and myocardial ischaemia in HCM were found to have important implications for arrhythmic risk, stress ECG manifestations of disease, and pharmacologic antiarrhythmic therapy in HCM patients.

9.2 Future directions

Although the key thesis aims were addressed, there are several further areas of research motivated by the present work.

A general understanding of the spatial distribution of ionic remodelling in HCM (previously detailed in section 3.3), and of its dependence on disease stage, would benefit from further study. This is particularly important because the repolarisation and refractoriness gradients introduced by ionic remodelling contributed to both ischaemic and non-ischaemic arrhythmic risk (Chapters 6 and 8), affected the ECG diagnosis of ischaemia (Chapter 7), and could be an important target for antiarrhythmic therapy (Chapter 8). This could in part be addressed computationally, by deriving novel ECG biomarkers proposed to be associated with repolarisation heterogeneity [317, 372] from simulations across a range of HCM biventricular geometries, with variable spatial distributions and severities of ionic remodelling. This study could yield *in vivo* markers of heterogeneous repolarisation in HCM, which could be used for arrhythmic risk stratification, or to measure the electrophysiological effects of pharmacologic therapies as a surrogate for antiarrhythmic efficacy and safety. Such measures could also be used for better in vivo calibration and/or validation of computational HCM models.

Furthermore, there is significant scope within computational modelling to optimise antiarrhythmic drug therapy, rather than just considering a single pre-specified agent at a given concentration. For example, for a given substrate, the framework used in this thesis could be applied to identify the specific ion channel effects that may optimally ameliorate arrhythmic risk. Although the impact of such an approach is first limited by the pace at which safe new compounds are developed (see the failure of eleclazine, for example), combinations of antiarrhythmic drug therapies could alternatively provide the flexibility in ion channel effects to achieve this goal. For example, combinations of ranolazine and dronedarone applied to experimental preparations are reported to effectively treat AF, whereas the agents individually had limited effect [35]. Similarly, combined mexiletine (which may be a more potent I_{NaL} blocker than ranolazine) with amiodarone (sometimes used in HCM [274]) prevented ventricular arrhythmias in one high-risk cohort [109]. The modelling of ranolazine in Chapter 8 could be extended to such combination approaches, however this would first benefit from further study of the dependence of the

relative contributions of I_{NaL} and I_{Kr} to ionic remodelling on disease stage. The framework in this thesis could also be extended to optimise non-pharmacologic antiarrhythmic therapy, such as ICD programming [346], by using the bidomain model of electrical propagation. Although effective at preventing SCD, ICDs still deliver inappropriate shocks [190]. Better ICD arrhythmia detection and novel techniques to deliver antitachycardia pacing (rather than large shocks) could in part be informed by modelling and simulation.

Although arrhythmia mechanisms related to combinations of disease factors were considered in Chapter 6, further work may consider comparative arrhythmic risk attributed to substrates formed purely by acute myocardial ischaemia, HCM ionic remodelling, or fibrosis. Although electrophysiological mechanisms related to these individual substrates are generally well understood, direct comparisons could yield insight as to the potency of each substrate and their contribution to arrhythmias in HCM. Arrhythmia mechanisms beyond just figure-of-eight re-entry may also benefit from further study. For example, future work could consider how existing ventricular repolarisation heterogeneities (e.g. transmural and apex-to-base) are affected by ionic remodelling and drug effects, and attempt to induce arrhythmias at sites with existing repolarisation gradients. Moreover, how the transition from VT to VF is affected by ionic remodelling, ischaemia, fibrosis and pharmacologic therapy could also be investigated by modifying the ToR-ORd model to have a steeper restitution gradient.

Moving beyond the study of general arrhythmia mechanisms, increasingly patient-specific biventricular HCM models could be developed to make patient-specific arrhythmic risk predictions and therapeutic recommendations. This may include imaging-derived patient-specific geometries and spatial distributions of myocardial ischaemia (perfusion CMR) and fibrosis (LGE-CMR). Moreover, electrophysiological personalisation is becoming increasingly feasible using the patient ECG to infer patient-specific electrical activity of the ventricles [39]. The construction of populations of HCM digital twins could enable *in silico* trials to test antiarrhythmic therapies, including ranolazine [80]. However, each personalisation step imposes unique challenges and limitations to be overcome in future work.

There is the further opportunity for computational modelling and simulation of cardiac electrophysiology to be used in combination with novel machine learning approaches, to offer mechanistic insight as to

the performance of such algorithms. This is particularly relevant as machine learning begins to overtake clinicians in diagnosing myocardial ischaemia on the ECG [401].

Finally, as a banal suggestion, further work could attempt to address any of the general limitations described next in section 9.3.

9.3 General limitations

The simulation studies in Chapters 5–8 were carefully designed to address the given hypotheses for each investigation. As such, the key strengths are that the mechanistic investigations considered a wide parameter space (including populations of AP models), where mechanisms identified in-tissue were preserved in biventricular simulations. Furthermore, human patch-clamp experimental validation was considered throughout, as well as comparisons to clinical ECGs in Chapters 7 and 8. However, there are a number of computational limitations present throughout this thesis.

Despite using a populations of models approach, only the ToR-ORd AP model was used as a baseline (as justified in section 4.1.2); therefore, possible dependence on the baseline AP model was not investigated. Moreover, the ToR-ORd AP model is electrophysiology-only, thus the possible influence of mechanoelectric feedback was not considered.

Only two meshes were used in the biventricular simulation studies presented in this thesis, derived from CMR scans of patients with septal and apical variants of HCM. Arrhythmic risk modulation by variability in ventricular geometries (e.g. due to increased muscle mass [297]) was not considered. In Chapter 7, benign T wave pseudonormalisation occurred differently between septal and apical HCM models, suggesting strong dependence on the anatomical and electrophysiological phenotype. CV in hypertrophied regions was considered as normal based on invasive measurements in the hypertrophied interventricular septum of obstructive HCM patients [364]. Therefore, differences in arrhythmic risk attributable to possible hypertrophy-associated differences in CV were not considered. Other pathological features in HCM such as myocardial disarray or replacement fibrosis were also not considered. Beta-adrenergic stimulation was not modelled, although refractoriness gradients in HCM may be enhanced by this factor [62]. Possible influences of the atria or patient torso were not accounted for. Furthermore,

despite using a realistic human activation sequence in biventricular simulations, the Purkinje system was not directly modelled, although it has a minor role in ischaemic re-entries as shown in other computational works [45].

In relation to modelling myocardial ischaemia, the ischaemic BZ was additionally assumed to be identical in width for all components of ischaemia, but differences in the size of the hyperkalaemic and hypoxic borders have been reported [45]. Arrhythmic risk was shown to be insensitive to this factor (Appendix Fig. A.5), but its possible influence on the ECG was not considered. Additionally, possible biphasic patterns of ischaemic K^+ accumulation in the BZ were not investigated, where $[K^+]$ has been reported to decrease in canine [81] or porcine [69] models of coronary ligation under longer timescales than the ones considered in this thesis. Also, consistent with the research hypotheses of this thesis, ischaemia was typically assumed to be confined to the most hypertrophied region, but microvascular dysfunction is frequently also present in mildly hypertrophied segments.

Furthermore, ectopic stimuli were assumed only to emerge in the ischaemic BZ (or just outside of the HCM-remodelled region in non-ischaemic simulations). This was based on experimental reports of ischaemic premature beats emerging adjacent to the BZ and inducing re-entries [148], and the reports that HCM-remodelled cells are particularly susceptible to cellular triggers [66, 282]. However, the spatial distribution of ectopy in HCM is unknown, but the late coupling intervals reported to induce arrhythmias in HCM suggest that ectopy can also emerge remote from the arrhythmic substrate [267]. Finally, measurements of arrhythmic risk considered only the transitions from a single applied PVC to PVC couplets or VT; further mechanisms are expected to mediate the initial PVC and the transition from VT to VF.

9.4 Conclusions

In summary, it was found that slowed repolarisation in HCM secondary to ionic remodelling makes independent contributions to ischaemic arrhythmic risk, facilitates HCM-specific manifestations of myocardial ischaemia on the ECG, and may be a therapeutic target for the amelioration of arrhythmias with ranolazine.

Altogether, this thesis highlights the general complexity associated with functional disease factors in HCM. Alteration of the ischaemic refractoriness and repolarisation response by chronic ionic remodelling in HCM had separate implications for arrhythmic risk and the stress ECG diagnosis of ischaemia. Correspondingly, both changes to the maximum refractory period, and to refractoriness gradients, were found to be individually important factors in arrhythmic risk, as well as antiarrhythmic drug efficacy and safety. In relation to the ECG manifestation of ischaemia in HCM, differential effects on repolarisation of regional and serum $[K^+]$ elevation between HCM-remodelled and non-remodelled myocardium, as well as heart rate effects, mechanistically explained T wave pseudonormalisation and the challenging diagnosis of ischaemia on the stress ECG.

More broadly, the work demonstrates the potential of *in silico* approaches to identify electrophysiological mechanisms with prognostic, diagnostic, and therapeutic implications. Multiscale computational modelling and simulation studies enabled human organ-scale arrhythmia mechanisms and ECG manifestations to be investigated, extending upon previous *in vitro* and *in silico* experiments in single cells [276], yet avoiding invasive clinical protocols. Such *in silico* identification of ECG biomarkers concomitant with arrhythmic risk and/or drug safety and efficacy may advance prognostic stratification and therapeutic targeting in HCM and beyond.

CHAPTER 10

References

[1] Omar M Abdelfattah, Matthew Martinez, Ahmed Sayed, et al. "Temporal and Global Trends of the Incidence of Sudden Cardiac Death in Hypertrophic Cardiomyopathy". In: *JACC Clin Electrophysiol* 8.11 (2022), pp. 1417–1427. DOI: 10.1016/j.jacep.2022.07.012.

[2] Khalid Abozguia, Perry Elliott, William McKenna, et al. "Metabolic Modulator Perhexiline Corrects Energy Deficiency and Improves Exercise Capacity in Symptomatic Hypertrophic Cardiomyopathy". In: *Circulation* 122.16 (2010), pp. 1562–1569. DOI: 10.1161/CIRCULATIONAHA.109.934059.

[3] A Selcuk Adabag, Barry J Maron, Evan Appelbaum, et al. "Occurrence and Frequency of Arrhythmias in Hypertrophic Cardiomyopathy in Relation to Delayed Enhancement on Cardiovascular Magnetic Resonance". In: *J Am Coll Cardiol* 51.14 (2008), pp. 1369–1374. DOI: 10.1016/j.jacc.2007.11.071.

[4] Pasquale Claudio Africa, Roberto Piersanti, Marco Fedele, et al. "lifex-fiber: an open tool for myofibers generation in cardiac computational models". In: *BMC Bioinform* 24.1 (2023), p. 143. DOI: 10.1186/s12859-023-05260-w.

[5] Sílvia Aguiar Rosa, Boban Thomas, António Fiarresga, et al. "The Impact of Ischemia Assessed by Magnetic Resonance on Functional, Arrhythmic, and Imaging Features of Hypertrophic Cardiomyopathy". In: *Front Cardiovasc Med* 8 (2021), p. 761860. DOI: 10.3389/fcvm.2021.761860.

[6] Takashi Akasaka, Junichi Yoshikawa, Kiyoshi Yoshida, et al. "Phasic Coronary Flow Characteristics in Patients With Hypertrophic Cardiomyopathy: A Study by Coronary Doppler Catheter". In: *J Am Soc Echocardiogr* 7.1 (1994), pp. 9–19. DOI: 10.1016/S0894-7317(14)80413-6.

[7] Sergio Alonso, Markus Bär, and Blas Echebarria. "Nonlinear physics of electrical wave propagation in the heart: a review". In: *Rep Prog Phys* 79.9 (2016), p. 096601. DOI: 10.1088/0034-4885/79/9/096601.

[8] Ali Amr, Jan Koelemen, Christoph Reich, et al. "Improving sudden cardiac death risk stratification in hypertrophic cardiomyopathy using established clinical variables and genetic information". In: *Clin Res Cardiol* (2023). DOI: 10.1007/s00392-023-02310-4.

[9] Bogdan Amuzescu, Razvan Airini, Florin Bogdan Epureanu, et al. "Evolution of mathematical models of cardiomyocyte electrophysiology". In: *Math Biosci* 334 (2021), p. 108567. DOI: 10.1016/j.mbs.2021.108567.

[10] Kiyoe Ando, Michinobu Nagao, Eri Watanabe, et al. "Association between myocardial hypoxia and fibrosis in hypertrophic cardiomyopathy: analysis by T2* BOLD and T1 mapping MRI". In: *Eur Radiol* 30.8 (2020), pp. 4327–4336. DOI: 10.1007/s00330-020-06779-9.

[11] Charles Antzelevitch, Luiz Belardinelli, Andrew C Zygmunt, et al. "Electrophysiological Effects of Ranolazine, a Novel Antianginal Agent With Antiarrhythmic Properties". In: *Circulation* 110.8 (2004), pp. 904–910. DOI: 10.1161/01.CIR.0000139333.83620.5D.

[12] Giovanni Donato Aquaro, Giancarlo Todiere, Andrea Barison, et al. "Myocardial Blood Flow and Fibrosis in Hypertrophic Cardiomyopathy". In: *J Card Fail* 17.5 (2011), pp. 384–391. DOI: 10.1016/j.cardfail.2011.01.006.

[13] V Aravindakshan, B Surawicz, and R D Allen. "Electrocardiographic exercise test in patients with abnormal T waves at rest". In: *Am Heart J* 93.6 (1977), pp. 706–714. DOI: 10.1016/s0002-8703(77)80065-3.

[14] Elena Arbelo, Alexandros Protonotarios, Juan R Gimeno, et al. "2023 ESC Guidelines for the management of cardiomyopathies: Developed by the task force on the management of cardiomyopathies of the European Society of Cardiology (ESC)". In: *Eur Heart J* 44.37 (2023), pp. 3503–3626. DOI: 10.1093/eurheartj/ehad194.

[15] Alessia Argirò, Mattia Zampieri, Lorenzo-Lupo Dei, et al. "Safety and efficacy of ranolazine in hypertrophic cardiomyopathy: Real-world experience in a National Referral Center". In: *Int J Cardiol* 370 (2023), pp. 271–278. DOI: 10.1016/j.ijcard.2022.10.014.

[16] Naoki Arima, Yuri Ochi, Makoto Takahashi, et al. "Transient decrease in the depth of the negative T wave in apical hypertrophic cardiomyopathy is a sign of left anterior descending artery stenosis: a case series". In: *Eur Heart J Case Rep* 7.1 (2023). DOI: 10.1093/ehjcr/ytad034.

[17] Houman Ashrafian, Charles Redwood, Edward Blair, et al. "Hypertrophic cardiomyopathy: a paradigm for myocardial energy depletion". In: *Trends Genet* 19.5 (2003), pp. 263–268. DOI: 10.1016/S0168-9525(03)00081-7.

[18] Elizabeth P Baskin and Joseph J Jr. Lynch. "Comparative Effects of Increased Extracellular Potassium and Pacing Frequency on the Class III Activities of Methanesulfonanilide IKr Blockers Dofetilide, d-Sotalol, E-4031, and MK-499". In: *J Cardiovasc Pharmacol* 24.2 (1994).

[19] Cristina Basso, Gaetano Thiene, Domenico Corrado, et al. "Hypertrophic cardiomyopathy and sudden death in the young: Pathologic evidence of myocardial ischemia". In: *Hum Pathol* 31.8 (2000), pp. 988–998. DOI: 10.1053/hupa.2000.16659.

[20] Cristina Basso, Gaetano Thiene, Shannon Mackey-Bojack, et al. "Myocardial bridging, a frequent component of the hypertrophic cardiomyopathy phenotype, lacks systematic association with sudden cardiac death". In: *Eur Heart J* 30.13 (2009), pp. 1627–1634. DOI: 10.1093/eurheartj/ehp121.

[21] Douglas E Befroy, Trevor Powell, George K Radda, et al. "Osmotic shock: modulation of contractile function, pHi, and ischemic damage in perfused guinea pig heart". In: *Am J Physiol Heart Circ Physiol* 276.4 (1999), H1236–H1244. DOI: 10.1152/ajpheart.1999.276.4.H1236.

[22] P Bélichard, D Pruneau, R Rouet, et al. "Electrophysiological responses of hypertrophied rat myocardium to combined hypoxia, hyperkalemia, and acidosis". In: *J Cardiovasc Pharmacol* 17 (1991), pp. 141–5. DOI: 10.1097/00005344-199117002-00034.

[23] Gray Belinda, Ingles Jodie, Medi Caroline, et al. "Prolongation of the QTc Interval Predicts Appropriate Implantable Cardioverter-Defibrillator Therapies in Hypertrophic Cardiomyopathy". In: *JACC: Heart Fail* 1.2 (2013), pp. 149–155. DOI: 10.1016/j.jchf.2013.01.004.

[24] Charles I Berul, Tammy L Sweeten, Anne M Dubin, et al. "Use of the rate-corrected JT interval for prediction of repolarization abnormalities in children". In: *Am J Cardiol* 74.12 (1994), pp. 1254–1257. DOI: 10.1016/0002-9149(94)90558-4.

[25] Elena Biagini, Chiara Pazzi, Iacopo Olivotto, et al. "Usefulness of Electrocardiographic Patterns at Presentation to Predict Long-term Risk of Cardiac Death in Patients With Hypertrophic Cardiomyopathy". In: *Am J Cardiol* 118.3 (2016), pp. 432–439. DOI: 10.1016/j.amjcard.2016.05.023.

[26] F Bogatyreva, V.ra Kaplunova, Maria Kozhevnikova, et al. "Assessment of the structural and functional state of blood vessels in patients with hypertrophic cardiomyopathy". In: *Kardiologiia* 61 (2021), pp. 16–21. DOI: 10.18087/cardio.2021.12.n1718.

[27] J Martijn Bos, Lia Crotti, Ram K Rohatgi, et al. "Mexiletine Shortens the QT Interval in Patients With Potassium Channel–Mediated Type 2 Long QT Syndrome". In: *Circ Arrhythm Electrophysiol* 12.5 (2019), e007280. DOI: 10.1161/CIRCEP.118.007280.

[28] Paco E Bravo, Aurélio Pinheiro, Takahiro Higuchi, et al. "PET/CT Assessment of Symptomatic Individuals with Obstructive and Nonobstructive Hypertrophic Cardiomyopathy". In: *J Nucl Med* 53.3 (2012), p. 407. DOI: 10.2967/jnumed.111.096156.

[29] Paco E Bravo, Stefan L Zimmerman, Hong-Chang Luo, et al. "Relationship of delayed enhancement by magnetic resonance to myocardial perfusion by positron emission tomography in hypertrophic cardiomyopathy". In: *Circ Cardiovasc Imaging* 6.2 (2013), pp. 210–217. DOI: 10.1161/CIRCIMAGING.112.000110.

[30] Oliver J Britton, Alfonso Bueno-Orovio, Karel Van Ammel, et al. "Experimentally calibrated population of models predicts and explains intersubject variability in cardiac cellular electrophysiology". In: *Proc Natl Acad Sci U S A* 110.23 (2013), E2098–E2105. DOI: 10.1073/pnas.1304382110.

[31] Oliver J Britton, Alfonso Bueno-Orovio, László Virág, et al. "The Electrogenic Na+/K+ Pump Is a Key Determinant of Repolarization Abnormality Susceptibility in Human Ventricular Cardiomyocytes: A Population-Based Simulation Study". In: *Front Physiol* 8 (2017). DOI: 10.3389/fphys.2017.00278.

[32] Oliver Bruder, Anja Wagner, Christoph J Jensen, et al. "Myocardial Scar Visualized by Cardiovascular Magnetic Resonance Imaging Predicts Major Adverse Events in Patients With Hypertrophic Cardiomyopathy". In: *J Am Coll Cardiol* 56.11 (2010), pp. 875–887. DOI: 10.1016/j.jacc.2010.05.007.

[33] Alfonso Bueno-Orovio, Ben Hanson, Jaswinder Gill, et al. "In Vivo Human Left-to-Right Ventricular Differences in Rate Adaptation Transiently Increase Pro-Arrhythmic Risk following Rate Acceleration". In: *PloS one* 7 (2012), e52234. DOI: 10.1371/journal.pone.0052234.

[34] Gianfranco Buja, Manuela Miorelli, Pietro Turrini, et al. "Comparison of QT dispersion in hypertrophic cardiomyopathy between patients with and without ventricular arrhythmias and sudden death". In: *Am J Cardiol* 72.12 (1993), pp. 973–976. DOI: 10.1016/0002-9149(93)91118-2.

[35] Alexander Burashnikov, Serge Sicouri, José M Di Diego, et al. "Synergistic Effect of the Combination of Ranolazine and Dronedarone to Suppress Atrial Fibrillation". In: *J Am Coll Cardiol* 56.15 (2010), pp. 1216–1224. DOI: 10.1016/j.jacc.2010.08.600.

[36] Claudia Camaioni, Kristopher D Knott, Joao B Augusto, et al. "Inline perfusion mapping provides insights into the disease mechanism in hypertrophic cardiomyopathy". In: *Heart* 106.11 (2020), p. 824. DOI: 10.1136/heartjnl-2019-315848.

[37] Paolo Camici, Giampaolo Chiriatti, Roberto Lorenzoni, et al. "Coronary vasodilation is impaired in both hypertrophied and nonhypertrophied myocardium of patients with hypertrophic cardiomyopathy: A study with nitrogen-13 ammonia and positron emission tomography". In: *J Am Coll Cardiol* 17.4 (1991), pp. 879–886. DOI: 10.1016/0735-1097(91)90869-B.

[38] Fernando Otaviano Campos, John Whitaker, Radhouene Neji, et al. "Factors promoting conduction slowing as substrates for block and reentry in infarcted hearts". In: *Biophys J* 117.12 (2019), pp. 2361–2374. DOI: 10.1016/j.bpj.2019.08.008.

[39] Julia Camps, Lucas Arantes Berg, Zhinuo Jenny Wang, et al. "Digital twinning of the human ventricular activation sequence to Clinical 12-lead ECGs and magnetic resonance imaging using realistic Purkinje networks for in silico clinical trials". In: *Med Image Anal* 94 (2024), p. 103108. DOI: 10.1016/j.media.2024.103108.

[40] Beatriz Carbonell-Pascual, Eduardo Godoy, Ana Ferrer, et al. "Comparison between Hodgkin–Huxley and Markov formulations of cardiac ion channels". In: *J Theor Biol* 399 (2016), pp. 92–102. DOI: 10.1016/j.jtbi.2016.03.039.

[41] Louie Cardone-Noott, Alfonso Bueno-Orovio, Ana Mincholé, et al. "Human ventricular activation sequence and the simulation of the electrocardiographic QRS complex and its variability in healthy and intraventricular block conditions". In: *Europace* 18.suppl 4 (2016), pp. iv4–iv15. DOI: 10.1093/europace/euw346.

[42] E Carmeliet. "Myocardial ischemia: reversible and irreversible changes." In: *Circulation* 70.1 (1984), pp. 149–151. DOI: 10.1161/01.CIR.70.1.149.

[43] Edward Carmeliet. "Cardiac Ionic Currents and Acute Ischemia: From Channels to Arrhythmias". In: *Physiol Rev* 79.3 (1999), pp. 917–1017. DOI: 10.1152/physrev.1999.79.3.917.

[44] E F Carpio, J F Gomez, J F Rodríguez-Matas, et al. "Computational Analysis of Vulnerability to Reentry in Acute Myocardial Ischemia". In: *Comput Cardiol*. 2020, pp. 1–4. DOI: 10.22489/CinC.2020.241.

[45] Edison F Carpio, Juan F Gomez, José F Rodríguez-Matas, et al. "Analysis of vulnerability to reentry in acute myocardial ischemia using a realistic human heart model". In: *Comput Biol Med* 141 (2022), p. 105038. DOI: 10.1016/j.compbiomed.2021.105038.

[46] Helga Castagnoli, Cecilia Ferrantini, Raffaele Coppini, et al. "Role of quantitative myocardial positron emission tomography for risk stratification in patients with hypertrophic cardiomyopathy: a 2016 reappraisal". In: *Eur J Nucl Med Mol Imaging* 43.13 (2016), pp. 2413–2422. DOI: 10.1007/s00259-016-3465-7.

[47] Franco Cecchi, Iacopo Olivotto, Roberto Gistri, et al. "Coronary Microvascular Dysfunction and Prognosis in Hypertrophic Cardiomyopathy". In: *N Engl J Med* 349.11 (2003), pp. 1027–1035. DOI: 10.1056/NEJMoa025050.

[48] Bernard R Chaitman. "Ranolazine for the Treatment of Chronic Angina and Potential Use in Other Cardiovascular Conditions". In: *Circulation* 113.20 (2006), pp. 2462–2472. DOI: 10.1161/CIRCULATIONAHA.105.597500.

[49] Bernard R Chaitman, Sandra L Skettino, John O Parker, et al. "Anti-ischemic effects and long-term survival during ranolazine monotherapy in patients with chronic severe angina". In: *J Am Coll Cardiol* 43.8 (2004), pp. 1375–1382. DOI: 10.1016/j.jacc.2003.11.045.

[50] Fang Chan-Dewar. "The cardiac cycle". In: *Anaesth Intensive Care Med* 13.8 (2012), pp. 391–396. DOI: 10.1016/j.mpaic.2012.05.010.

[51] A Chiribiri, S Leuzzi, M R Conte, et al. "Rest perfusion abnormalities in hypertrophic cardiomyopathy: correlation with myocardial fibrosis and risk factors for sudden cardiac death". In: *Clin Radiol* 70.5 (2015), pp. 495–501. DOI: 10.1016/j.crad.2014.12.018.

[52] Ehud Chorin, Dan Hu, Charles Antzelevitch, et al. "Ranolazine for Congenital Long-QT Syndrome Type III". In: *Circ Arrhythm Electrophysiol* 9.10 (2016), e004370. DOI: 10.1161/CIRCEP.116.004370.

[53] Lubna Choudhury, Heiko Mahrholdt, Anja Wagner, et al. "Myocardial scarring in asymptomatic or mildly symptomatic patients with hypertrophic cardiomyopathy". In: *J Am Coll Cardiol* 40.12 (2002), pp. 2156–2164. DOI: 10.1016/S0735-1097(02)02602-5.

[54] Quirino Ciampi, Iacopo Olivotto, Chiara Gardini, et al. "Prognostic role of stress echocardiography in hypertrophic cardiomyopathy: The International Stress Echo Registry". In: *Int J Cardiol* 219 (2016), pp. 331–338. DOI: 10.1016/j.ijcard.2016.06.044.

[55] R H Clayton, O Bernus, E M Cherry, et al. "Models of cardiac tissue electrophysiology: Progress, challenges and open questions". In: *Prog Biophys Mol Biol* 104.1 (2011), pp. 22–48. DOI: 10.1016/j.pbiomolbio.2010.05.008.

[56] R H Clayton, M P Nash, C P Bradley, et al. "Experiment-model interaction for analysis of epicardial activation during human ventricular fibrillation with global myocardial ischaemia". In: *Prog Biophys Mol Biol* 107.1 (2011), pp. 101–111. DOI: 10.1016/j.pbiomolbio.2011.06.010.

[57] Clipart Library. *Body*. URL: https://clipart-library.com/clipart/361875.htm.

[58] Clipart Library. *Unlabelled Diagram Of The Heart*. URL: https://clipart-library.com/clipart/di45ebgLT.htm.

[59] Caroline J Coats, Khadija Rantell, Aleksandra Bartnik, et al. "Cardiopulmonary Exercise Testing and Prognosis in Hypertrophic Cardiomyopathy". In: *Circ Heart Fail* 8.6 (2015), pp. 1022–1031. DOI: 10.1161/CIRCHEARTFAILURE.114.002248.

[60] Andrew Constantine and Konstantinos Dimopoulos. "Physiology of the normal heart". In: *J Med* 50.6 (2022), pp. 322–326. DOI: 10.1016/j.mpmed.2022.03.010.

[61] Jennifer Conway, Sandar Min, Chet Villa, et al. "The Prevalence and Association of Exercise Test Abnormalities with Sudden Cardiac Death and Transplant-Free Survival in Childhood Hypertrophic Cardiomyopathy". In: *Circulation* 147.9 (2022), pp. 718–727. DOI: 10.1161/CIRCULATIONAHA.122.062699.

[62] Raffaele Coppini, Matteo Beltrami, Ruben Doste, et al. "Paradoxical prolongation of QT interval during exercise in patients with hypertrophic cardiomyopathy: cellular mechanisms and implications for diastolic function". In: *Eur Heart J* 2.3 (2022), oeac034. DOI: 10.1093/ehjopen/oeac034.

[63] Raffaele Coppini, Cecila Ferrantini, Alessandro Aiazzi, et al. "Isolation and Functional Characterization of Human Ventricular Cardiomyocytes from Fresh Surgical Samples". In: *J Vis Exp* (2014). DOI: 10.3791/51116.

[64] Raffaele Coppini, Cecilia Ferrantini, Alessandro Mugelli, et al. "Altered Ca(2+) and Na(+) Homeostasis in Human Hypertrophic Cardiomyopathy: Implications for Arrhythmogenesis". In: *Front Physiol* 9 (2018), p. 1391. DOI: 10.3389/fphys.2018.01391.

[65] Raffaele Coppini, Cecilia Ferrantini, Manuel Pioner Josè, et al. "Electrophysiological and Contractile Effects of Disopyramide in Patients With Obstructive Hypertrophic Cardiomyopathy". In: *J Am Coll Cardiol Basic Trans Science* 4.7 (2019), pp. 795–813. DOI: 10.1016/j.jacbts.2019.06.004.

[66] Raffaele Coppini, Cecilia Ferrantini, Lina Yao, et al. "Late Sodium Current Inhibition Reverses Electromechanical Dysfunction in Human Hypertrophic Cardiomyopathy". In: *Circulation* 127.5 (2013), pp. 575–584. DOI: 10.1161/CIRCULATIONAHA.112.134932.

[67] Raffaele Coppini, Luca Mazzoni, Cecilia Ferrantini, et al. "Ranolazine Prevents Phenotype Development in a Mouse Model of Hypertrophic Cardiomyopathy". In: *Circ Heart Fail* 10.3 (2017), e003565. DOI: 10.1161/CIRCHEARTFAILURE.116.003565.

[68] G Coppola, P Carità, E Corrado, et al. "ST segment elevations: Always a marker of acute myocardial infarction?" In: *Indian Heart J* 65.4 (2013), pp. 412–423. DOI: 10.1016/j.ihj.2013.06.013.

[69] R Coronel, J W Fiolet, F J Wilms-Schopman, et al. "Distribution of extracellular potassium and its relation to electrophysiologic changes during acute myocardial ischemia in the isolated perfused porcine heart." In: *Circulation* 77.5 (1988), pp. 1125–1138. DOI: 10.1161/01.CIR.77.5.1125.

[70] Ruben Coronel, Michiel J Janse, Tobias Opthof, et al. "Postrepolarization refractoriness in acute ischemia and after antiarrhythmic drug administration: Action potential duration is not always an index of the refractory period". In: *Heart Rhythm* 9.6 (2012), pp. 977–982. DOI: 10.1016/j.hrthm.2012.01.021.

[71] Ruben Coronel, Francien J G Wilms-Schopman, and Joris R deGroot. "Origin of ischemia-induced phase 1b ventricular arrhythmias in pig hearts". In: *J Am Coll Cardiol* 39.1 (2002), pp. 166–176. DOI: 10.1016/S0735-1097(01)01686-2.

[72] Lauro Cortigiani, Fausto Rigo, Sonia Gherardi, et al. "Prognostic Implications of Coronary Flow Reserve on Left Anterior Descending Coronary Artery in Hypertrophic Cardiomyopathy". In: *Am J Cardiol* 102.12 (2008), pp. 1718–1723. DOI: 10.1016/j.amjcard.2008.08.023.

[73] P Coumel. "The management of clinical arrhythmias. An overview on invasive versus non-invasive electrophysiology". In: *Eur Heart J* 8.2 (1987), pp. 92–99. DOI: 10.1093/oxfordjournals.eurheartj.a062259.

[74] Keith Couper, Kurtis Poole, William Bradlow, et al. *Screening for cardiac conditions associated with sudden cardiac death in the young*. UK National Screening Committee, 2019.

[75] *Created with BioRender.com.*

[76] William J Crumb, Jose Vicente, Lars Johannesen, et al. "An evaluation of 30 clinical drugs against the comprehensive in vitro proarrhythmia assay (CiPA) proposed ion channel panel". In: *J Pharmacol Toxicol Methods* 81 (2016), pp. 251–262. DOI: 10.1016/j.vascn.2016.03.009.

[77] Hao Cui, Hartzell V Schaff, Thomas P Olson, et al. "Cardiopulmonary exercise test in patients with obstructive hypertrophic cardiomyopathy". In: *J Thorac Cardiovasc Surg* (2022). DOI: 10.1016/j.jtcvs.2022.05.025.

[78] Flavio D'Ascenzi, Francesca Valentini, Simone Pistoresi, et al. "Causes of sudden cardiac death in young athletes and non-athletes: systematic review and meta-analysis: Sudden cardiac death in the young". In: *Trends Cardiovasc Med* 32.5 (2021), pp. 299–308. DOI: 10.1016/j.tcm.2021.06.001.

[79] Arka Das, Christopher Kelly, Irvin Teh, et al. "Phenotyping hypertrophic cardiomyopathy using cardiac diffusion magnetic resonance imaging: the relationship between microvascular dysfunction and microstructural changes". In: *Eur Heart J Cardiovasc Imaging* 23.3 (2022), pp. 352–362. DOI: 10.1093/ehjci/jeab210.

[80] Albert Dasí, Aditi Roy, Rafael Sachetto, et al. "In-silico drug trials for precision medicine in atrial fibrillation: From ionic mechanisms to electrocardiogram-based predictions in structurally-healthy human atria". In: *Front Physiol* 13 (2022). DOI: 10.3389/fphys.2022.966046.

[81] Daniel David, Eric L Michelson, Masahito Naito, et al. "Extracellular potassium dynamics in the border zone during acute myocardial ischemia in a canine model". In: *J Am Coll Cardiol* 11.2 (1988), pp. 422–430. DOI: 10.1016/0735-1097(88)90111-8.

[82] Philippe Debonnaire, Spyridon Katsanos, Emer Joyce, et al. "QRS Fragmentation and QTc Duration Relate to Malignant Ventricular Tachyarrhythmias and Sudden Cardiac Death in Patients with Hypertrophic Cardiomyopathy". In: *J Cardiovasc Electrophysiol* 26.5 (2015), pp. 547–555. DOI: 10.1111/jce.12629.

[83] A Deviggiano, P Carrascosa, M D Zan, et al. "Wall Thickness and Patterns of Fibrosis in Hypertrophic Cardiomyopathy Assessed by Cardiac Magnetic Resonance Imaging". In: *Rev Argent Cardiol.* 84 (2016), pp. 208–214. DOI: 10.7775/RAC.84.3.7168.

[84] Stefan Dhein, Thomas Seidel, Aida Salameh, et al. "Remodeling of cardiac passive electrical properties and susceptibility to ventricular and atrial arrhythmias". In: *Front Physiol* 5 (2014). DOI: 10.3389/fphys.2014.00424.

[85] José M Di Diego and Charles Antzelevitch. "Ischemic ventricular arrhythmias: Experimental models and their clinical relevance". In: *Heart Rhythm* 8.12 (2011), pp. 1963–1968. DOI: 10.1016/j.hrthm.2011.06.036.

[86] Katharine M Dibb, Jessica D Clarke, Margaux A Horn, et al. "Characterization of an Extensive Transverse Tubular Network in Sheep Atrial Myocytes and its Depletion in Heart Failure". In: *Circ Heart Fail* 2.5 (2009), pp. 482–489. DOI: 10.1161/CIRCHEARTFAILURE.109.852228.

[87] Vasken Dilsizian, Robert O Bonow, Stephen E Epstein, et al. "Myocardial ischemia detected by thallium scintigraphy is frequently related to cardiac arrest and syncope in young patients with hypertrophic cardiomyopathy". In: *J Am Coll Cardiol* 22.3 (1993), pp. 796–804. DOI: 10.1016/0735-1097(93)90193-5.

[88] Thomas W Dohlen, L.Michael Prisant, and Martin J Frank. "Significance of positive or negative thallium-201 scintigraphy in hypertrophic cardiomyopathy". In: *Am J Cardiol* 64.8 (1989), pp. 498–503. DOI: 10.1016/0002-9149(89)90428-1.

[89] Ruben Doste, Raffaele Coppini, and Alfonso Bueno-Orovio. "Remodelling of potassium currents underlies arrhythmic action potential prolongation under beta-adrenergic stimulation in hypertrophic cardiomyopathy". In: *J Mol Cell Cardiol* 172 (2022), pp. 120–131. DOI: 10.1016/j.yjmcc.2022.08.361.

[90] Jonathan A Drezner, Aneil Malhotra, Jordan M Prutkin, et al. "Return to play with hypertrophic cardiomyopathy: are we moving too fast? A critical review". In: *Br J Sports Med* 55.18 (2021), p. 1041. DOI: 10.1136/bjsports-2020-102921.

[91] Sara Dutta, Ana Mincholé, T Alexander Quinn, et al. "Electrophysiological properties of computational human ventricular cell action potential models under acute ischemic conditions". In: *Prog Biophys Mol Biol* 129 (2017), pp. 40–52. DOI: 10.1016/j.pbiomolbio.2017.02.007.

[92] Sara Dutta, Ana Mincholé, Ernesto Zacur, et al. "Early afterdepolarizations promote transmural reentry in ischemic human ventricles with reduced repolarization reserve". In: *Prog Biophys Mol Biol* 120.1-3 (2016), pp. 236–248. DOI: 10.1016/j.pbiomolbio.2016.01.008.

[93] D A Eisner, K M Dibb, and A W Trafford. "The mechanism and significance of the slow changes of ventricular action potential duration following a change of heart rate". In: *Exp Physiol* 94.5 (2009), pp. 520–528. DOI: 10.1113/expphysiol.2008.044008.

[94] David A Eisner, Jessica L Caldwell, Kornél Kistamás, et al. "Calcium and Excitation-Contraction Coupling in the Heart". In: *Circ Res* 121.2 (2017), pp. 181–195. DOI: 10.1161/CIRCRESAHA.117.310230.

[95] P M Elliott, J C Kaski, K Prasad, et al. "Chest pain during daily life in patients with hypertrophic cardiomyopathy: an ambulatory electrocardiographic study". In: *Eur Heart J* 17.7 (1996), pp. 1056–1064. DOI: 10.1093/oxfordjournals.eurheartj.a015002.

[96] P M Elliott, G M Rosano, J S Gill, et al. "Changes in coronary sinus pH during dipyridamole stress in patients with hypertrophic cardiomyopathy." In: *Heart* 75.2 (1996), p. 179. DOI: 10.1136/hrt.75.2.179.

[97] Perry Elliott, Aris Anastasakis, Michael A Borger, et al. "2014 ESC Guidelines on diagnosis and management of hypertrophic cardiomyopathy: The Task Force for the Diagnosis and Management of Hypertrophic Cardiomyopathy of the European Society of Cardiology (ESC)". In: *Eur Heart J* 35.39 (2014), pp. 2733–2779. DOI: 10.1093/eurheartj/ehu284.

[98] Perry M Elliott, Juan R Gimeno, María T Tomé, et al. "Left ventricular outflow tract obstruction and sudden death risk in patients with hypertrophic cardiomyopathy". In: *Eur Heart J* 27.16 (2006), pp. 1933–1941. DOI: 10.1093/eurheartj/ehl041.

[99] A Esposito, F De Cobelli, G Perseghin, et al. "Impaired left ventricular energy metabolism in patients with hypertrophic cardiomyopathy is related to the extension of fibrosis at delayed gadolinium-enhanced magnetic resonance imaging". In: *Heart* 95.3 (2009), p. 228. DOI: 10.1136/hrt.2008.142562.

[100] J M Ferrero, B Trenor, J Saiz, et al. "Electrical activity and reentry in acute regional ischemia: insights from simulations". In: *Conf Proc IEEE Eng Med Biol Soc*. Vol. 1. 2003, pp. 17–20. DOI: 10.1109/IEMBS.2003.1279483.

[101] Jose M Ferrero, Ana Gonzalez-Ascaso, and Jose F Rodriguez Matas. "The mechanisms of potassium loss in acute myocardial ischemia: New insights from computational simulations". In: *Front Physiol* 14 (2023). DOI: 10.3389/fphys.2023.1074160.

[102] W F Fleet, T A Johnson, C A Graebner, et al. "Effect of serial brief ischemic episodes on extracellular K+, pH, and activation in the pig." In: *Circulation* 72.4 (1985), pp. 922–932. DOI: 10.1161/01.CIR.72.4.922.

[103] Alberto Foà, Valentina Agostini, Claudio Rapezzi, et al. "Histopathological comparison of intramural coronary artery remodeling and myocardial fibrosis in obstructive versus end-stage

hypertrophic cardiomyopathy". In: *Int J Cardiol* 291 (2019), pp. 77–82. DOI: 10.1016/j.ijcard.2019.03.060.

[104] Nikolaos G Frangogiannis. "The extracellular matrix in myocardial injury, repair, and remodeling". In: *J Clin Invest* 127.5 (2017), pp. 1600–1612. DOI: 10.1172/JCI87491.

[105] Pedro Freitas, António Miguel Ferreira, Edmundo Arteaga-Fernández, et al. "The amount of late gadolinium enhancement outperforms current guideline-recommended criteria in the identification of patients with hypertrophic cardiomyopathy at risk of sudden cardiac death". In: *J Cardiovasc Magn Reson* 21.1 (2019), p. 50. DOI: 10.1186/s12968-019-0561-4.

[106] Hiroshi Furushima, Masaomi Chinushi, Kenichi Iijima, et al. "Ventricular Tachyarrhythmia Associated with Hypertrophic Cardiomyopathy: Incidence, Prognosis, and Relation to Type of Hypertrophy". In: *J Cardiovasc Electrophysiol* 21.9 (2010), pp. 991–999. DOI: 10.1111/j.1540-8167.2010.01769.x.

[107] David C Gadsby. "Ion channels versus ion pumps: the principal difference, in principle". In: *Nat Rev Mol Cell Biol* 10.5 (2009), pp. 344–352. DOI: 10.1038/nrm2668.

[108] Giuseppe Galati, Ornella Leone, Ferdinando Pasquale, et al. "Histological and Histometric Characterization of Myocardial Fibrosis in End-Stage Hypertrophic Cardiomyopathy". In: *Circ Heart Fail* 9.9 (2016), e003090. DOI: 10.1161/CIRCHEARTFAILURE.116.003090.

[109] Dongsheng Gao, Hugo Herendael, Lamia Alshengeiti, et al. "Mexiletine as an Adjunctive Therapy to Amiodarone Reduces the Frequency of Ventricular Tachyarrhythmia Events in Patients With an Implantable Defibrillator". In: *J Cardiovasc Pharmacol* 62 (2013). DOI: 10.1097/FJC.0b013e31829651fe.

[110] Pedro Garcia Brás, Sílvia Aguiar Rosa, Boban Thomas, et al. "Associations between perfusion defects, tissue changes and myocardial deformation in hypertrophic cardiomyopathy, uncovered by a cardiac magnetic resonance segmental analysis". In: *Rev Port Cardiol* 41.7 (2022), pp. 559–568. DOI: 10.1016/j.repc.2022.03.003.

[111] Monica Gaspari, Cristina Basso, Martina Perazzolo Marra, et al. "Small Vessel Disease: Another Component of the Hypertrophic Cardiomyopathy Phenotype Not Necessarily Associated with Fibrosis". In: *J Clin Med* 10.4 (2021), p. 575. DOI: 10.3390/jcm10040575.

[112] Bernard J Gersh, Barry J Maron, Robert O Bonow, et al. "2011 ACCF/AHA Guideline for the Diagnosis and Treatment of Hypertrophic Cardiomyopathy". In: *Circulation* 124.24 (2011), e783–e831. DOI: 10.1161/CIR.0b013e318223e2bd.

[113] Juan R Gimeno, Maite Tomé-Esteban, Carla Lofiego, et al. "Exercise-induced ventricular arrhythmias and risk of sudden cardiac death in patients with hypertrophic cardiomyopathy". In: *Eur Heart J* 30.21 (2009), pp. 2599–2605. DOI: 10.1093/eurheartj/ehp327.

[114] Alexey V Glukhov, Vadim V Fedorov, Qing Lou, et al. "Transmural Dispersion of Repolarization in Failing and Nonfailing Human Ventricle". In: *Circ Res* 106.5 (2010), pp. 981–991. DOI: 10.1161/CIRCRESAHA.109.204891.

[115] Frank Gommans, Jeannette Bakker, Etienne Cramer, et al. "Elevated high-sensitivity cardiac troponin is associated with hypertrophy and fibrosis assessed with CMR in patients with hypertrophic cardiomyopathy". In: *J Cardiovasc Magn Reson* 15.1 (2013), P144. DOI: 10.1186/1532-429X-15-S1-P144.

[116] Franca Gori, Cristina Basso, and Gaetano Thiene. "Myocardial Infarction in a Patient with Hypertrophic Cardiomyopathy". In: *N Engl J Med* 342.8 (2000), pp. 593–594. DOI: 10.1056/NEJM200002243420817.

[117] Christoph Gräni. "Prime time for CMR imaging of arrhythmogenic substrate in hypertrophic cardiomyopathy". In: *Eur Heart J* 44.45 (2023), pp. 4793–4795. DOI: 10.1093/eurheartj/ehad686.

[118] Augustus O Grant. "Cardiac Ion Channels". In: *Circ Arrhythm Electrophysiol* 2.2 (2009), pp. 185–194. DOI: 10.1161/CIRCEP.108.789081.

[119] Suchi Grover, Rachael Lloyd, Rebecca Perry, et al. "Assessment of myocardial oxygenation, strain, and diastology in MYBPC3-related hypertrophic cardiomyopathy: a cardiovascular magnetic resonance and echocardiography study". In: *Eur Heart J Cardiovasc Imaging* 20.8 (2019), pp. 932–938. DOI: 10.1093/ehjci/jey220.

[120] Ahmet Güçlü, Chris Happé, Seyma Eren, et al. "Left ventricular outflow tract gradient is associated with reduced capillary density in hypertrophic cardiomyopathy irrespective of genotype". In: *Eur J Clin Invest* 45.12 (2015), pp. 1252–1259. DOI: 10.1111/eci.12544.

[121] Ahmet Güner, Macit Kalçık, Mehmet Çelik, et al. "Impaired repolarization parameters may predict fatal ventricular arrhythmias in patients with hypertrophic cardiomyopathy (from the CILICIA Registry)". In: *J Electrocardiol* 63 (2020), pp. 83–90. DOI: 10.1016/j.jelectrocard.2020.10.009.

[122] Antonio Gutiérrez Díez, Amalia Tamariz-Martel Moreno, Antonio Baño Rodrigo, et al. "Muerte súbita y fibrilación ventricular de posible origen isquémico en un niño con miocardiopatía hipertrófica". In: *Rev Esp Cardiol* 53.2 (2000), pp. 290–293. DOI: 10.1016/s0300-8932(00)75093-7..

[123] Tom Gyllenhammar, Eva Fernlund, Robert Jablonowski, et al. "Young patients with hypertrophic cardiomyopathy, but not subjects at risk, show decreased myocardial perfusion reserve quantified with CMR". In: *Eur Heart J Cardiovasc Imaging* 15.12 (2014), pp. 1350–1357. DOI: 10.1093/ehjci/jeu137.

[124] Radek Halfar, Brodie A J Lawson, Rodrigo Weber dos Santos, et al. "Recurrence quantification analysis for fine-scale characterisation of arrhythmic patterns in cardiac tissue". In: *Sci Rep* 13.1 (2023), p. 11828. DOI: 10.1038/s41598-023-38256-w.

[125] Mareomi Hamada, Yuji Shigematsu, Shigeru Nakata, et al. "Predicting the clinical course in hypertrophic cardiomyopathy using thallium-201 myocardial scintigraphy". In: *ESC Heart Fail* 8.2 (2021), pp. 1378–1387. DOI: 10.1002/ehf2.13218.

[126] Michèle Hamon, Georges Fau, Guillaume Née, et al. "Meta-analysis of the diagnostic performance of stress perfusion cardiovascular magnetic resonance for detection of coronary artery disease". In: *J Cardiovasc Magn Reson* 12.1 (2010), p. 29. DOI: 10.1186/1532-429X-12-29.

[127] Adam Hartley, Joseph Shalhoub, Fu Siong Ng, et al. "Size matters in atrial fibrillation: the underestimated importance of reduction of contiguous electrical mass underlying the effectiveness of catheter ablation". In: *EP Europace* 23.11 (2021), pp. 1698–1707. DOI: 10.1093/europace/euab078.

[128] David J Hearse, Lionel H Opie, Issy E Katzeff, et al. "Characterization of the "border zone" in acute regional ischemia in the dog". In: *Am J Cardiol* 40.5 (1977), pp. 716–726. DOI: 10.1016/0002-9149(77)90187-4.

[129] Bence Hegyi, Ye Chen-Izu, Leighton Izu, et al. "Altered K+ current profiles underlie cardiac action potential shortening in hyperkalemia and β adrenergic stimulation". In: *Can J Physiol Pharmacol* 97 (2019). DOI: 10.1139/cjpp-2019-0056.

[130] Lazaro E Hernandez. "Myocardial stress perfusion magnetic resonance in children with hypertrophic cardiomyopathy". In: *Cardiol Young* 28.5 (2018), pp. 702–708. DOI: 10.1017/S1047951118000094.

[131] M N Hicks, M A McIntosh, K A Kane, et al. "The electrophysiology of rabbit hearts with left ventricular hypertrophy under normal and ischaemic conditions". In: *Cardiovasc Res* 30.2 (1995), pp. 181–186. DOI: 10.1016/S0008-6363(95)00065-8.

[132] S Hirasaki, T Nakamura, T Kuribayashi, et al. "Abnormal course, abnormal flow, and systolic compression of the septal perforator associated with impaired myocardial perfusion in hypertrophic cardiomyopathy". In: *Am Heart J* 137 (1999), pp. 109–117. DOI: 10.1016/s0002-8703(99)70466-7.

[133] Hj. Hirche, Chr. Franz, L Bös, et al. "Myocardial extracellular K+ and H+ increase and noradrenaline release as possible cause of early arrhythmias following acute coronary artery occlusion in pigs". In: *J Mol Cell Cardiol* 12.6 (1980), pp. 579–593. DOI: 10.1016/0022-2828(80)90016-4.

[134] Siew Yen Ho. "Anatomy and myoarchitecture of the left ventricular wall in normal and in disease". In: *Eur J Echocardiogr* 10.8 (2009), pp. iii3–iii7. DOI: 10.1093/ejechocard/jep159.

[135] A L Hodgkin and A F Huxley. "A quantitative description of membrane current and its application to conduction and excitation in nerve". In: *J Physiol* 117.4 (1952), pp. 500–544. DOI: 10.1113/jphysiol.1952.sp004764.

[136] Margaux Horn and Andrew Trafford. "Aging and the cardiac collagen matrix: Novel mediators of fibrotic remodelling". In: *J Mol Cell Cardiol* 93 (2015). DOI: 10.1016/j.yjmcc.2015.11.005.

[137] L Huang, R Han, T Ai, et al. "Assessment of coronary microvascular dysfunction in hypertrophic cardiomyopathy: First-pass myocardial perfusion cardiovascular magnetic resonance imaging at 1.5 T". In: *Clin Radiol* 68.7 (2013), pp. 676–682. DOI: 10.1016/j.crad.2013.01.003.

[138] Rebecca K Hughes, Claudia Camaioni, João B Augusto, et al. "Myocardial Perfusion Defects in Hypertrophic Cardiomyopathy Mutation Carriers". In: *J Am Heart Assoc* 10.15 (2021), e020227. DOI: 10.1161/JAHA.120.020227.

[139] Lee Hyun-Jung, Kim Hyung-Kwan, Lee Sang Chol, et al. "Performance of 2020 AHA/ACC HCM Guidelines and Incremental Value of Myocardial Strain for Predicting SCD". In: *JACC: Asia* 4.1 (2024), pp. 10–22. DOI: 10.1016/j.jacasi.2023.09.002.

[140] Praveen Indraratna, Daniel Tardo, Madeline Delves, et al. "Measurement and Management of QT Interval Prolongation for General Physicians". In: *J Gen Intern Med* 35 (2019), pp. 1–9. DOI: 10.1007/s11606-019-05477-7.

[141] H Irisawa and R Sato. "Intra- and extracellular actions of proton on the calcium current of isolated guinea pig ventricular cells." In: *Circ Res* 59.3 (1986), pp. 348–355. DOI: 10.1161/01.RES.59.3.348.

[142] S Ishiwata, H Maruno, M Senda, et al. "Mechanical efficiency in hypertrophic cardiomyopathy assessed by positron emission tomography with carbon 11 acetate". In: *Am Heart J* 133.5 (1997), pp. 497–503. DOI: 10.1016/s0002-8703(97)70143-1.

[143] Tevfik Ismail, Li-Yueh Hsu, Anders Greve, et al. "Coronary microvascular ischemia in hypertrophic cardiomyopathy - A pixel-wise quantitative cardiovascular magnetic resonance perfusion study". In: *J Cardiovasc Magn Reson* 16 (2014), p. 49. DOI: 10.1186/s12968-014-0049-1.

[144] Ziad F Issa, John M Miller, and Douglas P Zipes. "4 - Electrophysiological Testing: Tools and Techniques". In: *Clinical Arrhythmology and Electrophysiology*. Ed. by Ziad F Issa, John M Miller, and Douglas P Zipes. Philadelphia: Elsevier, 2019, pp. 81–124. DOI: 10.1016/B978-0-323-52356-1.00004-9.

[145] Robert Jablonowski, Eva Fernlund, Anthony H Aletras, et al. "Regional Stress-Induced Ischemia in Non-fibrotic Hypertrophied Myocardium in Young HCM Patients". In: *Pediatr Cardiol* 36.8 (2015), pp. 1662–1669. DOI: 10.1007/s00246-015-1214-5.

[146] R I Jabr and W C Cole. "Alterations in electrical activity and membrane currents induced by intracellular oxygen-derived free radical stress in guinea pig ventricular myocytes." In: *Circ Res* 72.6 (1993), pp. 1229–1244. DOI: 10.1161/01.RES.72.6.1229.

[147] M J Janse and F J van Capelle. "Electrotonic interactions across an inexcitable region as a cause of ectopic activity in acute regional myocardial ischemia. A study in intact porcine and canine hearts and computer models." In: *Circ Res* 50.4 (1982), pp. 527–537. DOI: 10.1161/01.RES.50.4.527.

[148] M J Janse, F J van Capelle, H Morsink, et al. "Flow of "injury" current and patterns of excitation during early ventricular arrhythmias in acute regional myocardial ischemia in isolated porcine and canine hearts. Evidence for two different arrhythmogenic mechanisms." In: *Circ Res* 47.2 (1980), pp. 151–165. DOI: 10.1161/01.RES.47.2.151.

[149] M J Janse, J Cinca, H Moréna, et al. "The "border zone" in myocardial ischemia. An electrophysiological, metabolic, and histochemical correlation in the pig heart." In: *Circ Res* 44.4 (1979), pp. 576–588. DOI: 10.1161/01.RES.44.4.576.

[150] M J Janse and A G Kléber. "Electrophysiological changes and ventricular arrhythmias in the early phase of regional myocardial ischemia." In: *Circ Res* 49.5 (1981), pp. 1069–1081. DOI: 10.1161/01.RES.49.5.1069.

[151] Michael Janse, Andre Kleber, Capucci Alessandro, et al. "Electrophysiological basis for arrhythmias caused by acute ischemia". In: *J Mol Cell Cardiol* 18.4 (1986), pp. 339–355. DOI: 10.1016/S0022-2828(86)80898-7.

[152] Markus Jerling. "Clinical Pharmacokinetics of Ranolazine". In: *Clin Pharmacokinet* 45.5 (2006), pp. 469–491. DOI: 10.2165/00003088-200645050-00003.

[153] Markus Jerling, Bee-Lian Huan, Kwan Leung, et al. "Studies to Investigate the Pharmacokinetic Interactions Between Ranolazine and Ketoconazole, Diltiazem, or Simvastatin During Combined Administration in Healthy Subjects". In: *J Clin Pharmacol* 45.4 (2005), pp. 422–433. DOI: 10.1177/0091270004273992.

[154] Bengt Johansson, Stellan Mörner, Anders Waldenström, et al. "Myocardial capillary supply is limited in hypertrophic cardiomyopathy: A morphological analysis". In: *Int J Cardiol* 126.2 (2008), pp. 252–257. DOI: 10.1016/j.ijcard.2007.04.003.

[155] Jonathan N Johnson, Camilla Grifoni, J Martijn Bos, et al. "Prevalence and clinical correlates of QT prolongation in patients with hypertrophic cardiomyopathy". In: *Eur Heart J* 32.9 (2011), pp. 1114–1120. DOI: 10.1093/eurheartj/ehr021.

[156] X Jouven, A Hagege, Philippe Charron, et al. "Relation between QT duration and maximal wall thickness in familial hypertrophic cardiomyopathy". In: *Heart* 88 (2002), pp. 153–157. DOI: 10.1136/heart.88.2.153.

[157] George Joy, Luis R Lopes, Matthew Webber, et al. "Electrophysiological Characterization of Subclinical and Overt Hypertrophic Cardiomyopathy by Magnetic Resonance Imaging-Guided Electrocardiography". In: *J Am Coll Cardiol* (2024). DOI: 10.1016/j.jacc.2024.01.006.

[158] Wulf-Ingo Jung, Ludger Sieverding, Johannes Breuer, et al. "31P NMR Spectroscopy Detects Metabolic Abnormalities in Asymptomatic Patients With Hypertrophic Cardiomyopathy". In: *Circulation* 97.25 (1998), pp. 2536–2542. DOI: 10.1161/01.CIR.97.25.2536.

[159] Satoshi Kaimoto, Tatsuya Kawasaki, Toshiro Kuribayashi, et al. "Myocardial perfusion abnormality in the area of ventricular septum-free wall junction and cardiovascular events in nonobstructive hypertrophic cardiomyopathy". In: *Int J Cardiovasc Imaging* 28.7 (2012), pp. 1829–1839. DOI: 10.1007/s10554-011-9994-z.

[160] Liang Kang, Yi-Hua Li, Rong Li, et al. "Predicting apical hypertrophic cardiomyopathy using T-wave inversion: Three case reports". In: *World J Clin Cases* 11.25 (2023), pp. 5970–5976. DOI: 10.12998/wjcc.v11.i25.5970.

[161] S Kang and W.-H. Choi. "Pseudonormalization of Negative T Wave during Stress Test in Asymptomatic Patients without Ischemic Heart Disease: A Clue to Apical Hypertrophic Cardiomyopathy?" In: *Cardiol* 124.2 (2013), pp. 91–96. DOI: 10.1159/000346235.

[162] E Kaplinsky, S Ogawa, C W Balke, et al. "Two periods of early ventricular arrhythmia in the canine acute myocardial infarction model." In: *Circulation* 60.2 (1979), pp. 397–403. DOI: 10.1161/01.CIR.60.2.397.

[163] Theodoros D Karamitsos, Sairia Dass, Joseph Suttie, et al. "Blunted Myocardial Oxygenation Response During Vasodilator Stress in Patients With Hypertrophic Cardiomyopathy". In: *J Am Coll Cardiol* 61.11 (2013), pp. 1169–1176. DOI: 10.1016/j.jacc.2012.12.024.

[164] Anthony Kashou, Hajira Basit, and Ahmad Malik. "ST Segment". In: Treasure Island (FL): StatPearls Publishing, 2023.

[165] Philipp Kaufmann, Giuseppe Vassalli, Simonetta Lupi-Wagner, et al. "Coronary artery dimensions in primary and secondary left ventricular hypertrophy". In: *J Am Coll Cardiol* 28.3 (1996), pp. 745–750. DOI: 10.1016/0735-1097(96)00194-5.

[166] Tatsuya Kawasaki, Akihiro Azuma, Toshiro Kuribayashi, et al. "Resting ST-segment depression predicts exercise-induced subendocardial ischemia in patients with hypertrophic cardiomyopathy". In: *Int J Cardiol* 107.2 (2006), pp. 267–274. DOI: 10.1016/j.ijcard.2005.03.031.

[167] Ivan V Kazbanov, Richard H Clayton, Martyn P Nash, et al. "Effect of global cardiac ischemia on human ventricular fibrillation: insights from a multi-scale mechanistic model of the human heart". In: *PLoS Comput Biol* 10.11 (2014), e1003891–e1003891. DOI: 10.1371/journal.pcbi.1003891.

[168] Moa Kihlgren, Christina Almqvist, Fereydoun Amankhani, et al. "The U-wave: A remaining enigma of the electrocardiogram". In: *J Electrocardiol* 79 (2023), pp. 13–20. DOI: 10.1016/j.jelectrocard.2023.03.001.

[169] Eun Kyoung Kim, Sang-Chol Lee, Sung-A Chang, et al. "Prevalence and clinical significance of cardiovascular magnetic resonance adenosine stress-induced myocardial perfusion defect in hypertrophic cardiomyopathy". In: *J Cardiovasc Magn Reson* 22.1 (2020), p. 30. DOI: 10.1186/s12968-020-00623-1.

[170] Woo-Shik Kim, Shinichi Minagoe, Naoko Mizukami, et al. "No reflow-like pattern in intramyocardial coronary artery suggests myocardial ischemia in patients with hypertrophic cardiomyopathy". In: *J Cardiol* 52.1 (2008), pp. 7–16. DOI: 10.1016/j.jjcc.2008.04.004.

[171] Brian P Kimball, Victor LiPreti, Sanh Bui, et al. "Comparison of proximal left anterior descending and circumflex coronary artery dimensions in aortic valve stenosis and hypertrophic cardiomyopathy". In: *Am J Cardiol* 65.11 (1990), pp. 767–771. DOI: 10.1016/0002-9149(90)91385-J.

[172] Andrè G Kléber. "ST-segment elevation in the electrocardiogram: a sign of myocardial ischemia". In: *Cardiovasc Res* 45.1 (2000), pp. 111–118. DOI: 10.1016/S0008-6363(99)00301-6.

[173] Paul Knaapen, Tjeerd Germans, Paolo G Camici, et al. "Determinants of coronary microvascular dysfunction in symptomatic hypertrophic cardiomyopathy". In: *Am J Physiol Heart Circ Physiol* 294.2 (2008), H986–H993. DOI: 10.1152/ajpheart.00233.2007.

[174] Itsuo Kodama, Arthur Wilde, Michiel J Janse, et al. "Combined effects of hypoxia, hyperkalemia and acidosis on membrane action potential and excitability of guinea-pig ventricular muscle". In: *J Mol Cell Cardiol* 16.3 (1984), pp. 247–259. DOI: 10.1016/S0022-2828(84)80591-X.

[175] Tetsuro Kohya, Shinichi Kimura, Robert J Myerburg, et al. "Susceptibility of hypertrophied rat hearts to ventricular fibrillation during acute ischemia". In: *J Mol Cell Cardiol* 20.2 (1988), pp. 159–168. DOI: 10.1016/S0022-2828(88)80029-4.

[176] Jin Komuro, Nobuo Iguchi, Yuko Utanohara, et al. "Prediction of Serious Adverse Events of Patients with Hypertrophic Cardiomyopathy by Magnetic Resonance". In: *Int Heart J* 62.1 (2021), pp. 135–141. DOI: 10.1536/ihj.20-479.

[177] S Koyanagi, C Eastham, and M L Marcus. "Effects of chronic hypertension and left ventricular hypertrophy on the incidence of sudden cardiac death after coronary artery occlusion in conscious dogs." In: *Circulation* 65.6 (1982), pp. 1192–1197. DOI: 10.1161/01.CIR.65.6.1192.

[178] R Krams, M J M Kofflard, D J Duncker, et al. "Decreased Coronary Flow Reserve in Hypertrophic Cardiomyopathy Is Related to Remodeling of the Coronary Microcirculation". In: *Circulation* 97.3 (1998), pp. 230–233. DOI: 10.1161/01.CIR.97.3.230.

[179] Rob Krams, Folkert J Cate, Stéphane G Carlier, et al. "Diastolic coronary vascular reserve: a new index to detect changes in the coronary microcirculation in hypertrophic cardiomyopathy". In: *J Am Coll Cardiol* 43.4 (2004), pp. 670–677. DOI: 10.1016/j.jacc.2003.09.046.

[180] Shankarjee Krishnamoorthi, Mainak Sarkar, and William S Klug. "Numerical quadrature and operator splitting in finite element methods for cardiac electrophysiology". In: *Int J Numer Methods Biomed Eng* 29.11 (2013), pp. 1243–1266. DOI: 10.1002/cnm.2573.

[181] K Kroll and G V Martin. "Comparison of myocardial ATP, blood flow, and cytosolic adenosine in demand ischemia and coronary occlusion". In: *Am J Physiol Heart Circ Physiol* 269.3 (1995), H819–H828. DOI: 10.1152/ajpheart.1995.269.3.H819.

[182] I Kubota, M Yamaki, T Shibata, et al. "Role of ATP-sensitive K+ channel on ECG ST segment elevation during a bout of myocardial ischemia. A study on epicardial mapping in dogs." In: *Circulation* 88.4 (1993), pp. 1845–1851. DOI: 10.1161/01.CIR.88.4.1845.

[183] Deborah H Kwon, Nicholas G Smedira, E Rene Rodriguez, et al. "Cardiac Magnetic Resonance Detection of Myocardial Scarring in Hypertrophic Cardiomyopathy: Correlation With

Histopathology and Prevalence of Ventricular Tachycardia". In: *J Am Coll Cardiol* 54.3 (2009), pp. 242–249. DOI: 10.1016/j.jacc.2009.04.026.

[184] Michael K Kyriakidis, John M Dernellis, Aristides E Androulakis, et al. "Changes in Phasic Coronary Blood Flow Velocity Profile and Relative Coronary Flow Reserve in Patients With Hypertrophic Obstructive Cardiomyopathy". In: *Circulation* 96.3 (1997), pp. 834–841. DOI: 10.1161/01.CIR.96.3.834.

[185] Fananapazir Lameh, Mohiddin Saidi A, and Shih Joanna. "Myocardial bridging of the left anterior descending coronary artery in children with hypertrophic cardiomyopathy: Reply". In: *J Am Coll Cardiol* 38.3 (2001), p. 922. DOI: 10.1016/S0735-1097(01)01462-0.

[186] Carl J Lavie, Jae K Oh, Harold T Mankin, et al. "Significance of T-Wave Pseudonormalization during Exercise: A Radionuclide Angiographic Study". In: *Chest* 94.3 (1988), pp. 512–516. DOI: 10.1378/chest.94.3.512.

[187] Ettore Lazzeroni, Eugenio Picano, Letizia Morozzi, et al. "Dipyridamole-Induced Ischemia as a Prognostic Marker of Future Adverse Cardiac Events in Adult Patients With Hypertrophic Cardiomyopathy". In: *Circulation* 96.12 (1997), pp. 4268–4272. DOI: 10.1161/01.CIR.96.12.4268.

[188] Philip J Leisy, Remy R Coeytaux, Galen S Wagner, et al. "ECG-based signal analysis technologies for evaluating patients with acute coronary syndrome: A systematic review". In: *J Electrocardiol* 46.2 (2013), pp. 92–97. DOI: 10.1016/j.jelectrocard.2012.11.010.

[189] Giuseppe Limongelli, Paolo Calabro', Giuseppe Pacileo, et al. "Myocardial infarction in a young athlete with non-obstructive hypertrophic cardiomyopathy and normal coronary arteries". In: *Int J Cardiol* 115.2 (2007), e71–e73. DOI: 10.1016/j.ijcard.2006.07.206.

[190] G Lin, R A Nishimura, B J Gersh, et al. "Device complications and inappropriate implantable cardioverter defibrillator shocks in patients with hypertrophic cardiomyopathy". In: *Heart* 95.9 (2009), p. 709. DOI: 10.1136/hrt.2008.150656.

[191] Fang Liu, Yue Ma, Hailong Ge, et al. "Long-Term Outcomes of Acute Myocardial Infarction in Patients With Hypertrophic Cardiomyopathy". In: *Angiology* 69.10 (2018), pp. 900–908. DOI: 10.1177/0003319718778418.

[192] Wen Liu, Dandan Sun, and Jun Yang. "Diastolic Dysfunction of Hypertrophic Cardiomyopathy Genotype-Positive Subjects Without Hypertrophy Is Detected by Tissue Doppler Imaging: A Systematic Review and Meta-analysis". In: *J Ultrasound Med* 36.10 (2017), pp. 2093–2103. DOI: 10.1002/jum.14250.

[193] Robert W Loar, J Martijn Bos, Melissa L Will, et al. "Genotype–phenotype Correlations of Hypertrophic Cardiomyopathy When Diagnosed in Children, Adolescents, and Young Adults". In: *Congenit Heart Dis* 10.6 (2015), pp. 529–536. DOI: 10.1111/chd.12280.

[194] Henry S Loeb and Nicholas C Friedman. "Normalization of abnormal T-waves during stress testing does not identify patients with reversible perfusion defects". In: *Clin Cardiol* 30.8 (2007), pp. 403–407. DOI: 10.1002/clc.20111.

[195] Massimiliano Lorenzini, Zacharias Anastasiou, Constantinos O'Mahony, et al. "Mortality Among Referral Patients With Hypertrophic Cardiomyopathy vs the General European Population". In: *JAMA Cardiol* 5.1 (2020), pp. 73–80. DOI: 10.1001/jamacardio.2019.4534.

[196] R Lorenzoni, R Gistri, F Cecchi, et al. "Syncope and ventricular arrhythmias in hypertrophic cardiomyopathy are not related to the derangement of coronary microvascular function". In: *Eur Heart J* 18.12 (1997), pp. 1946–1950. DOI: 10.1093/oxfordjournals.eurheartj.a015204.

[197] Roberto Lorenzoni, Roberto Gistri, Franco Cecchi, et al. "Coronary vasodilator reserve is impaired in patients with hypertrophic cardiomyopathy and left ventricular dysfunction". In: *Am Heart J* 136.6 (1998), pp. 972–981. DOI: 10.1016/S0002-8703(98)70152-8.

[198] Dai-Yin Lu, Hulya Yalçin, Fatih Yalçin, et al. "Stress Myocardial Blood Flow Heterogeneity Is a Positron Emission Tomography Biomarker of Ventricular Arrhythmias in Patients With Hypertrophic Cardiomyopathy". In: *Am J Cardiol* 121.9 (2018), pp. 1081–1089. DOI: 10.1016/j.amjcard.2018.01.022.

[199] Mark Luedde, Ulrich Flögel, Maike Knorr, et al. "Decreased contractility due to energy deprivation in a transgenic rat model of hypertrophic cardiomyopathy". In: *J Mol Med* 87.4 (2009), pp. 411–422. DOI: 10.1007/s00109-008-0436-x.

[200] Aurore Lyon, Rina Ariga, Ana Mincholé, et al. "Distinct ECG Phenotypes Identified in Hypertrophic Cardiomyopathy Using Machine Learning Associate With Arrhythmic Risk Markers". In: *Front Physiol* 9 (2018). DOI: 10.3389/fphys.2018.00213.

[201] Aurore Lyon, Alfonso Bueno-Orovio, Ernesto Zacur, et al. "Electrocardiogram phenotypes in hypertrophic cardiomyopathy caused by distinct mechanisms: apico-basal repolarization gradients vs. Purkinje-myocardial coupling abnormalities". In: *Europace* 20.suppl_3 (2018), pp. iii102–iii112. DOI: 10.1093/europace/euy226.

[202] Fei Ma, Yating Yang, Jingwen Tao, et al. "Twenty-four hour variability of inverted T-waves in patients with apical hypertrophic cardiomyopathy". In: *Front Cardiovasc Med* 9 (2022). DOI: 10.3389/fcvm.2022.1004178.

[203] Peter Magnusson, Jonny Nordström, Hendrik J Harms, et al. "Positron emission tomography (15O-water, 11C-acetate, 11C-HED) risk markers and nonsustained ventricular tachycardia in hypertrophic cardiomyopathy". In: *IJC Heart Vasc* 26 (2020), p. 100452. DOI: 10.1016/j.ijcha.2019.100452.

[204] Damiano Magrì, Giuseppe Limongelli, Federica Re, et al. "Cardiopulmonary exercise test and sudden cardiac death risk in hypertrophic cardiomyopathy". In: *Heart* 102.8 (2016), p. 602. DOI: 10.1136/heartjnl-2015-308453.

[205] Damiano Magrì, Caterina Santolamazza, Luca Limite, et al. "QT spatial dispersion and sudden cardiac death in hypertrophic cardiomyopathy: Time for reappraisal". In: *J Cardiol* 70.4 (2017), pp. 310–315. DOI: 10.1016/j.jjcc.2017.01.006.

[206] Masliza Mahmod, Jane M Francis, Nikhil Pal, et al. "Myocardial perfusion and oxygenation are impaired during stress in severe aortic stenosis and correlate with impaired energetics and subclinical left ventricular dysfunction". In: *J Cardiovasc Magn Reson* 16.1 (2014), p. 29. DOI: 10.1186/1532-429X-16-29.

[207] Aita Makoto, Takeuchi Toshiharu, Sakamoto Naka, et al. "Microcirculatory dysfunction determines the long-term prognosis in asymptomatic patients with non-obstructive hypertrophic cardiomyopathy". In: *J Am Coll Cardiol* 61.10_Supplement (2013), E1308–E1308. DOI: 10.1016/S0735-1097(13)61308-X.

[208] Maan Malahfji, Alpana Senapati, Dany Debs, et al. "Examining the impact of inducible ischemia on myocardial fibrosis and exercise capacity in hypertrophic cardiomyopathy". In: *Sci Rep* 10.1 (2020), p. 15977. DOI: 10.1038/s41598-020-71394-z.

[209] E Marban, M Kitakaze, Y Koretsune, et al. "Quantification of [Ca2+]i in perfused hearts. Critical evaluation of the 5F-BAPTA and nuclear magnetic resonance method as applied to the study of ischemia and reperfusion." In: *Circ Res* 66.5 (1990), pp. 1255–1267. DOI: 10.1161/01.RES.66.5.1255.

[210] Gregory M Marcus. "Evaluation and Management of Premature Ventricular Complexes". In: *Circulation* 141.17 (2020), pp. 1404–1418. DOI: 10.1161/CIRCULATIONAHA.119.042434.

[211] Ali J Marian and Eugene Braunwald. "Hypertrophic Cardiomyopathy". In: *Circ Res* 121.7 (2017), pp. 749–770. DOI: 10.1161/CIRCRESAHA.117.311059.

[212] Jairo J Marin, Ming K Heng, Roger Sevrin, et al. "Significance of T wave normalization in the electrocardiogram during exercise stress test". In: *Am Heart J* 114.6 (1987), pp. 1342–1348. DOI: 10.1016/0002-8703(87)90535-7.

[213] Barry J Maron. "Hypertrophic Cardiomyopathy". In: *Circulation* 106.19 (2002), pp. 2419–2421. DOI: 10.1161/01.CIR.0000034170.83171.0B.

[214] Barry J Maron, Joseph J Doerer, Tammy S Haas, et al. "Sudden Deaths in Young Competitive Athletes". In: *Circulation* 119.8 (2009), pp. 1085–1092. DOI: 10.1161/CIRCULATIONAHA.108.804617.

[215] Barry J Maron, Stephen E Epstein, and William C Roberts. "Hypertrophic cardiomyopathy and transmural myocardial infarction without significant atherosclerosis of the extramural coronary arteries". In: *Am J Cardiol* 43.6 (1979), pp. 1086–1102. DOI: 10.1016/0002-9149(79)90139-5.

[216] Barry J Maron, Mark J Leyhe, Susan A Casey, et al. "Assessment of QT dispersion as a prognostic marker for sudden death in a regional nonreferred hypertrophic cardiomyopathy cohort". In: *Am J Cardiol* 87.1 (2001), pp. 114–115. DOI: 10.1016/S0002-9149(00)01285-6.

[217] Barry J Maron, Shannon Mackey-Bojack, Emily Facile, et al. "Hypertrophic Cardiomyopathy and Sudden Death Initially Identified at Autopsy". In: *Am J Cardiol* 127 (2020), pp. 139–141. DOI: 10.1016/j.amjcard.2020.04.021.

[218] Barry J Maron, Martin S Maron, and Christopher Semsarian. "Genetics of Hypertrophic Cardiomyopathy After 20 Years: Clinical Perspectives". In: *J Am Coll Cardiol* 60.8 (2012), pp. 705–715. DOI: 10.1016/j.jacc.2012.02.068.

[219] Barry J Maron, Iacopo Olivotto, Paolo Spirito, et al. "Epidemiology of Hypertrophic Cardiomyopathy–Related Death". In: *Circulation* 102.8 (2000), pp. 858–864. DOI: 10.1161/01.CIR.102.8.858.

[220] Barry J Maron, James K Wolfson, Stephen E Epstein, et al. "Intramural ("small vessel") coronary artery disease in hypertrophic cardiomyopathy". In: *J Am Coll Cardiol* 8.3 (1986), pp. 545–557. DOI: 10.1016/S0735-1097(86)80181-4.

[221] Martin S Maron, Barry J Maron, Caitlin Harrigan, et al. "Hypertrophic Cardiomyopathy Phenotype Revisited After 50 Years With Cardiovascular Magnetic Resonance". In: *J Am Coll Cardiol* 54.3 (2009), pp. 220–228. DOI: 10.1016/j.jacc.2009.05.006.

[222] Martin S Maron, Iacopo Olivotto, Barry J Maron, et al. "The Case for Myocardial Ischemia in Hypertrophic Cardiomyopathy". In: *J Am Coll Cardiol* 54.9 (2009), pp. 866–875. DOI: 10.1016/j.jacc.2009.04.072.

[223] Martin S Maron, Iacopo Olivotto, Andrey G Zenovich, et al. "Hypertrophic Cardiomyopathy Is Predominantly a Disease of Left Ventricular Outflow Tract Obstruction". In: *Circulation* 114.21 (2006), pp. 2232–2239. DOI: 10.1161/CIRCULATIONAHA.106.644682.

[224] Martin S Maron, Ethan J Rowin, Benjamin S Wessler, et al. "Enhanced American College of Cardiology/American Heart Association Strategy for Prevention of Sudden Cardiac Death in High-Risk Patients With Hypertrophic Cardiomyopathy". In: *J Am Coll Cardiol* 4.7 (2019), pp. 644–657. DOI: 10.1001/jamacardio.2019.1391.

[225] Richard J Marszalek, R John Solaro, and Beata M Wolska. "Coronary arterial vasculature in the pathophysiology of hypertrophic cardiomyopathy". In: *Pflug Arch Eur J Physiol* 471.5 (2019), pp. 769–780. DOI: 10.1007/s00424-018-2224-y.

[226] J P Martinez, R Almeida, S Olmos, et al. "A wavelet-based ECG delineator: evaluation on standard databases". In: *IEEE Trans Biomed Eng* 51.4 (2004), pp. 570–581. DOI: 10.1109/TBME.2003.821031.

[227] Marine Martinez, Richard Walton, Jason Bayer, et al. "Role of the Purkinje-Muscle Junction on the Ventricular Repolarization Heterogeneity in the Healthy and Ischemic Ovine Ventricular Myocardium". In: *Front Physiol* 9 (2018). DOI: 10.3389/fphys.2018.00718.

[228] Hector Martinez-Navarro, Ana Mincholé, Alfonso Bueno-Orovio, et al. "High arrhythmic risk in antero-septal acute myocardial ischemia is explained by increased transmural reentry occurrence". In: *Sci Rep* 9.1 (2019), p. 16803. DOI: 10.1038/s41598-019-53221-2.

[229] Hector Martinez-Navarro, Xin Zhou, Alfonso Bueno-Orovio, et al. "Electrophysiological and anatomical factors determine arrhythmic risk in acute myocardial ischaemia and its modulation by sodium current availability". In: *Interface Focus* 11 (2020). DOI: 10.1098/rsfs.2019.0124.

[230] Attilio Maseri, Silva Severi, Maurizio de Nes, et al. ""Variant" angina: One aspect of a continuous spectrum of vasospastic myocardial ischemia: Pathogenetic Mechanisms, Estimated Incidence and Clinical and Coronary Arteriographic Findings in 138 Patients". In: *Am J Cardiol* 42.6 (1978), pp. 1019–1035. DOI: 10.1016/0002-9149(78)90691-4.

[231] Niccolò Maurizi, Chiara Chiriatti, Carlo Fumagalli, et al. "Real-World Use and Predictors of Response to Disopyramide in Patients with Obstructive Hypertrophic Cardiomyopathy". In: *J Clin Med* 12.7 (2023). DOI: 10.3390/jcm12072725.

[232] Niccolò Maurizi, Silvia Passantino, Gaia Spaziani, et al. "Long-term Outcomes of Pediatric-Onset Hypertrophic Cardiomyopathy and Age-Specific Risk Factors for Lethal Arrhythmic Events". In: *JAMA Cardiol* 3.6 (2018), pp. 520–525. DOI: 10.1001/jamacardio.2018.0789.

[233] Andrea Mazzanti, Riccardo Maragna, Alessandro Faragli, et al. "Gene-Specific Therapy With Mexiletine Reduces Arrhythmic Events in Patients With Long QT Syndrome Type 3". In: *J Am Coll Cardiol* 67.9 (2016), pp. 1053–1058. DOI: 10.1016/j.jacc.2015.12.033.

[234] B W McCrindle and A T Yetman. "Myocardial bridging of the left anterior descending coronary artery in children with hypertrophic cardiomyopathy". In: *J Am Coll Cardiol* 38.3 (2001), pp. 921–922. DOI: 10.1016/S0735-1097(01)01461-9.

[235] Paola Melacini, Francesco Corbetti, Chiara Calore, et al. "Cardiovascular magnetic resonance signs of ischemia in hypertrophic cardiomyopathy". In: *Int J Cardiol* 128.3 (2008), pp. 364–373. DOI: 10.1016/j.ijcard.2007.06.023.

[236] Alexey Melkikh and Maria Sutormina. "Model of active transport of ions in cardiac cell". In: *J Theor Biol* 252 (2008), pp. 247–254. DOI: 10.1016/j.jtbi.2008.02.006.

[237] Elena Mershina, Olga Blagova, Valentin Sinitsyn, et al. "A case of hypertrophic cardiomyopathy with "burned-out" apex of the left ventricle due to mid-ventricular obstruction". In: *Clin Case Rep* 2 (2016). DOI: 10.15761/CCRR.1000S2002.

[238] Anushka Michailova, Jeffrey Saucerman, Mary Belik, et al. "Modeling regulation of cardiac KATP and L-type Ca2+ currents by ATP, ADP, and Mg2+". In: *Biophys J* 88 (2005), pp. 2234–2249. DOI: 10.1529/biophysj.104.046284.

[239] Manuela Miorelli, Gianfranco Buja, Paola Melacini, et al. "QT-interval variability in hypertrophic cardiomyopathy patients with cardiac arrest". In: *Int J Cardiol* 45.2 (1994), pp. 121–127. DOI: 10.1016/0167-5273(94)90267-4.

[240] Sergey Mironov, José Jalife, and Elena G Tolkacheva. "Role of Conduction Velocity Restitution and Short-Term Memory in the Development of Action Potential Duration Alternans in Isolated Rabbit Hearts". In: *Circulation* 118.1 (2008), pp. 17–25. DOI: 10.1161/CIRCULATIONAHA.107.737254.

[241] S Mishra, A Mishra, and JP Mishra. "Pseudo-normalization of t-waves: review & update". In: *Blood Heart Circ* 2 (2018). DOI: 10.15761/BHC.1000128.

[242] Marjeta Misigoj-Durakovic, Zijad Durakovic, and Ivan Prskalo. "Heart Rate-Corrected QT and JT Intervals in Electrocardiograms in Physically Fit Students and Student Athletes". In: *Ann Noninvasive Electrocardiol* 21 (2016). DOI: 10.1111/anec.12374.

[243] Shunichiro Miyoshi, Toshthisa Miyazakt, Mika Asanagi, et al. "Differential Role of Epicardial and Endocardial KATP Channels in Potassium Accumulation During Regional Ischemia Induced by Embolization of a Coronary Artery with Latex". In: *J Cardiovasc Electrophysiol* 9.3 (1998), pp. 292–298. DOI: 10.1111/j.1540-8167.1998.tb00914.x.

[244] Saidi A Mohiddin, David Begley, Joanna Shih, et al. "Myocardial bridging does not predict sudden death in children with hypertrophic cardiomyopathy but is associated with more severe cardiac disease". In: *J Am Coll Cardiol* 36.7 (2000), pp. 2270–2278. DOI: 10.1016/S0735-1097(00)00987-6.

[245] Jeonggeun Moon, In Jeong Cho, Chi Young Shim, et al. "Abnormal Myocardial Capillary Density in Apical Hypertrophic Cardiomyopathy Can Be Assessed by Myocardial Contrast

Echocardiography". In: *Circulation* 74.10 (2010), pp. 2166–2172. DOI: 10.1253/circj.CJ-10-0241.

[246] Gil Moravsky, Efrat Ofek, Harry Rakowski, et al. "Myocardial Fibrosis in Hypertrophic Cardiomyopathy: Accurate Reflection of Histopathological Findings by CMR". In: *JACC Cardiovasc Imaging* 6.5 (2013), pp. 587–596. DOI: 10.1016/j.jcmg.2012.09.018.

[247] H Moréna, M J Janse, J W Fiolet, et al. "Comparison of the effects of regional ischemia, hypoxia, hyperkalemia, and acidosis on intracellular and extracellular potentials and metabolism in the isolated porcine heart." In: *Circ Res* 46.5 (1980), pp. 634–646. DOI: 10.1161/01.RES.46.5.634.

[248] Jonathan D Moreno, Pei-Chi Yang, John R Bankston, et al. "Ranolazine for Congenital and Acquired Late INa-Linked Arrhythmias". In: *Circ Res* 113.7 (2013), e50–e61. DOI: 10.1161/CIRCRESAHA.113.301971.

[249] David A Morrow, Benjamin M Scirica, Ewa Karwatowska-Prokopczuk, et al. "Effects of Ranolazine on Recurrent Cardiovascular Events in Patients With Non–ST-Elevation Acute Coronary SyndromesThe MERLIN-TIMI 36 Randomized Trial". In: *JAMA* 297.16 (2007), pp. 1775–1783. DOI: 10.1001/jama.297.16.1775.

[250] A J Moss, W Zareba, K Q Schwarz, et al. "Ranolazine Shortens Repolarization in Patients with Sustained Inward Sodium Current Due to Type-3 Long-QT Syndrome". In: *J Cardiovasc Electrophysiol* 19.12 (2008), pp. 1289–1293. DOI: 10.1111/j.1540-8167.2008.01246.x.

[251] David K Murdock, Jeff Kaliebe, and Naomi Overton. "Ranolozine-Induced Suppression of Ventricular Tachycardia in a Patient with Nonischemic Cardiomyopathy: A Case Report". In: *Pacing Clin Electrophysiol* 31.6 (2008), pp. 765–768. DOI: 10.1111/j.1540-8159.2008.01083.x.

[252] Beatrice Musumeci, Giacomo Tini, Domitilla Russo, et al. "Left Ventricular Remodeling in Hypertrophic Cardiomyopathy: An Overview of Current Knowledge". In: *J Clin Med* 10 (2021), p. 1547. DOI: 10.3390/jcm10081547.

[253] Anna Muszkiewicz, Oliver J Britton, Philip Gemmell, et al. "Variability in cardiac electrophysiology: Using experimentally-calibrated populations of models to move beyond the single virtual physiological human paradigm". In: *Prog Biophys Mol Biol* 120.1 (2016), pp. 115–127. DOI: 10.1016/j.pbiomolbio.2015.12.002.

[254] Victor Nauffal, Peter Marstrand, Larry Han, et al. "Worldwide differences in primary prevention implantable cardioverter defibrillator utilization and outcomes in hypertrophic cardiomyopathy". In: *Eur Heart J* 42.38 (2021), pp. 3932–3944. DOI: 10.1093/eurheartj/ehab598.

[255] M E Nelson. *Databasing the Brain: From Data to Knowledge*. New York: Wiley, 2004.

[256] Louise L A M Nijenkamp, Ilse A E Bollen, Hans W M Niessen, et al. "Sex-specific cardiac remodeling in early and advanced stages of hypertrophic cardiomyopathy". In: *PLoS One* 15.5 (2020), e0232427. DOI: 10.1371/journal.pone.0232427.

[257] T Nishimura, S Nagata, T Uehara, et al. "Prognosis of hypertrophic cardiomyopathy: assessment by 123I-BMIPP (beta-methyl-p-(123I)iodophenyl pentadecanoic acid) myocardial single photon emission computed tomography". In: *Ann Nucl Med* 10.1 (1996), pp. 71–78. DOI: 10.1007/bf03165056.

[258] D Noble. "A modification of the Hodgkin-Huxley equations applicable to Purkinje fibre action and pacemaker potentials". In: *J Physiol* 160.2 (1962), pp. 317–352. DOI: 10.1113/jphysiol.1962.sp006849.

[259] D Noble. "Cardiac Action and Pacemaker Potentials based on the Hodgkin-Huxley Equations". In: *Nature* 188.4749 (1960), pp. 495–497. DOI: 10.1038/188495b0.

[260] G Norrish, T Ding, E Field, et al. "The relationship between left ventricular outflow tract gradient and sudden cardiac death in childhood hypertrophic cardiomyopathy". In: *Eur Heart J* 41.Supplement_2 (2020), ehaa946.0732. DOI: 10.1093/ehjci/ehaa946.0732.

[261] Gabrielle Norrish, Chen Qu, Ella Field, et al. "External validation of the HCM Risk-Kids model for predicting sudden cardiac death in childhood hypertrophic cardiomyopathy". In: *Eur J Prev Cardiol* 29.4 (2022), pp. 678–686. DOI: 10.1093/eurjpc/zwab181.

[262] Gabrielle Norrish, Cristian Topriceanu, Chen Qu, et al. "The role of the electrocardiographic phenotype in risk stratification for sudden cardiac death in childhood hypertrophic cardiomyopathy". In: *Eur J Prev Cardiol* 29.4 (2022), pp. 645–653. DOI: 10.1093/eurjpc/zwab046.

[263] Npatchett. *File:Hypertrophic obstructive cardiomyopathy.png*. URL: https://commons.wikimedia.org/wiki/File:Hypertrophic_obstructive_cardiomyopathy.png.

[264] P T O'Gara, R O Bonow, B J Maron, et al. "Myocardial perfusion abnormalities in patients with hypertrophic cardiomyopathy: assessment with thallium-201 emission computed tomography." In: *Circulation* 76.6 (1987), pp. 1214–1223. DOI: 10.1161/01.CIR.76.6.1214.

[265] Thomas O'Hara, László Virág, András Varró, et al. "Simulation of the Undiseased Human Cardiac Ventricular Action Potential: Model Formulation and Experimental Validation". In: *PLoS Comput Biol* 7.5 (2011), e1002061–. DOI: 10.1371/journal.pcbi.1002061.

[266] Constantinos O'Mahony, Fatima Jichi, Menelaos Pavlou, et al. "A novel clinical risk prediction model for sudden cardiac death in hypertrophic cardiomyopathy (HCM Risk-SCD)". In: *Eur Heart J* 35.30 (2014), pp. 2010–2020. DOI: 10.1093/eurheartj/eht439.

[267] Constantinos O'Mahony, Pier D Lambiase, Shafiqur M Rahman, et al. "The relation of ventricular arrhythmia electrophysiological characteristics to cardiac phenotype and circadian patterns in hypertrophic cardiomyopathy". In: *EP Europace* 14.5 (2012), pp. 724–733. DOI: 10.1093/europace/eur362.

[268] Constantinos O'Mahony, Perry Elliott, and William McKenna. "Sudden Cardiac Death in Hypertrophic Cardiomyopathy". In: *Circ Arrhythm Electrophysiol* 6.2 (2013), pp. 443–451. DOI: 10.1161/CIRCEP.111.962043.

[269] Christopher O'Shea, Davor Pavlovic, Kashif Rajpoot, et al. "Examination of the Effects of Conduction Slowing on the Upstroke of Optically Recorded Action Potentials". In: *Front Physiol* 10 (2019). DOI: 10.3389/fphys.2019.01295.

[270] Iacopo Olivotto, Paolo G Camici, Piera Angelica Merlini, et al. "Efficacy of Ranolazine in Patients With Symptomatic Hypertrophic Cardiomyopathy". In: *Circ Heart Fail* 11.1 (2018), e004124. DOI: 10.1161/CIRCHEARTFAILURE.117.004124.

[271] Iacopo Olivotto, Franco Cecchi, Roberta Bini, et al. "Tunneled left anterior descending artery in a child with hypertrophic cardiomyopathy". In: *Nat Clin Pract Cardiovasc Med* 6.2 (2009), pp. 134–139. DOI: 10.1038/ncpcardio1420.

[272] Iacopo Olivotto, Franco Cecchi, Roberto Gistri, et al. "Relevance of Coronary Microvascular Flow Impairment to Long-Term Remodeling and Systolic Dysfunction in Hypertrophic Cardiomyopathy". In: *J Am Coll Cardiol* 47.5 (2006), pp. 1043–1048. DOI: 10.1016/j.jacc.2005.10.050.

[273] Iacopo Olivotto, Franco Cecchi, Corrado Poggesi, et al. "Developmental origins of hypertrophic cardiomyopathy phenotypes: a unifying hypothesis". In: *Nat Rev Cardiol* 6.4 (2009), pp. 317–321. DOI: 10.1038/nrcardio.2009.9.

[274] Steve R Ommen, Seema Mital, Michael A Burke, et al. "2020 AHA/ACC Guideline for the Diagnosis and Treatment of Patients With Hypertrophic Cardiomyopathy". In: *Circulation* 142.25 (2020), e558–e631. DOI: 10.1161/CIR.0000000000000937.

[275] Ingegerd Östman-Smith, Aase Wisten, Eva Nylander, et al. "Electrocardiographic amplitudes: a new risk factor for sudden death in hypertrophic cardiomyopathy". In: *Eur Heart J* 31.4 (2010), pp. 439–449. DOI: 10.1093/eurheartj/ehp443.

[276] Chiara Palandri, Lorenzo Santini, Alessia Argirò, et al. "Pharmacological Management of Hypertrophic Cardiomyopathy: From Bench to Bedside". In: *Drugs* 82.8 (2022), pp. 889–912. DOI: 10.1007/s40265-022-01728-w.

[277] Clement Papadacci, Victor Finel, Jean Provost, et al. "Imaging the dynamics of cardiac fiber orientation in vivo using 3D Ultrasound Backscatter Tensor Imaging". In: *Sci Rep* 7.1 (2017), p. 830. DOI: 10.1038/s41598-017-00946-7.

[278] Despoina Parcharidou, Thomas Zegkos, Dimitris Ntelios, et al. "The natural history of hypertrophic cardiomyopathy in a large Mediterranean cohort". In: *J Cardiovasc Med* 21.6 (2020). DOI: 10.2459/JCM.0000000000000945.

[279] Chul Hwan Park, Hyemoon Chung, Yoonjung Kim, et al. "Electrocardiography based prediction of hypertrophy pattern and fibrosis amount in hypertrophic cardiomyopathy: comparative study with cardiac magnetic resonance imaging". In: *Int J Cardiovasc Imaging* 34.10 (2018), pp. 1619–1628. DOI: 10.1007/s10554-018-1365-6.

[280] Young Jun Park, Seung-Jung Park, Eun-Kyung Kim, et al. "Semi-quantitative versus quantitative assessments of late gadolinium enhancement extent for predicting spontaneous ventricular tachyarrhythmia events in patients with hypertrophic cardiomyopathy". In: *Sci Rep* 10.1 (2020), p. 2920. DOI: 10.1038/s41598-020-59804-8.

[281] Elisa Passini, Oliver J Britton, Hua Rong Lu, et al. "Human In Silico Drug Trials Demonstrate Higher Accuracy than Animal Models in Predicting Clinical Pro-Arrhythmic Cardiotoxicity". In: *Front Physiol* 8 (2017). DOI: 10.3389/fphys.2017.00668.

[282] Elisa Passini, Ana Mincholé, Raffaele Coppini, et al. "Mechanisms of pro-arrhythmic abnormalities in ventricular repolarisation and anti-arrhythmic therapies in human hypertrophic cardiomyopathy". In: *J Mol Cell Cardiol* 96 (2016), pp. 72–81. DOI: 10.1016/j.yjmcc.2015.09.003.

[283] Parag Patel, Ashwat Dhillon, Zoran B Popovic, et al. "Left Ventricular Outflow Tract Obstruction in Hypertrophic Cardiomyopathy Patients Without Severe Septal Hypertrophy". In: *Circ Cardiovasc Imaging* 8.7 (2015), e003132. DOI: 10.1161/CIRCIMAGING.115.003132.

[284] Antonio Pelliccia, Douglas P Zipes, and Barry J Maron. "Bethesda Conference #36 and the European Society of Cardiology Consensus Recommendations Revisited: A Comparison of U.S. and European Criteria for Eligibility and Disqualification of Competitive Athletes With Cardiovascular Abnormalities". In: *J Am Coll Cardiol* 52.24 (2008), pp. 1990–1996. DOI: 10.1016/j.jacc.2008.08.055.

[285] Francesco Pelliccia, Giuseppe Campolongo, Rosalba Massaro, et al. "Ranolazine reduces symptoms of palpitations and documented arrhythmias in patients with ischemic heart disease — The RYPPLE randomized cross-over trial". In: *IJC Metabolic & Endocrine* 7 (2015), p. 8. DOI: 10.1016/j.ijcme.2015.05.016.

[286] Francesco Pelliccia, Bernard J Gersh, and Paolo G Camici. "Gaps in Evidence for Risk Stratification for Sudden Cardiac Death in Hypertrophic Cardiomyopathy". In: *Circulation* 143.2 (2021), pp. 101–103. DOI: 10.1161/CIRCULATIONAHA.120.051968.

[287] Jesús Peteiro, Alberto Bouzas-Mosquera, Xusto Fernandez, et al. "Prognostic Value of Exercise Echocardiography in Patients with Hypertrophic Cardiomyopathy". In: *J Am Soc Echocardiogr* 25.2 (2012), pp. 182–189. DOI: 10.1016/j.echo.2011.11.005.

[288] Jesús Peteiro, Xusto Fernandez, Alberto Bouzas-Mosquera, et al. "Exercise echocardiography and cardiac magnetic resonance imaging to predict outcome in patients with hypertrophic cardiomyopathy". In: *Eur Heart J Cardiovasc Imaging* 16.4 (2015), pp. 423–432. DOI: 10.1093/ehjci/jeu225.

[289] Bradley J Petek, Timothy W Churchill, Nathaniel Moulson, et al. "Sudden Cardiac Death in National Collegiate Athletic Association Athletes: A 20-Year Study". In: *Circulation* 149.2 (2024), pp. 80–90. DOI: 10.1161/CIRCULATIONAHA.123.065908.

[290] Steffen E Petersen, Michael Jerosch-Herold, Lucy E Hudsmith, et al. "Evidence for Microvascular Dysfunction in Hypertrophic Cardiomyopathy". In: *Circulation* 115.18 (2007), pp. 2418–2425. DOI: 10.1161/CIRCULATIONAHA.106.657023.

[291] Gunnar Plehn, Julia Vormbrock, Axel Meissner, et al. "Effects of exercise on the duration of diastole and on interventricular phase differences in patients with hypertrophic cardiomyopathy: relationship to cardiac output reserve". In: *J Nucl Cardiol* 16.2 (2009), pp. 233–243. DOI: 10.1007/s12350-008-9031-3.

[292] Aron F Popov, Christian Bireta, Jan D Schmitto, et al. "Myocardial ischemia with left ventricular outflow obstruction". In: *J Cardiothorac Surg* 4.1 (2009), p. 51. DOI: 10.1186/1749-8090-4-51.

[293] N G Poteshkina, E A Kovalevskaya, N S Krylova, et al. "Myocardial ischemia in patients with hypertrophic cardiomyopathy". In: *Probl Sotsialnoi Gig Zdravookhranenniiai Istor Med* 27 (2020), pp. 671–676. DOI: 10.32687/0869-866X-2019-27-si1-671-676.

[294] M Potse, B Dube, J Richer, et al. "A Comparison of Monodomain and Bidomain Reaction-Diffusion Models for Action Potential Propagation in the Human Heart". In: *IEEE Trans Biomed Eng* 53.12 (2006), pp. 2425–2435. DOI: 10.1109/TBME.2006.880875.

[295] Tuija Poutanen, Tero Tikanoja, Pertti Jääskeläinen, et al. "Diastolic dysfunction without left ventricular hypertrophy is an early finding in children with hypertrophic cardiomyopathy–causing mutations in the β-myosin heavy chain, α-tropomyosin, and myosin-binding protein C genes". In: *Am Heart J* 151.3 (2006), pp. 1–725. DOI: 10.1016/j.ahj.2005.12.005.

[296] Silvia G Priori, Arthur A Wilde, Minoru Horie, et al. "HRS/EHRA/APHRS Expert Consensus Statement on the Diagnosis and Management of Patients with Inherited Primary Arrhythmia Syndromes: Document endorsed by HRS, EHRA, and APHRS in May 2013 and by ACCF, AHA, PACES, and AEPC in June 2013." In: *Heart Rhythm* 10.12 (2013), pp. 1932–1963. DOI: 10.1016/j.hrthm.2013.05.014.

[297] Zhilin Qu. "Critical mass hypothesis revisited: Role of dynamical wave stability in spontaneous termination of cardiac fibrillation". In: *Am J Physiol Heart Circ Physiol* 290 (2006), pp. 255–63. DOI: 10.1152/ajpheart.00668.2005.

[298] Giovanni Quarta, Attilio Iacovoni, Chiara Marrone, et al. "Microvascular ischaemia after cardiac arrest in a patient with hypertrophic cardiomyopathy". In: *Glob Cardiol Sci Pract* 2015.4 (2015), p. 51. DOI: 10.5339/gcsp.2015.51.

[299] Betty Raman, Rina Ariga, Marco Spartera, et al. "Progression of myocardial fibrosis in hypertrophic cardiomyopathy: mechanisms and clinical implications". In: *Eur Heart J Cardiovasc Imaging* 20.2 (2019), pp. 157–167. DOI: 10.1093/ehjci/jey135.

[300] Betty Raman, Elizabeth M Tunnicliffe, Kenneth Chan, et al. "Association Between Sarcomeric Variants in Hypertrophic Cardiomyopathy and Myocardial Oxygenation: Insights From a Novel Oxygen-Sensitive Cardiovascular Magnetic Resonance Approach". In: *Circulation* 144.20 (2021), pp. 1656–1658. DOI: 10.1161/CIRCULATIONAHA.121.054015.

[301] Charu Ramanathan, Ping Jia, Raja Ghanem, et al. "Activation and repolarization of the normal heart under complete physiological conditions". In: *Proc Natl Acad Sci U S A* 103 (2006), pp. 6309–6314. DOI: 10.1073/pnas.0601533103.

[302] Kishin Ramani, W.David Lust, Tim S Whittingham, et al. "ATP catabolism and adenosine generation during ischemia in the aging heart". In: *Mech Ageing Dev* 89.2 (1996), pp. 113–124. DOI: 10.1016/0047-6374(96)01732-0.

[303] Anupam Rao, Austin Chin Chwan Ng, Raymond Sy, et al. "Electrocardiographic QRS duration is influenced by body mass index and sex". In: *Int J Cardiol Heart Vasc* 37 (2021), p. 100884. DOI: 10.1016/j.ijcha.2021.100884.

[304] Claire E Raphael, Robert Cooper, Kim H Parker, et al. "Mechanisms of Myocardial Ischemia in Hypertrophic Cardiomyopathy: Insights From Wave Intensity Analysis and Magnetic Resonance". In: *J Am Coll Cardiol* 68.15 (2016), pp. 1651–1660. DOI: 10.1016/j.jacc.2016.07.751.

[305] Claire E Raphael, Frances Mitchell, Gajen Sunthar Kanaganayagam, et al. "Cardiovascular magnetic resonance predictors of heart failure in hypertrophic cardiomyopathy: the role of myocardial replacement fibrosis and the microcirculation". In: *J Cardiovasc Magn Reson* 23.1 (2021), p. 26. DOI: 10.1186/s12968-021-00720-9.

[306] Ciprian Rezuș, Victor Moga, Anca Ouatu, et al. "QT interval variations and mortality risk: Is there any relationship?" In: *Anatol J Cardiol* 15 (2015). DOI: 10.5152/akd.2015.5875.

[307] Ellis Rochelson, Lynn Nappo, and Robert H Pass. "Hypertrophic cardiomyopathy: Ischemia progressing to ventricular fibrillation". In: *Hear Case Rep* 4.9 (2018), pp. 386–388. DOI: 10.1016/j.hrcr.2018.03.004.

[308] Tiago Rodrigues, Sofia Cavaco Raposo, Dulce Brito, et al. "Prognostic relevance of exercise testing in hypertrophic cardiomyopathy. A systematic review". In: *Int J Cardiol* 339 (2021), pp. 83–92. DOI: 10.1016/j.ijcard.2021.06.051.

[309] Blanca Rodríguez, Natalia Trayanova, and Denis Noble. "Modeling cardiac ischemia". In: *Annals of the New York Academy of Sciences* 1080 (2006), pp. 395–414. DOI: 10.1196/annals.1380.029.

[310] Stephan Rohr. "Role of gap junctions in the propagation of the cardiac action potential". In: *Cardiovasc Res* 62.2 (2004), pp. 309–322. DOI: 10.1016/j.cardiores.2003.11.035.

[311] Guillermo Romero-Farina, Jaume Candell-Riera, Enrique Galve, et al. "Do myocardial perfusion SPECT and radionuclide angiography studies in adult patients with hypertrophic cardiomyopathy have prognostic implications?" In: *J Nucl Cardiol* 11 (2004), pp. 578–586. DOI: 10.1016/j.nuclcard.2004.05.008.

[312] Andrea Rossi, Alberto Giannoni, Martina Nesti, et al. "Prognostic value of right ventricular refractory period heterogeneity in Type-1 Brugada electrocardiographic pattern". In: *EP Europace* 25.2 (2023), pp. 651–659. DOI: 10.1093/europace/euac168.

[313] Aigars Rubulis, Jens Jensen, Gunilla Lundahl, et al. "Ischemia induces aggravation of baseline repolarization abnormalities in left ventricular hypertrophy: a deleterious interaction". In: *J Appl Physiol* 101.1 (2006), pp. 102–110. DOI: 10.1152/japplphysiol.01334.2005.

[314] Rafael Sachetto, Sergio Alonso, and Rodrigo Weber dos Santos. "Killing Many Birds With Two Stones: Hypoxia and Fibrosis Can Generate Ectopic Beats in a Human Ventricular Model". In: *Front Physiol* 9 (2018). DOI: 10.3389/fphys.2018.00764.

[315] Rafael Sachetto Oliveira, Bernardo Martins Rocha, Denise Burgarelli, et al. "Performance evaluation of GPU parallelization, space-time adaptive algorithms, and their combination for simulating cardiac electrophysiology". In: *Int J Numer Methods Biomed Eng* 34.2 (2018), e2913. DOI: 10.1002/cnm.2913.

[316] J E Saffitz, H L Kanter, K G Green, et al. "Tissue-specific determinants of anisotropic conduction velocity in canine atrial and ventricular myocardium." In: *Circ Res* 74.6 (1994), pp. 1065–1070. DOI: 10.1161/01.RES.74.6.1065.

[317] P Sahu, P O Lim, B S Rana, et al. "QT dispersion in medicine: electrophysiological Holy Grail or fool's gold?" In: *QJM* 93.7 (2000), pp. 425–431. DOI: 10.1093/qjmed/93.7.425.

[318] S Said. "Unroofing of LAD Myocardial Bridge Combined With Right Ventricular Septal Myectomy in a Child With Noonan Syndrome and HCM". In: *World J Pediatr Congenit Heart Surg.* 12 (2020), pp. 659–660. DOI: 10.1177/2150135120943869.

[319] K Sakata, M Shimizu, H Ino, et al. "QT dispersion and left ventricular morphology in patients with hypertrophic cardiomyopathy". In: *Heart* 89.8 (2003), p. 882. DOI: 10.1136/heart.89.8.882.

[320] Arend F L Schinkel, Pieter A Vriesendorp, Eric J G Sijbrands, et al. "Outcome and Complications After Implantable Cardioverter Defibrillator Therapy in Hypertrophic Cardiomyopathy". In: *Circ Heart Fail* 5.5 (2012), pp. 552–559. DOI: 10.1161/CIRCHEARTFAILURE.112.969626.

[321] Frédéric Schnell, Nathan Riding, Rory O'Hanlon, et al. "Recognition and Significance of Pathological T-Wave Inversions in Athletes". In: *Circulation* 131.2 (2015), pp. 165–173. DOI: 10.1161/CIRCULATIONAHA.114.011038.

[322] Bodo Schwartzkopff, Markus Mundhenke, and Bodo E Strauer. "Alterations of the Architecture of Subendocardial Arterioles in Patients With Hypertrophic Cardiomyopathy and Impaired Coronary Vasodilator Reserve: A Possible Cause for Myocardial Ischemia". In: *J Am Coll Cardiol* 31.5 (1998), pp. 1089–1096. DOI: 10.1016/S0735-1097(98)00036-9.

[323] Roberto Sciagrà, Barbara Sotgia, Iacopo Olivotto, et al. "Relationship between atrial fibrillation and blunted hyperemic myocardial blood flow in patients with hypertrophic cardiomyopathy". In: *J Nucl Cardiol* 16.1 (2009), pp. 92–96. DOI: 10.1007/s12350-008-9005-5.

[324] Benjamin M Scirica, David A Morrow, Hanoch Hod, et al. "Effect of Ranolazine, an Antianginal Agent With Novel Electrophysiological Properties, on the Incidence of Arrhythmias in Patients With Non–ST-Segment–Elevation Acute Coronary Syndrome". In: *Circulation* 116.15 (2007), pp. 1647–1652. DOI: 10.1161/CIRCULATIONAHA.107.724880.

[325] Simon Sedej and Burkert Pieske. "Mechanisms of Ca2+-Triggered Arrhythmias". In: *Tachycardia*. Ed. by Takumi Yamada. Rijeka: IntechOpen, 2012, Ch. 8. DOI: 10.5772/25906.

[326] A Seitz, S Greulich, D Herter, et al. "Long-term risk of sudden cardiac death in hypertrophic cardiomyopathy - a cardiac magnetic resonance outcome study". In: *Eur Heart J Cardiovasc Imaging* 22.Supplement_1 (2021). DOI: 10.1093/ehjci/jeaa356.327.

[327] Stephanie L Sellers, Tim A Fonte, Rominder Grover, et al. "Hypertrophic Cardiomyopathy (HCM): New insights into Coronary artery remodelling and ischemia from FFRCT". In: *J Cardiovasc Comput Tomogr* 12.6 (2018), pp. 467–471. DOI: 10.1016/j.jcct.2018.08.002.

[328] Christopher Semsarian, Jodie Ingles, Martin S Maron, et al. "New Perspectives on the Prevalence of Hypertrophic Cardiomyopathy". In: *J Am Coll Cardiol* 65.12 (2015), pp. 1249–1254. DOI: 10.1016/j.jacc.2015.01.019.

[329] Vasco Sequeira, Edoardo Bertero, and Christoph Maack. "Energetic drain driving hypertrophic cardiomyopathy". In: *FEBS Lett* 593.13 (2019), pp. 1616–1626. DOI: 10.1002/1873-3468.13496.

[330] Nicholas J Severs. "Gap junction remodeling and cardiac arrhythmogenesis: cause or coincidence?" In: *J Cell Mol Med* 5.4 (2001), pp. 355–366. DOI: 10.1111/j.1582-4934.2001.tb00170.x.

[331] J S Shah, M T T Esteban, R Thaman, et al. "Prevalence of exercise-induced left ventricular outflow tract obstruction in symptomatic patients with non-obstructive hypertrophic cardiomyopathy". In: *Heart* 94.10 (2008), p. 1288. DOI: 10.1136/hrt.2007.126003.

[332] Masoud Shariat, Paaladinesh Thavendiranathan, Elsie Nguyen, et al. "Utility of coronary CT angiography in outpatients with hypertrophic cardiomyopathy presenting with angina symptoms". In: *J Cardiovasc Comput Tomogr* 8.6 (2014), pp. 429–437. DOI: 10.1016/j.jcct.2014.09.007.

[333] R Shaw and Y Rudy. "Electrophysiological changes of ventricular tissue under ischemic conditions: a simulation study". In: *Comput Cardiol*. 1994, pp. 641–644. DOI: 10.1109/CIC.1994.470110.

[334] Robin M Shaw and Yoram Rudy. "Electrophysiologic Effects of Acute Myocardial Ischemia". In: *Circ Res* 80.1 (1997), pp. 124–138. DOI: 10.1161/01.RES.80.1.124.

[335] Yasuyuki Shimada and Metin Avkiran. "Susceptibility to Ischemia and Reperfusion Arrhythmias in Myocardial Hypertrophy". In: *Jpn Heart J* 44.6 (2003), pp. 989–1004. DOI: 10.1536/jhj.44.989.

[336] Masami Shimizu, Hiroyuki Yoshio, Hidekazu Ino, et al. "Myocardial scintigraphic study with 123I 15-(p-iodophenyl)-3(R,S)-methylpentadecanoic acid in patients with hypertrophic cardiomyopathy". In: *Int J Cardiol* 54.1 (1996), pp. 51–59. DOI: 10.1016/0167-5273(95)02536-7.

[337] A A Shiozaki, T Senra, E Arteaga, et al. "Myocardial fibrosis in patients with hypertrophic cardiomyopathy and high risk for sudden death". In: *Arq Bras Cardiol* 94.4 (2010), pp. 535–540. DOI: 10.1590/s0066-782x2010005000017.

[338] Anna Simon, J Robins, T E H Hooghoudt, et al. "Pseudonormalisation of the T wave: old wine?" In: *Neth Heart J* 15 (2007), pp. 257–259. DOI: 10.1007/BF03085994.

[339] William T Smith, William F Fleet, Timothy A Johnson, et al. "The Ib Phase of Ventricular Arrhythmias in Ischemic In Situ Porcine Heart Is Related to Changes in Cell-to-Cell Electrical Coupling". In: *Circulation* 92.10 (1995), pp. 3051–3060. DOI: 10.1161/01.CIR.92.10.3051.

[340] Osama I I Soliman, Paul Knaapen, Marcel L Geleijnse, et al. "Assessment of intravascular and extravascular mechanisms of myocardial perfusion abnormalities in obstructive hypertrophic cardiomyopathy by myocardial contrast echocardiography". In: *Heart* 93.10 (2007), pp. 1204–1212. DOI: 10.1136/hrt.2006.110460.

[341] Paul Sorajja, Steve R Ommen, Rick A Nishimura, et al. "Adverse Prognosis of Patients With Hypertrophic Cardiomyopathy Who Have Epicardial Coronary Artery Disease". In: *Circulation* 108.19 (2003), pp. 2342–2348. DOI: 10.1161/01.CIR.0000097110.55312.BF.

[342] Paul Sorajja, Steve R Ommen, Rick A Nishimura, et al. "Myocardial bridging in adult patients with hypertrophic cardiomyopathy". In: *J Am Coll Cardiol* 42.5 (2003), pp. 889–894. DOI: 10.1016/S0735-1097(03)00854-4.

[343] Barbara Sotgia, Roberto Sciagrà, Iacopo Olivotto, et al. "Spatial Relationship Between Coronary Microvascular Dysfunction and Delayed Contrast Enhancement in Patients with Hypertrophic Cardiomyopathy". In: *J Nucl Med* 49.7 (2008), p. 1090. DOI: 10.2967/jnumed.107.050138.

[344] Daniel D Streeter, Henry M Spotnitz, Dali P Patel, et al. "Fiber Orientation in the Canine Left Ventricle during Diastole and Systole". In: *Circ Res* 24.3 (1969), pp. 339–347. DOI: 10.1161/01.RES.24.3.339.

[345] P M I Sutton, P Taggart, T Opthof, et al. "Repolarisation and refractoriness during early ischaemia in humans". In: *Heart* 84.4 (2000), p. 365. DOI: 10.1136/heart.84.4.365.

[346] Darrell J Swenson, Robert T Taepke, Josh J E Blauer, et al. "Direct comparison of a novel antitachycardia pacing algorithm against present methods using virtual patient modeling". In: *Heart Rhythm* 17.9 (2020), pp. 1602–1608. DOI: 10.1016/j.hrthm.2020.05.009.

[347] Norbert Szentadrassy, Tamas Banyasz, Tamas Biro, et al. "Apico–basal inhomogeneity in distribution of ion channels in canine and human ventricular myocardium". In: *Cardiovasc Res* 65.4 (2005), pp. 851–860. DOI: 10.1016/j.cardiores.2004.11.022.

[348] Peter Taggart, Peter M I Sutton, Tobias Opthof, et al. "Inhomogeneous Transmural Conduction During Early Ischaemia in Patients with Coronary Artery Disease". In: *J Mol Cell Cardiol* 32.4 (2000), pp. 621–630. DOI: 10.1006/jmcc.2000.1105.

[349] Jun Takata, Peter J Counihan, Jeff N Gane, et al. "Regional thallium-201 washout and myocardial hypertrophy in hypertrophic cardiomyopathy and its relation to exertional chest pain". In: *Am J Cardiol* 72.2 (1993), pp. 211–217. DOI: 10.1016/0002-9149(93)90162-6.

[350] Qin-You Tan, Huan-De Li, Rong-Hua Zhu, et al. "Tolerability and Pharmacokinetics of Ranolazine Following Single and Multiple Sustained-release Doses in Chinese Healthy Adult Volunteers". In: *Am J Cardiovasc Drugs* 13.1 (2013), pp. 17–25. DOI: 10.1007/s40256-013-0006-7.

[351] M Tanaka, H Fujiwara, T Onodera, et al. "Quantitative analysis of narrowings of intramyocardial small arteries in normal hearts, hypertensive hearts, and hearts with hypertrophic cardiomyopathy." In: *Circulation* 75.6 (1987), pp. 1130–1139. DOI: 10.1161/01.CIR.75.6.1130.

[352] Polakit Teekakirikul, Seda Eminaga, Okan Toka, et al. "Cardiac fibrosis in mice with hypertrophic cardiomyopathy is mediated by non-myocyte proliferation and requires Tgf-β". In: *J Clin Invest* 120.10 (2010), pp. 3520–3529. DOI: 10.1172/JCI42028.

[353] Milorad Tesic, Ana Djordjevic-Dikic, Branko Beleslin, et al. "Regional Difference of Microcirculation in Patients with Asymmetric Hypertrophic Cardiomyopathy: Transthoracic Doppler Coronary Flow Velocity Reserve Analysis". In: *J Am Soc Echocardiogr* 26.7 (2013), pp. 775–782. DOI: 10.1016/j.echo.2013.03.023.

[354] Daisuke Tezuka, Hisanori Kosuge, Masahiro Terashima, et al. "Myocardial perfusion reserve quantified by cardiac magnetic resonance imaging is associated with late gadolinium enhancement in hypertrophic cardiomyopathy". In: *Heart Vessels* 33.5 (2018), pp. 513–520. DOI: 10.1007/s00380-017-1088-y.

[355] H Tian, C Yang, Y Song, et al. "Microvascular Rarefaction and Myocardial Fibrosis in Hypertrophic Obstructive Cardiomyopathy". In: *Cardiol* 141.4 (2018), pp. 202–211. DOI: 10.1159/000493005.

[356] Stefan A J Timmer, Tjeerd Germans, Marco J W Götte, et al. "Determinants of myocardial energetics and efficiency in symptomatic hypertrophic cardiomyopathy". In: *Eur J Nucl Med Mol Imaging* 37.4 (2010), pp. 779–788. DOI: 10.1007/s00259-009-1350-3.

[357] Jakub Tomek, Alfonso Bueno-Orovio, Elisa Passini, et al. "Development, calibration, and validation of a novel human ventricular myocyte model in health, disease, and drug block". In: *eLife* 8 (2019), e48890. DOI: 10.7554/eLife.48890.

[358] Yasuaki Tomochika, Nobuaki Tanaka, Yuichiro Wasaki, et al. "Assessment of flow profile of left anterior descending coronary artery in hypertrophic cardiomyopathy by transesophageal pulsed Doppler echocardiography". In: *Am J Cardiol* 72.18 (1993), pp. 1425–1430. DOI: 10.1016/0002-9149(93)90191-E.

[359] Sergio Trevethan, Rafael Castilla, Gustavo Medrano, et al. "Giant T waves simulating apical hypertrophic myocardiopathy that disappear with sodium nitroprusside administration: Case report of pheochromocytoma". In: *J Electrocardiol* 24.3 (1991), pp. 267–275. DOI: 10.1016/0022-0736(91)90033-I.

[360] Chung Chun Tyan, Sarah Armstrong, David Scholl, et al. "Stress Hypoperfusion and Tissue Injury in Hypertrophic Cardiomyopathy". In: *Circ Cardiovasc Imaging* 6.2 (2013), pp. 229–238. DOI: 10.1161/CIRCIMAGING.112.000170.

[361] Takumi Uchida, Masaaki Yashima, Masamichi Gotoh, et al. "Mechanism of Acceleration of Functional Reentry in the Ventricle". In: *Circulation* 99.5 (1999), pp. 704–712. DOI: 10.1161/01.CIR.99.5.704.

[362] J E Udelson, R O Bonow, P T O'Gara, et al. "Verapamil prevents silent myocardial perfusion abnormalities during exercise in asymptomatic patients with hypertrophic cardiomyopathy." In: *Circulation* 79.5 (1989), pp. 1052–1060. DOI: 10.1161/01.CIR.79.5.1052.

[363] Aditya J Ullal, Ramy S Abdelfattah, Euan A Ashley, et al. "Hypertrophic Cardiomyopathy as a Cause of Sudden Cardiac Death in the Young: A Meta-Analysis". In: *Am J Med* 129.5 (2016), pp. 486–496. DOI: 10.1016/j.amjmed.2015.12.027.

[364] R Van Dam, J P Roos, and D Durrer. "Electrical activation of ventricles and interventricular septum in hypertrophic obstructive cardiomyopathy". In: *Br Heart J* 34.1 (1972), pp. 100–112. DOI: 10.1136/hrt.34.1.100.

[365] Bert Vandenberk, Eline Vandael, Tomas Robyns, et al. "Which QT Correction Formulae to Use for QT Monitoring?" In: *J Am Heart Assoc* 5.6 (2016), e003264. DOI: 10.1161/JAHA.116.003264.

[366] A M Varnava, P M Elliott, S Sharma, et al. "Hypertrophic cardiomyopathy: the interrelation of disarray, fibrosis, and small vessel disease". In: *Heart* 84.5 (2000), pp. 476–482. DOI: 10.1136/heart.84.5.476.

[367] Amanda M Varnava, Perry M Elliott, Niall Mahon, et al. "Relation between myocyte disarray and outcome in hypertrophic cardiomyopathy". In: *Am J Cardiol* 88.3 (2001), pp. 275–279. DOI: 10.1016/S0002-9149(01)01640-X.

[368] Jolanda van der Velden, Carlo G Tocchetti, Gilda Varricchi, et al. "Metabolic changes in hypertrophic cardiomyopathies: scientific update from the Working Group of Myocardial Function of the European Society of Cardiology". In: *Cardiovasc Res* 114.10 (2018), pp. 1273–1280. DOI: 10.1093/cvr/cvy147.

[369] Jessica T Vermeulen, Hanno L Tan, Han Rademaker, et al. "Electrophysiologic and Extracellular Ionic Changes During Acute Ischemia in Failing and Normal Rabbit Myocardium". In: *J Mol Cell Cardiol* 28.1 (1996), pp. 123–131. DOI: 10.1006/jmcc.1996.0012.

[370] Adriana Villa, Nuno Bettencourt, Niloufar Zarinabad, et al. "Stress perfusion CMR in hypertrophic cardiomyopathy: comparison with late gadolinium enhancement". In: *J Cardiovasc Magn Reson* 16 (2014), P324–P324. DOI: 10.1186/1532-429X-16-S1-P324.

[371] Adriana D M Villa, Eva Sammut, Niloufar Zarinabad, et al. "Microvascular ischemia in hypertrophic cardiomyopathy". In: *J Cardiovasc Magn Reson* 18 (2016). DOI: 10.1186/s12968-016-0223-8.

[372] Jeanne van der Waal, Laura Bear, Veronique Meijborg, et al. "Steep repolarization time gradients in pig hearts cause distinct changes in composite electrocardiographic T-wave parameters". In: *Ann Noninvasive Electrocardiol* 27.6 (2022), e12994. DOI: 10.1111/anec.12994.

[373] Galen S Wagner, Peter Macfarlane, Hein Wellens, et al. "AHA/ACCF/HRS Recommendations for the Standardization and Interpretation of the Electrocardiogram: Part VI: Acute Ischemia/Infarction A Scientific Statement From the American Heart Association Electrocardiography and Arrhythmias Committee, Council on Clinical Cardiology; the American College of Cardiology Foundation; and the Heart Rhythm Society Endorsed by the International Society for Computerized Electrocardiology". In: *J Am Coll Cardiol* 53.11 (2009), pp. 1003–1011. DOI: 10.1016/j.jacc.2008.12.016.

[374] Zhinuo J Wang, Alfonso Santiago, Xin Zhou, et al. "Human biventricular electromechanical simulations on the progression of electrocardiographic and mechanical abnormalities in post-myocardial infarction". In: *EP Europace* 23.Supplement_1 (2021), pp. i143–i152. DOI: 10.1093/europace/euaa405.

[375] J N Weiss, N Venkatesh, and S T Lamp. "ATP-sensitive K+ channels and cellular K+ loss in hypoxic and ischaemic mammalian ventricle." In: *J Physiol* 447.1 (1992), pp. 649–673. DOI: 10.1113/jphysiol.1992.sp019022.

[376] Adaya Weissler Snir, Kim A Connelly, Jack M Goodman, et al. "Exercise in hypertrophic cardiomyopathy: restrict or rethink". In: *Am J Physiol Heart Circ Physiol* 320.5 (2021), H2101–H2111. DOI: 10.1152/ajpheart.00850.2020.

[377] Adaya Weissler-Snir, Katherine Allan, Kristopher Cunningham, et al. "Hypertrophic Cardiomyopathy–Related Sudden Cardiac Death in Young People in Ontario". In: *Circulation* 140.21 (2019), pp. 1706–1716. DOI: 10.1161/CIRCULATIONAHA.119.040271.

[378] Zhen Weng, Jialu Yao, Raymond H Chan, et al. "Prognostic Value of LGE-CMR in HCM: A Meta-Analysis". In: *JACC Cardiovasc Imaging* 9.12 (2016), pp. 1392–1402. DOI: https://doi.org/10.1016/j.jcmg.2016.02.031.

[379] A A Wilde, D Escande, C A Schumacher, et al. "Potassium accumulation in the globally ischemic mammalian heart. A role for the ATP-sensitive potassium channel." In: *Circ Res* 67.4 (1990), pp. 835–843. DOI: 10.1161/01.RES.67.4.835.

[380] R L Wilensky, J Tranum-Jensen, R Coronel, et al. "The subendocardial border zone during acute ischemia of the rabbit heart: an electrophysiologic, metabolic, and morphologic correlative study." In: *Circulation* 74.5 (1986), pp. 1137–1146. DOI: 10.1161/01.CIR.74.5.1137.

[381] R Wolk. "Arrhythmogenic mechanisms in left ventricular hypertrophy". In: *Europace* 2.3 (2000), pp. 216–223. DOI: 10.1053/eupc.2000.0110.

[382] Robert Wolk, Kenneth P Sneddon, John Dempster, et al. "Regional electrophysiological effects of left ventricular hypertrophy in isolated rabbit hearts under normal and ischaemic conditions". In: *Cardiovasc Res* 48.1 (2000), pp. 120–128. DOI: 10.1016/S0008-6363(00)00149-8.

[383] Victor Chien-Chia Wu, Tien-Hsing Chen, Michael Wu, et al. "Outcomes of patients with hypertrophic cardiomyopathy and acute myocardial infarction: a propensity score-matched, 15-year nationwide population-based study in Asia". In: *BMJ Open* 8.8 (2018), e019741. DOI: 10.1136/bmjopen-2017-019741.

[384] Hua-yan Xu, Zhi-gang Yang, Jia-yu Sun, et al. "The regional myocardial microvascular dysfunction differences in hypertrophic cardiomyopathy patients with or without left ventricular outflow tract obstruction: Assessment with first-pass perfusion imaging using 3.0-T cardiac magnetic resonance". In: *Eur Radiol* 83.4 (2014), pp. 665–672. DOI: 10.1016/j.ejrad.2014.01.008.

[385] M Yamada, P M Elliott, J C Kaski, et al. "Dipyridamole stress thallium-201 perfusion abnormalities in patients with hypertrophic cardiomyopathy. Relationship to clinical presentation and outcome". In: *Eur Heart J* 19.3 (1998), pp. 500–507. DOI: 10.1053/euhj.1997.0769.

[386] Masatoshi Yamazaki, Naoki Tomii, Koichi Tsuneyama, et al. "Rotors anchored by refractory islands drive torsades de pointes in an experimental model of electrical storm". In: *Heart Rhythm* 19.2 (2022), pp. 318–329. DOI: 10.1016/j.hrthm.2021.10.012.

[387] Yin-Jian Yang, Chao-Mei Fan, Jin-Qing Yuan, et al. "Long-term survival after acute myocardial infarction in patients with hypertrophic cardiomyopathy". In: *Clin Cardiol* 40.1 (2017), pp. 26–31. DOI: 10.1002/clc.22601.

[388] Ying Yang, Ting-ting Lv, Si-yuan Li, et al. "Sodium channel blockers in the management of long QT syndrome types 3 and 2: A system review and meta-analysis". In: *J Cardiovasc Electrophysiol* 32.11 (2021), pp. 3057–3067. DOI: 10.1111/jce.15223.

[389] Z Yao, I Cavero, and G J Gross. "Activation of cardiac KATP channels: an endogenous protective mechanism during repetitive ischemia". In: *Am J Physiol Heart Circ Physiol* 264.2 (1993), pp. 495–504. DOI: 10.1152/ajpheart.1993.264.2.H495.

[390] Yee Guan Yap and A John Camm. "Drug induced QT prolongation and torsades de pointes". In: *Heart* 89.11 (2003), p. 1363. DOI: 10.1136/heart.89.11.1363.

[391] A Yatani, A M Brown, and N Akaike. "Effect of extracellular pH on sodium current in isolated, single rat ventricular cells". In: *J Membrane Biol* 78.2 (1984), pp. 163–168. DOI: 10.1007/BF01869203.

[392] Derek M Yellon, David J Hearse, Renata Crome, et al. "Temporal and spatial characteristics of evolving cell injury during regional myocardial ischemia in the dog: The "border zone" controversy". In: *J Am Coll Cardiol* 2.4 (1983), pp. 661–670. DOI: 10.1016/S0735-1097(83)80306-4.

[393] Anji T Yetman, Brian W McCrindle, Cathy MacDonald, et al. "Myocardial Bridging in Children with Hypertrophic Cardiomyopathy — A Risk Factor for Sudden Death". In: *N Engl J Med* 339.17 (1998), pp. 1201–1209. DOI: 10.1056/NEJM199810223391704.

[394] Gang Yi, Jan Poloniecki, Shaughan Dickie, et al. "Is QT Dispersion Associated with Sudden Cardiac Death in Patients with Hypertrophic Cardiomyopathy?" In: *Ann Noninvasive Electrocardiol* 6.3 (2001), pp. 209–215. DOI: 10.1111/j.1542-474X.2001.tb00110.x.

[395] Okan Yildiz, Firat H Altin, Oyku Tosun, et al. "Myocardial Bridging in a Child With Hypertrophic Obstructive Cardiomyopathy". In: *World J Pediatr Congenit Heart Surg* 5.4 (2014), pp. 611–614. DOI: 10.1177/2150135114536901.

[396] Liang Yin, Hai-yan Xu, Sui-sheng Zheng, et al. "3.0 T magnetic resonance myocardial perfusion imaging for semi-quantitative evaluation of coronary microvascular dysfunction in hypertrophic cardiomyopathy". In: *Int J Card Imaging* 33.12 (2017), pp. 1949–1959. DOI: 10.1007/s10554-017-1189-9.

[397] Noriko Yoshida, Hisao Ikeda, Toyofumi Wada, et al. "Exercise-induced abnormal blood pressure responses are related to subendocardial ischemia in hypertrophic cardiomyopathy". In: *J Am Coll Cardiol* 32.7 (1998), pp. 1938–1942. DOI: 10.1016/S0735-1097(98)00498-7.

[398] Ho-Joong Youn, Jong-Min Lee, Chul-Soo Park, et al. "The impaired flow reserve capacity of penetrating intramyocardial coronary arteries in apical hypertrophic cardiomyopathy". In: *J Am Soc Echocardiogr* 18.2 (2005), pp. 128–132. DOI: 10.1016/j.echo.2004.08.043.

[399] Arwa Younis, Ilan Goldenberg, Shamroz Farooq, et al. "Reduction in Ventricular Tachyarrhythmia Burden in Patients Enrolled in the RAID Trial". In: *JACC Clin Electrophysiol* 8.6 (2022), pp. 754–762. DOI: 10.1016/j.jacep.2022.02.018.

[400] Wei Yu, Mi-Mi Huang, Guo-Hong Zhang, et al. "Whole-exome sequencing reveals MYH7 p.R671C mutation in three different phenotypes of familial hypertrophic cardiomyopathy". In: *Exp Ther Med* 22 (2021). DOI: 10.3892/etm.2021.10434.

[401] Salah S Al-Zaiti, Christian Martin-Gill, Jessica K Zègre-Hemsey, et al. "Machine learning for ECG diagnosis and risk stratification of occlusion myocardial infarction". In: *Nat Med* 29.7 (2023), pp. 1804–1813. DOI: 10.1038/s41591-023-02396-3.

[402] Karolina M Zareba, Vien T Truong, Wojciech Mazur, et al. "T-wave and its association with myocardial fibrosis on cardiovascular magnetic resonance examination". In: *Ann Noninvasive Electrocardiol* 26.2 (2021), e12819. DOI: 10.1111/anec.12819.

[403] Ming-Kui Zhang, Zhengjie Zhang, Hui Xue, et al. "Microvascular Rarefaction and Myocardial Fibrosis in Hypertrophic Obstructive Cardiomyopathy: A Histopathological Comparison of Pediatric and Adult Patients". In: *Heart Surg Forum* 25.1 (2022), E042–E047. DOI: 10.1532/hsf.4277.

[404] Nixiao Zhang, Sijing Cheng, Hongxia Niu, et al. "Association of QTc Interval and V4-S Wave With Appropriate ICD Therapy in Hypertrophic Cardiomyopathy". In: *Front Cardiovasc Med* 9 (2022). DOI: 10.3389/fcvm.2022.882662.

[405] Xin Zhang and Geng Li. "Effects of a mitochondrial-acting drug on ischemia/reperfusion-induced ventricular arrhythmias, cardiac mitochondrial function and inflammatory cytokines in rat: Role of adenosine triphosphate-sensitive potassium channels". In: *Eur J Inflamm* 20 (2022), p. 1721727X2211150. DOI: 10.1177/1721727X221115041.

[406] Xian-Liang Zhou, Yan Xiao, Kun-Qi Yang, et al. "Clinical Characteristics and Prognosis of End-stage Hypertrophic Cardiomyopathy". In: *Chin Med J* 128 (2015), p. 1483. DOI: 10.4103/0366-6999.157656.

[407] Lidia Ziolkowska, Agnieszka Boruc, Dorota Sobielarska-Lysiak, et al. "Prognostic Significance of Myocardial Ischemia Detected by Single-Photon Emission Computed Tomography in Children with Hypertrophic Cardiomyopathy". In: *Pediatr Cardiol* 42.4 (2021), pp. 960–968. DOI: 10.1007/s00246-021-02570-9.

[408] Jerzy Zoladz, K Duda, Joanna Majerczak, et al. "Effect of different cycling frequencies during incremental exercise on the venous plasma potassium concentration in humans". In: *Physiol Res* 51 (2002), pp. 581–586. DOI: 10.33549/physiolres.930262.

APPENDIX A

Appendix

A.1 Single Cells Supplementary Material

A.1.1 Patch-clamp methods

Septal specimens were prepared as previously described [66]. Briefly, septal samples from HCM patients and non-failing non-hypertrophic aortic stenosis controls who underwent surgical myectomy were rapidly washed in ice-cold cardioplegic solution containing (in mmol/L): KH_2PO_4 50, $MgSO_4$ 8, HEPES 10, adenosine 5, glucose 140, mannitol 100, taurine 10 (pH 7.4 with KOH). Samples were then minced to small pieces (around 1 mm^3) and subjected to enzymatic and mechanical dissociation to obtain viable single myocytes, as described before [63]. In brief, small tissue chunks were transferred into a scraping device, while the bathing solution was changed to Ca^{2+}-free dissociation buffer containing (in mM): NaCl 113, KCl 4.7, KH_2PO_4 0.6, Na_2HPO_4 0.6, $MgSO_4$-$7H_2O$ 1.2, $NaHCO_3$ 12, $KHCO_3$ 10, HEPES 10, taurine 20, Na pyruvate 4, glucose 10, BDM 10 (pH 7.3 with NaOH) and heated to 37 °C. Collagenase Type V and Protease Type XXIV (Sigma) were subsequently added and tissue chunks digested for a total 2 hours' time. During the digestion, the buffer containing dissociated myocytes was collected every 15 minutes from the scraping device and diluted with KB solution at room temperature. KB solution contained (in mM): KCl 20, KH_2PO_4 10, glucose 25, mannitol 5, L-glutamic acid monopotassium salt 70, β-hydroxybutyric acid 10, EGTA 10 and 2 mg/mL albumin (pH 7.2 with KOH). The myocytes

were left to settle and then resuspended in Ca^{2+}-free Tyrode solution containing (in mM): 132 NaCl, 5 KCl, 1.2 $MgCl_2$, 10 HEPES, and 11 glucose (pH 7.35 NaOH), supplemented with bovine serum albumin (1 mg/ml). $CaCl_2$ was added stepwise up to 0.6 mM. Cells were stored in this solution and used within 3 hours. Cells were washed and transferred to a temperature-controlled recording chamber (experimental temperature = 35 $\pm$ 0.5 $^{\circ}$), mounted on the stage of an inverted microscope. Current-clamp experiments were conducted as previously [66]. APs were measured simultaneously using the perforated-patch configuration (amphotericin-B method). Specifically, for AP recordings, the pipette solution contained (in mM) 115 K methanesulfonate, 25 KCl, 10 HEPES, 3 $MgCl_2$ and cells were superfused with Tyrode buffer (see above) containing 1.8 mM $CaCl_2$. APs were elicited with short depolarizing stimuli ($<$ 3 ms) at different frequencies of stimulation (0.2 Hz and 0.5 Hz, 1 minute at each frequency). $[K^+]_e$ was then raised from 5 mM up to 9 mM and AP recordings were repeated using the same stimulation protocol. All patch-clamp experimental data was provided by Dr. Raffaele Coppini, University of Florence.

A.1.2 Computational Results

Effects of ischaemia on Ca^{2+} handling

The impact of acute myocardial ischaemia on Ca^{2+} handling in the populations of control and HCM AP models was also investigated (Appendix Fig. A.1). At baseline, HCM AP models had longer Ca^{2+} transient durations than controls (530 $\pm$ 50 vs. 390 $\pm$ 50 ms; HCM vs control), elevated diastolic Ca^{2+} (82 $\pm$ 7 vs. 77 $\pm$ 5 nM) and lower Ca^{2+} transient amplitudes (340 $\pm$ 90 vs. 380 $\pm$ 80 nM), as reported experimentally [66]. Ca^{2+} transient amplitudes were reduced similarly in control and HCM populations during hyperkalaemia (-60 $\pm$ 40 vs. -80 $\pm$ 60 nM), hypoxia (-120 $\pm$ 30 vs. -90 $\pm$ 40 nM), acidosis (-150 $\pm$ 30 vs. -130 $\pm$ 40 nM) and ischaemia (-240 $\pm$ 50 vs. -220 $\pm$ 80 nM). Small changes in Ca^{2+} transient durations were observed in control and HCM populations during hyperkalaemia (8 $\pm$ 10 vs. 7 $\pm$ 20 ms) and hypoxia (9 $\pm$ 10 vs. 0 $\pm$ 20 ms). During acidosis, Ca^{2+} transient durations were increased similarly in control and HCM populations (40 $\pm$ 5 vs. 40 $\pm$ 20 ms), and this was also observed during ischaemia (50 $\pm$ 20 vs. 40 $\pm$ 40 ms).

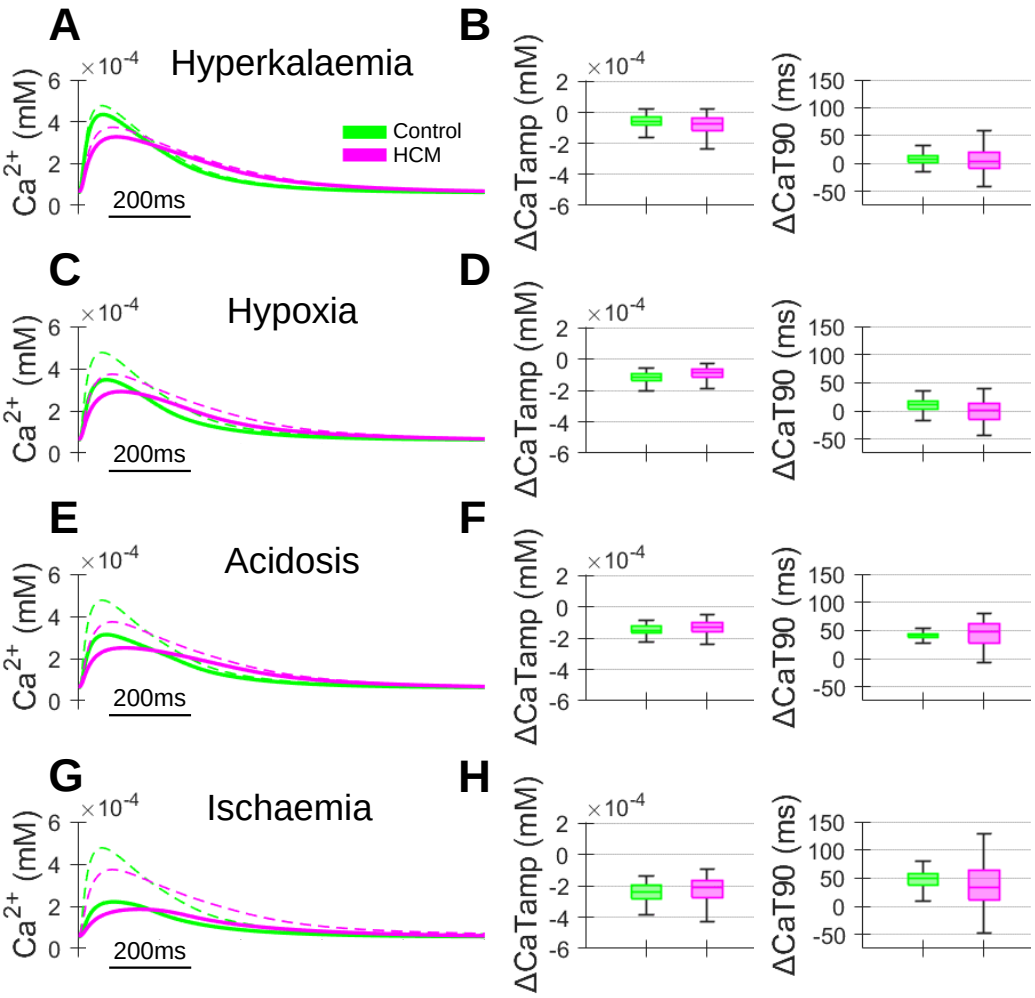


Figure A.1: Effects of ischaemia on Ca^{2+} handling in control and HCM populations of AP models. (A, C, E, G) Representative Ca^{2+} transients under basal conditions (dashed) compared to during (A) hyperkalaemia ($[K^+]_e$ = 9 mM), (C) hypoxia (f_{KATP} = 0.09), (E) acidosis (-25% I_{Na} & I_{CaL}) and (G) ischaemia ($[K^+]_e$ = 8 mM, f_{KATP} = 0.06, -25% I_{Na} & I_{CaL}), (solid). (B, D, F, H) Changes in Ca^{2+} transient amplitudes (ΔCaTamp) (left) and changes in Ca^{2+} transient durations measured at 90% decay (ΔCaT90) (right) undergone for each respective condition.

In summary, myocardial ischaemia led to similar prolongation of Ca^{2+} transients and similar impairment of Ca^{2+} transient amplitudes in control and HCM AP models. The Ca^{2+} durations which were prolonged in HCM models under basal conditions remained significantly prolonged during ischaemia compared to

controls (570 ± 30 ms vs. 440 ± 50 ms), which contrasts with the changes observed in APD in HCM models.

Sensitivity of AP biomarkers to ischaemic effects on I_{NaK}, I_{NaL} and I_{NCX}

Although hyperkalaemia, hypoxia and acidosis are the main causes of electrical changes during acute myocardial ischaemia [247], there are various formulations of hypoxic and acidotic effects in computational cardiac electrophysiology models. In addition to hypoxic activation of I_{KATP} and the acidotic effects on I_{Na} and I_{CaL} modelled in this thesis and in previous works [45, 91, 100, 228], more detailed models of hypoxia and acidosis include changes in I_{NaK} and I_{NCX} [45]. Furthermore, the accumulation of the ischaemic metabolite lysphosphatidylcholine and its upregulation of I_{NaL} [45] may be of relevance to the present study, in which ionic remodelling in I_{NaL} is a key component of HCM cells. The sensitivity of the results to these additional ischaemic effects were analysed by repeating cellular and in-tissue simulations with changes in I_{NaK}, I_{NCX} and I_{NaL} extracted directly from a more detailed computational model of ischaemia [44].

Appendix Fig. A.2 shows how AP biomarkers were affected by these additional ischaemia components. Compared with the original model of ischaemia, the inclusion of moderate changes in $I_{NaK}/I_{NCX}/I_{NaL}$ led to longer APDs in control cells (190 ± 40 vs. 180 ± 50 ms), an effect which was slightly more pronounced in HCM cells (330 ± 50 vs. 310 ± 50 ms) due to basal I_{NaL} upregulation in HCM (Appendix Fig. A.2A). There were also marginal reductions in CV in control myocardium (44 ± 6 vs. 45 ± 6 cm/s) due to the less negative RMP caused by impairment of I_{NaK}, which was slightly more pronounced in HCM cells (37 ± 7 vs. 40 ± 6 cm/s) (Appendix Fig. A.2B). Differences in ERPs (Appendix Fig. A.2C) were largely secondary to differences in APDs, where moderate changes in $I_{NaK}/I_{NCX}/I_{NaL}$ led to longer ERPs in control cells (310 ± 60 vs. 290 ± 50 ms), an effect which was again more pronounced in HCM cells (490 ± 90 vs. 460 ± 80 ms). PRRs (Appendix Fig. A.2D) were largely unchanged in control cells (120 ± 50 vs. 120 ± 70 ms) but were slightly increased in HCM cells (160 ± 70 vs. 150 ± 60 ms). When compared with non-ischaemic cells, all models of ischaemia caused similar changes to AP biomarkers in both control and HCM.

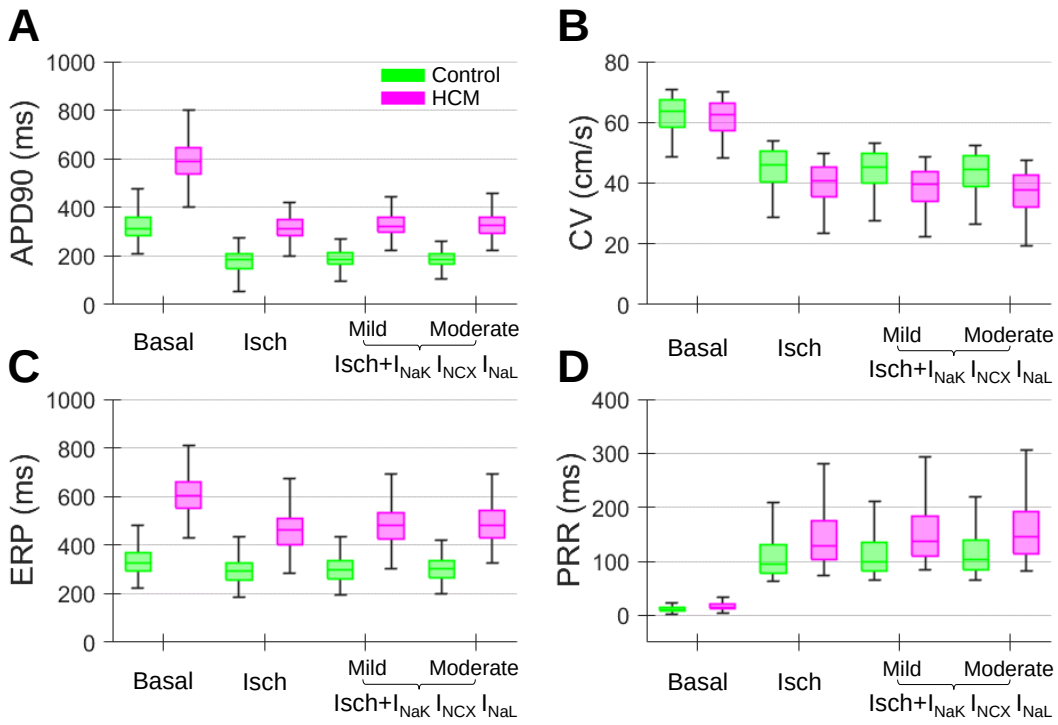


Figure A.2: Effects on AP biomarkers of extending the model of ischaemia to include changes in I_{NaK}, I_{NCX} and I_{NaL}. (A) APD, (B) CV, (C) ERP and (D) PRR for control and HCM populations of models subjected to basal conditions, the original ischaemia conditions ($[K^+]_e$ = 8 mM, f_{KATP} = 0.06, -25% I_{Na} & I_{CaL}), and ischaemia with mild/moderate effects on I_{NaK} I_{NCX} I_{NaL} ($[K^+]_e$ = 8 mM, f_{KATP}=0.06, -25% I_{Na} & I_{CaL}, -20%/-40% I_{NaK} & I_{NCX}, +40%/+70% I_{NaL}).

A.2 Arrhythmic Risk Supplementary Material

A.2.1 Perfusion imaging cohort clinical characteristics

All perfusion imaging data was provided by Prof. Betty Raman, University of Oxford.

Demographic / Clinical Data	
Age (years)	49 ± 14
Male sex	23 (82%)
Weight (kg)	82 ± 5
Height (cm)	175 ± 8
Body mass index (kg/m^2)	27 ± 4
LVOT obstruction	9 (32%)
VT	5 (18%)
CMR	
LVEDV (ml)	166 ± 32
LVESV (ml)	49 ± 16
Stroke volume (ml)	117 ± 24
Ejection fraction (%)	71 ± 7
Max wall thickness (mm)	20 ± 4
Mid-LV Segmental MPRI	
Anterior	1.3 ± 0.4
Anteroseptal	1.1 ± 0.4
Inferoseptal	1.2 ± 0.4
Inferior	1.3 ± 0.5
Inferolateral	1.5 ± 0.5
Anferolateral	1.3 ± 0.4

Table A.1: Characteristics and demographics of HCM patients (N = 28) that underwent perfusion imaging. LVEDV: LV end-diastolic volume; LVESV: LV end-systolic volume; LVOT: left ventricular outflow tract; VT: ventricular tachycardia; CMR: cardiac magnetic resonance; LV: left ventricle; MPRI: myocardial perfusion reserve index.

A.2.2 Computational Results

Effects of variable I_{Kr} block on ischaemic arrhythmic risk

As in previous work [282], the modelling of HCM ionic remodelling was informed by cardiomyocyte current measurements, protein expression, and mRNA data from surgical samples of HCM patients undergoing septal myectomy [66]. However, patients undergoing septal myectomy may represent a narrow window of advanced disease progression. Evidence from murine models suggests that ionic remodelling in HCM is instead progressive [67]. To further investigate how arrhythmic risk might be sensitive to the degree of ionic remodelling in HCM, arrhythmic risk studies were performed in ischaemic HCM tissue for a range of regional K^+ channel blocks in [50%, 60%, 70%, 75%, 80%] to characterise different extents of AP prolongation as a primary hallmark of the HCM cellular phenotype. This involved applying ectopic S1-S2 stimulus protocols to regionally ischaemic ($[K^+]_e = 7$ mM, $f_{KATP} = 0.06$) tissue, across 50 AP models, for variable degrees of ionic remodelling.

Appendix Fig. A.3 shows how arrhythmic risk varied across the considered 50 AP models as the APD of the ischaemic region was increased. Arrhythmic risk (both single and multiple re-entries) did not monotonically increase with increasing APD, illustrating competing mechanisms of ionic remodelling in HCM on arrhythmic risk. These findings indicate that ischaemia-induced arrhythmic risk in HCM may progressively increase in the early stages of HCM as the disease-associated ionic remodelling develops, but this may be partially subverted at later stages of the disease where more sizeable regional increases in APD/ERP counterbalance re-entries.

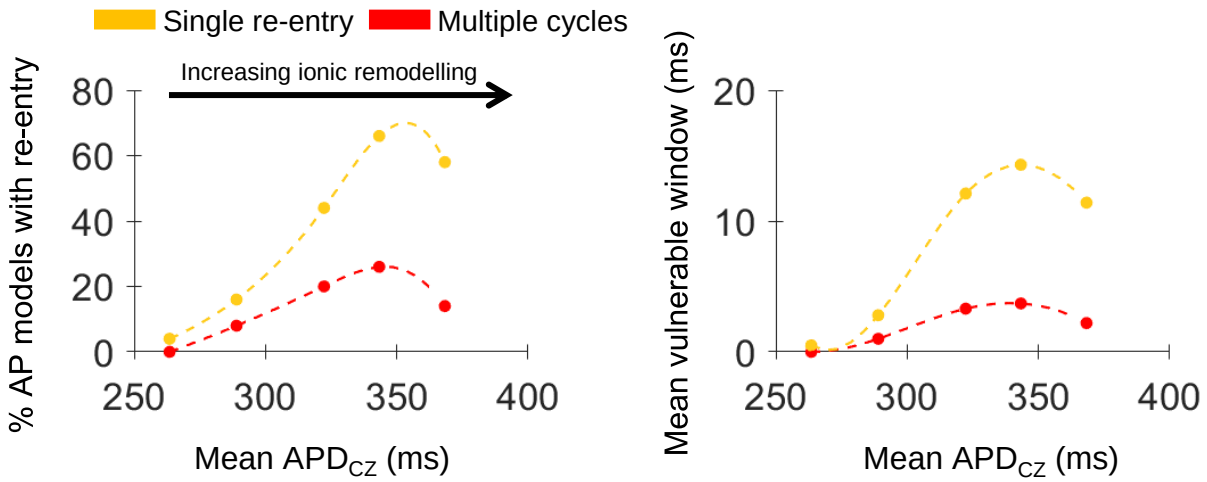


Figure A.3: Modulation of ischaemic arrhythmic risk by extent of HCM ionic remodelling. Summary statistics of arrhythmic risk over the population of 50 AP models, subjected to regional ischaemia with $[K^+]_e = 7$ mM and $f_{KATP} = 0.06$, for I_{Kr}, I_{K1} and I_{Ks} block in [50%, 60%, 70%, 75%, 80%]. Increasing block of K^+ currents led to increased arrhythmic risk up to a peak in APD, beyond which arrhythmic risk fell.

Sensitivity of in-tissue arrhythmic risk to ischaemic effects on I_{NaK}, I_{NaL} and I_{NCX}

Appendix Fig. A.4 shows how arrhythmic risk as measured in tissue was affected by extending the model of ischaemia to include effects on I_{NaK}, I_{NCX} and I_{NaL}. When compared with the original ischaemia conditions (Appendix Fig. A.4A), the more detailed model of ischaemia (Appendix Fig. A.4B) supported similar patterns of arrhythmic risk across the hyperkalaemia/hypoxia parameter space, with re-entries again occurring at a lesser hyperkalaemic extent in HCM models than in controls. As before with the AP biomarkers, the sensitivity of arrhythmic risk to ischaemic changes in I_{NaK}, I_{NCX} and I_{NaL} was greater in HCM models, due to basal upregulation of I_{NaL} and reduced conduction reserve in HCM.

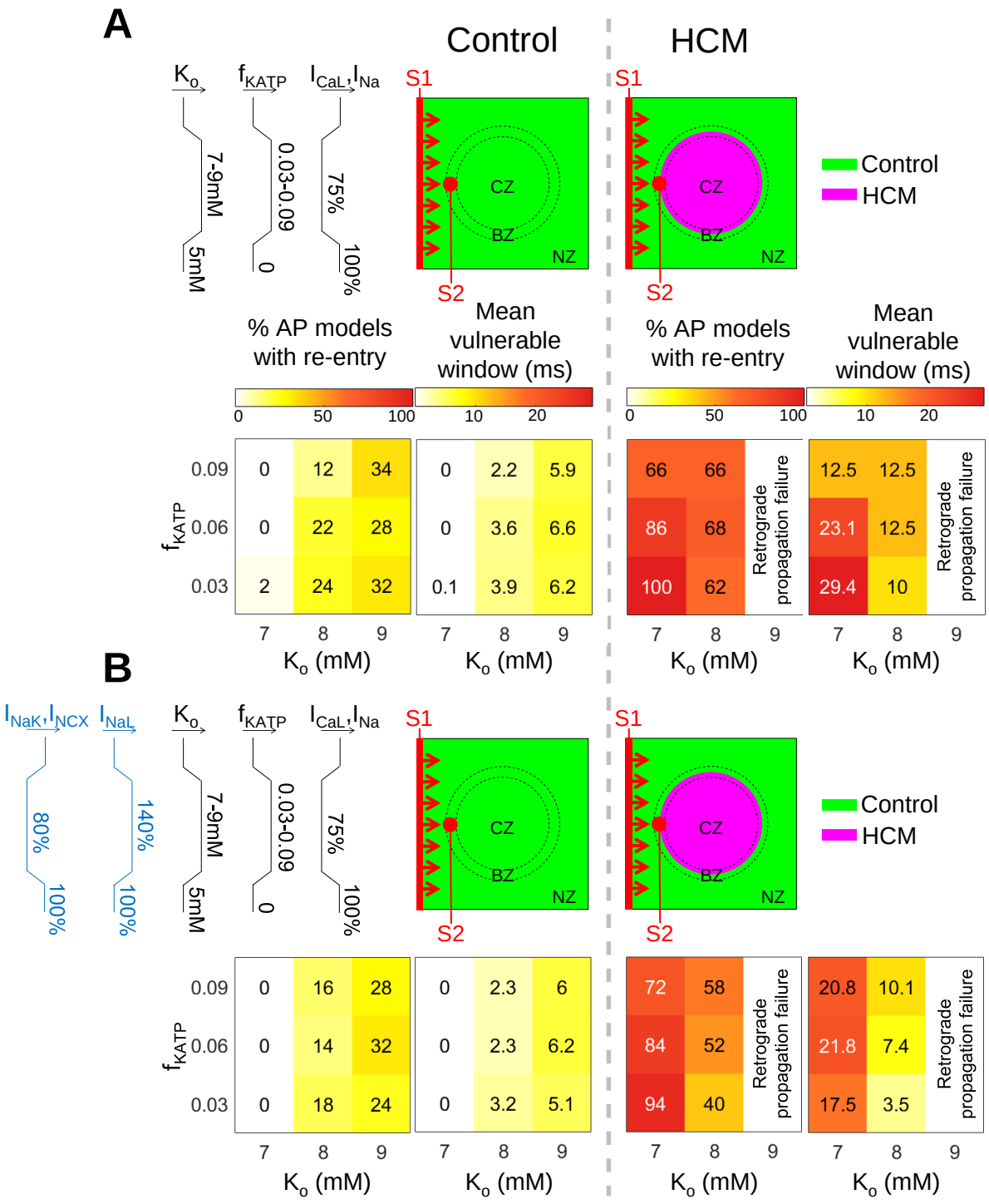


Figure A.4: Effects on in-tissue arrhythmic risk of extending the model of ischaemia to include changes in I_{NaK}, I_{NCX} and I_{NaL}. Summary statistics of arrhythmic risk over the hyperkalaemia/hypoxia parameter space for the 50 AP models in tissue, as characterised using S1-S2 pacing protocols, for (A) the original

ischaemia conditions ($[K^+]_e$ = 7–9 mM, f_{KATP} = 0.03– 0.09, -25% I_{Na} & I_{CaL}) and (B) ischaemia with additional mild effects on I_{NaK}, I_{NCX}, and I_{NaL} ($[K^+]_e$ = 7–9 mM, f_{KATP} = 0.03–0.09, -25% I_{Na} & I_{CaL}, -20% I_{NaK} & I_{NCX}, +40% I_{NaL}).

Sensitivity of in-tissue arrhythmic risk to hypoxic border zone width

The in-tissue models of ischaemia assumed that the lateral BZ width of hyperkalaemia, hypoxia and acidosis were equal [149]. Previous works have used different lateral BZ widths for the components of ischaemia [45], to include steeper gradients of ATP than K^+ in the lateral BZ. To analyse whether the choice of BZ affected the in-tissue results, in-tissue simulations at $[K^+]_e$ = 8 mM, f_{KATP} = 0.06 were repeated for a sharp transition in I_{KATP} activation (no hypoxic BZ) as shown in Appendix Fig. A.5.

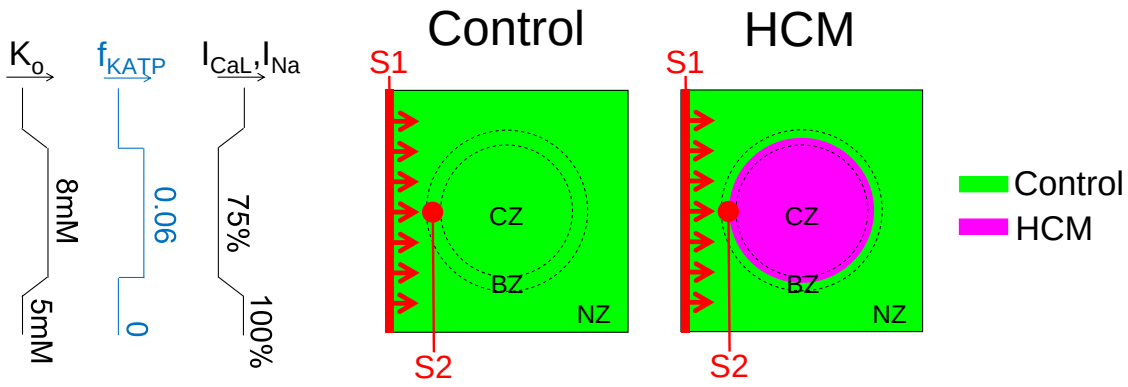


Figure A.5: Tissue domains used to test the sensitivity of arrhythmic risk to the hypoxic lateral BZ width.

Compared to simulations with a BZ in hypoxia (Appendix Fig. A.4A), the mean vulnerable window width and the percentage of AP models with re-entry was similar in simulations without a hypoxic BZ (2.7 ms, 20% vs. 3.6 ms, 22% with hypoxic BZ, in controls). This also applied to HCM tissue models (14.0 ms, 74% vs. 12.5 ms, 68% with hypoxic BZ).

Sensitivity of in-tissue arrhythmic risk to spatial resolution

To analyse how spatial resolution affected the in-tissue results, in-tissue simulations in ischaemic control models (n = 50) at $[K^+]_e$ = 8 mM, f_{KATP} = 0.06 were compared between dx = [200, 250, 500] μm. The corresponding mean vulnerable window widths were [3.1, 3.6, 2.6] ms, and corresponding the percentages of AP models with re-entry were [20, 22, 18]%, showing modest sensitivity to dx at the AP population level. In individual tissue models, despite the occurrence of re-entry being similar, the patterns of re-entry were not identical, reflecting greater CV at dx = 200 μm (Appendix Fig. A.6A) than at dx = 500 μm (Appendix Fig. A.6B).

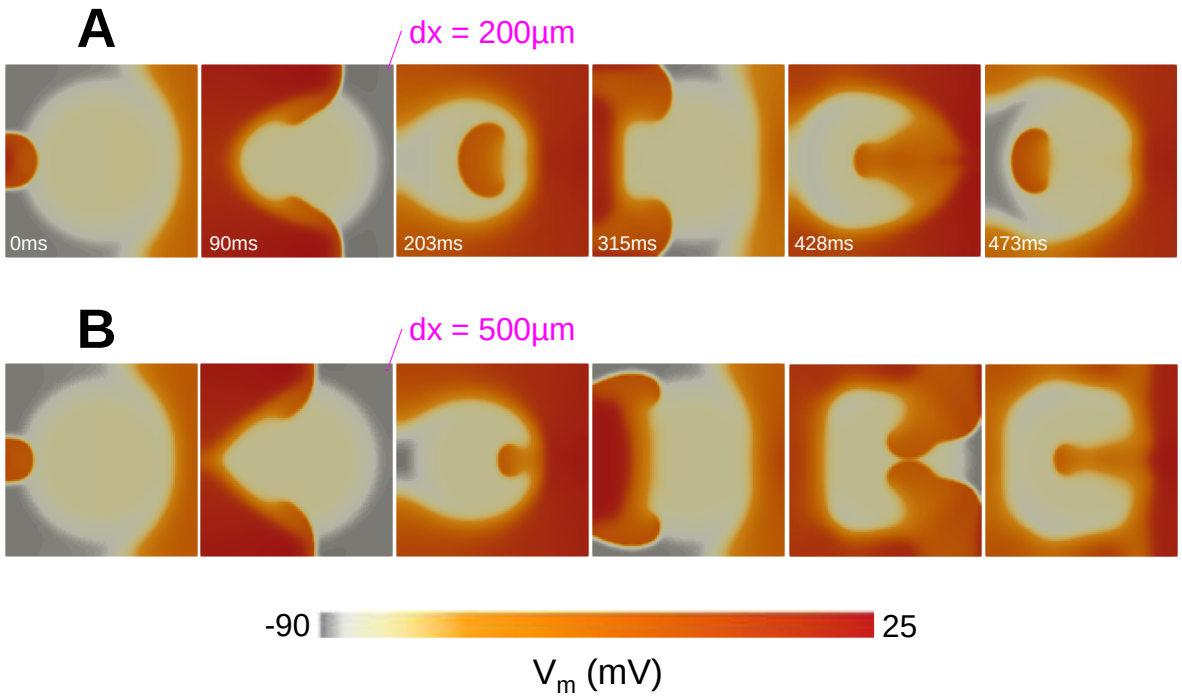


Figure A.6: Representative re-entries in ischaemic control tissue using spatial resolutions. (A) dx = 200 μm and (B) dx = 500 μm. Time elapsed following S2 (ms) is denoted in each frame.

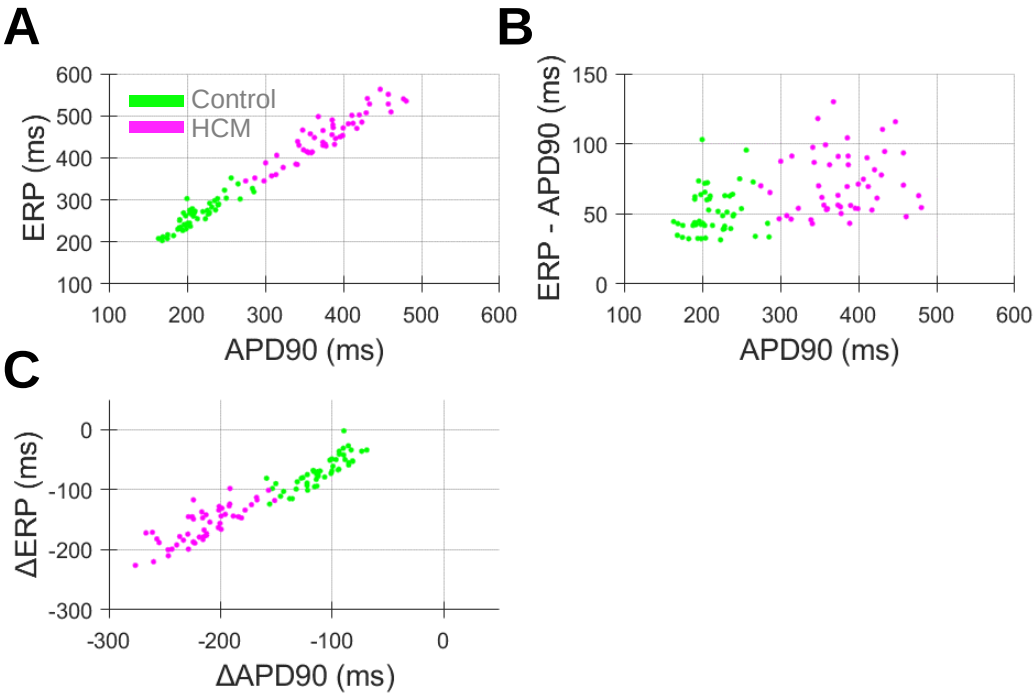


Figure A.7: Refractoriness and repolarisation under ischaemic conditions ($[K^+]_e$ = 7 mM, f_{KATP} = 0.06, -25% I_{Na} & I_{CaL}, -20% I_{NaK} & I_{NCX}, +40% I_{NaL}), as measured in n = 50 control and HCM cable simulations. (A) ERP and (B) PRR, vs. APD. (C) The difference in ERP during ischaemia with respect to basal conditions (ΔERP) vs. the difference in APD during ischaemia with respect to basal conditions (ΔAPD90).

Sensitivity of AP biomarkers to further ischaemic effects on J_{up} and I_{pCa}

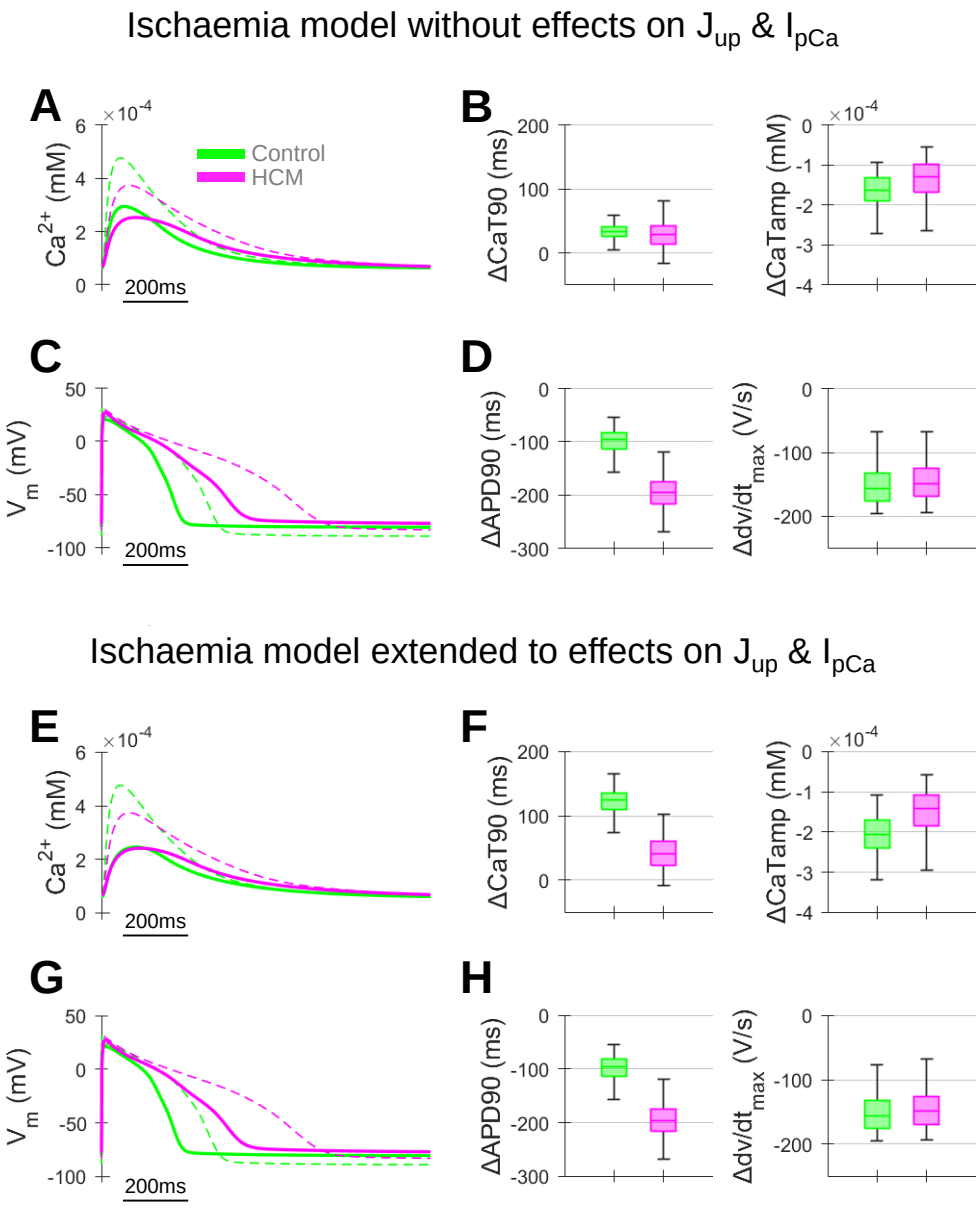


Figure A.8: Effects on AP and Ca^{2+} transient biomarkers of further extending the model of ischaemia to include impairment of J_{up} and I_{pCa}. (A, E) Representative Ca^{2+} transients and (C, G) representative AP traces, under basal conditions (dashed) compared to (A, C) ischaemia without impairment of J_{up} and I_{pCa} ($[K^+]_e$ = 7 mM, f_{KATP} = 0.06, -25% I_{Na} & I_{CaL}, -20% I_{NaK} & I_{NCX}, +40% I_{NaL}) (solid) and (E, G) ischaemia with impairment of J_{up} and I_{pCa} ($[K^+]_e$ = 7 mM, f_{KATP} = 0.06, -25% I_{Na} & I_{CaL},

-20% I_{NaK} & I_{NCX}, +40% I_{NaL}, -30% J_{up} & I_{pCa}) (solid). (B, F) Changes in Ca^{2+} transient durations measured at 90% decay (ΔCaT90) (left) and Ca^{2+} transient amplitudes (ΔCaTamp) (right) undergone for each respective condition. (D, H) Changes in APD (ΔAPD) (left) and maximal upstroke velocities ($\Delta dv/dt_{max}$) (right) undergone for each respective condition.

A.3 Diagnosis Supplementary Material

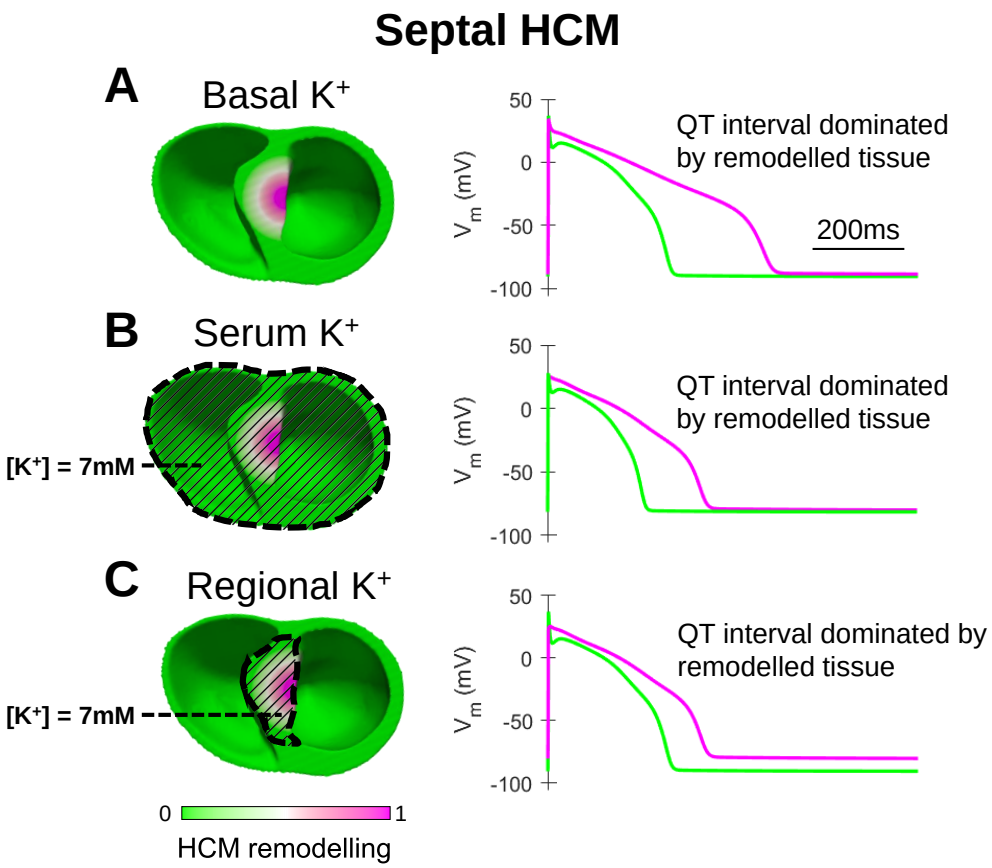


Figure A.9: Representative APs under mild increases of serum [K^+] and regional [K^+]. (A) At baseline, prolonged APD in the HCM-remodelled myocardium determined the max QT interval. (B) Mild serum [K^+] increases reduced the APD of the control and HCM-remodelled myocardium, but the prolonged APD in the HCM-remodelled myocardium still determined the max QT interval. (C) Mild regional [K^+] increases reduced the APD of the HCM-remodelled myocardium, but the APD remained prolonged and still determined the max QT interval.

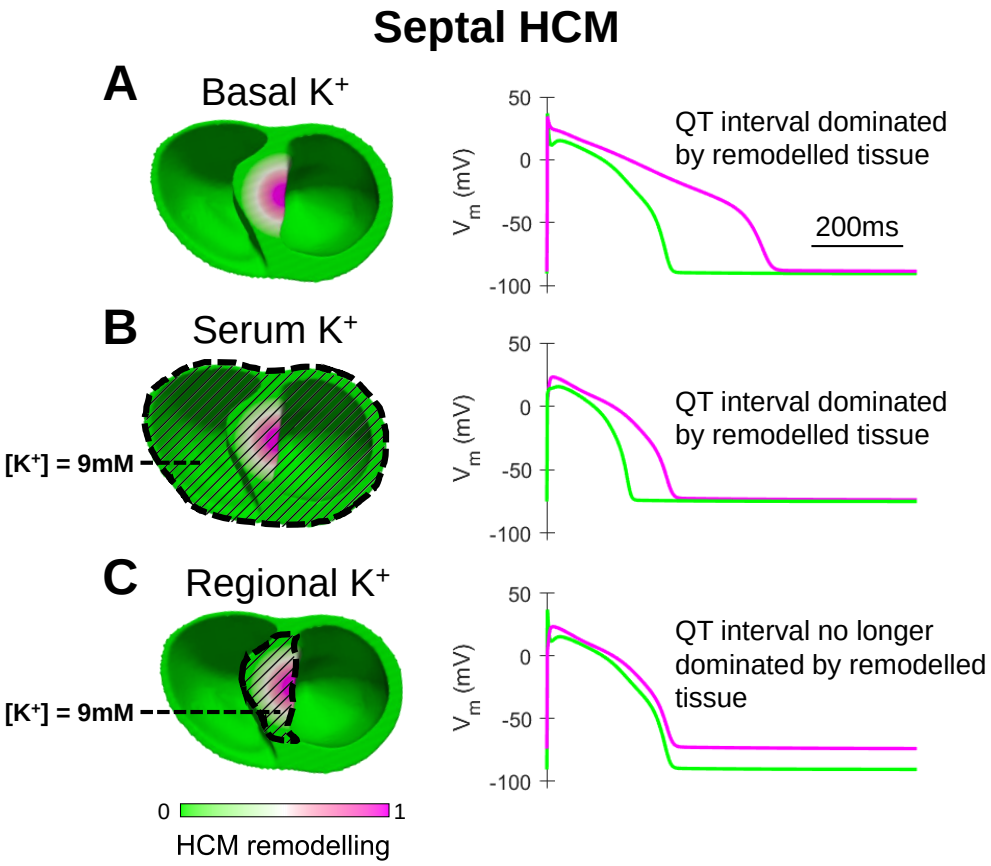


Figure A.10: Representative APs under severe increases of serum [K^+] and regional [K^+]. (A) At baseline, prolonged APD in the HCM-remodelled myocardium determined the max QT interval. (B) Severe serum [K^+] increases reduced the APD of the control and HCM-remodelled myocardium, but the prolonged APD in the HCM-remodelled myocardium still determined the max QT interval. (C) Severe regional [K^+] increases reduced the APD of the HCM-remodelled myocardium to that (or less than that) of the control myocardium, such that the QT interval was insensitive to further regional K^+ accumulation.

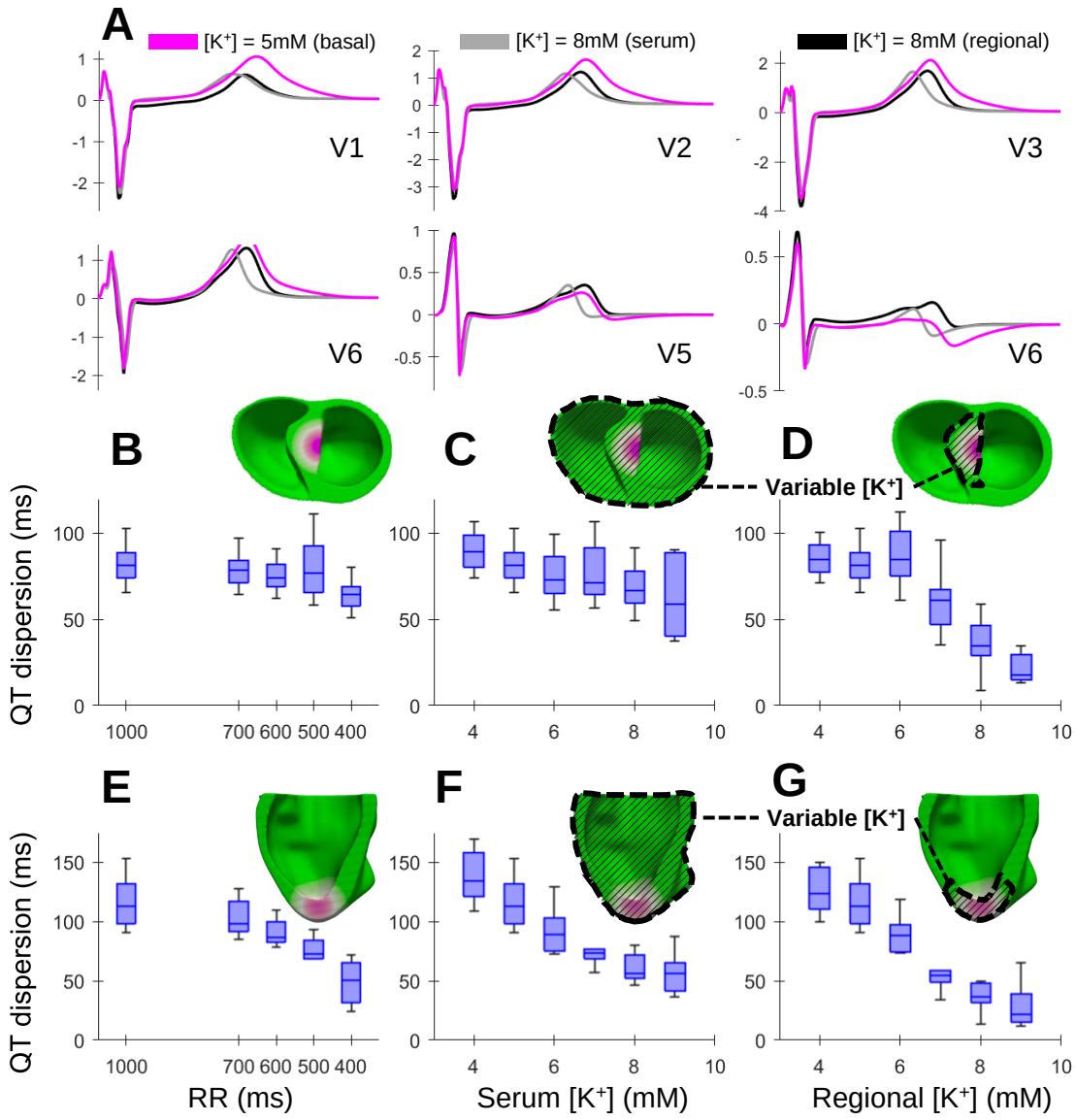


Figure A.11: Effects of pacing rate and [K^+] increases on leads V1-V6. (A) Representative lead V1-V6 traces in septal HCM for basal [K^+], serum [K^+] increases, and regional [K^+] increases. (B, C, D) Leads V1-V6 QT dispersion plotted against RR interval, serum [K^+], and regional [K^+], respectively in septal HCM. (E, F, G) Leads V1-V6 QT dispersion plotted against RR interval, serum [K^+], and regional [K^+], respectively in apical HCM. All results presented at 1 Hz pacing.

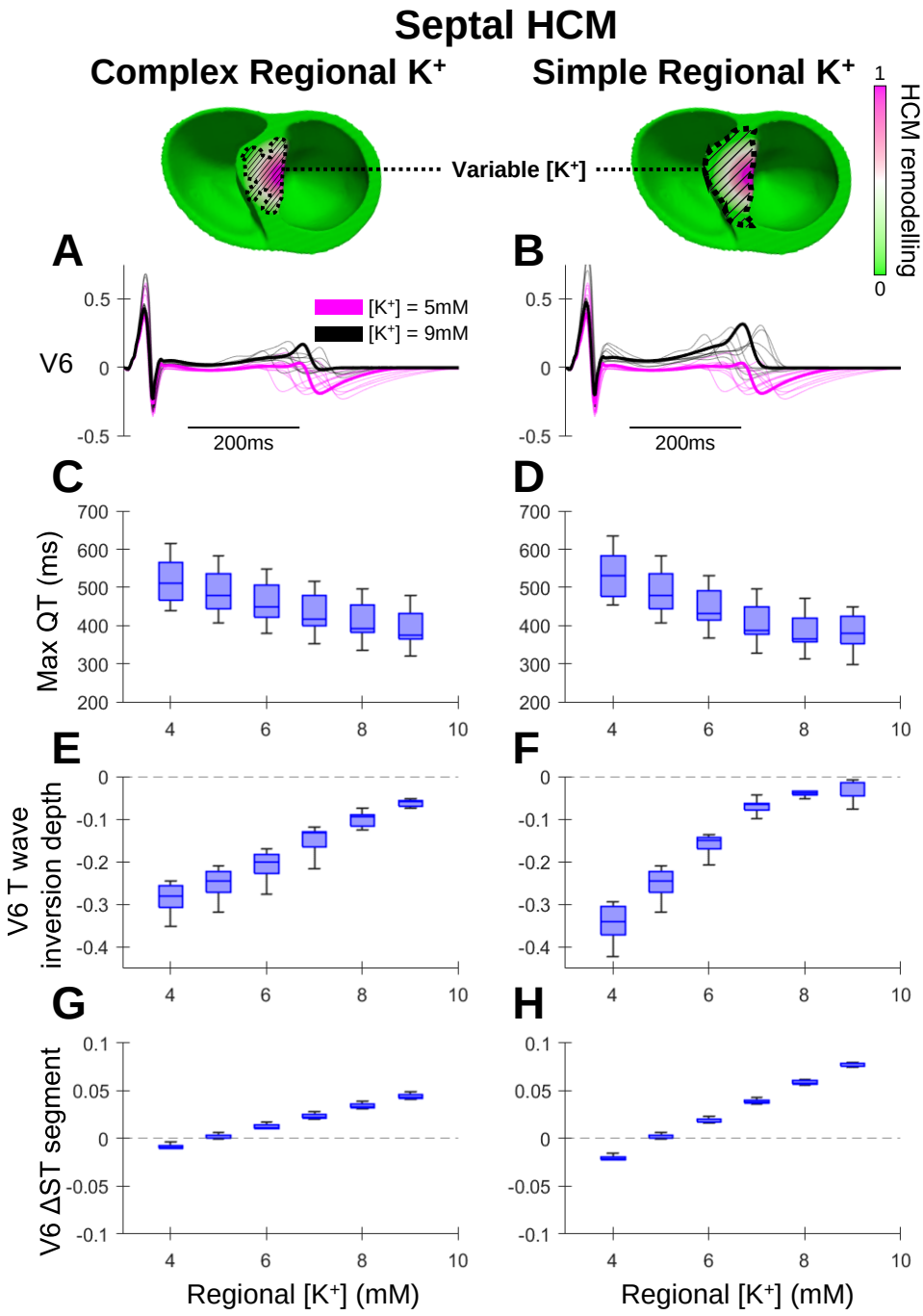


Figure A.12: Comparisons of the effect of increased regional [K^+] in a complex pattern vs. a simple pattern on ECG biomarkers in septal HCM. (A, B) Representative lead V6 traces, showing that T wave morphology was normalised by both complex (A), and simple (B), regional distributions of increased

[K^+]. (C, D) Max QT interval, (E, F) lead V6 T wave inversion depth, and (G, H) lead V6 ST segment changes, plotted against complex and simple distributions of regional [K^+] changes, respectively. All results presented at 1 Hz pacing. The complex pattern of regional ischaemic changes was informed by a clinical case of myocardial infarction in HCM [116].

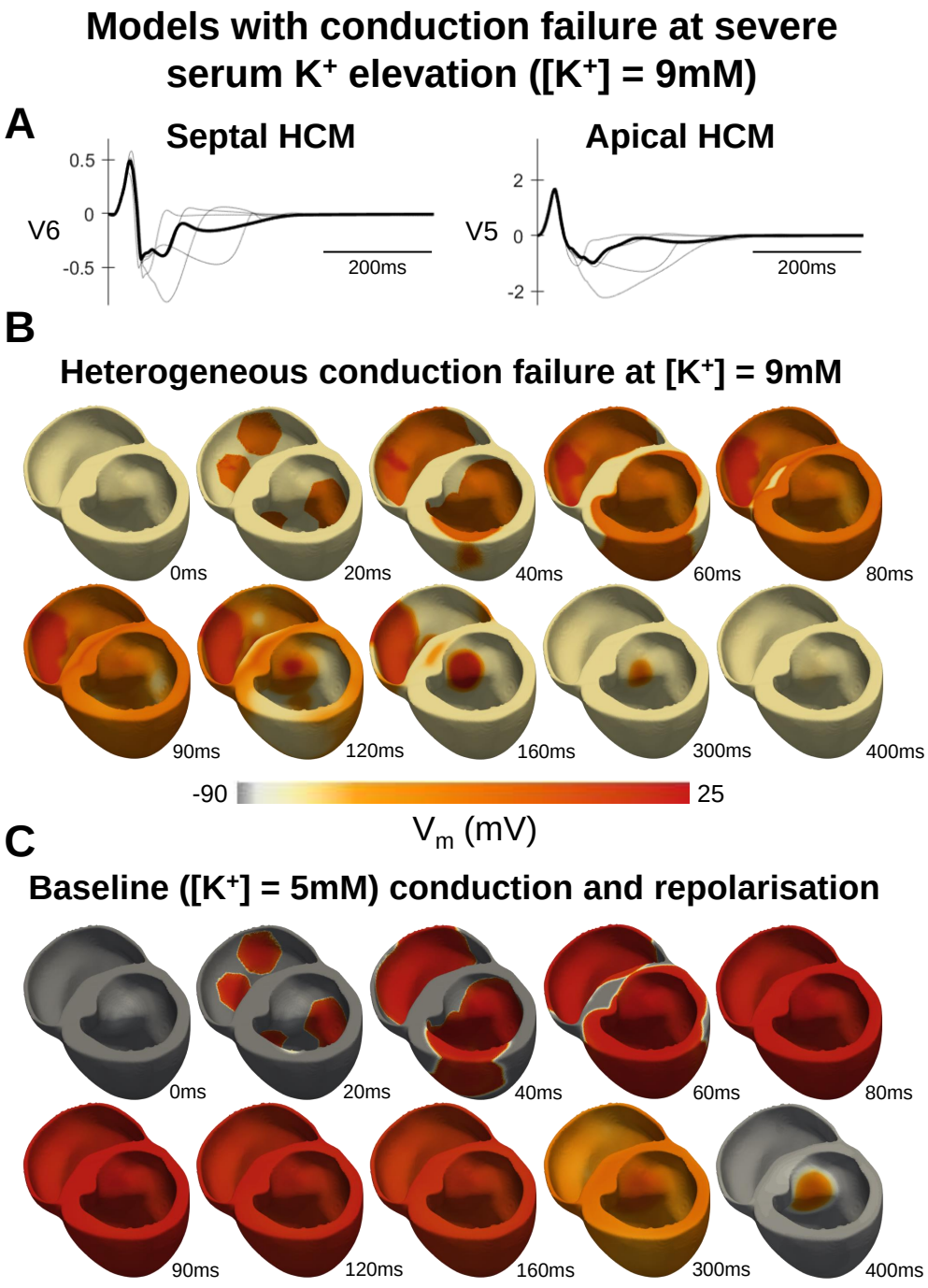


Figure A.13: Biventricular models with AP propagation failure during severe global hyperkalaemia. (A) ECG traces in models where a T wave was not discernible from the QRS complex. (B) Slowed propagation of stunted APs resulted in simultaneous ventricular depolarisation and repolarisation among different regions, as compared to (C) baseline $[K^+]$ in which ventricular depolarisation and repolarisation phases are clearly discernible. All results presented at 1 Hz pacing.

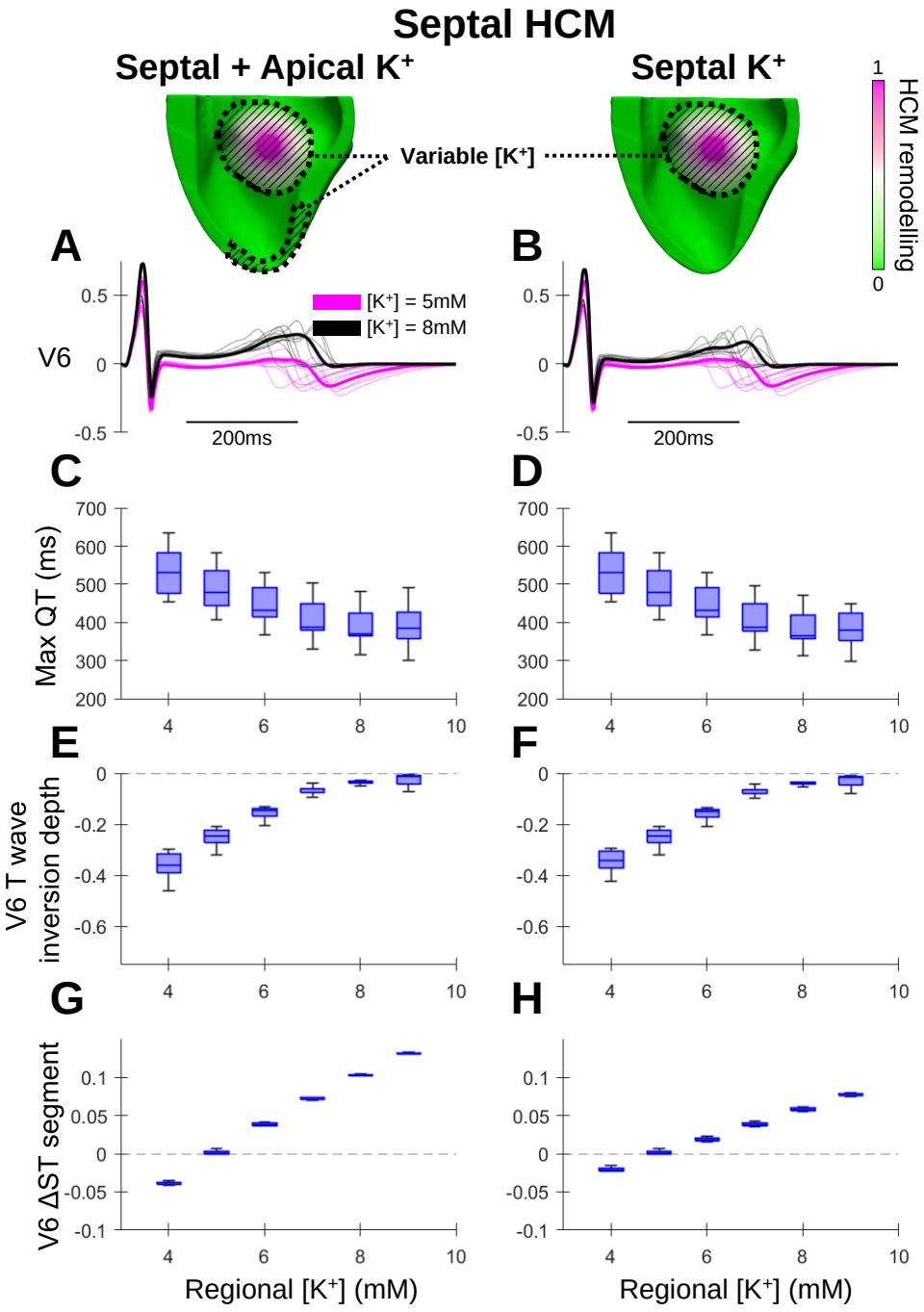


Figure A.14: Comparisons of the effect of increased regional [K^+] in the septum and apex vs. only the septum on ECG biomarkers in septal HCM. (A, B) Representative lead V6 traces, showing that T wave morphology was normalised by both the septal and apical (A), and septal only (B), distributions of [K^+] increases. (C, D) Max QT interval, (E, F) lead V6 T wave inversion depth, and (G, H) lead V6

ST segment changes, plotted against septal and apical, and septal only, distributions of regional [K^+] changes, respectively. All results presented at 1 Hz pacing.

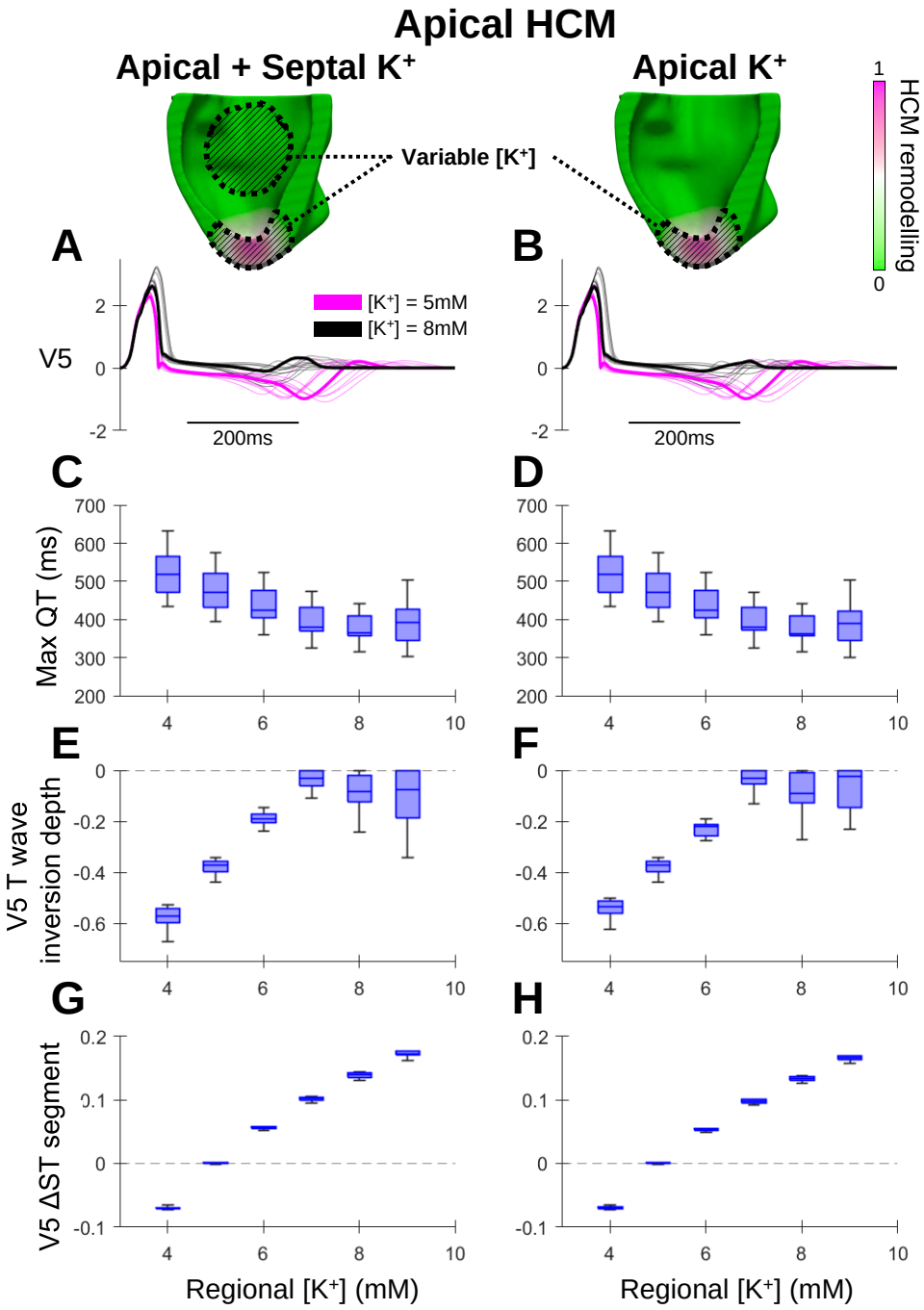


Figure A.15: Comparisons of the effect of increased regional [K^+] in the apex and septum vs. only the

apex on ECG biomarkers in apical HCM. (A, B) Representative lead V6 traces, showing that T wave morphology was normalised by both the apical and septal (A), and apical only (B), distributions of $[K^+]$ increases. (C, D) Max QT interval, (E, F) lead V6 T wave inversion depth, and (G, H) lead V6 ST segment changes, plotted against apical and septal, and apical only, distributions of regional $[K^+]$ changes, respectively. All results presented at 1 Hz pacing.

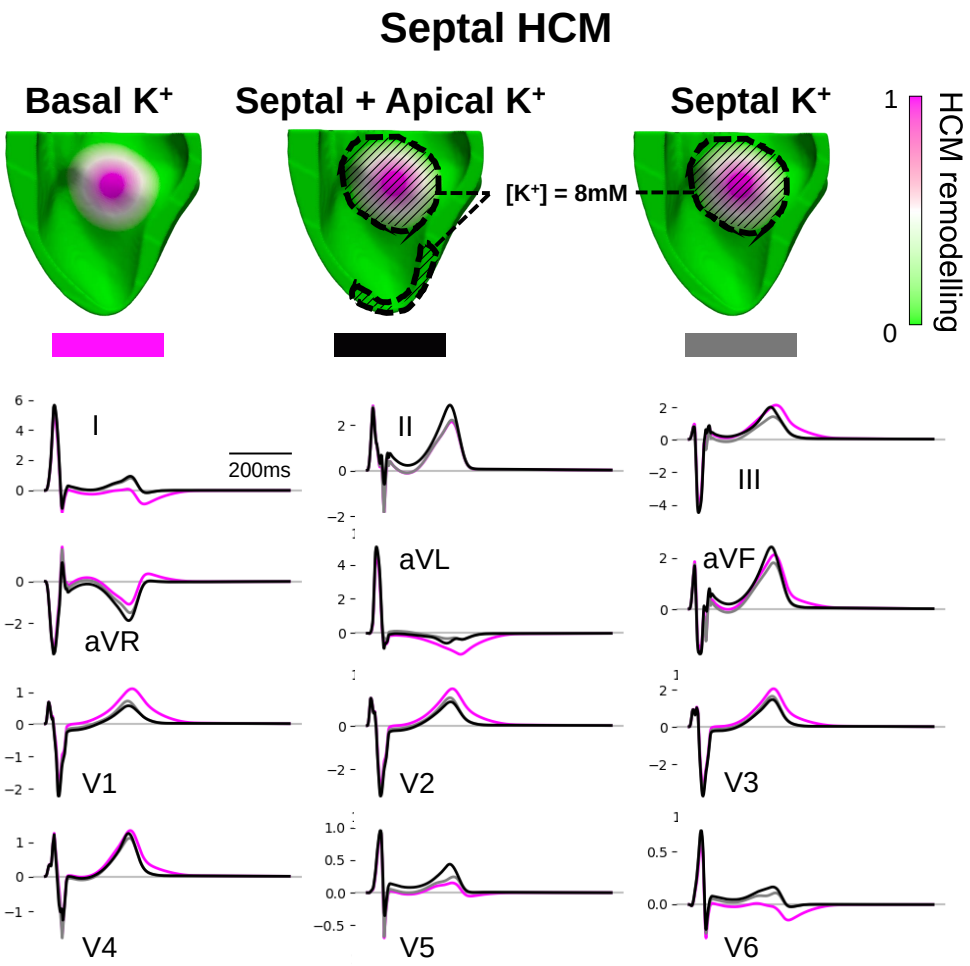


Figure A.16: Comparisons of the effect of increased regional $[K^+]$ in the septum and apex vs. only the septum on 12-lead ECG in septal HCM. Concomitant apical $[K^+]$ increases in septal HCM did not significantly affect T wave pseudonormalisation, but additional ST segment changes occurred.

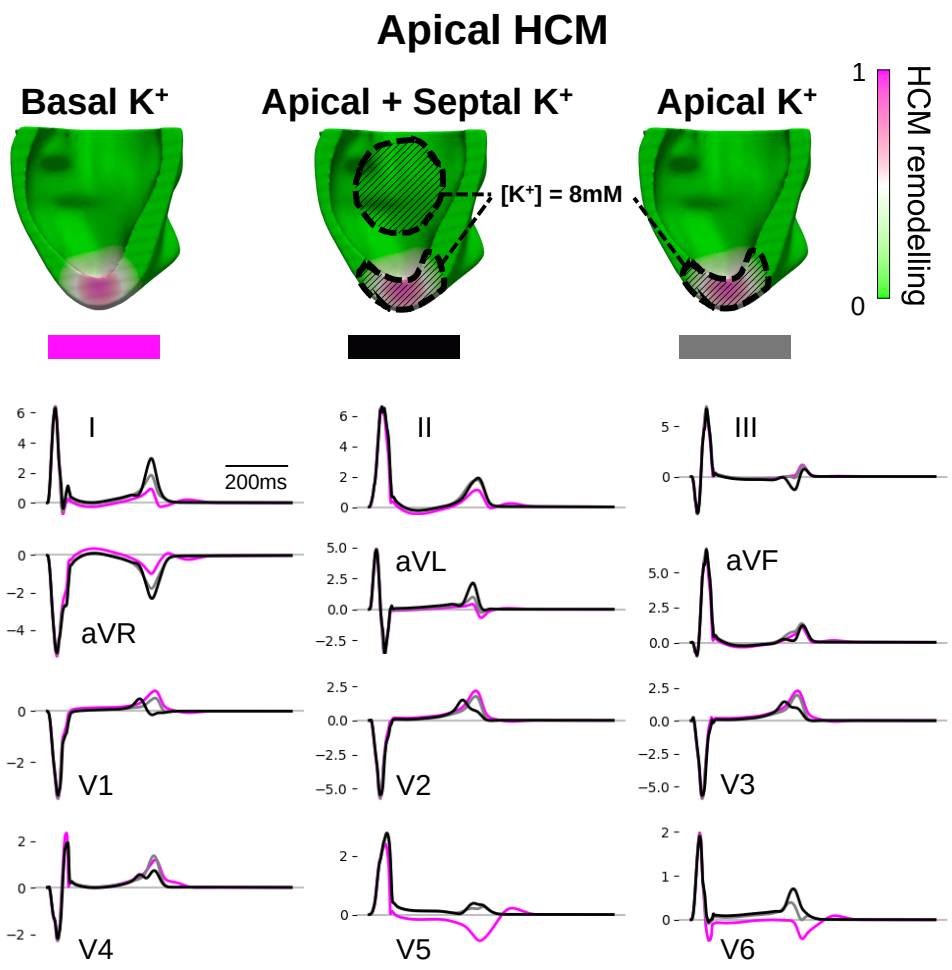


Figure A.17: Comparisons of the effect of increased regional [K^+] in the apex and septum vs. only the apex on 12-lead ECG in apical HCM. Concomitant septal [K^+] increases in apical HCM did not significantly affect T wave pseudonormalisation, but additional ischaemic T wave notching in leads V1-V4 occurred.

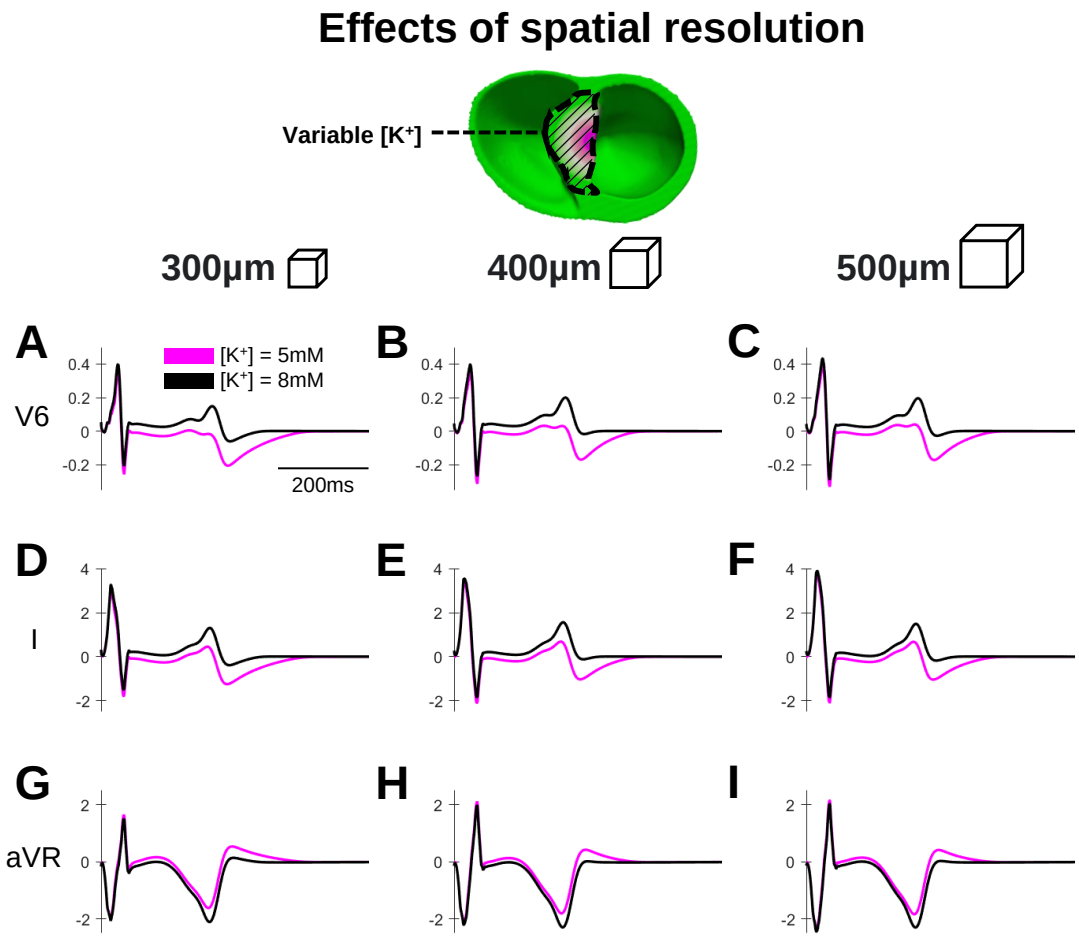


Figure A.18: Example effects of biventricular mesh resolution on ischaemic T wave pseudonormalisation in the septal HCM model. (A, B, C) Lead V6, (D, E, F) lead I, and (G, H, I) lead aVR, for varying spatial resolutions of 300 μm (A, D, G), 400 μm (B, E, H), and 500 μm (C, F, I), under regional $[K^+]$ increases to 8 mM (black traces) as compared to basal $[K^+]$ of 5 mM (magenta traces). Leads V6, I, and aVR are shown as they exhibited baseline repolarisation abnormalities in the form of inverted T waves. In all cases, T wave pseudonormalisation effects due to regional $[K^+]$ increases were insensitive to the spatial resolution (300–500 μm) used in the discretisation of the virtual heart models.

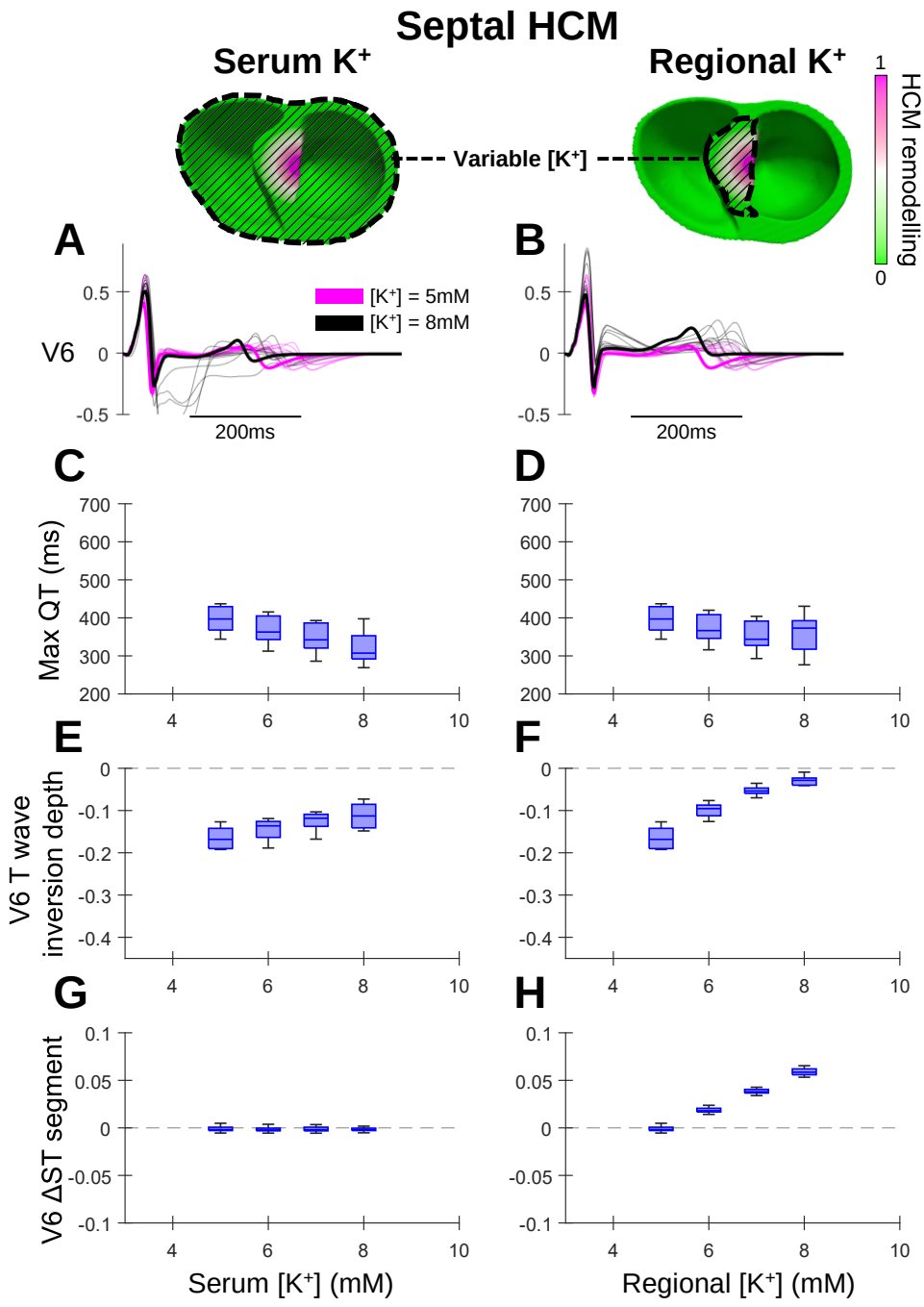


Figure A.19: Comparisons of the effect of serum [K^+] vs. regional [K^+] on ECG biomarkers in septal HCM. (A & B) Representative lead V6 traces, showing that (A) T wave morphology is modulated, but not totally pseudonormalised, by serum [K^+], and (B) T wave pseudonormalisation can occur due to regional [K^+] increases. (C & D) Max QT interval, (E & F) lead V6 T wave inversion depth and (G &

H) lead V6 ST segment changes, plotted against (C & E & G) serum [K^+] and (D & F & H) regional [K^+]. All results presented at 2 Hz pacing.
